REPORT DOCUMENTATION PAGE

1a. REPORT SECURITY CLASSIFICATION	1b. RESTRICTIVE MARKINGS
2a. SECURITY CLASSIFICATION AUTHORITY	3. DISTRIBUTION/AVAILABILITY OF REPORT
2b. DECLASSIFICATION/DOWNGRADING SCHEDULE	Approved for public release; distribution is unlimited

4. PERFORMING ORGANIZATION REPORT NUMBER(S)	5. MONITORING ORGANIZATION REPORT NUMBER(S)
	AFWAL-TR-87-3060

6a. NAME OF PERFORMING ORGANIZATION	6b. OFFICE SYMBOL (If applicable)	7a. NAME OF MONITORING ORGANIZATION
McDonnell Aircraft Company		Air Force Wright Aeronautical Laboratory Flight Dynamics Laboratory (AFWAL/FIBEC)

6c. ADDRESS (City, State, and ZIP Code)	7b. ADDRESS (City, State, and ZIP Code)
P. O. Box 516 St. Louis, Missouri 63166	Wright-Patterson AFB, Ohio 45433-6553

8a. NAME OF FUNDING/SPONSORING ORGANIZATION Air Force Wright Aeronautical Laboratory	8b. OFFICE SYMBOL (If applicable) AFWAL/FIBEC	9. PROCUREMENT INSTRUMENT IDENTIFICATION NUMBER
		F33615-83-C-3219

8c. ADDRESS (City, State, and ZIP Code)	10. SOURCE OF FUNDING NUMBERS			
	PROGRAM ELEMENT NO.	PROJECT NO.	TASK NO.	WORK UNIT ACCESSION NO.
Wright-Patterson AFB, Ohio 45433	62201F	2401	01	67

11. TITLE (Include Security Classification)

Durability of Continuous Fiber Reinforced Metal Matrix Composites

12. PERSONAL AUTHOR(S)

C. R. Saff, D. M. Harmon, and Dr. C. T. Sun

13a. TYPE OF REPORT	13b. TIME COVERED	14. DATE OF REPORT (Year, Month, Day)	15. PAGE COUNT
Final	FROM Sep 83 TO Dec 86	1987 October	219

16. SUPPLEMENTARY NOTATION

17.	COSATI CODES		18. SUBJECT TERMS (Continue on reverse if necessary and identify by block number)
FIELD	GROUP	SUB-GROUP	Fatigue Life Composite Materials
11	04		Static Strength Metal Matrix
			Stress Analysis

19. ABSTRACT (Continue on reverse if necessary and identify by block number)

The objective of this program was to develop the test data and analysis techniques required to insure the structural integrity of fiber reinforced metal matrix composites (FRMMC) when applied to airframe structures. Approximately 300 tests of unidirectional boron/6061 aluminum, (B4C)/15-3-3-3 titanium, and crossplied boron/6061 aluminum were performed. Testing was concentrated on notched (central hole) specimens to evaluate the notch sensitivity of these materials and to discriminate between the failure modes of aluminum and titanium matrix composites.

It was found that the relative fiber and matrix stiffnesses and strengths determine primary failure modes in fatigue. Analysis methods were developed based on fiber and matrix properties to predict notched and unnotched static strength, crack initiation, fatigue failure mode, life to failure, and residual strength. One half of the tests (150 specimens) were performed to verify the predicted properties of the aluminum and titanium matrix composites.

20. DISTRIBUTION/AVAILABILITY OF ABSTRACT	21. ABSTRACT SECURITY CLASSIFICATION
☐ UNCLASSIFIED/UNLIMITED ☐ SAME AS RPT. ☒ DTIC USERS	Unclassified

22a. NAME OF RESPONSIBLE INDIVIDUAL	22b. TELEPHONE (Include Area Code)	22c. OFFICE SYMBOL
Lt. D. Graves	(513) 255-6104	AFWAL/FIBEC

DD FORM 1473, 84 MAR
83 APR edition may be used until exhausted.
All other editions are obsolete.

AFWAL-TR-87-3060

DURABILITY OF CONTINUOUS FIBER REINFORCED METAL MATRIX COMPOSITES

D.M. Harmon and C.R. Saff
McDonnell Aircraft Company
P.O. Box 516
St. Louis, Missouri 63166

Dr. C.T. Sun
Purdue University
W. Lafayette, IN

October 1987

Final Report for Period September 1983 to December 1986

Approved for public release; distribution unlimited

FLIGHT DYNAMICS LABORATORY
AIR FORCE WRIGHT AERONAUTICAL LABORATORIES
AIR FORCE SYSTEMS COMMAND
WRIGHT-PATTERSON AIR FORCE BASE, OHIO 45433-6553

NOTICE

When Government drawings, specifications, or other data are
used for any purpose other than in connection with a definitely
related Government Procurement operation, the United States
Government thereby incurs no responsibility nor any obligation
whatsoever; and the fact that the government may have formulated,
furnished, or in any way supplied the said drawings, specifica-
tions, or other data, is not to be regarded by implication or
otherwise as in any manner licensing the holder or any other
person or corporation, or conveying any rights or permission to
manufacture, use, or sell any patented invention that may in any
way be related thereto.

This report has been reviewed by the Information Office (IO)
and is releasable to the National Technical Information Service
(NTIS). At NTIS, it will be available to the general public,
including foreign nationals.

This technical report has been reviewed and is approved for
publication.

DAVID L. GRAVES, 1st Lt, USAF
Project Engineer

FRANK D. ADAMS, Chief
Structural Integrity Branch
Structures Division

FOR THE COMMANDER

HENRY A. BONDARUK, Jr., Colonel, USAF
Chief, Structures Division

FOREWORD

This report was prepared by McDonnell Aircraft Company (MCAIR), St. Louis, Missouri, for the Structural Integrity Branch, Structures Division, Flight Dynamics Laboritory, Air Force Wright Aeronautical Laboritories, Wright-Patterson Air Force Base, Ohio, under contract F33615-83-C-3219, Project 2401, Work Unit 24010167, "Durability of Continuous Fiber Metal Matrix Composites." The contract monitor is Capt. David Graves, AFWAL/FIBEC.

The Structural Research Department of McDonnell Aircraft Company is responsible for the performance of this program. The Program Manager is H. D. Dill. Principal Investigator and principal author of this report is C. R. Saff. Development of a unified analysis procedure for metal matrix composites and direction of MCAIR testing was performed by D. M. Harmon.

Dr. C. T. Sun, of Purdue University, was a primary subcontractor, contributing testing of crossplied metal matrix laminate specimens and stress and fatigue life analyses of both unidirectional and crossplied metal matrix composites.

TABLE OF CONTENTS

TABLE OF CONTENTS (Continued)

TABLE OF CONTENTS (Concluded)

LIST OF ILLUSTRATIONS

LIST OF ILLUSTRATIONS (Continued)

xi

LIST OF ILLUSTRATIONS (Continued)

LIST OF ILLUSTRATIONS (Continued)

LIST OF TABLES

SECTION I

INTRODUCTION

Metal matrix composites have received renewed interest in recent years for applications in aerospace structures in which temperature and/or stiffness requirements preclude the use of resin matrix composites and strength and durability requirements tax monolithic metal structures. These applications are addressed in a number of USAF-funded efforts (References 1-7). While durability of metal matrix composites (MMC) is being assessed in these programs there is no requirement to develop life prediction capability which can be used to assure durability during design of future MMC structures.

This program was an outgrowth of these larger Advanced Development Programs. The objective of this program was to develop fatigue life and crack growth prediction methodologies required to assure the durability of MMC structures according to current military specifications. This program involved four tasks: a literature survey to select life analysis methodologies for evaluation, an analysis model development test program, the analysis development itself, and an analysis model verification test program.

The results of the literature survey task were reported in AFWAL-TR-85-3107 (Reference 8). This report summarizes the analysis methods used by previous investigators to predict strength, fatigue life, and residual strength of MMC materials, and it presents a compilation of fatigue life test data from various literature sources. In that literature data, it was noted that the fatigue failure mode was related to the fiber to matrix stiffness and strength ratios. It was also noted that the methods used to predict stiffness and strength of resin matrix composite systems apply equally well to metal matrix systems.

1

In the analysis model development test task, 150 static, fatigue, and residual strength tests were performed to determine the effects of notch sensitivity, load level, stress ratio, and layup on fatigue life of MMC materials. Throughout the formulation of this test plan and analysis of the data, the results of the MMC tests were related to the known behaviors of metals and resin matrix composite systems. These comparisons led to some basic insights into the relative behavior of MMC materials for application to primary airframe structures. All of the unidirectional material tests were performed at McDonnell Aircraft Company (MCAIR). The crossplied laminate tests were performed by Dr. C. T. Sun of Purdue University. During the model development testing numerous methods for nondestructive examination of the damage state in MMC materials were evaluated. Specimen thicknesses were selected to eliminate the need for buckling guides for compression testing so that in-situ examinations could be carried out during these tests. Dye penetrant, ultrasonic C-scans, X radiography, displacement monitoring, and acoustic emission monitoring were all evaluated during this test program. Specimen sectioning, deplying, and scanning electron microscopy (SEM) were all used at various points in post test examinations to determine the failure mechanisms.

Analytical model development was primarily based on a simple stress analysis technique. This analysis technique, described completely herein, allows rapid stress analysis of finite width, orthotropic or isotropic plates having circular or elliptical notches. This analysis, along with a nonlinear laminated plate theory analysis, forms the backbone of the analytical development. Dr. Sun developed a discrete finite element model of the yield behavior of the matrix between fibers in cracked aluminum and titanium matrix materials. His analyses along with others available in the literature, showed the way toward development of a simple analysis scheme capable of accurately predicting strength, stiffness, fatigue life, fatigue failure mode, and residual strength of MMC materials.

2

This analytical model was verified by 150 static, fatigue, and residual strength tests of both aluminum and titanium matrix composite coupons in which the test results were predicted before the tests were performed. The accuracy of these analysis procedures was demonstrated in these tests of MMC materials having very different fiber to matrix strength ratios and fatigue failure modes. Again crossplied laminate tests were performed by Dr. Sun and the unidirectional tests were performed at MCAIR.

SECTION II

SELECTION OF ANALYTICAL METHODS AND DATA REQUIREMENTS

1. <u>LITERATURE SURVEY</u> - In the first phase of this program a literature survey was performed to identify the state-of-the-art in testing and analysis of metal matrix composites. This survey formed the basis for the model development effort performed during this program. The literature survey results are summarized in a separate report, AFWAL-TR-85-3107 (Reference 8). Some of these results provide an important background for the model of MMC behavior that was developed in this program and for the test plan rationale used for model development and testing. Therefore this section provides a brief review of the effect of matrix properties and notch geometry on strength, fatigue life, and failure mode behavior on metal matrix composites.

    a. <u>Failure Modes</u> - One of the primary goals of the literature survey was to review the test data available in the literature to determine the range of fatigue failure modes found by previous investigators. Testing performed under MCAIR IRAD had previously shown that failure modes in fiber reinforced metals differ with matrix strength. In aluminum matrix materials cracks appear to initiate at the location around a notch at which the matrix shear stresses are highest (indicated by the arrows in Figure 1).

    In titanium matrix materials, the cracks initiate where the strains in the fibers are greatest. These cracks grow irregularly at first, the path apparently selected by where fibers fail. Eventually these cracks become large enough that the energy at the crack tip becomes great enough to fail fibers at the crack tip. Then crack propagation proceeds as it would in the matrix metal, across the specimen net section. In aluminum matrix composites,

and certainly in epoxy resin composites, the matrix stiffness and strength will not generate enough energy at the crack tip to fail fibers as it does in titanium matrix composites.

B/6061 Aluminum   **(B₄C)B/Ti 15-3-3-3**

Load Direction
Fiber Direction

Load Direction
Fiber Direction

⬆ Predicted failure initiation sites
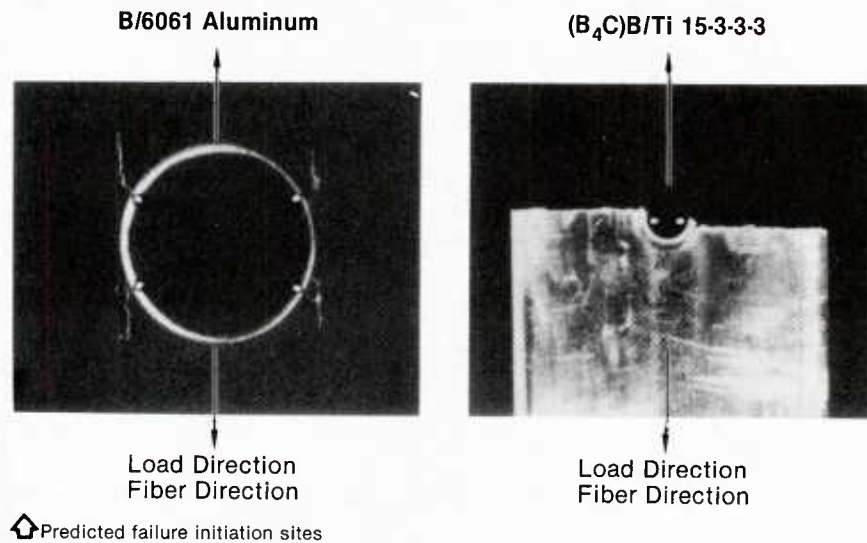
**Figure 1. Fatigue Failure Modes in Unidirectionally Reinforced
Metal Matrix Composites**

This same effect of the matrix strength to affect the crack initiation behavior of MMC materials was demonstrated in tests performed by Midwest Research Institute in 1976. In a series of tests of notched aluminum metal matrix composites examining the effect of heat treatment on crack growth and crack initiation, J. R. Hancock found that even aluminum MMC materials, heat treated to peak strength conditions, can develop flaws that initiate and propagate from the notches as they do in the parent metal. For the vast majority of the lower strength (6061 and 2XXX series) aluminums, the flaws will grow along the fibers.

b. Notch Sensitivity - Another interesting effect of fiber reinforcement on material properties is notch sensitivity. Notch sensitivities in fatigue and static strength are shown in Figure 2 for metals, unidirectionally reinforced metal matrix composites

and fiber dominated (50 percent 0 degree fibers or more) resin matrix composites. In the comparison shown, the static strength sensitivity is defined as the ratio of the net strength of a notched specimen to the strength of an unnotched coupon under tension loading. The fatigue sensitivity is the ratio of net stress in a notched specimen to that in an unnotched specimen at a given life (10,000 cycles at R=-1).
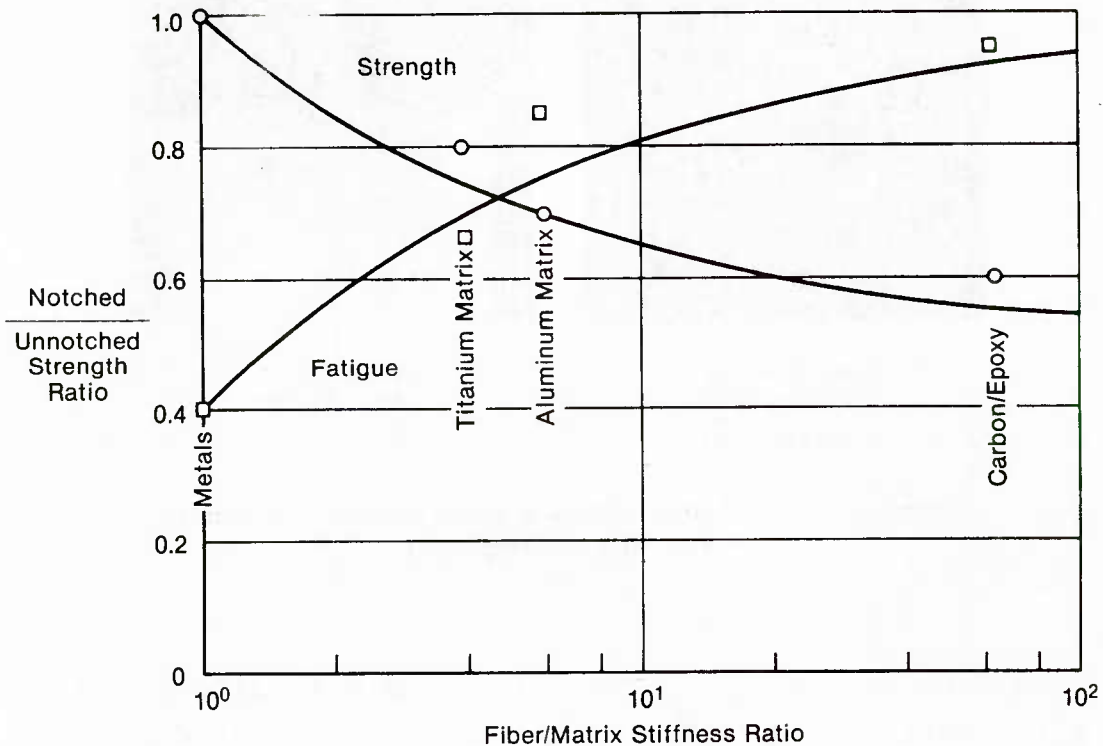
Figure 2. Effects of Fiber Reinforcement on Notch Sensitivity

Metals and resin matrix composites form a convenient framework in which to discuss the mechanical behavior of FRMMC materials. Metals, because of their ability to plastically deform, have notch strengths close to net section ultimate strength. In contrast, carbon/epoxy shows a significant effect of notches on static strength because the notch interrupts load carrying fibers and forces load through the weak matrix. Consequently, it is not surprising to find that MMC materials are ranked between these limits by the ratio of fiber strength to matrix strength. For metals, the "fiber" to "matrix" strength ratio is selected as unity.

6

In fatigue, the reverse ordering takes place. In weak matrix composites, initial cracking occurs along the fibers, reducing stress concentrations and promoting long fatigue lives in composites loaded along the fibers. In metals, notches are the primary source of failure origination in fatigue. While interface strength can influence flaw growth in metal matrix composites, these materials appear to be ranked by the ratio of fiber stiffness to matrix stiffness.

Figure 2 shows the superposition of notch sensitivity in strength and fatigue for the materials studied. The notch sensitivity of continuous fiber reinforced metal matrix composites lies between that of metals and that of resin matrix composites and the relative sensitivity of metals and resin matrix composites is reversed between strength and fatigue. The comparison shown in Figure 2 demonstrates why we think of metals as being fatigue sensitive and resin matrix composites as strength sensitive.

Metal matrix composites fall in an area balanced between strength and fatigue sensitivity. The failure progression in these materials reflects this balance. In unidirectionally reinforced boron/aluminum, static failure modes were across the net section, but fatigue cracks grew in the matrix along the fibers. Even when static failures occur across the net section, the matrix yields enough to isolate the notch and remove the notch sensitivity (Figure 3).

2. SELECTED METHODS & DATA REQUIREMENTS - Based on the literature survey, and the testing we performed preceding this program, methods of analysis were tentatively selected for evaluation in this program. Each of these methods required a certain type of input data to be provided by the model development test program.
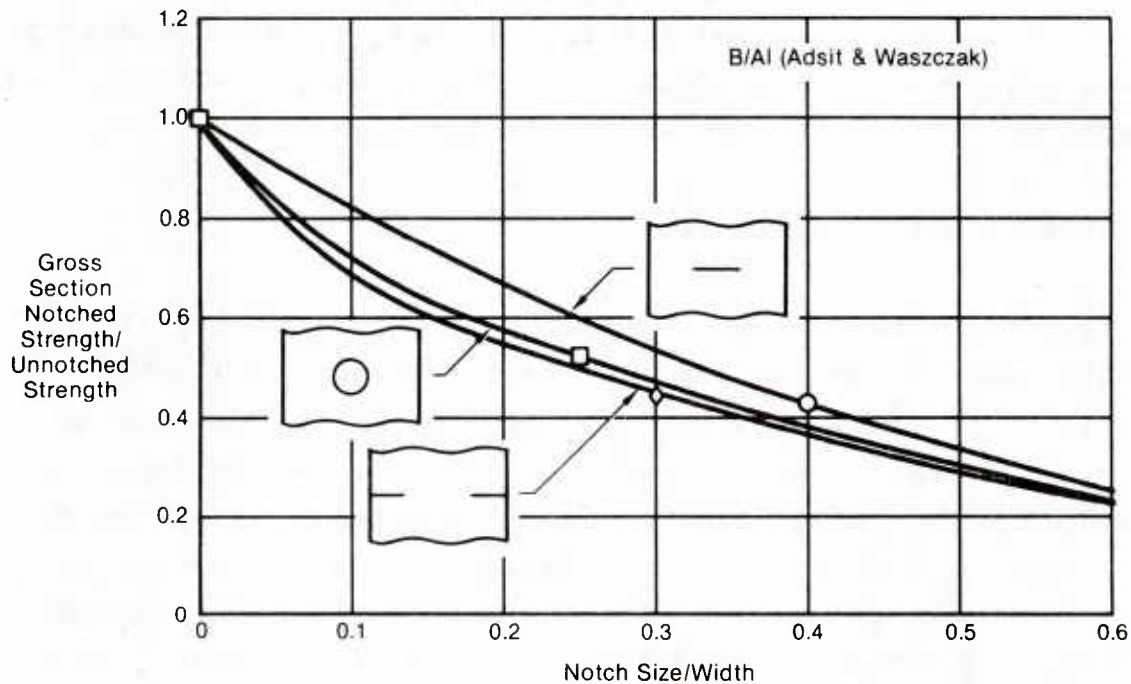
Figure 3. Effect of Notch Severity on Strength

a. <u>Stiffness</u> - For lamina stiffness we used rule of mixtures and verified that approach using literature data on fiber, matrix, and unidirectionally reinforced composite, stiffnesses. Tests of unnotched coupons were used to verify the stiffnesses used in analysis development within this program.

Laminate stiffnesses were computed using laminated plate theory and verified through ultimate strength tests of unnotched specimens. The plies were modeled as elastic-perfectly plastic materials, based on the lamina test results from unnotched specimens. Off-axis plies were predicted to lose stiffness as they yielded or failed.

Similarly, laminate stiffnesses were reduced as fatigue failures occurred within various plies, as predicted by Johnson and associates at NASA, Langley.

8

b.   Stress - Stress analyses were performed using a very simple orthotropic plate analysis technique developed during the course of this program. It's accuracy was demonstrated by comparison with classical elasticity solutions and by comparisons with displacement measurements taken during open hole tests.

c.   Strength - Strength analysis development was based on the above stress and stiffness analyses, and were influenced by the shear lag analyses developed by Goree and associates at Clemson University (References 9 - 11). These strength analyses require lamina property stiffness and strength data from unnotched specimens and were verified by notched specimen data.

d.   Crack Initiation - Crack initiation analyses are based on the stresses around the notch. Two conditions, shear stress within the matrix parallel to the fibers and stress in the fiber adjacent to the notch, are examined to determine failure mode. Unnotched lamina tests were used to determine stiffness and strength properties for the laminae. Crack initiation data from open or filled hole specimens was the basis for development of matrix cracking and fiber breakage life curves. Model development and verification was provided by tests of other notch geometries, stress levels, and stress ratios.

In crossplied laminates, the same types of testing were performed, although lamina test data are sufficient to allow initiation prediction with the model.

e. Crack Growth - Crack growth data can be obtained from either center cracked panels of the matrix material, or from center cracked or open hole tests of MMC materials. In the case of weak matrix composites (B/Al) the crack propagation will usually be in the matrix parallel to the fibers, so off-axis specimens are usually more useful for data generation. Very little crack growth information was obtained in crossplied MMC because the outermost plies were longitudinal in each case.

Cracking behavior was noted in these plies, but it was obvious that it was heavily influenced by subsurface flaw growth in the off-axis plies.

Crack growth analysis verification was obtained from tests of center cracked and center hole specimens at different stress levels and stress ratios.

f. <u>Residual Strength</u> - Residual strength analyses depend on two potential failure modes: strength failures that occur in weak matrix composites when yielding and cracking progress along the fibers, and fracture that occurs in strong matrix materials in which the cracking in the matrix can induce fiber failures. Residual strength analyses were developed and verified through tests of center hole specimens.

SECTION III

LIFE PREDICTION METHODOLOGY DEVELOPMENT TESTING

This test program is divided into two phases using 150 specimens in each; the first directed toward methodology development, the second toward model verification and extension. Model development testing concentrated on unidirectionally reinforced aluminum matrix material, although some crossplied boron/aluminum was also tested. Unidirectional titanium matrix material was tested only in the model verification phase.

The objective of the model development test program was to generate the data required to determine how flaws originate and grow to failure in fiber reinforced metal matrix composites (FRMMC) under fatigue loading. This data was used to develop an analysis procedure which can be used to predict fatigue life (durability) of FRMMC structures. To verify the analysis the strengths and lives were predicted for the specimens and loading conditions used in the verification test plan.

In the analysis development test program we concentrated on tracking fatigue damage growth in notched specimens. We believe that in FRMMC structures fatigue failures will initiate at stress concentration sites such as fastener holes or cut-outs. This is true even when FRMMC is used as selective reinforcement. Our tests of selectively reinforced material show that failures occur in the base material at the end of reinforcements, rather than in the unnotched reinforcements.

Fatigue tests of unnotched specimens were performed to evaluate the notch sensitivity of FRMMC structures. This is of interest because notch sensitivity in these materials falls between that of metals, which show severe notch sensitivity, and that of epoxy matrix composites, which often show little or no notch sensitivity. We evaluated many methods for identifying

11

damage initiation in these tests to aid in developing stress analyses of notches in FRMMC. We monitored damage growth in these tests and measured residual strength to help evaluate damage parameters. The majority of tests were run to failure in fatigue to provide data for developing life analyses.

1. <u>MATERIAL SELECTION</u> - Two FRMMC materials were used: boron/6061 aluminum and $(B_4C)B/15V-3Al-3Sn-3Cr$ titanium. One of the primary effects to be investigated in this program was the difference in initiation and growth of flaws between aluminum and titanium matrix materials. Previous tests had shown that flaws in aluminum matrix materials initiate at locations of highest matrix principal stress and propagate parallel to the fibers, Figure 1. In titanium matrix materials the flaws will propagate through the fibers. Because MCAIR had developed sufficient data on titanium matrix materials in our Reference 1 program, model development testing in this program concentrated on the aluminum matrix materials.

Boron fibers, due to their longer period of development, are believed to have the most consistently high strengths of the fibers available at the outset of this program, Figure 4. Boron and B_4C coated boron fibers have about the same properties. Only the B_4C coated fiber is shown in Figure 4. Within this test program many variables were investigated. A consistent material system was essential to provide reproducible results with few replications. Boron fibers are used in both materials. B_4C coated boron is used in the titanium material to reduce fiber degradation during the higher temperature consolidation. Properties of the bare and B_4C coated fibers are the same, as given in Figure 5, thus differences in flaw growth behavior should be attributable to either matrix or fiber/matrix interface properties.

The boron/aluminum material was primarily unidirectional in 8 ply and 24 ply thicknesses. Two crossplied laminates were also tested: $[0°_2/90°_2]_{3S}$ and $[0°_2/+45°]_{3S}$, hereafter termed (0/90) and (0/45) layups, respectively. These layups are representative

of those used in the aluminum matrix demonstration program
(Reference 3). The stacking sequences are based on two considera-
tions: (1) to increase bending stiffness for a given axial
stiffness by having 0° plies outermost, and (2) to reduce inter-
laminar shear stresses caused by grouping similar ply orientations.
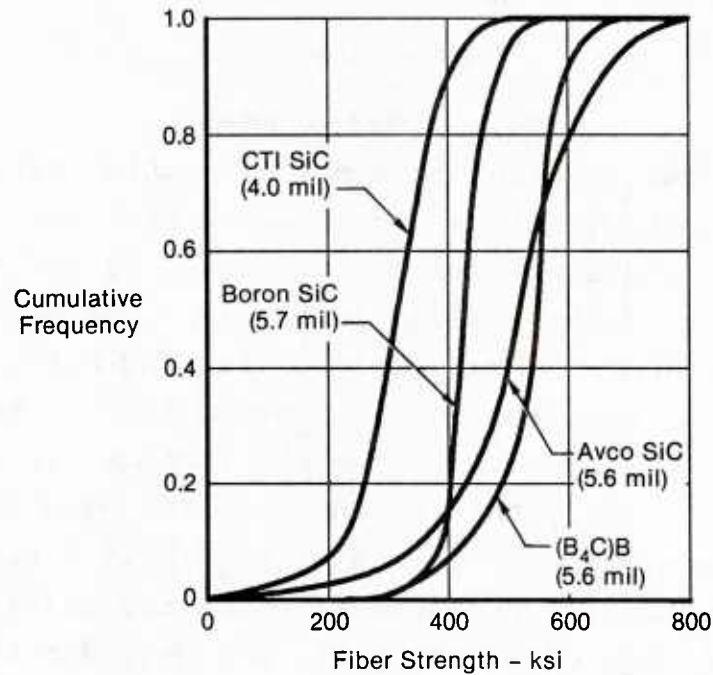
	Fiber Strength (ksi)		
	Average	Standard Deviation	B-Basis Value
Avco SiC	538	131	370
CTI SiC	335	89	221
Boron SiC	443	49	380
(B₄C) Boron	552	85	443

Figure 4. Fiber Strength Distributions

13

Tungsten

Boron

Boron

Tungsten

Boron

B₄C Layer

B₄C-Boron

Tensile Strength = 550 ksi
Modulus = 58 msi
Density = 0.091 lb/in.³
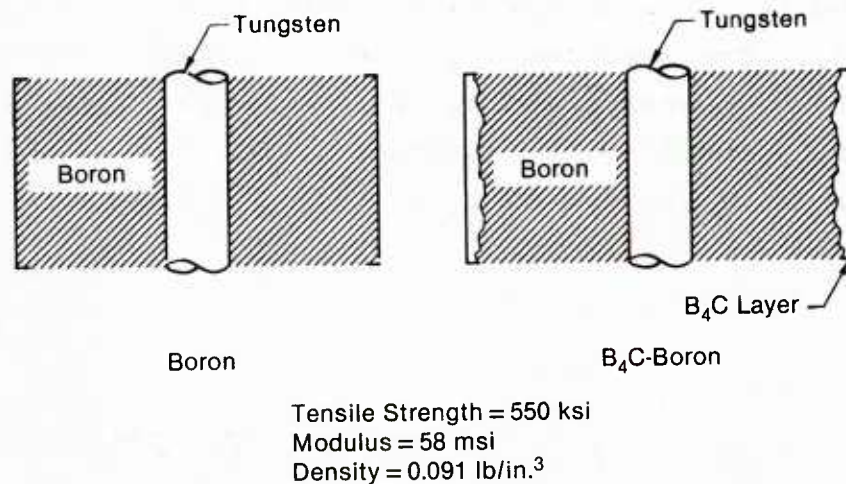
Figure 5. Selected Fibers

Unidirectionally reinforced boron/titanium material was tested in the model verification program. The high transverse and shear strengths and stiffnesses of titanium matrix composites, Figure 6, eliminate the need to cross-ply. The material was subjected to a simulated superplastic forming/diffusion bonding (SPF/DB) cycle by the fabricator (Amercom Inc.). We feel that a major advantage of the titanium matrix material is its SPF/DB capability. Currently, the SPF/DB cycle has been found to significantly reduce static properties of (B₄C)B/15-3 titanium, Figure 7. The reinforced 15-3 properties, which are initially higher than comparable (B₄C)B/6-4 material, are degraded to nearly the same low values after SPF/DB.

2. <u>INITIAL QUALITY OF FRMMC MATERIAL</u> - All FRMMC material used in this program was fabricated by hot vacuum pressing by Amercom, Inc. All fibers were identified as to reactor run and recorded along with fiber tension strengths. A transverse strip of the drum wrap (the foil used in preparing the MMC) was removed and retained by Amercom for traceability.

Consolidation pressure, temperature-time histories, and as-consolidated tensile strengths were recorded for each lot of FRMMC material. Strength results are shown in Figure 8 for the unidirectionally reinforced B/Al panels.

14
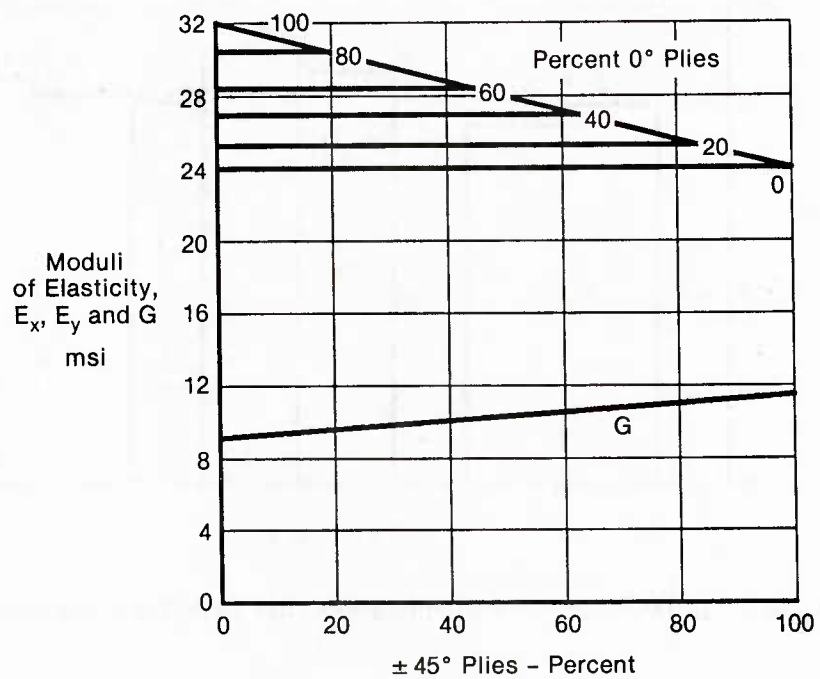
Figure 6. Moduli of Cross-Plied Boron/Titanium
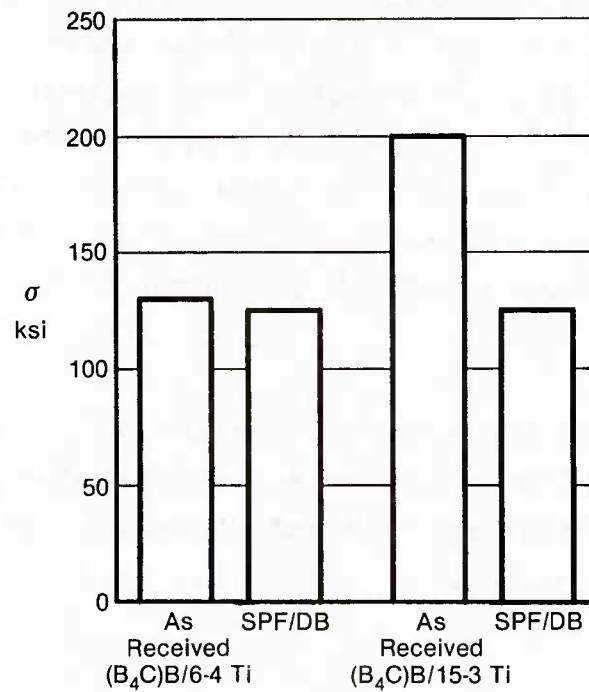
Figure 7. Effect of Thermal Processing on Longitudinal Strength of Titanium FRMMC
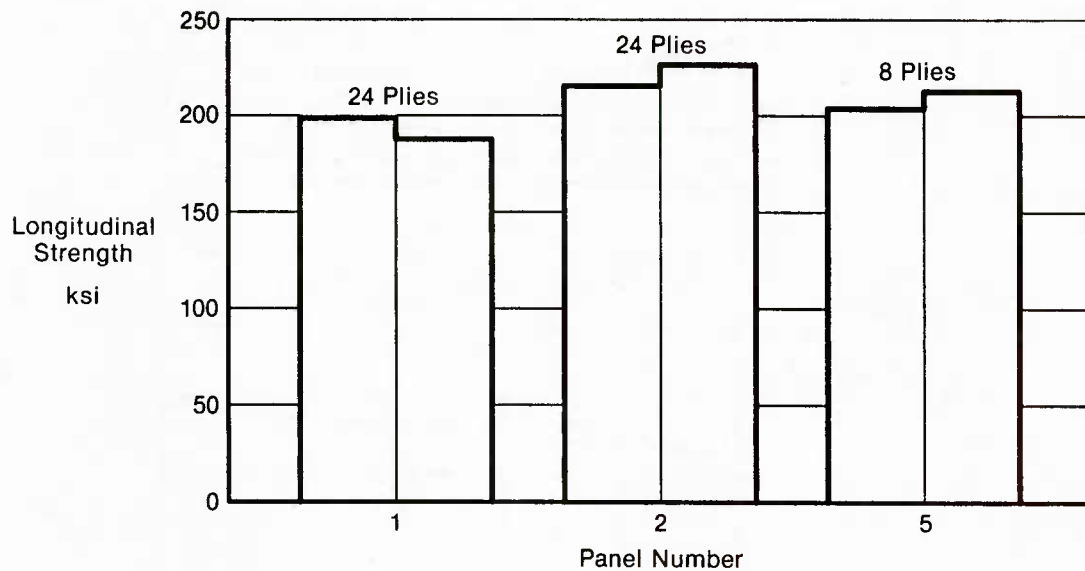
Figure 8. Boron/Aluminum Qualification Test Data /From Amercom

All FRMMC panels were nondestructively inspected following fabrication to verify specimen quality. Low kilowatt radiography was used to inspect the panels for non-uniform fiber spacing and for broken fibers. Figure 9 shows these initial defects as detected by X-ray examination of a thin boron/titanium panel from a previous program. The panels used in this test program showed no such damage, at most they showed a waviness in the fiber, as shown in Figure 10. The material received from Amercom was exceptionally well consolidated in comparison to previous MMC materials.

In addition to the X-ray inspection all panels were subjected to an ultrasonic through transmission reflector plate inspection to detect interlaminar debonds and incomplete fiber impregnation. Test specimens machined from the panels were also inspected for quality.

3. SPECIMENS AND TEST PROCEDURES - The principle specimens used in the analysis model development test program are shown in Figure 11. Central unloaded holes with fasteners installed were selected

as the primary specimens for test in this program to provide a
realistic flaw initiation site. Unnotched specimens were tested
to compare initiation lives with those determined from the central
hole specimens. Center cracked panel specimens were tested to
develop crack growth data, where such data were meaningful.
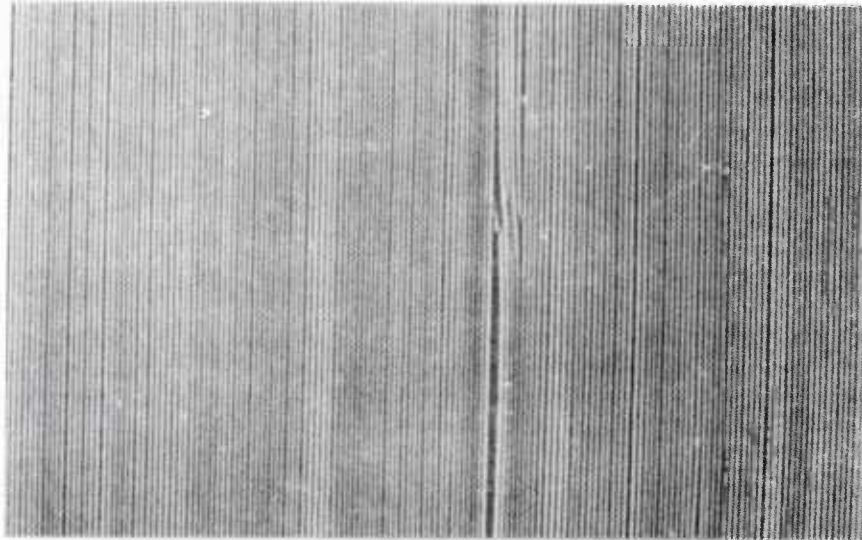
Magnification 4.5 ×

**Figure 9. Initial Damage in Unidirectional FRMMC
Detected by X-Radiography**
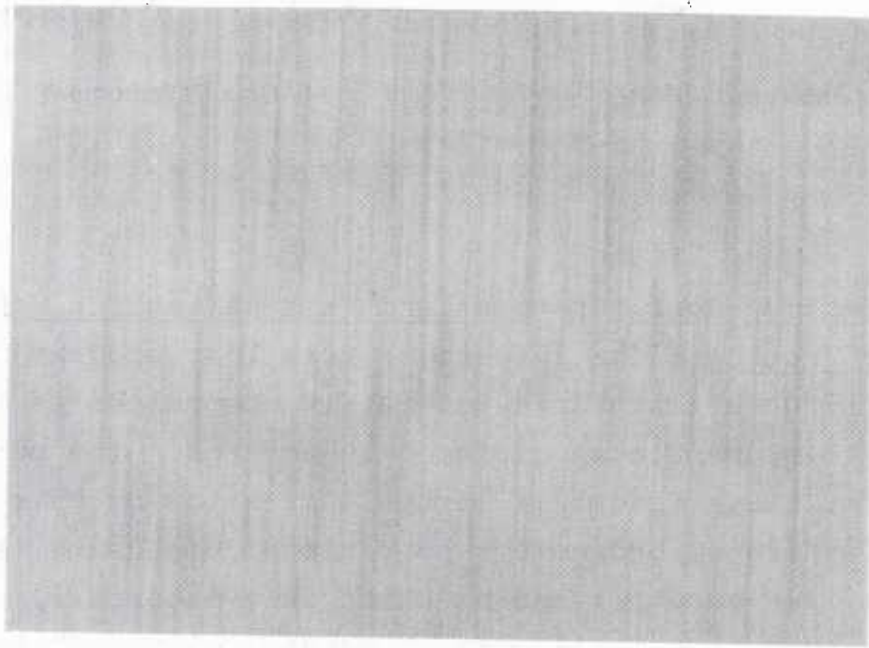
Figure 10. Typical X-Radiography Photograph of Panels Used in This Program
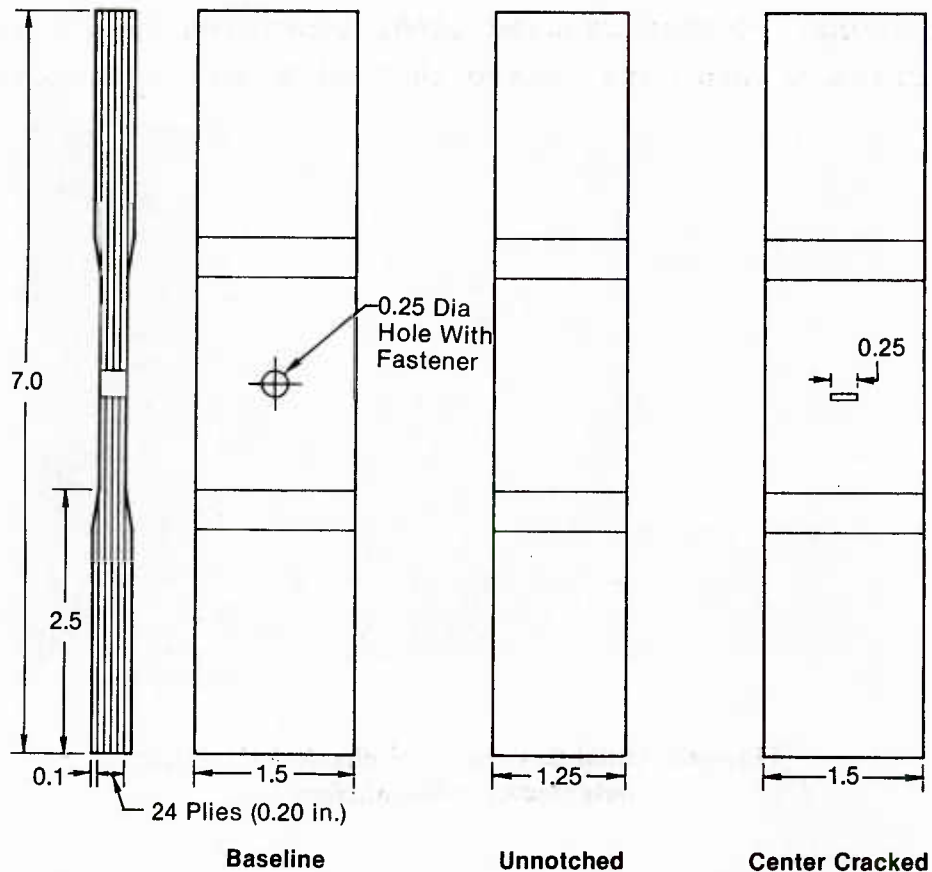
Figure 11. Primary Test Specimens for Analysis Development

a. <u>Specimen Configurations and Fabrication for Model Development Testing</u> - The purpose of this test program was to determine the durability of metal matrix composites as they would be applied to conventional airframe structures. The primary uses projected for these materials at the initiation of this program were as selective reinforcement of various components (such as those shown in Figure 12) and as stiff skin materials, either diffusion bonded to a metal core or mechanically fastened to a conventional spar-rib structure.

18
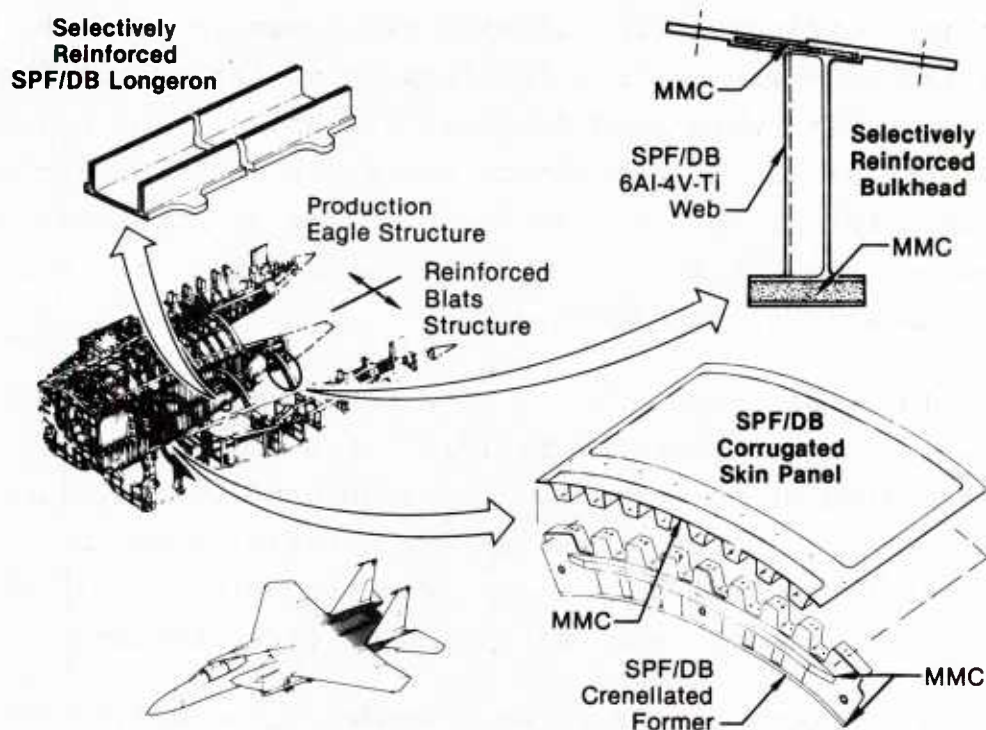
Figure 12. Reinforced Aft Fuselage Design

It was felt that emphasis on unnotched specimens to measure crack initiation lives would produce data that would not reflect the failure modes possible within unidirectionally reinforced MMC structures, particularly those involving notched or mechanically fastened skins. Previous tests at MCAIR had shown that failure modes at holes in FRMMC materials can differ markedly from material to material. Thus we felt it to be imperative that a notched specimen be used to characterize failure in MMCs because the use of either an unnotched or center cracked specimen to develop data presupposes a knowledge of failure modes, knowledge which the tests are intended to produce.

The central hole specimen, shown in Figure 11, is representative of airframe bolted attachments having little or no load transfer. Similar specimens have been used for development of fatigue life data in metals, carbon/epoxy, as well as in metal matrix composites (References 12-15). A steel pin was inserted

19

into the hole to provide realistic stress concentrations under compression loadings. The fastener was taped in place so that one side of the hole was visible for inspection throughout the test. Diamond core bits were used to drill the holes. The holes were not reamed because our experience has shown that reaming can break fibers near the holes. Polishing the sides of unnotched specimens was shown to break fibers in much the same way in the Air Force testing summarized in Reference 16.

Aluminum tabs were used on both aluminum and titanium MMC specimens to prevent fatigue failures from originating at the ends of the serrated grips, especially in the unnotched specimen tests. Generally, there is too little matrix material covering the surface fibers to keep serrations from producing significant damage to the specimen and initiating an early failure.

In this program the tabs were bonded using AF136 adhesive. This adhesive requires a 4 hour cure at 150°F. This cure cycle was not expected to produce any significant residual stress states in either the specimen or adhesive. There were no failures in this test program caused by the use of the aluminum loading tabs.

Specimen thicknesses for the model development tests were based on precluding buckling during R=-1 testing so that the specimens could be monitored without buckling guides. The 24 ply thickness was selected so that buckling loads would exceed the maximum load by more than 30 percent. Static tests showed that this criterion was met, however, in R=-1 fatigue tests of cross-plied B/Al, the stiffness lost as the crossplies cracked reduced the buckling load until buckling became the eventual failure mode in these tests.

Unnotched specimens (Figure 11) were used to determine crack initiation life and modulus changes in the parent material and to provide a comparison with the notched fatigue data. The net section area was nominally the same for both notched and unnotched specimens to simplify these comparisons.

For unnotched specimens, edge conditions are known to significantly affect fatigue life, as previously shown by AFML testing, Reference 16. A diamond wheel was used at low feed rates to produce reproducible quality of cut edges.

Once the fatigue failure modes were determined using the central hole specimens, data from center cracked panel specimens could be used to characterize flaw growth rates and for direct comparison of the effects of stress concentration on initiation and growth lives. The specimen configuration is shown in Figure 11 and, in greater detail in Figure 13. The 0° and 90° specimens had elox slots perpendicular to the loading direction, while the 45° specimens had the slots cut along the fibers to examine the growth of flaws between fibers under shear loads. The elox slots in the crossplied specimens were all at 90° to the applied load.
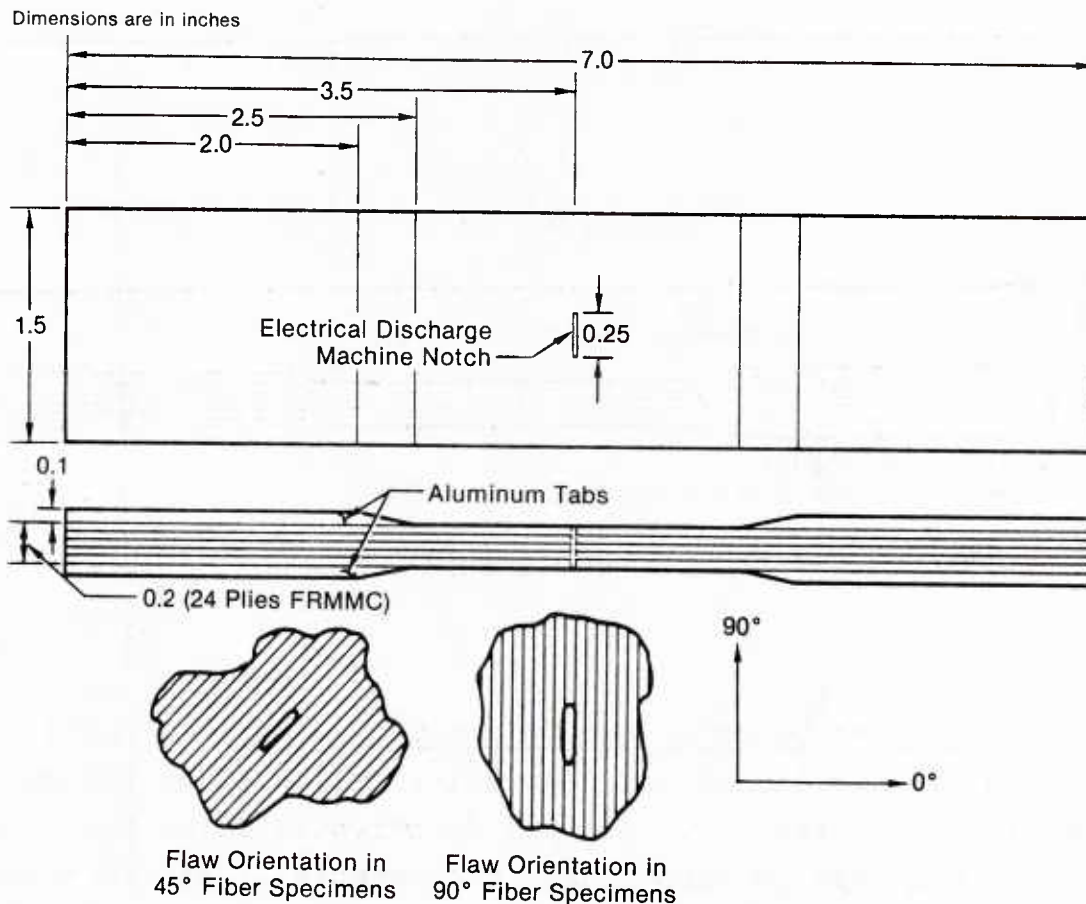
Figure 13. Center Cracked Panel

21

To examine the effects of specimen width on static strength
and fatigue failure modes and life, a small number of wider
specimens were tested. These specimens had a width to hole
diameter (W/D) of 10 to preclude any interaction of the specimen
edge with the failure mode or life (Figure 14). Tests of these
specimens, and the baseline W/D=6 specimens, were performed before
any other specimens were fabricated to satisfy ourselves that the
W/D=6 configuration would not behave differently under static or
fatigue loadings due to its smaller W/D.
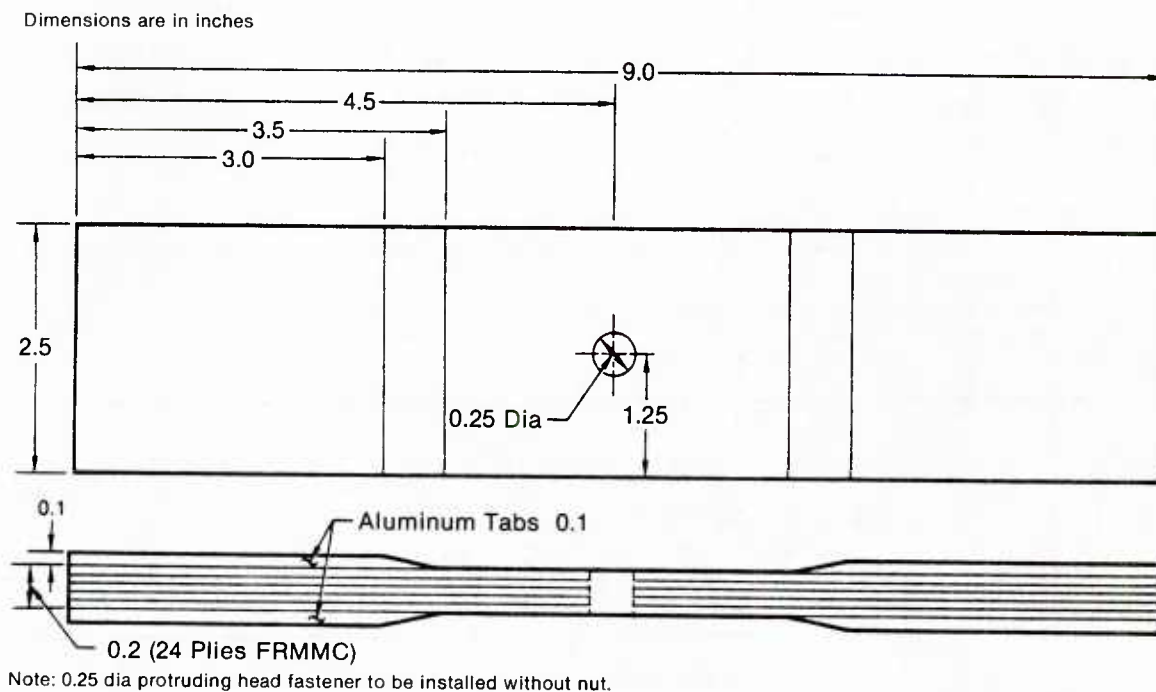
Figure 14. Width Effects Specimen

b.   Specimen Location and Orientation - Maximum panel sizes
are about 350 sq. inches in boron/aluminum and about 144 sq.
inches in boron/titanium, with the differences being due to the
pressures required to consolidate the material. Within these
limitations, the panels required for this program are shown in
Figures 15 through 17.
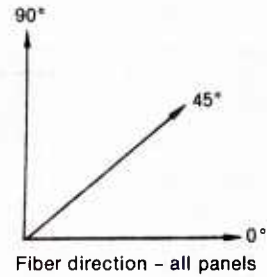
(Panel 1) 16 in. × 23 in. × 24 Plies
22 Specimens

1-1-61	1-1-92					
1-1-51		1-1-24	1-1-25	1-1-26	1-1-27	1p1-28
1-1-41						
	1-1-52					
	1-1-42					
1-1-31						
1-1-21	1-1-12 1-1-13 1-1-14 1-1-15				1-1-22	1-1-23
1-1-11						

(Panel 2) 16 in. × 23 in. × 24 Plies
27 Specimens

1-2-91		1-2-93
1-2-11	1-2-12	1-2-13

(Panel 3) 16 in. × 23 in. × 24 Plies
27 Specimens

1-3-91		1-3-93
1-3-11		1-3-13

(Panel 4) 16 in. × 23 in. × 24 Plies
27 Specimens

1-4-91		1-4-91
1-4-11		1-4-13

(Panel 5) 6 in. × 16 in. × 8 Plies
10 Specimens

1-5-91	1-5-92
1-5-71	1-5-72
1-5-51	1-5-52
1-5-31	1-5-32
1-5-11	1-5-12

(Panel 6) 16 in. × 16 in. × 8 Plies
18 Specimens

1-6-91	1-6-92
1-6-11	1-6-12

Fiber direction – all panels

Figure 15. Panel Layouts for Unidirectional Boron/Aluminum

23

(Panel 1) 16 in. × 23 in. × 24 Plies
22 Specimens

Fiber direction – all panels

(Panel 2) 16 in. × 23 in. × 24 Plies
27 Specimens

(Panel 3) 12.5 in. × 16 in. × 8 Plies
14 Specimens

Figure 16. Panel Layouts for Cross-Plied Boron/Aluminum Laminates

(Panel 1) 9 in. × 12 in. × 24 Plies
6 Specimens

(Panel 2 – 4) 9 in. × 16 in. × 24 Plies
10 Specimens Each

(Panel 5 – 6) 9 in. × 16 in. × 8 Plies
10 Specimens Each

0° fiber direction – all panels

Figure 17. Panel Layouts for Unidirectional Boron/Titanium

Specimen locations and orientations are indicated on the panels, and marked as shown in the photographs of Figures 18 and 19. Specimen numbers were given to these specimens to indicate:

    (a)   the material number
          1   for unidirectional boron/aluminum
          2   for 0/90 boron/aluminum
          3   for 0/45 boron/aluminum
          4   for unidirectional boron/titanium
    (b)   the panel number
    (c)   the location

The location numbers initiated in the lower left hand corner at 11 and progressed to the upper right hand corner at 9X, depending upon the number and orientation of the specimens cut from the panels. Static strength specimens were taken from opposing corners where possible, to characterize the strength variation across the panel.
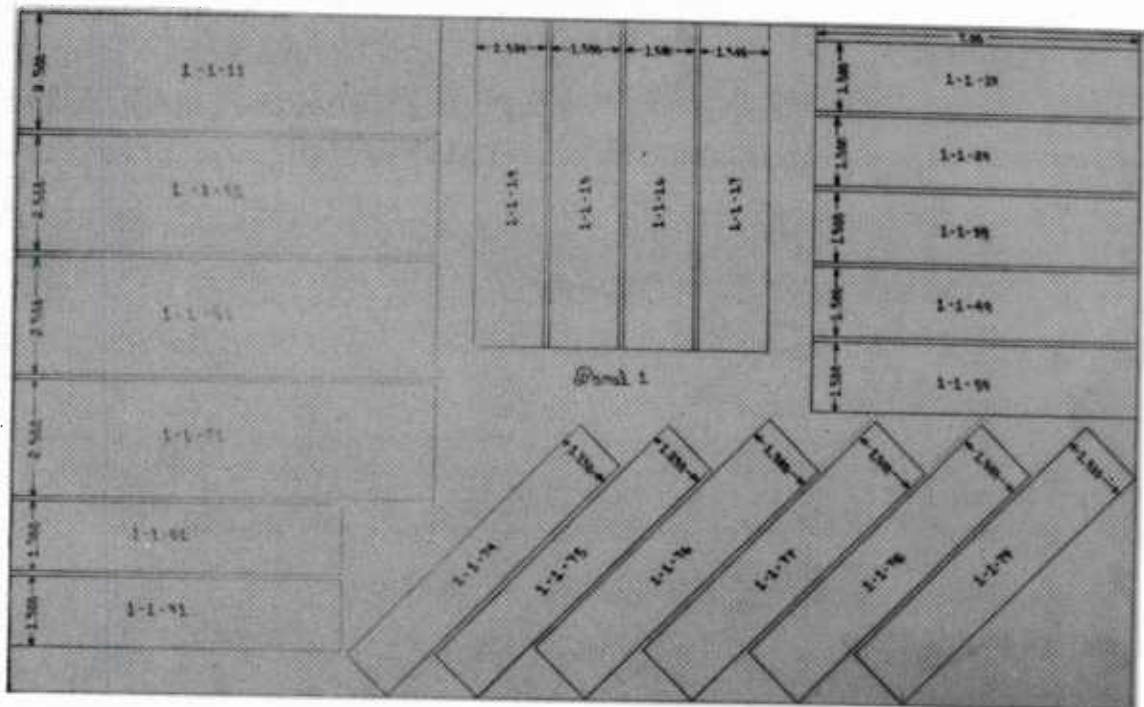
Figure 18. Photograph of Specimen Layouts for Unidirectional Boron/Aluminum
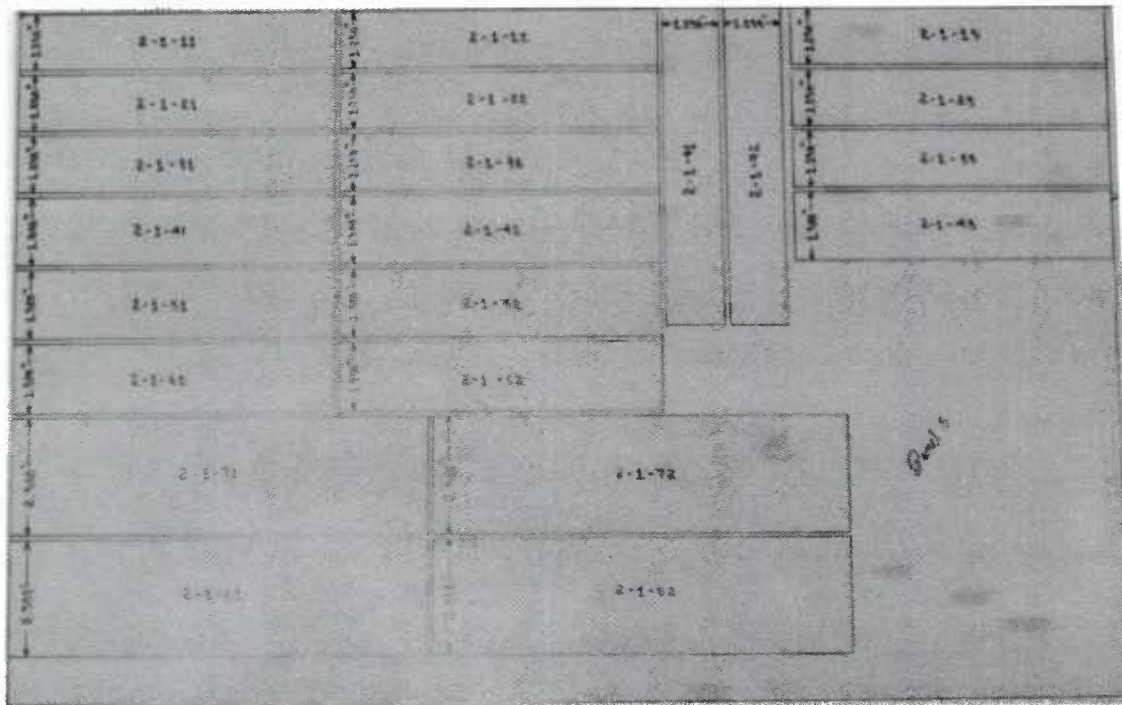
Figure 19. Photograph of Specimen Layouts for Crossplied Boron/Aluminum

c. <u>Replication</u> - The number of variables included in the testing performed precluded any extensive evaluation of scatter in fatigue lives or strength. However, the test plan was configured so that one static and one fatigue test condition were repeated ten times. These tests allowed evaluation of panel-to-panel variability and overall scatter.

In general, the minimum replication of two was used throughout the test program to maximize the variables which could be evaluated.

d. <u>Loading</u> - All specimens were loaded through self-aligning hydraulic grips in MTS, Inc. test equipment. Aluminum tabs were used to protect the specimen surfaces from damage from the serrated grips.

Buckling guides were not required for compression tests because the specimen thickness selected precluded initial specimen buckling, however, in the crossplied boron/aluminum tests, the modulus reduction caused by cracking in the off-axis plies often caused eventual buckling failures in compression tests of these laminates.

Fatigue load cycles were applied at about 10-20 Hz to minimize test time. No noticeable heating of the specimens (like that that occurs in carbon/epoxy specimens) was observed in any of the tests.

e. <u>Identification of Failure Modes</u> - During testing of the FRMMC specimens damage progression was monitored and failure modes identified. Failure modes and NDE techniques that were used to monitor these modes during test are outlined below:

Failure Mode	NDE Technique
Matrix cracks	Photomicrographic, Ultrasonics
Fiber breakage,Rupture	X-ray, Displacement, Acoustic Emission
Through-flaws	Photomicrographic
Part-Through flaws	Photomicrographic, Sectioning
Delamination	Ultrasonics, X-ray

After failure occurred, the failure modes and mechanism(s) were identified. Our primary tool for this examination was the scanning electron microscope.

f. <u>Monitoring Damage Progression During Test</u> - The primary method used to monitor surface cracking was a photomicrographic technique (Figure 20). Early in our testing of FRMMC materials, we found that fluorescent penetrant enhances the photographic quality of the damage (Figure 21). Damage progression typical of unidirectionally reinforced aluminum under tension-tension loading is shown in Figure 22.
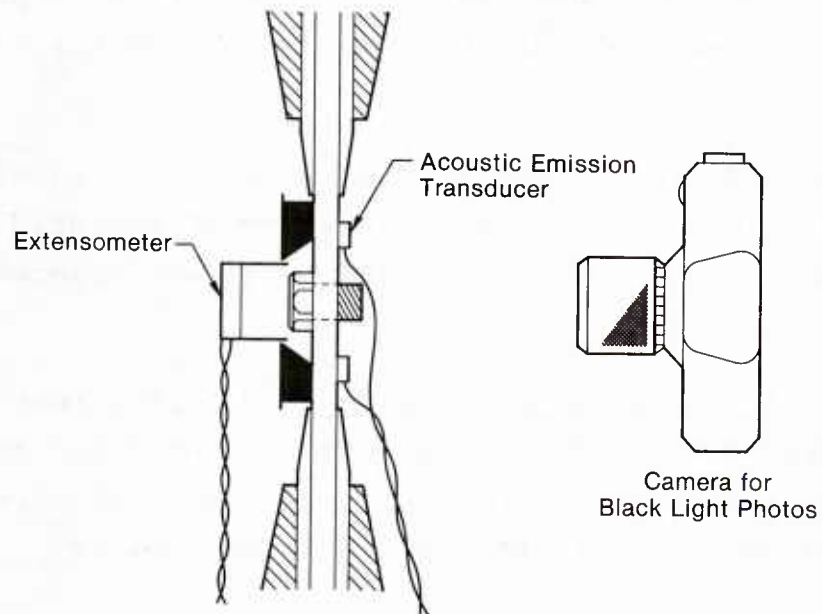
Figure 20. Test Specimen Monitoring During Test

Without Dye Penetrant   **With Dye Penetrant**
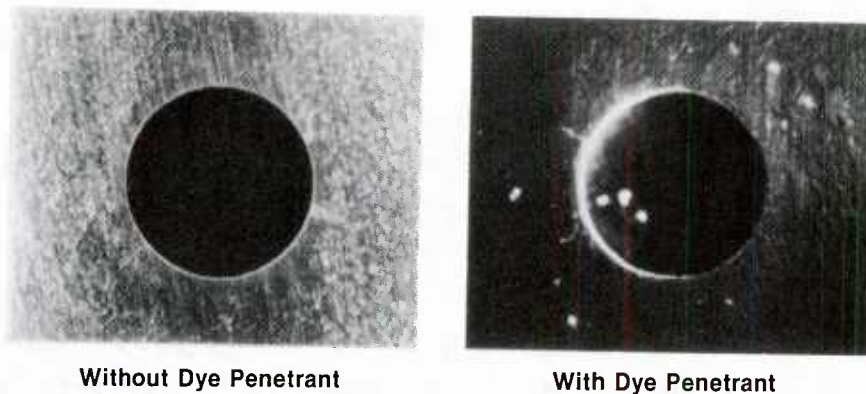
Figure 21. Photographic Enhancement Using Dye Penetrant

28

At 5,000 Cycles

At 703,000 Cycles
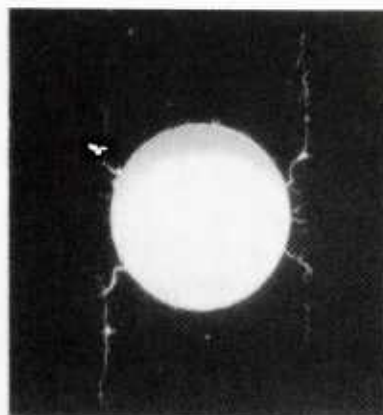
At 2,170,000 Cycles
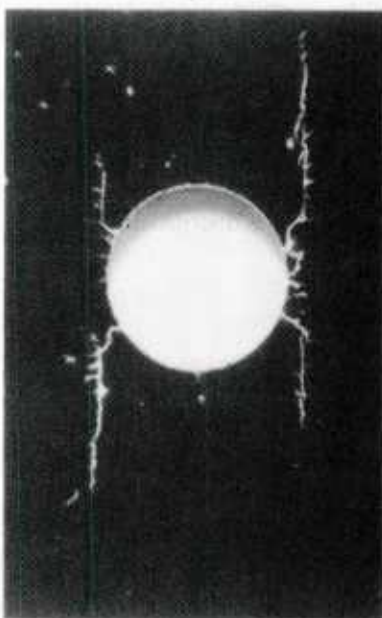
At 3,260,000 Cycles
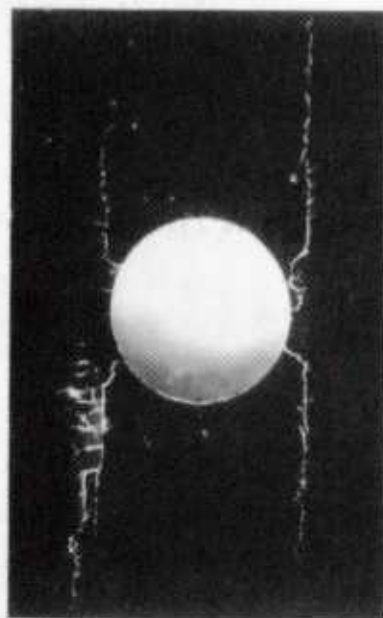
Figure 22. Crack Growth in Fiber Reinforcement Aluminum
as Revealed by Dye Penetrant

While numerous other damage monitoring techniques were tried and several showed promise for determining specific failure modes, we found none that gave better definition of the damage state in unidirectionally reinforced MMC materials than the photomicrographic technique. Using this technique we were able to define flaw growth such as that shown in Figure 23, recording flaw growth very accurately throughout the test.
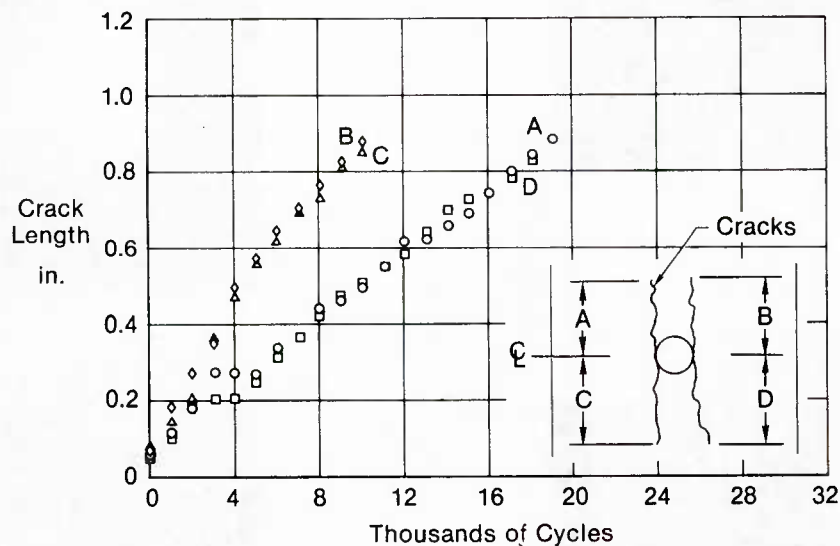
Figure 23. Crack Growth in Notched, Unindirectional Boron/Aluminum

Another monitoring method that was found useful was simple displacement monitoring during fatigue tests. Initially this was done to examine the kinds of stiffness reduction in MMC materials that had been reported by Johnson (References 17 and 18) and others. In this program we used the MTS control computer and a standard 1/2 inch extensometer to continuously monitor displacements throughout the fatigue tests. This was particularly effective when monitoring displacements across the hole (rather than in the net section) because those displacements are sensitive to damage that initiates near the hole.

By letting the computer monitor displacement ranges occurring across the hole during fatigue tests, it was possible to automatically stop the test when a specified change in displacement range occurred. In the crossplied boron/aluminum specimen test data shown in Figure 24, the displacement range rapidly reached a plateau value. This plateau value was found to correspond to matrix cracking along the fibers as shown in the inset photograph. The test was stopped to obtain the photograph, and on restarting the test a small perturbation in the displacement range was evident. However, from that point on the range increased progressively until failure occurred.
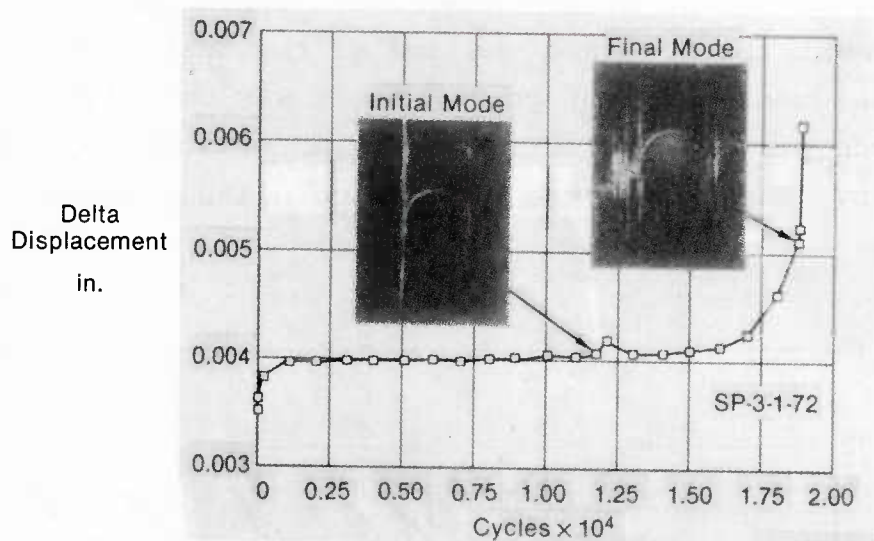
Figure 24. Specimen Displacements Can Identify Fatigue Failure Modes in Crossplied Boron/Aluminum

The displacement monitoring was helpful in recording the change in failure mode that occurs in crossplied laminates near the end of life when the interior ply failures cause cracking and eventual failure in the 0° plies that control life. Because net section failures occur rapidly once fibers fail, this change in failure mode can often be very difficult to record photographically. Attempts to catch this mode change (from cracking along the fibers to fiber breaks and net section failure) by visual monitoring proved to be nearly impossible - the failure occurred before

31

the machine could be shut down, even at slow cycle rates. Only by setting the machine to shut down when a specified increase in displacement range occurred could the photo shown in the second insert in Figure 24 be obtained.

Displacement monitoring showed interesting results throughout the testing of crossplied boron/aluminum materials. As shown in Figure 25, this data allowed continuous monitoring of progressive stiffness loss in tension tests. In R=-1 tests this loss became even more. Data such as that shown in Figure 26 was the first direct evidence we had that this progressive stiffness loss would eventually contribute to a buckling failure of the specimen, as demonstrated by the highly non-linear appearance of the load displacement trace toward the end of the test. When this change in displacement behavior occurred, it was correlated with the appearance of matrix cracks, at the outer surface of the specimen, induced by cracking in the subsurface plies (Figure 27).
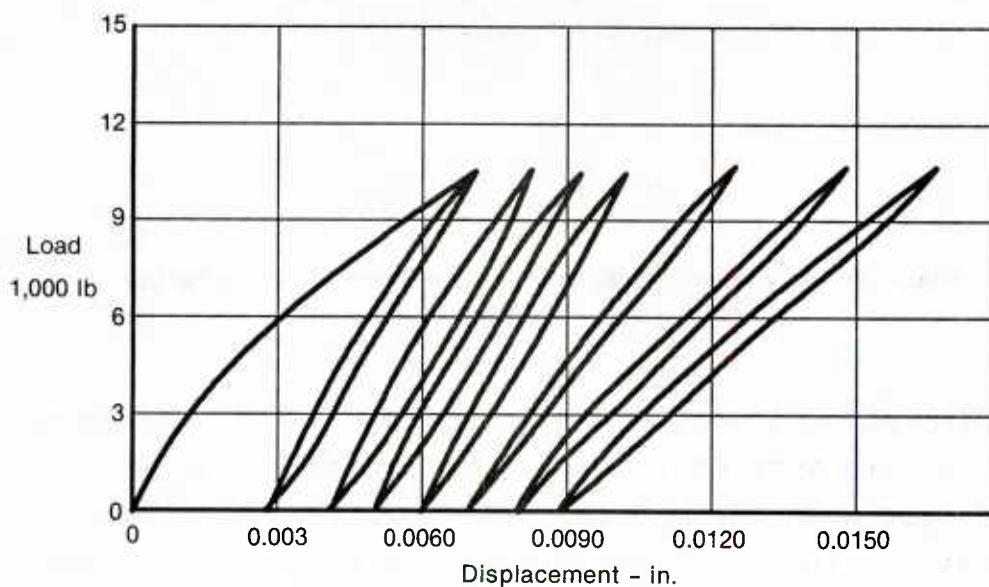
Figure 25. Progressive Stiffness Loss in Tension-Tension Fatigue Test of a 0/90 Boron/Aluminum Laminate

32
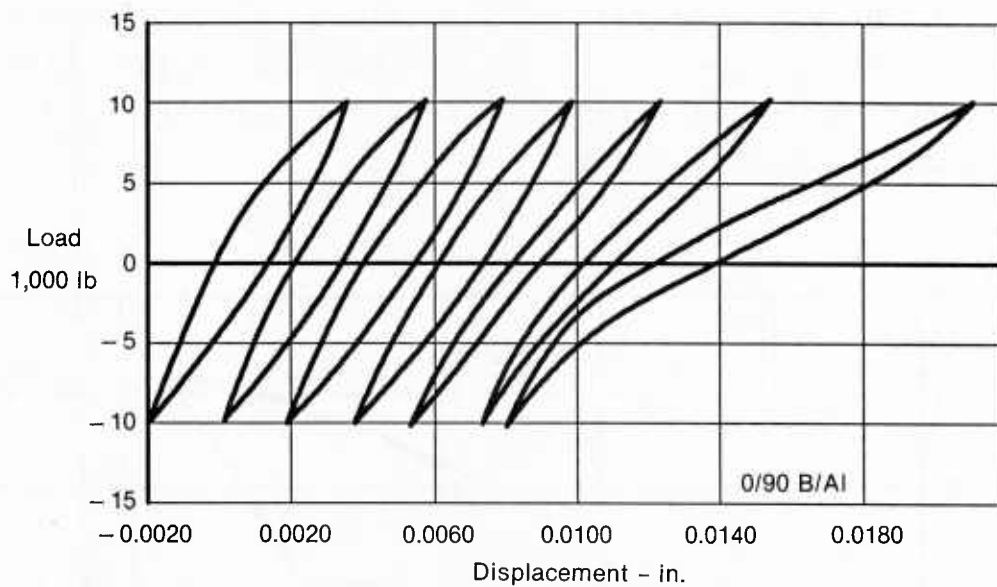
Figure 26. Stiffness Loss in Fatigue Can Cause Specimen Buckling in R = − 1 Fatigue Tests
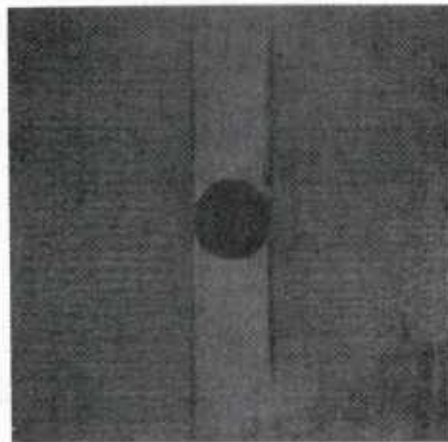
Figure 27. Cracking in 90° Plies Can Cause Fatigue Cracks in 0° Plies in 0/90 Boron/Aluminum

33

Displacement records taken during static tests were also informative. The trace taken from a 0/90 boron/aluminum tension test (Figure 28) shows dramatically the change in specimen stiffness that occur when the 90° plies re-yield in compression during unloading. This is one reason why the crossplied laminates show so much larger hysteresis behavior that the unidirectional materials during fatigue tests.
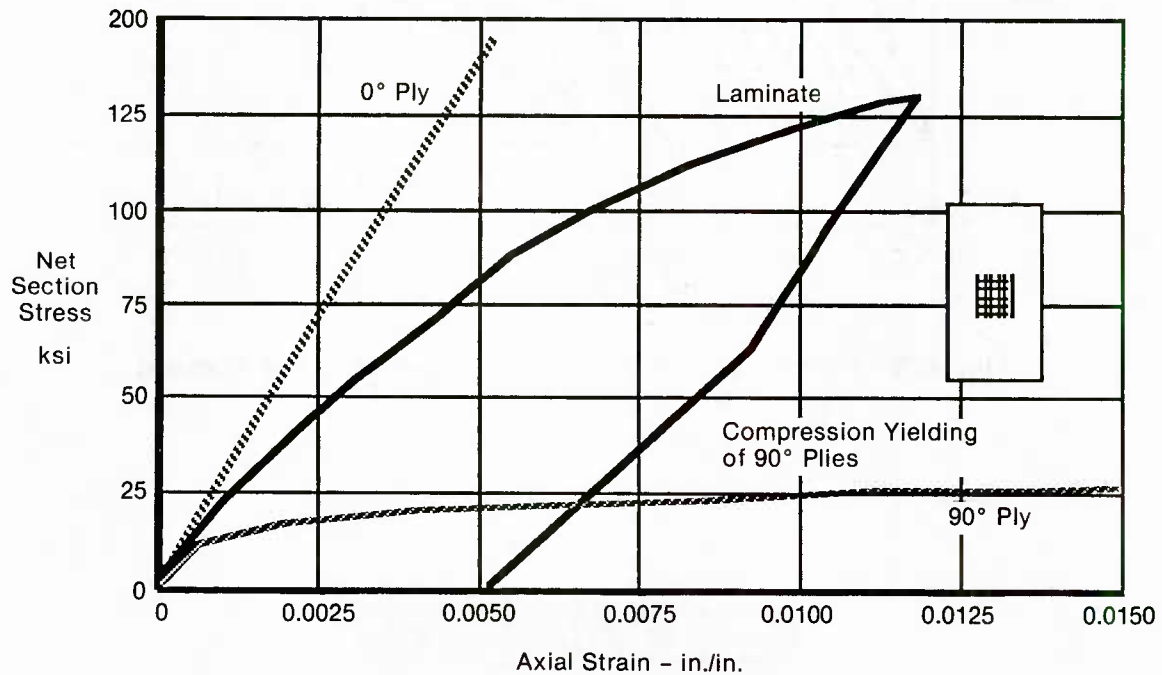
Figure 28. Uniaxial Load-Deformation Response of an Orthotropic B-Al Laminate [0°/90°]$_s$

Both ultrasonic and X-radiographic techniques were used to determine their applicability to FRMMC materials, but, as shown in Figure 29, they were not as effective as the photomicrographic technique. Pulse echo and through transmission reflector plate ultrasonic techniques were used to monitor and identify the progress of delamination damage in certain specimens. Frequencies of 5 to 15 MHz were found to provide the best detectability of small damage sites.

34
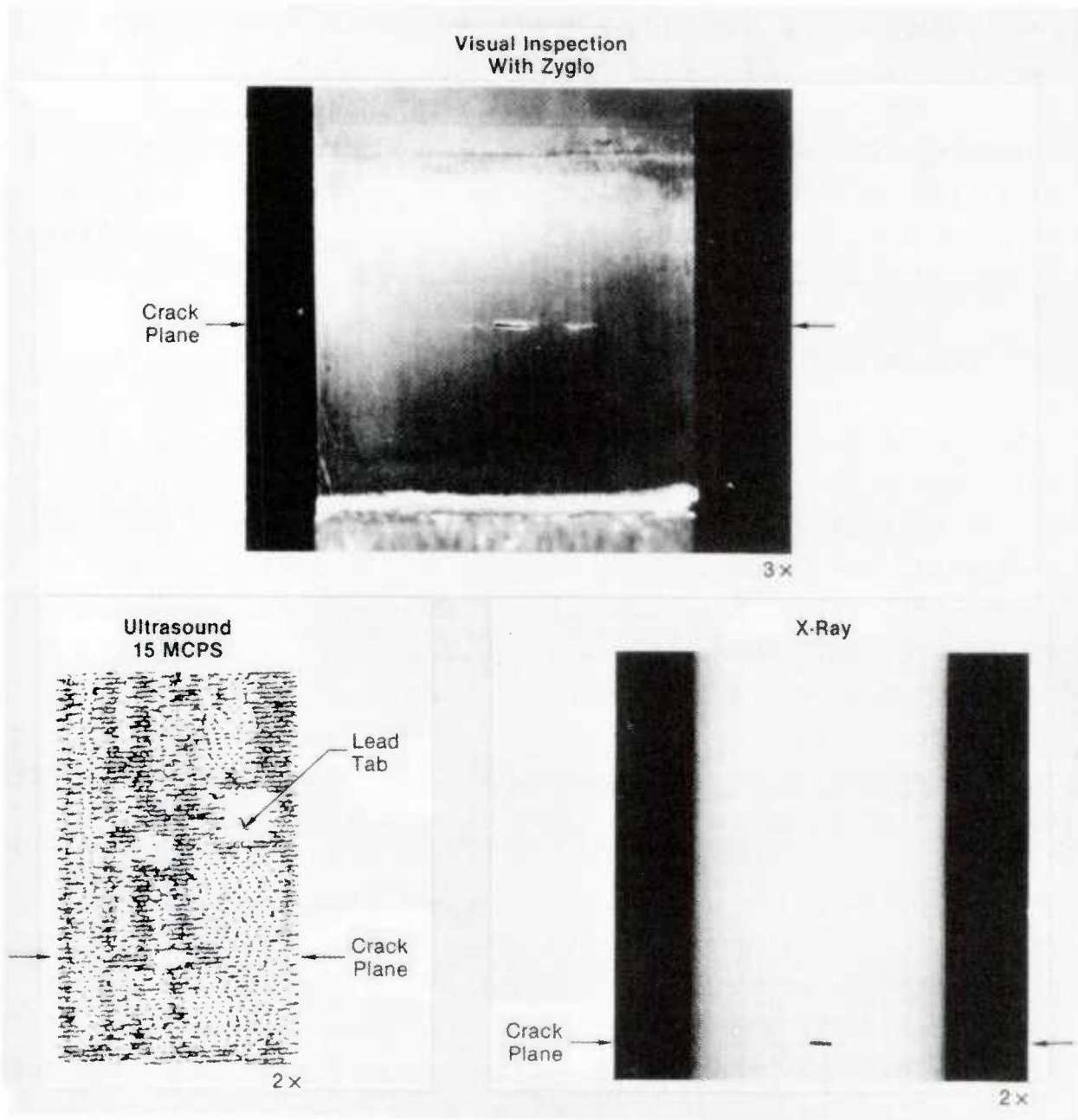
Figure 29. Comparison of Three Nondestructive Examination Techniques

35

X-radiographic techniques were evaluated for use in monitoring the development and progression of fiber breakage and matrix cracking. As shown by Johnson (Reference 19), fiber breakage in very thin FRMMC laminates is detectable by low kV radiography. The low tube potential provides high subject contrast permitting clear detectability of the fibers in FRMMC. But for the thicker laminates tested in this program, X-radiography could not be used to distinguish matrix cracking or fiber breaks because fibers in other plies masked the damage. A comparison of dye-penetrant enhanced visual inspection, ultrasound, and X-radiography is shown in Figure 29.

One of the most intriguing methods for monitoring damage progression in MMC materials is acoustic emission monitoring. Long promoted by Jonathan Awerbuch of Drexel University (Reference 20), this method has undergone a dramatic rejuvenation with the advent of small, powerful microprocessor driven data retrieval and analysis. The newer systems can monitor several different AE parameters in real time and display them as well, while the test is in progress. While the applicability of this monitoring technique has yet to be proven for resin matrix composites reinforced by bundles of very small fibers, in metal matrix composites the fibers are generally large, stiff members whose failure send an appreciable, identifiable AE signal.

We performed a small test program to examine the applicability of AE methods for monitoring damage initiation and progression in metal matrix composites. The materials used in the tests are identified in Figure 30. The test specimen used was slightly narrower than the baseline specimen used in this program (Figure 31), resulting in a smaller W/D.

A number of interesting results came from this test program. First it was found that the number of AE counts, or events, rose with increasing crack length in unidirectionally reinforced titanium matrix composites. Higher amplitude events were

36

especially noticeable as the cracks progressed across the net section (Figure 32). Comparison of the static and fatigue tests of duplicate titanium MMC specimens showed that the number and distribution of high amplitude events was about the same for both tests, but the number of low amplitude counts was much greater for the fatigue test than for the static test (Figure 33). Because both specimens failed across the net section, failing roughly the same number of fibers, it appears that these high amplitude events may be related to fiber breaks during crack growth. Awerbuch has shown that actual fiber breaks occur at higher AE amplitudes than those recorded in these tests, yet the relationship of static and fatigue results seems indisputable. The discrepancy between static and fatigue test results at the lower amplitudes is thought to be due to matrix cracking and yielding, obviously more plentiful during the repeated load fatigue test than during the short static test.

Material Type	Test Type	No. of Tests
Titanium 6Al-4V	Static	2
	Fatigue	2
$(B_4C)B/Ti-6-4$	Static	2
	Fatigue	2
$(B_4C)B/6061$ (Ti Clad)	Static	2
	Fatigue	2
SIC/TI-6-4	Static	2
	Fatigue	2

Note:
⚠ R = 0.02, max stress of 35 ksi used initially for each test set.

Figure 30. Testing to Examine Acoustic Emission Results
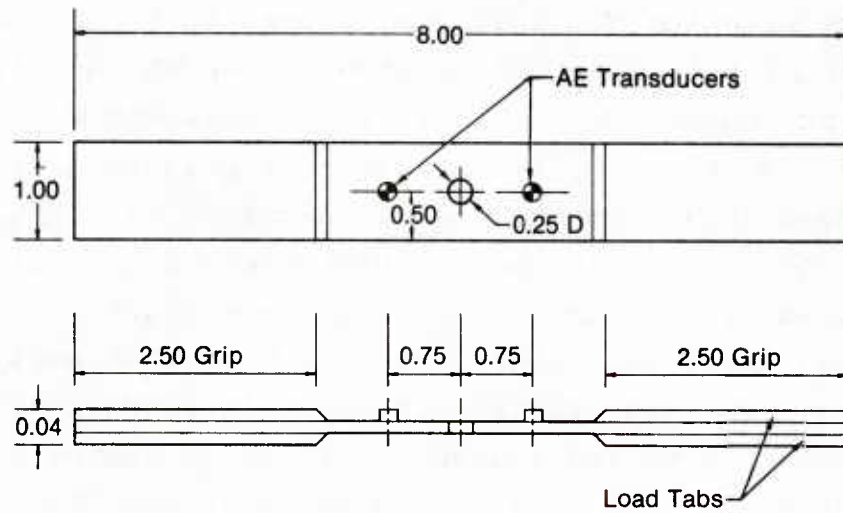
Figure 31. Acoustic Emission Test Specimen
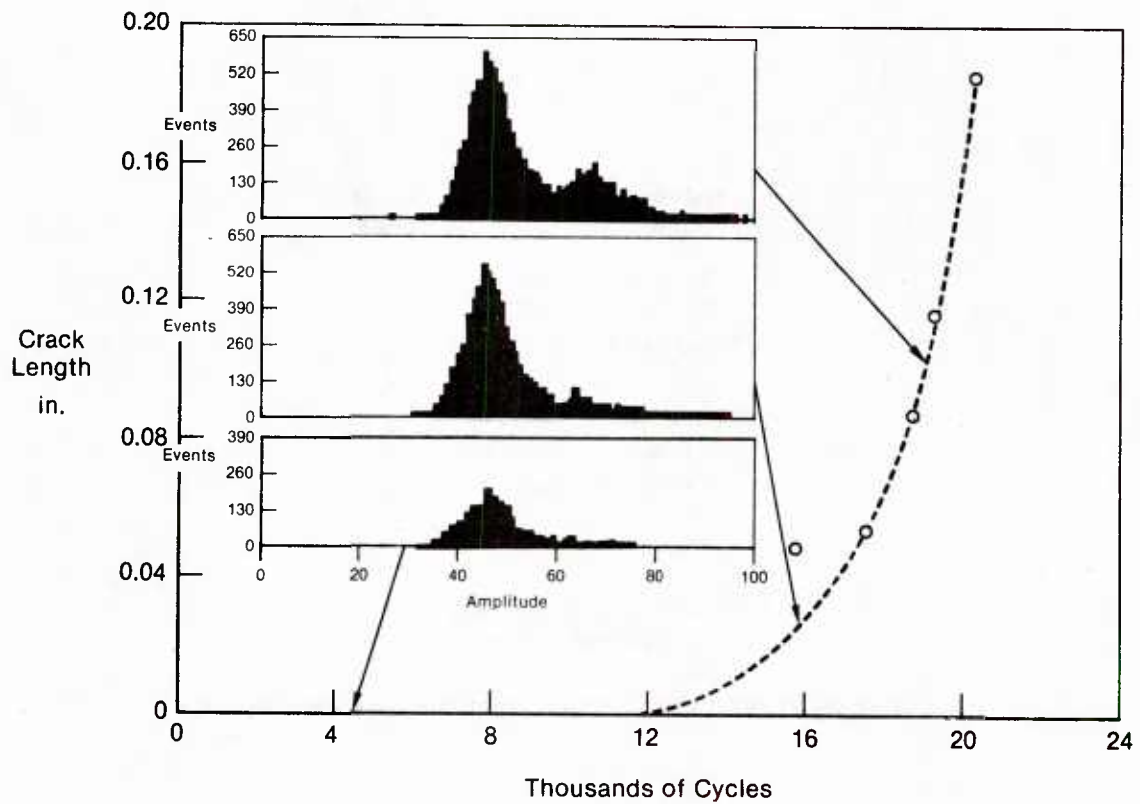
Figure 32. Correlation of Acoustic Emission Results With Crack Growth in SiC/Ti

38
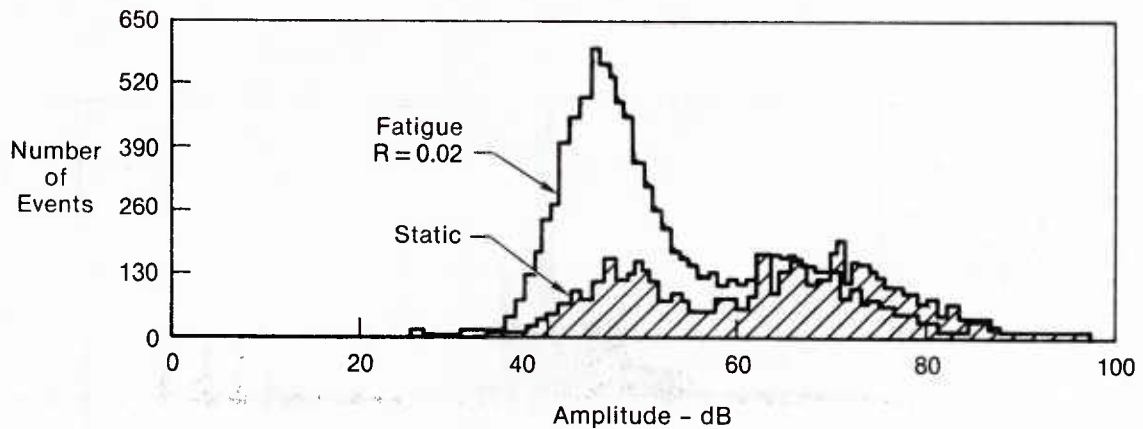
Figure 33. Comparison of Acoustic Emission Amplitudes From Static and Fatigue Tests of SiC/Ti MMC

Current AE systems can also be used to monitor crack initiation location in real time by using two transducers. By setting a gate to exclude signals that come from the grips and monitoring events received at both transducers, one can use the difference in time for the two signals to determine where the event occurs in the specimen. Our best example of location discrimination is shown in Figure 34, where the results of two different tests of unidirectionally reinforced titanium MMC are shown. In one test the cracks initiated and grew across the net section in a single plane. In the second specimen the cracks initiated and grew across the net section in parallel planes, one side in a different plane than the other. This was effectively displayed by the AE monitor.

In a later test of a titanium clad boron/aluminum coupon, the AE emissions showed a much more diffuse distribution of event locations (Figure 35). X-ray examinations showed that cracks had initiated in the titanium cladding material (Figure 36), but they showed no reason for the distributed emissions found from AE. Ultrasonic C-scans of the specimen (Figure 37) showed that the unidirectionally reinforced boron/aluminum material was cracking along the fibers, beneath the titanium cladding.

39
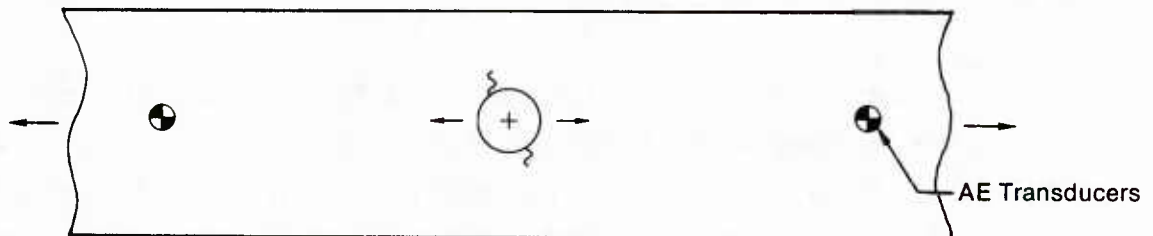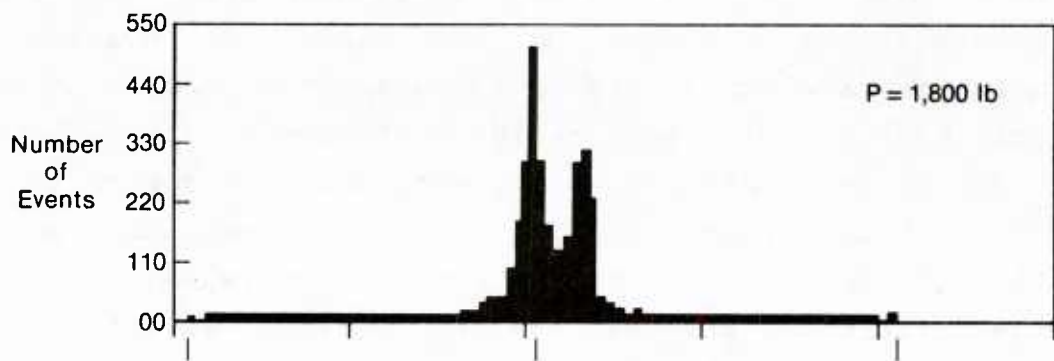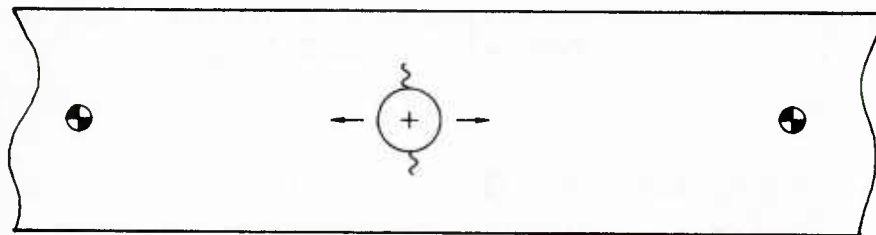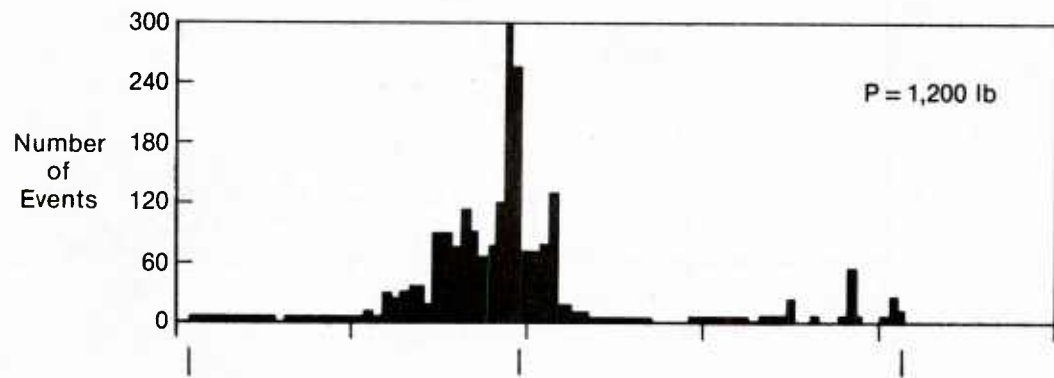
Figure 34. Acoustic Emission Can Define Cracking Location During a Test (SiC/Ti)
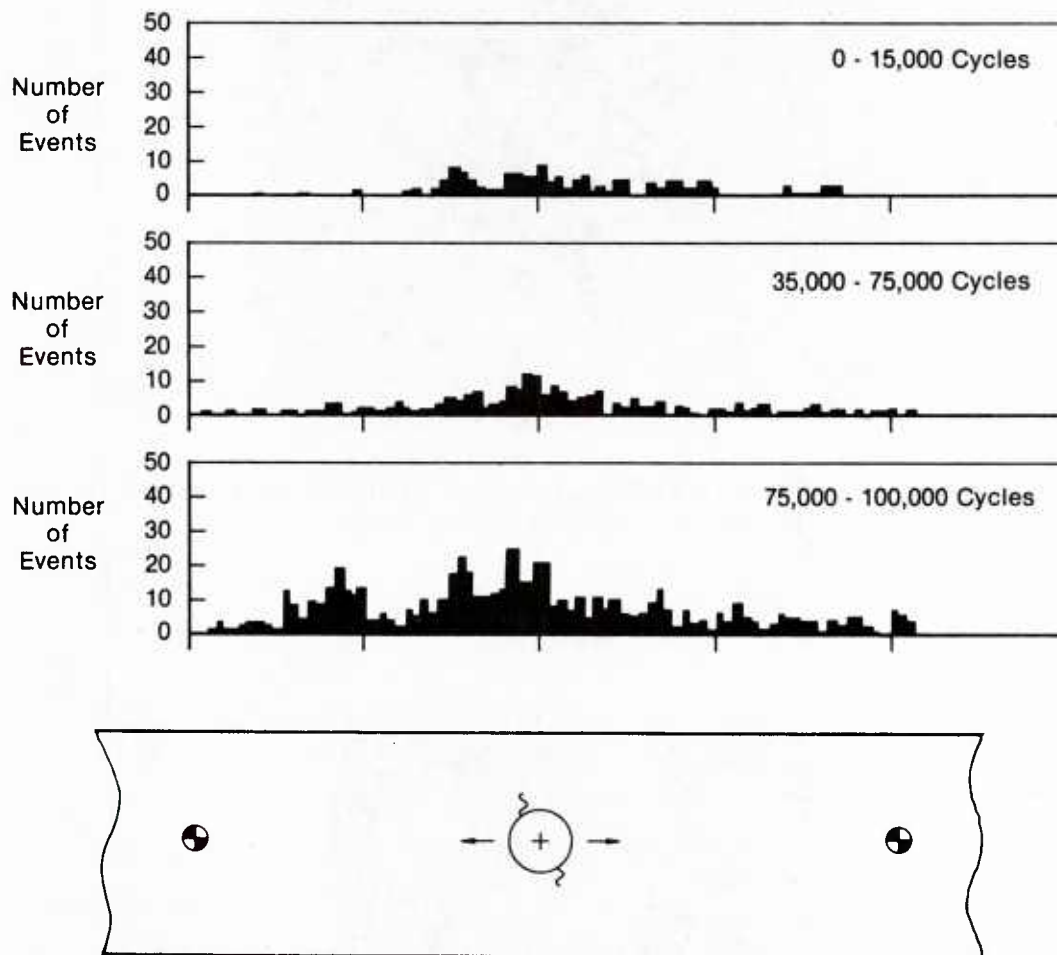
Figure 35. Cracking Progression in Ti-Clad-(B₄C)B/Al as Shown by Acoustic Emission
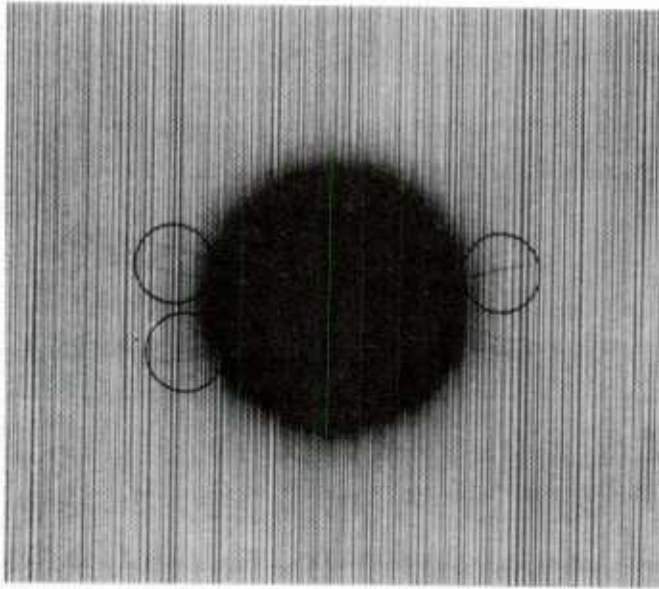
Figure 36. X-Radiography Show Cracks in Titanium Face Sheets But No Cracking in Boron/Aluminum
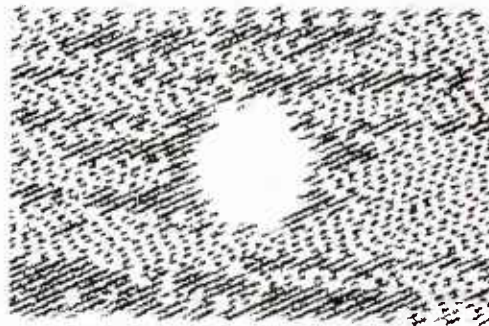
Figure 37. C-Scan Shows Matrix Cracking and Delamination at Edges of Titanium-Clad – Boron/Aluminum Specimen

The most effective use of acoustic emission monitoring currently seems to be in the area of determining crack initiation in crossplied laminates and, perhaps, in full scale structural tests where triangulation can be used to determine when and where failure initiates. In this program AE was not extensively used because the testing concentrated on tests of unidirectional fiber reinforced MMCs where visual monitoring was as effective as the AE monitoring.

g. <u>Post Failure Analysis</u> - After specimen rupture, we inspected failure surfaces using a scanning electron microscope (SEM). The SEM was found to be a valuable tool for obtaining information concerning damage progression in MMC materials. In addition, several of the crossplied laminate specimens tested at Purdue University by Dr. C. T. Sun were sectioned after testing to determine the cracking behavior of the internal plies of the laminates.

The SEM was used to examine the fracture surfaces of the boron/aluminum fatigue specimens to show that the cracking which occurred along the fiber in this material system was not at the fiber/matrix interface but in the matrix material itself (Figure 38). Even in 90° specimens, where one would expect the fiber/matrix interface to be weakest, the cracking in boron/aluminum was within the matrix (Figure 39).

In our SEM studies of boron/titanium center cracked tension specimens we identified several recurrent fatigue phenomena. Our first observation was that fatigue crack growth is impeded by disbonding along fiber/matrix interfaces. Figure 40 shows sections of a boron/titanium center cracked panel from near the elox slot and from the static failure region near the free edge.

In the fatigue region, the fracture surface is characterized by an irregular appearance, indicative of discontinuous, start/stop growth. In the static failure region, the surface is much smoother, indicating a single, swift failure.

43

18×
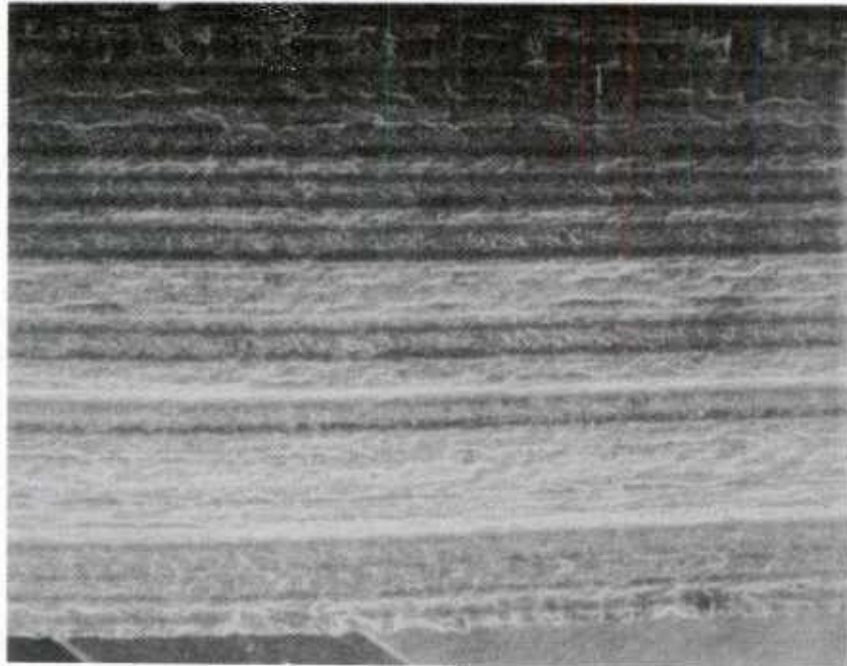
Figure 38. Photomicrograph of Matrix Cracking Along Fibers
in 0° Boron/Aluminum

12×
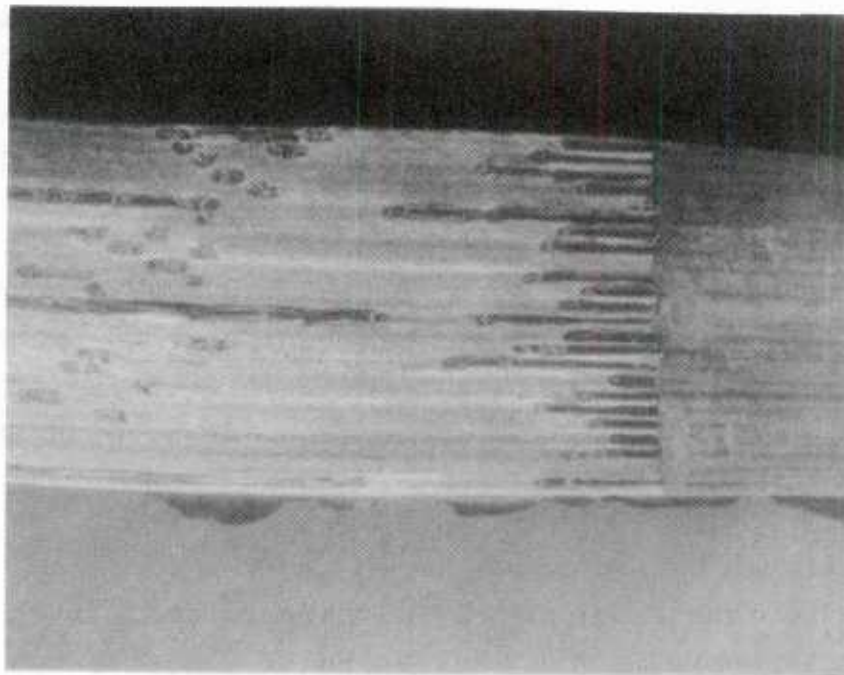
Figure 39. Photomicrograph of Fracture Surface in 90° Boron/Aluminum

44
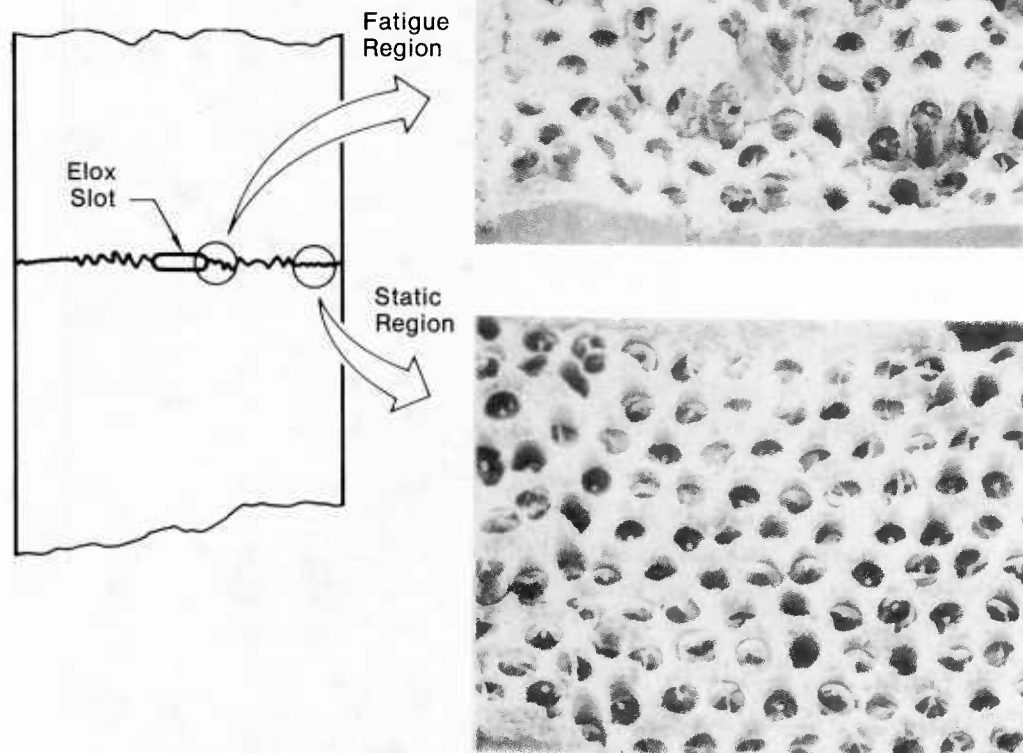
Figure 40. Comparison of Fatigue and Static Failure Surface Topographies in a Boron/Titanium Center Cracked Panel

Regions of retarded growth rate followed by a burst in growth rate appear as jumps in the da/dN versus elastic stress intensity, K, curve shown in Figure 41. The "stall/burst" regions correspond directly to an elevation change of the crack plane. Creation of a new fracture surface by fiber failures in a new plane is thus seen to inhibit crack growth. Inspection of these SEM photos indicate that the damage model must take into account the ability of disbonded fibers to inhibit crack growth in titanium matrix composites.

45
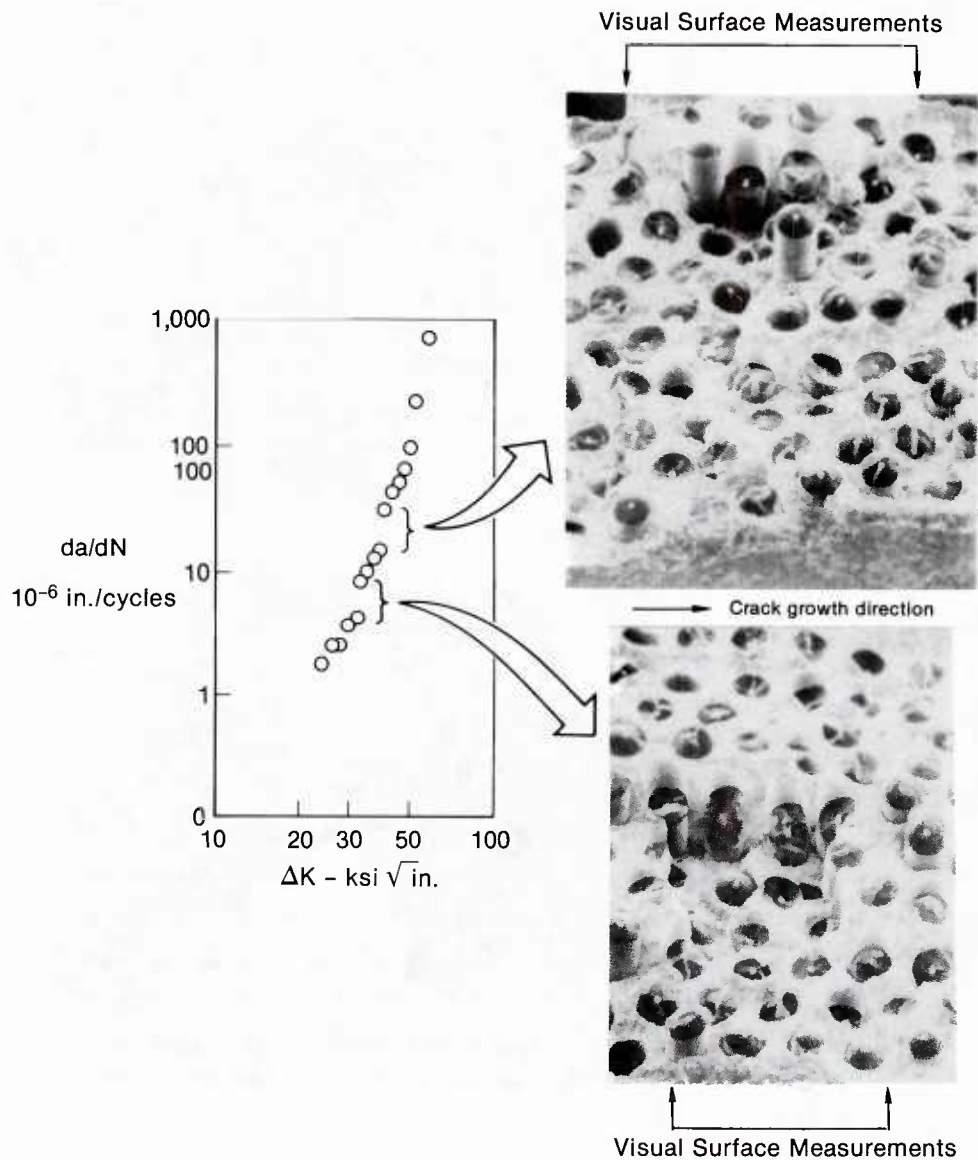
Figure 41. Changes in Crack Growth Rate Correspond to Elevation Changes of the Fatigue Crack Plane

The matrix surface in the fatigue region of a center cracked panel is markedly different from the familiar ductile fracture surface of the matrix in the static rupture region, as shown in Figure 42.

46
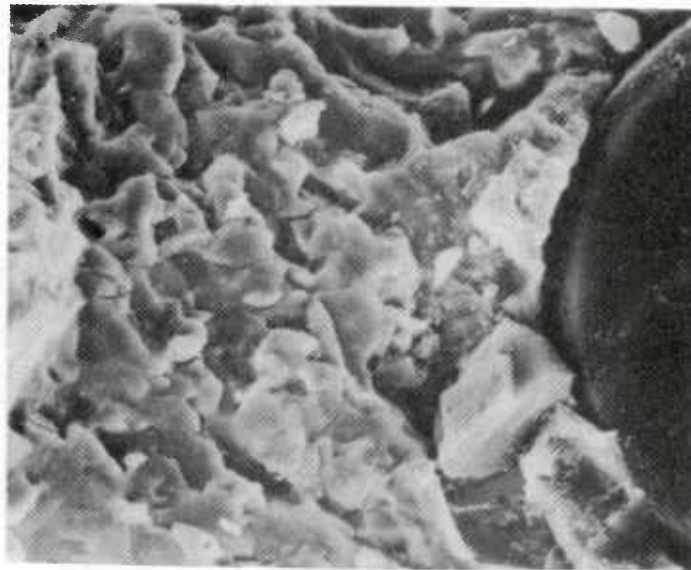
└─0.001 in.─┘

a) Fatigue Region
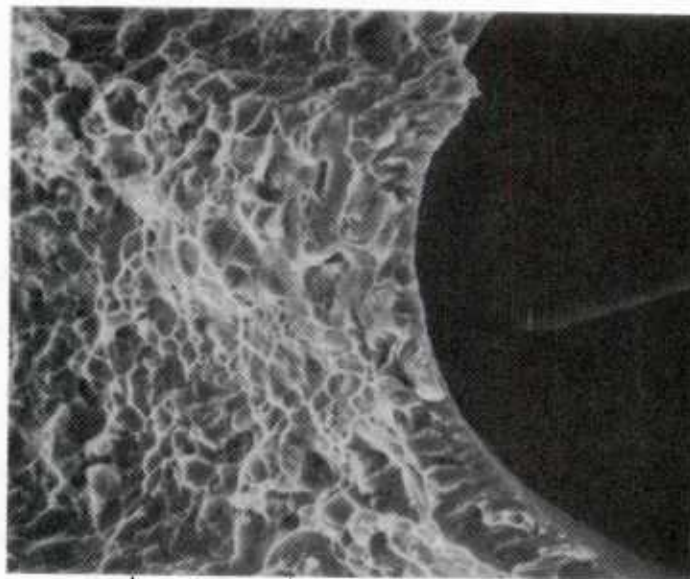
└─0.001 in.─┘

b) Static Region

Figure 42. Comparison of Fatigue and Static Failure Regions in a
Center Cracked Panel of $B_4C/6$-4 Titanium

Evidence of fatigue striations in the matrix can be seen in Figure 43. Note that these striations indicate flaw growth away from the adjacent fiber rather than along the primary fracture path. In later tests we found that fibers fail very early in the $(B_4C)B/15$-3 titanium material. This may explain why the matrix striations appear to show crack propagation away from the fiber rather than along the primary crack path.
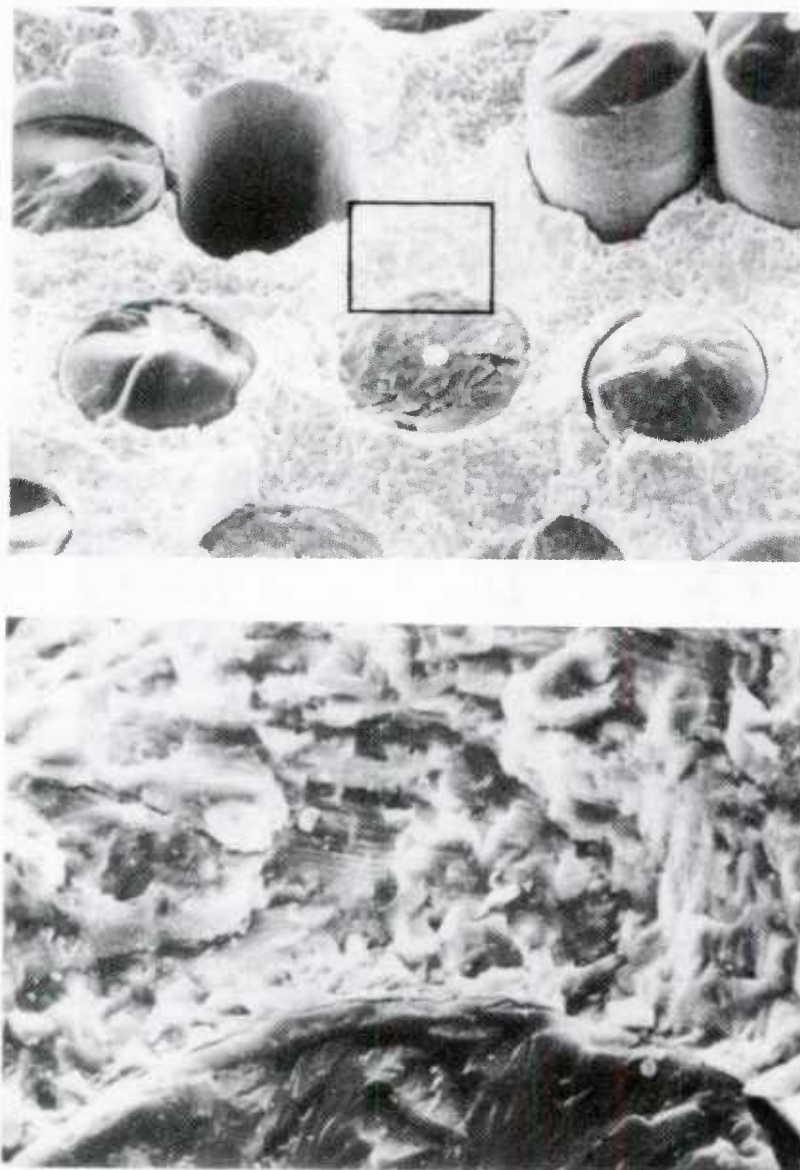
Figure 43. Fatigue Striations in the Matrix Can Be Seen Emanating From the Fiber/Matrix Interface in $B_4C/6$-4 Titanium

Our SEM examinations have also shown that fibers in titanium matrix materials are often disbonded from the matrix at the fracture surface, both in the fatigue and static regions. Fibers failed in fatigue (Figure 42a) have rougher texture in their fracture surfaces than do those failed statically (Figure 42b).

Fiber pull-out length (the length of fiber above or below the matrix failure surface) is indicative of the amount of fiber disbond occurring at the fracture surface. Statistical studies of measurements from SEM photos indicate that the mean fiber pullout length in the fatigue region of the specimens is 10% of the fiber diameter, about 25% longer than the pullout length in the static rupture region of the same specimen. Furthermore, the scatter in pullout length is larger in the fatigue region than in the static region. These findings point to different mechanisms controlling static and fatigue crack growth.

Our studies have demonstrated the importance of the SEM for defining damage mechanisms in FRMMC and verifying results of damage sequence analyses.

An attractive feature of our SEM system is an integrated Energy Dispersion System, EDS, which can detect the concentration of various elements present on the observation surface. This feature is particularly useful to us in describing the nature of the fracture surface and the character of suspected local initiation sites and inclusions. An example of the SEM capability is shown in Figure 44 where the titanium-carbide reaction zone for a misheat-treated SCS-6/15-3 titanium MMC panel is evident from the element analysis.

Dr. C. T. Sun, of Purdue University, sectioned a number of crossplied boron/aluminum specimens after failure to determine the cracking within the specimen. During the test very careful photographic tracking of the failure progression was recorded. Prior to failure the crack growth in the outermost ply was evident as

shown in Figure 45. The specimen shown is one of the countersink
hole specimens from the verification tests in a 0/45 laminate.
The cracking on the back side indicated that the 45° plies had a
significant effect on the crack growth pattern in the outermost 0°
plies.

Sections cut in this specimen, as shown in Figure 46, show
that in this specimen there appears to be a single dominant flaw
traversing the entire specimen thickness, even a significant
distance from the hole edge. Not only has the flaw grown through
the 45° plies, but it has also broken fibers in the 0° plies
throughout the thickness. The flaw does not grow in a single
plane but has a tortuous path through the specimen thickness.

As shown, careful specimen sectioning can be a useful tool to
determine the flaw progression in crossplied MMC materials. Other
results of Dr. Sun's sectioning work is described in Section V.

4. <u>ANALYTICAL MODEL DEVELOPMENT TESTING</u> - The testing performed in
this test phase is summarized in Figure 47. A total of 150 tests
were performed using boron/aluminum specimens to develop the data
required to formulate the analysis model. No tests were felt to
be required to model the $(B_4C)B/15-3$ titanium material because
MCAIR had sufficient data in house from fatigue testing and
previous materials characterization tests performed under the Two
Sheet Available Fiber/Matrix Composite Design Development for
Airframes program (Reference 1). The majority of the boron/
aluminum specimens were unidirectional laminates, with the
remaining tests equally divided between the two crossplied
laminates.

These tests provided data on static strength, damage
initiation, crack growth, fatigue failure mode and life, and
residual strength under a wide variety of stress levels and stress
ratios.
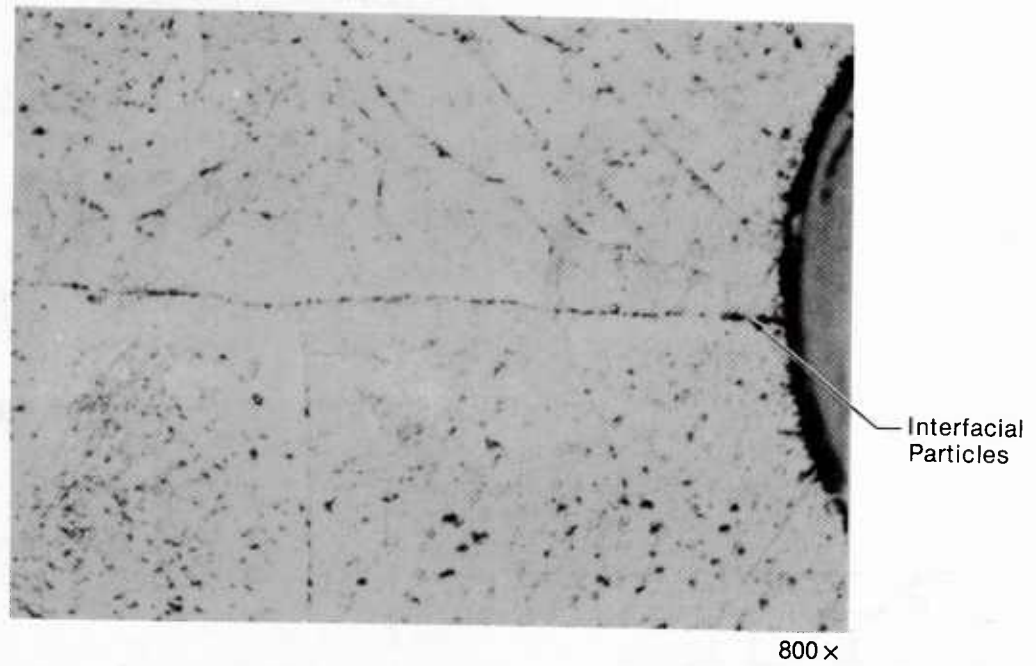
Figure 44. Interfacial Particles in the Bondline of $(B_4C)B/15$-3 Titanium
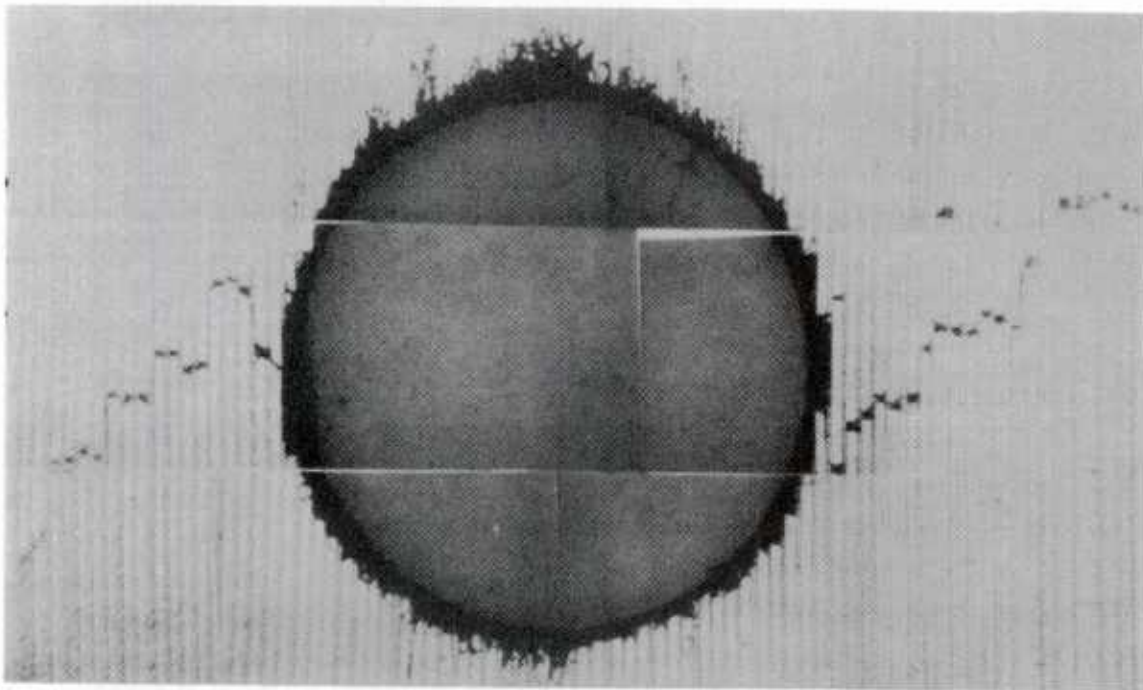
Figure 45. Fatigue Crack Growth in Countersink Hole Specimen
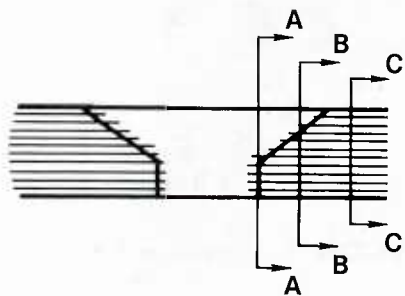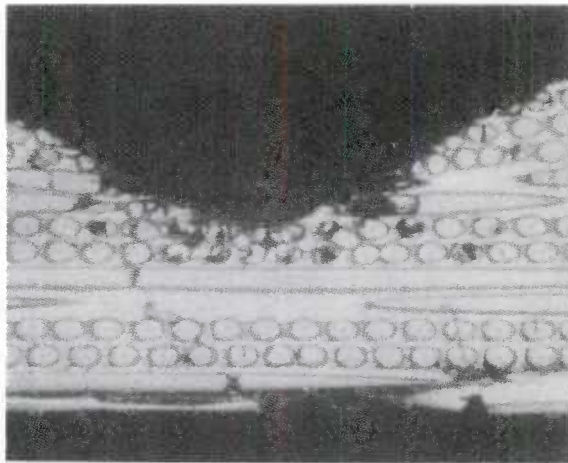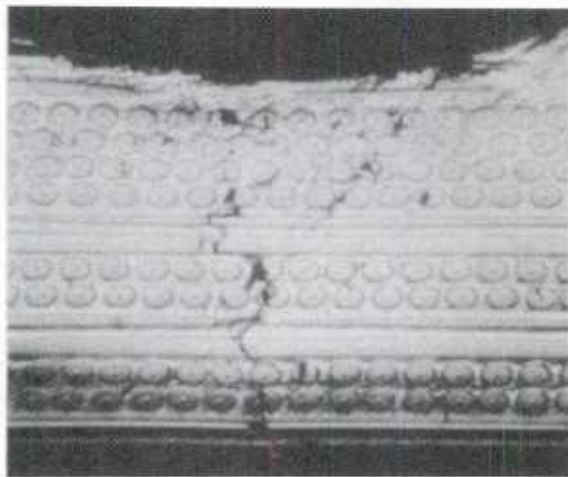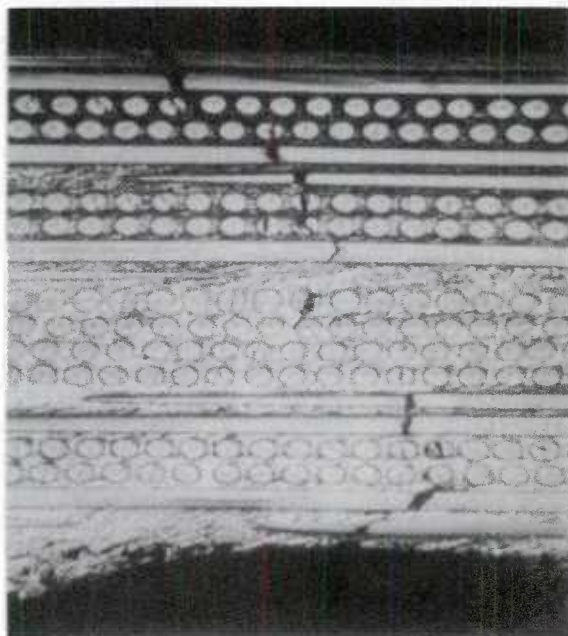
Figure 46. Sectioning Shows Crack Growth in
0/ ± 45 Countersink Hole Specimen

52

Test Objective	Laminate Description/No. of Tests			Total Tests
	0°	0°/90°	0°/+45°	
Width Effects				
Notched Strength	4	4	4	12
Notched Fatigue	4	4	4	12
Static Properties				
Unnotched Strength	6	6	6	18
Panel-to-Panel Bias/Strength[1]	8	2	2	12
Fatigue Life Tests				
Stress Ratio Effects	18	6	6	28
Strain Threshold	6	—	—	6
Panel-to-Panel Bias[1]	6	2	2	10
Unnotched Specimens	8	4	4	16
Center Cracked Specimens	8	—	—	8
Residual Strength Tests				
Fatigue/Static	20	4	4	28
Total Tests	**86**	**32**	**32**	**150**

(1) These tests include tension, compression, or fatigue of panels
    not previously characterized.

Figure 47. Analytical Model Development Testing in Boron/Aluminum

A filled hole specimen was selected as the simplest baseline
specimen which would produce fatigue damage representative of
bolted or riveted FRMMC structures. These specimens were
nominally unflawed so that damage could initiate naturally. For
investigations into new material systems, in which the modes of
failure are uncertain, we consider unflawed hole specimens to be
superior to preflawed specimens which impose a given damage state,
or unnotched specimens, whose lives are almost completely subject
to the specimen fabrication at the specimen edges. Once failure
modes are identified in the notched coupon specimens then
unnotched or center cracked specimens can be used to develop
initiation life and flaw growth data for the failure modes
identified.

Specimen width effects were investigated to ensure that the
baseline specimen width produced realistic damage growth and
failure modes. Static tests were performed to characterize the
strength of each material and laminate and assess panel-to-panel
variability in fabrication and processing. The primary tests in

this program measured fatigue life and residual strength. During these tests, specimen stiffnesses were continuously monitored and automatically stored. Detailed visual damage measurements were recorded at intervals determined by damage growth or expended life, to relate damage growth to stiffness loss and residual strength.

    a. <u>Specimen Width Effects</u> - Tests were performed in both baseline and wider specimens to determine strength and fatigue failure modes in each boron/aluminum laminate. The specimen geometries and data taken are summarized in Figures 48 and 49.

Test Type	Laminate	Specimen Type	Spec No.	Width (in.)	Thick (in.)	Dia (in.)	Load (KIP)	Net Stress (ksi)	Gross Stress (ksi)	Cycles to Crack to Grips	Cycles to Failure	Comments
Static Tension	0	Baseline	1-1-19	1.388	0.1720	0.2526	26.75	136.98	112.05	—	—	
	0	Baseline	1-1-91	1.511	0.1719	0.2508	25.50	117.71	98.17	—	—	
	0	Large W/D	1-1-11	2.508	0.1711	0.2540	48.60	126.02	113.36	—	—	
	0	Large W/D	1-1-51	2.205	0.1716	0.2545	45.50	117.82	105.85	—	—	
	0/45	Baseline	3-1-61	1.504	0.1728	0.2519	15.05	69.56	57.91	—	—	
	0/45	Baseline	3-1-62	1.487	1.1723	0.2569	13.05	61.57	50.93	—	—	
	0/45	Large W/D	3-1-81	2.475	0.1720	0.2570	23.45	61.47	55.09	—	—	
	0/45	Large W/D	3-1-82	2.526	0.1725	0.2571	20.80	53.38	47.93	—	—	
	0/90	Baseline	2-1-61	1.507	0.1720	0.2537	13.20	61.23	50.93	—	—	
	0/90	Baseline	2-1-62	1.510	0.1729	0.2610	10.78	49.92	41.29	—	—	
	0/90	Large W/D	2-1-81	2.509	0.1712	0.2535	20.15	52.18	46.91	—	—	
	0/90	Large W/D	2-1-82	2.510	0.1721	0.2530	18.90	48.66	43.75	—	—	
Fatigue												
R = −0.02	0	Baseline	1-1-81	1.508	0.1700	0.2500	23.50	109.88	91.67	—	8	
R = −0.02	0	Large W/D	1-1-71	2.517	0.1710	0.2500	41.90	108.09	97.35	—	3	
R = −1.0	0	Baseline	1-1-29	1.510	0.1720	0.2500	17.60	81.21	67.77	183,375	—	Runout-NF
R = −1.0	0	Large W/D	1-1-31	2.498	0.1720	0.2500	31.70	81.99	73.78	400,000	—	Runout-NF
R = −1.0	0/45	Baseline	3-1-51	1.505	0.1730	0.2500	11.24	51.77	43.17	—	174,232	
							12.10	55.73	46.47	—	4,611	Grip Failure
R = −1.0	0/45	Baseline	3-1-52	1.495	0.1710	0.2500	11.95	56.13	46.74	—	2,038	Grip Failure
R = −1.0	0/45	Large W/D	3-1-72	2.509	0.1730	0.2500	18.80	48.11	43.31	—	18,881	
R = −1.0	0/45	Large W/D	3-1-71	2.511	0.1720	0.2500	18.80	48.34	43.53	—	65,848	
R = −1.0	0/90	Baseline	2-1-52	1.508	0.1730	0.2500	8.00	36.76	30.66	—	190,949	NF
							11.14	51.19	42.70	—	—	Overloaded
R = −1.0	0/90	Baseline	2-1-52	1.507	0.1730	0.2500	9.60	44.15	36.82	—	10,113	
R = −1.0	0/90	Large W/D	2-1-72	2.505	0.1720	0.2500	15.00	40.22	36.21	—	9,317	
R = −1.0	0/90	Large W/D	2-1-71	2.509	0.1710	0.2500	15.60	40.38	36.36	—	26,741	

Figure 48. Specimen Width Effects in Boron/Aluminum

54
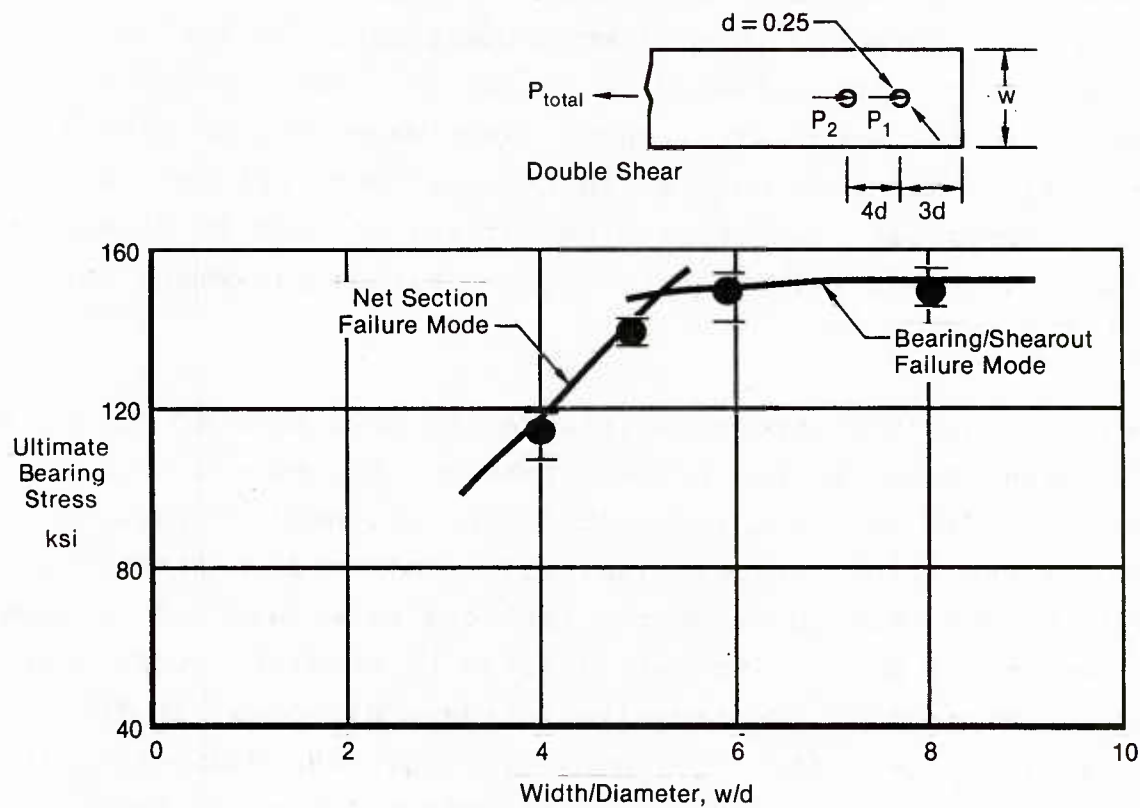
Figure 49. Effect of Specimen Width on Carbon/Epoxy Joint Strength

Based on our previous carbon/epoxy and FRMMC work, we believe that the W/D = 6 specimen is representative of aircraft structural applications and does not show significant influence of its finite width. When W/D is less than 6, crossplied carbon/epoxy joint specimens have shown a change in failure mode, from locally induced bearing/shearout failures to net section failures (Figure 49). In addition, failure progresses much more rapidly in specimens having small W/D. This makes tracking more difficult, a detriment for model development. Smaller W/D specimens were tested in the verification test program, to examine the influence of higher stress concentrations and finite width effects.

b.   Static Properties - We performed static strength tests
using unnotched specimens (Figure 11) to determine material
strengths, moduli, and strains at failure for each of the
laminates tested.   Specimen geometries and test results are
summarized in Figure 50.   Load displacement data for the 0°, 90°,
and 45° specimens are displayed in Figure 51.   The unnotched
specimens used for material strength tests were removed from a
single panel in each laminate so that comparisons between the
tension, compression, and transverse strengths could be directly
made.   Extensometers were used to obtain load-displacement data
during the tests.

Notched baseline specimens (Figure 11) were used to determine
tensile strength variations between panels.   One set of
compression tests was used to evaluate the notched compression
strength of the unidirectional laminate.   Compressive strengths
generally exceed tensile strengths in these materials and fatigue
stress levels for most tests were limited by tensile rather than
compression strengths.   Compression failures did occur in the
crossplied laminates after cycling in fatigue caused cracking in
the off-axis plies and reduced the stiffness of the laminate.

c.   Fatigue Life Tests - Sixty-eight fatigue tests were
performed as outlined in Figure 52 to determine the effects of
stress ratio, stress level, panel-to-panel variability, and notch
sensitivity of boron/aluminum laminates.   The majority of these
tests used the notched baseline specimen of Figure 11.   Displace-
ments were continuously monitored and automatically stored by
computer during each test.   Detailed damage propagation measure-
ments were made at intervals during these tests to track damage-
growth so that it could be related to modulus and residual
strength changes.

Test Type	Laminate	Specimen Type	Spec No	Width (in.)	Thick (in.)	Dia (in.)	Load (KIP)	Net Stress (ksi)	Gross Stress (ksi)
Tension	0	Unnotched	1-2-13	1.255	0.1714	—	41.90	194.79	194.79
	0	Unnotched	1-2-33	1.254	0.1725	—	36.30	167.81	167.81
	15	Unnotched	1-2-93	1.272	0.1716	—	14.04	64.32	64.32
	15	Unnotched	1-2-94	1.257	0.1739	—	13.30	60.84	60.84
	45	Unnotched	1-1-74	1.272	0.1714	—	5.55	25.46	25.46
	45	Unnotched	1-1-75	1.274	0.1722	—	5.34	24.34	24.34
	0/90	Unnotched	2-1-11	1.250	0.1720	—	24.62	114.51	114.51
	0/90	Unnotched	2-1-12	1.250	0.1720	—	20.93	97.35	97.35
	0/45	Unnotched	3-1-11	1.250	0.1720	—	26.97	125.44	125.44
	0/45	Unnotched	3-1-12	1.250	0.1720	—	27.00	125.58	125.58
Compression	0	Unnotched	1-2-31	1.271	0.1736	—	−39.70	−179.93	−179.93
	0	Unnotched	1-2-21	1.269	0.1735	—	−39.90	−181.22	−181.22
	0/90	Unnotched	2-1-13	1.250	0.1720	—	−27.06	−125.86	−125.86
	0/90	Unnotched	2-1-21	1.250	0.1720	—	−27.10	−126.05	−126.05
	0/45	Unnotched	3-1-13	1.250	0.1720	—	−26.30	−122.33	−122.30
	0/45	Unnotched	3-1-21	1.250	0.1720	—	−26.50	−123.26	−123.26
Traverse	0	Unnotched	1-4-14	1.262	0.1704	—	5.59	25.99	25.99
	0	Unnotched	1-4-24	1.248	0.1702	—	5.44	25.61	25.61
	0/90	Unnotched	2-1-91	1.250	0.1720	—	21.13	98.28	98.28
	0/90	Unnotched	2-1-92	1.250	0.1720	—	21.00	97.68	97.68
	0/45	Unnotched	3-1-91	1.250	0.1720	—	6.83	31.77	31.77
	0/45	Unnotched	3-1-92	1.250	0.1720	—	6.38	29.67	29.67
Panel-to-Panel Bias									
Tension	0	Baseline	1-2-43	1.510	0.1719	0.2505	25.05	115.70	96.51
	0	Baseline	1-2-42	1.510	0.1715	0.2510	25.35	117.41	97.89
	0	Baseline	1-3-13	1.516	0.1720	0.2527	29.95	137.84	114.86
	0	Baseline	1-3-31	1.521	0.1711	0.2528	25.00	115.21	96.06
	0	Baseline	1-4-52	1.501	0.1712	0.2512	21.00	98.15	81.72
	0	Baseline	1-4-23	1.504	0.1711	0.2517	22.45	104.78	87.24
	0/90	Baseline	2-1-42	1.250	0.1720	0.2500	11.66	67.79	54.23
	0/90	Baseline	2-2-91	1.250	0.1720	0.2500	14.00	81.40	65.12
	0/45	Baseline	3-1-42	1.250	0.1720	0.2500	14.61	84.94	67.95
	0/45	Baseline	3-2-91	1.250	0.1720	0.2500	16.50	95.93	76.74
Compression	0	Baseline	1-4-41	1.506	0.1720	0.2508	−14.50	−192.22	−160.21
	0	Baseline	1-4-92	1.497	0.1706	0.2510	−41.30	−194.29	−161.71

Figure 50. Static Properties Tests in Boron/Aluminum

57
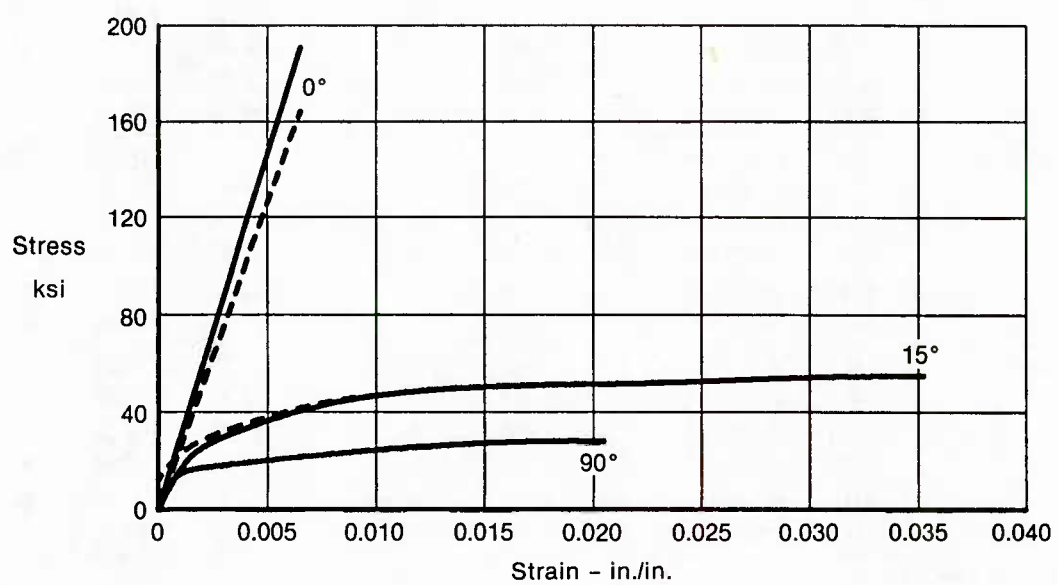
Figure 51. Stress-Strain Curves for Unnotched, Unidirectionally Reinforced Boron/Aluminum

58

Test Type	Laminate	Specimen Type	Spec No.	Width (in.)	Thick (in.)	Dia (in.)	Cr Len (in.)	Load (KIP)	Net Stress (ksi)	Gross Stress (ksi)	Cycles to 0.05 Crack	Cycles to Crack to Grips	Cycles to Failure	Comments
Stress Ratio Effects														
R = 0.02	0	Baseline	1-3-63	1.511	0.1701	0.2500	—	21.98	102.47	85.52	—	—	60	
R = 0.02	0	Baseline	1-3-33	1.513	0.1710	0.2500	—	21.73	100.61	83.99	70	7,200	—	
R = 0.02	0	Baseline	1-3-73	1.512	0.1703	0.2500	—	21.63	100.64	84.00	—	—	48	
R = 0.02	0	Baseline	1-3-93	1.515	0.1698	0.2500	—	20.61	95.95	80.12	—	—	66	
R = 0.02	0	Baseline	1-3-32	1.510	0.1720	0.2500	—	19.92	91.92	76.70	—	—	1,960,000	
R = 0.02	0	Baseline	1-3-42	1.515	0.1710	0.2500	—	19.24	88.94	74.27	—	—	2,170,000	
R = 0.02	0	Baseline	1-3-23	1.517	0.1710	0.2500	—	15.56	71.82	59.98	430	70,000	—	
R = 0.02	0	Baseline	1-3-22	1.497	0.1701	0.2515	—	15.28	72.12	60.01	490	73,250	—	
R = − 1.0	0	Baseline	1-3-11	1.517	0.1720	0.2500	—	21.98	100.86	84.24	—	—	1,161	
R = − 1.0	0	Baseline	1-4-51	1.506	0.1720	0.2500	—	21.76	100.73	84.01	26	225	775	
R = − 1.0	0	Baseline	1-4-31	1.500	0.1708	0.2510	—	21.52	100.88	84.00	49	300	1,000	
R = − 1.0	0	Baseline	1-3-12	1.514	0.1725	0.2500	—	20.61	94.52	78.92	—	—	1,720	
R = − 1.0	0	Baseline	1-3-21	1.520	0.1709	0.2500	—	88.65	74.07		—	—	44,635	
R = − 1.0	0	Baseline	1-4-11	1.493	0.1702	0.2500	—	15.25	72.08	60.01	25	850	—	
R = − 1.0	0	Baseline	1-4-21	1.506	0.1708	0.2500	—	15.43	71.93	59.99	46	750	—	
R = 10.0	0	Baseline	1-3-62	1.518	0.1707	0.2500	—	31.60	145.99	121.95	—	—	3,981	
R = 10.0	0	Baseline	1-3-51	1.513	0.1707	0.2500	—	27.48	127.46	106.40	—	—	403,000	NF
R = 10.0	0	Baseline	1-4-32	1.502	0.1708	0.2515	—	25.65	120.00	99.98	227	14,000	—	
R = 10.0	0	Baseline	1-4-42	1.500	0.1709	0.2510	—	25.64	120.12	100.02	164	45,000	—	
R = 10.0	0	Baseline	1-3-83	1.510	0.1715	0.2500	—	24.73	114.44	95.40	—	—	411,000	NF
R = 10.0	0	Baseline	1-3-61	1.513	0.1710	0.2500	—	21.98	101.77	84.96	—	—	430,000	NF
R = 10.0	0	Baseline	1-4-12	1.501	0.1701	0.2500	—	21.45	100.80	84.01	290	1,320,000	—	
R = 10.0	0	Baseline	1-4-22	1.507	0.1707	0.2515	—	21.62	100.83	84-01	447	190,000	—	
Open Hole														
R = 0.02	0	Baseline	1-3-72	1.510	0.1710	0.2500	—	19.24	89.30	74.51	—	—	8	
R = 0.02	0	Baseline	1-3-91	1.513	0.1690	0.2500	—	17.86	83.67	69.85	—	—	2,150,000	NF
R = 0.02	0	Baseline	1-3-52	1.519	0.1709	0.2500	—	16.49	76.04	63.52	—	—	859,000	NF
R = 0.02	0/90	Baseline	2-2-11	1.500	0.1720	0.2500	—	10.50	48.84	40.70	—	—	162,400	
R = 0.02	0/90	Baseline	2-2-13	1.500	0.1720	0.2500	—	10.50	48.84	40.70	—	—	8	
R = 0.02	0/45	Baseline	3-2-11	1.500	0.1720	0.2500	—	12.00	55.81	46.51	—	—	73,800	
R = 0.02	0/45	Baseline	3-2-13	1.500	0.1720	0.2500	—	12.00	55.81	46.51	—	—	119,910	
R = − 1.0	0/90	Baseline	2-2-31	1.500	0.1720	0.2500	—	9.50	44.19	36.82	—	—	150,700	
R = − 1.0	0/90	Baseline	2-2-32	1.500	0.1720	0.2500	—	9.50	44.19	36.82	—	—	41	
R = − 1.0	0/90	Baseline	2-1-43	1.500	0.1720	0.2500	—	9.00	41.86	34.88	—	—	6,890	
R = − 1.0	0/90	Baseline	2-2-41	1.500	0.1720	0.2500	—	9.00	41.86	34.88	—	—	402,800	
R = − 1.0	0/45	Baseline	3-2-31	1.500	0.1720	0.2500	—	9.50	44.19	36.82	—	—	200,290	
R = − 1.0	0/45	Baseline	3-2-33	1.500	0.1720	0.2500	—	9.50	44.19	36.82	—	—	3,750,000	NF
R = − 1.0	0/45	Baseline	3-1-43	1.500	0.1720	0.2500	—	11.00	51.16	42.64	—	—	369,970	
R = − 1.0	0/45	Baseline	3-2-41	1.500	0.1720	0.2500	—	11.0	51.16	42.64	—	—	73,170	
Stress Threshold														
R = 0.02	0	Baseline		1.500	0.1720	0.2500	—	3.87	18.00	15.00	—	—	—	5 ksi incr.
								9.00	48.00	40.00	—	—	600,000	No Damage
R = 0.02	0	Baseline		1.500	0.1720	0.2500	—	11.61	54.00	45.00	—	—	100,000	0.1 Cracks
R = − 1.0	0	Baseline		1.500	0.1720	0.2500	—	2.58	12.00	10.00	—	—	—	5 ksi incr.
		Baseline						6.45	30.00	25.00	—	—	400,000	No Damage
R = − 1.0	0	Baseline		1.500	0.1720	0.2500	—	7.74	36.00	30.00	—	—	100,000	—
R = 0.02	0	Center Crack		1.500	0.1720	—	0.2500	3.87	18.00	15.00	—	—	—	5 ksi incr.
								9.03	42.00	35.00	—	—	500,000	No Damage
R = 0.02	0	Center Crack		1.500	0.1720	—	0.2500	10.32	48.00	40.00	—	—	100,000	0.02 Cracks
R = 0.02	0	Center Crack		1.500	0.1720	—	0.2500	10.32	48.00	40.00	—	—	1,300,000	0.2 Cracks
R = 0.02	0	Center Crack		1.500	0.1720	—	0.2500	11.61	54.00	45.00	—	?	—	
R = − 1.0	0	Center Crack		1.500	0.1720	—	0.2500	2.58	12.00	10.00	—	—	—	5 ksi incr.
								3.87	18000	15.00	—	—	200,000	No Damage
R = − 1.0	0	Center Crack		1.500	0.1720	—	0.2500	5.16	24.00	20.00	—	50,000	—	

Figure 52. Fatigue Life Tests in Boron/Aluminum

Test Type	Laminate	Specimen Type	Spec No.	Width (in.)	Thick (in.)	Dia (in.)	Cr Len (in.)	Load (KIP)	Net Stress (ksi)	Gross Stress (ksi)	Cycles to 0.05 Crack	Cycles to Crack to Grips	Cycles to Failure	Comments
Panel-to-Panel Bias														
R = −1.0	0/90	Baseline	2-2-21	1.500	0.1720	0.2500	—	10.00	46.51	38.76	—	—	172,500	
R = −1.0	0/90	Baseline	2-2-22	1.500	0.1720	0.2500	—	10.00	46.51	38.76	—	—	48	
R = −1.0	0/45	Baseline	3-2-21	1.500	0.1720	0.2500	—	11.00	51.16	42.64	—	—	48,870	
R = −1.0	0/45	Baseline	3-2-23	1.500	0.1720	0.2500	—	11.00	51,16	42.64	—	—	75,290	
Unnotched														
R = 0.02	0	Unnotched	1-2-41	1.250	0.1710	—	—	31.00	145.03	145.03	—	—	65,586	
R = 0.02	0	Unnotched	1-2-51	1.250	0.1710	—	—	31.00	145.03	145.03	—	—	68,827	
R = 0.02	0/90	Unnotched	2-1-22	1.250	0.1710	—	—	20.00	93.57	93.57	—	—	3	
R = 0.02	0/90	Unnotched	2-1-23	1.250	0.1710	—	—	19.00	88.89	88.89	—	—	3,980	
R = 0.02	0/45	Unnotched	3-1-22	1.250	0.1710	—	—	23.00	107.60	107.60	—	—	17	
R = 0.02	0/45	Unnotched	3-1-31	1.250	0.1710	—	—	23.00	107.60	107.60	—	—	36,190	
R = −1.0	0	Unnotched	1-2-81	1.250	0.1710	—	—	31.00	145.03	145.03	—	—	25	
R = −1.0	0	Unnotched	1-2-32	1.250	0.1710	—	—	31.00	145-03	145.03	—	—	5	
R = −1.0	15	Unnotched	1-2-95	1.250	0.1710	—	—	6.41	29.99	29.99	—	—	76,202	
R = −1.0	45	Unnotched	1-1-77	1.250	0.1710	—	—	2.67	12.49	12.49	—	—	1,067,659	NF
R = −1.0	90	Unnotched	1-1-15	1.250	0.1710	—	—	3.21	15.00	15.00	—	—	79,625	
R = −1.0	90	Unnotched	1-1-17	1.250	0.1710	—	—	2.67	12.50	12.50	—	—	126,199	
R = −1.0	0/90	Unnotched	2-1-32	1.250	0.1710	—	—	17.00	79.53	79.53	—	—	90	
R = −1.0	0/90	Unnotched	2-1-33	1.250	0.1710	—	—	15.00	70.18	70.18	—	—	321	
R = −1.0	0/45	Unnotched	3-1-32	1.250	0.1710	—	—	21.00	98.25	98.25	—	—	51	
R = −1.0	0/45	Unnotched	3-1-33	1.250	0.1710	—	—	20.00	93.57	93.57	—	—	70	
Center Cracked Specimens														
R = 0.02	0	Center Crack	1-2-52	1.517	0.717	—	0.2500	16.32	75.02	62.66	181	6,000	—	
R = −1.0	0	Center Crack	1-2-92	1.522	0.1711	—	0.2500	16.32	74.99	62.67	12	210	—	
R = 0.02	45	Center Crack	1-1-76	1.518	0.1708	—	0.1768	1.30	5.66	5.00	—	—	367,000	NF
								2.29	10.00	8.83	210	—	79,897	
R = 0.02	45	Center Crack	1-1-78	1.518	0.1712	—	0.1768	3.44	14.98	13.24	50	—	1,600	
R = 0.02	90	Center Crack	1-1-14	1.486	0.1719	—	0.2500	3.19	15.01	12.49	—	—	100	Overload
R = 0.02	90	Center Crack	1-1-16	1.510	0.1716	—	0.2500	2.16	9.99	8.34	30,250	—	72,250	

Figure 52. (Continued) Fatigue Life Tests in Boron/Aluminum

Fatigue tests were performed at three stress ratios, R = 0, −1, and ∞. Because these tests developed the primary data for model development, we tested three load levels for the unidirectional laminate. Load levels were selected to produce lives of 500; 10,000; and 200,000 cycles. Similar tests were performed for R = 0 and R = −1 in the crossplied laminates. A series of tests were performed to determine the stress threshold levels below which cracking would not initiate in boron/aluminum center hole and center cracked specimens at R = 0 and −1. The data from the stress ratio effects tests were used to estimate stress thresholds in the unidirectional laminate specimens. In the first test in the series an intentionally low stress level was selected for

testing to obtain 200,000 cycles of loading without cracking. The load was then increased in small increments, at the end of each block of 200,000 cycles, until a crack initiated. The final stress level was used for the remaining tests.

We selected one loading condition to evaluate panel-to-panel variability in fatigue life: R = -1 testing at the same load level used in the specimen width tests. These tests allowed characterization of panel-to-panel variability in fatigue life, and evaluation of overall scatter.

Unnotched specimens were tested in fatigue to determine the initiation life and to compare these results with those from the notched specimens to determine the notch sensitivity of life in FRMMC materials. Unnotched specimens were configured to provide the same net section stress as in the notched baseline specimens.

Once failure modes in the fastener hole specimens were identified, we developed data on crack growth rates in those modes through tests of center cracked panels in which the crack and fiber orientations were selected to propagate flaws within the matrix or across the net section. These tests characterized growth: (1) perpendicular to 0° fibers, (2) along 45° fibers to correlate with shear and tension mode cracking noted from our tests, and (3) along 90° fibers, which was used along with the 45° test results to evaluate cracking in the crossplied laminates.

d. <u>Residual Strength Tests</u> - Twenty-eight residual strength tests, predominantly in unidirectional boron/aluminum were performed as summarized in Figure 53. In this test series constant amplitude fatigue tests of baseline notched specimens were performed until a particular damage state (crack length) was obtained. The specimens were then failed statically to determine residual strength. Tests were duplicated for each stress level and damage configuration tested. For the R = -1 testing, residual strengths in both tension and compression were measured.

61

Test Type	Laminate	Specimen Type	Spec No.	Width (in.)	Thick (in.)	Dia (in.)	Fatigue Stress (ksi)	Cr Len (in.)	Load (KIP)	Net Stress (ksi)	Gross Stress (ksi)
Open Hole											
R = 0.02	0	Baseline	1-3-71	1.500	0.1720	0.2500	50	0.0625	22.70	105.58	87.98
R = 0.02	0	Baseline	1-1-59	1.500	0.1720	0.2500	75	0.0625	26.50	123.26	102.71
R = 0.02	0	Baseline	1-3-23	1.500	0.1720	0.2500	75	0.5000	22.33	103.84	86.53
R = 0.02	0	Baseline	1-2-62	1.500	0.1720	0.2500	75	0.5000	26.85	124.88	104.07
R = 0.02	0	Baseline	1-3-43	1.500	0.1720	0.2500	77	Grips	30.40	141.40	117.83
R = −1.0	0	Baseline	1-1-39	1.500	0.1720	0.2500	50	0.0625	27.90	129.77	108.14
R = −1.0	0	Baseline	1-2-73	1.500	0.1720	0.2500	75	0.0625	25.40	118.14	98.45
R = −1.0	0	Baseline	1-3-81	1.500	0.1720	0.2500	50	0.5000	27.50	127.91	106.59
R = −1.0	0	Baseline	1-2-53	1.500	0.1720	0.2500	75	0.5000	28.80	133.95	111.63
R = −1.0	0/90	Baseline	2-2-51	1.500	0.1720	0.2500	42	—	10.26	47.72	39.77
R = −1.0	0/90	Baseline	2-2-61	1.500	0.1720	0.2500	42	—	− 22.33	− 103.86	− 86.55
R = −1.0	0/45	Baseline	3-2-51	1.500	0.1720	0.2500	53	—	12.62	58.70	48.91
R = −1.0	0/45	Baseline	3-2-61	1.500	0.1720	0.2500	53	—	13.10	60.93	50.78
R = −1.0	0/45	Baseline	3-2-71	1.500	0.1720	0.2500	53	—	− 28.42	− 132.19	− 110.16
R = −1.0	0/45	Baseline	3-2-81	1.500	0.1720	0.2500	53	—	− 27.05	− 125.81	− 104.84
Filled Hole											
R = −1.0	0	Baseline	1-2-72	1.500	0.1720	0.2500	50	0.0625	− 42.20	− 196.28	− 163.57
R = −1.0	0	Baseline	1-4-31	1.500	0.1720	0.2500	75	0.0625	− 33.50	− 155.81	− 129.84
R = −1.0	0	Baseline	1-1-49	1.500	0.1720	0.2500	50	0.5000	− 45.89	− 213.02	− 177.52
R = −1.0	0	Baseline	1-2-63	1.500	0.1720	0.2500	75	0.5000	− 46.70	− 217.21	− 181.01
R = 10.0	0	Baseline	1-4-42	1.500	0.1720	0.2500	100	0.1200	− 38.40	− 178.60	− 148.84
R = 10.0	0	Baseline	1-4-12	1.500	0.1720	0.2500	84	0.5000	− 36.60	− 170.23	− 141.86
R = 10.0	0	Baseline	1-4-32	1.500	0.1720	0.2500	100	0.7500	− 40.20	− 186.98	− 155.81
R = 10.0	0	Baseline	1-3-61	1.500	0.1720	0.2500	84	Grips	− 36.39	− 169.77	− 141.47

Figure 53. Residual Strength Tests in Boron/Aluminum

62

MODEL DEVELOPMENT

During the course of this program, analysis methods were derived for the prediction of static strength of notched and unnotched MMC structures, fatigue crack initiation life to an assumed 0.05 inch flaw, crack growth of such flaws, and residual strength of flawed MMC structures. These analyses were developed based on our knowledge about the behaviors of metal and resin matrix composite structures. Thus, wherever possible, metallic and composite structural analysis provide the limiting cases for these techniques. In addition, the analyses developed were derived to be as simple as possible and yet still describe the test results obtained in this program. These analysis techniques were embodied in a computer routine, MMCAN, and a User's Guide for this routine is presented in Appendix A.

1. <u>STIFFNESS AND STRENGTH OF UNNOTCHED METAL MATRIX COMPOSITES</u> - For unidirectional, continuous fiber reinforced composites the most common method for examining strength and stiffness behavior is to compare test values with a Rule of Mixtures analysis. This analysis assures that composite stiffness or strength is related only to the matrix and fiber properties and the fiber volume fraction, v_{fiber}.

$$P_{composite} = P_{fiber} \, v_{fiber} + P_{matrix} \, v_{matrix}$$

Where P is the property (strength or stiffness) and v is the ratio of cross-sectional areas of fibers or matrix to total area.

$$v_{matrix} = 1 - v_{fiber}$$

Figure 54 shows the Rule of Mixtures (ROM) prediction of composite stiffness for various ratios of fiber to matrix stiffness. Both MMC and resin matrix composites show good correlation

with this analysis. The correlation is even more evident in Figure 55 where measured composite stiffness is plotted against that predicted by the Rule of Mixtures.
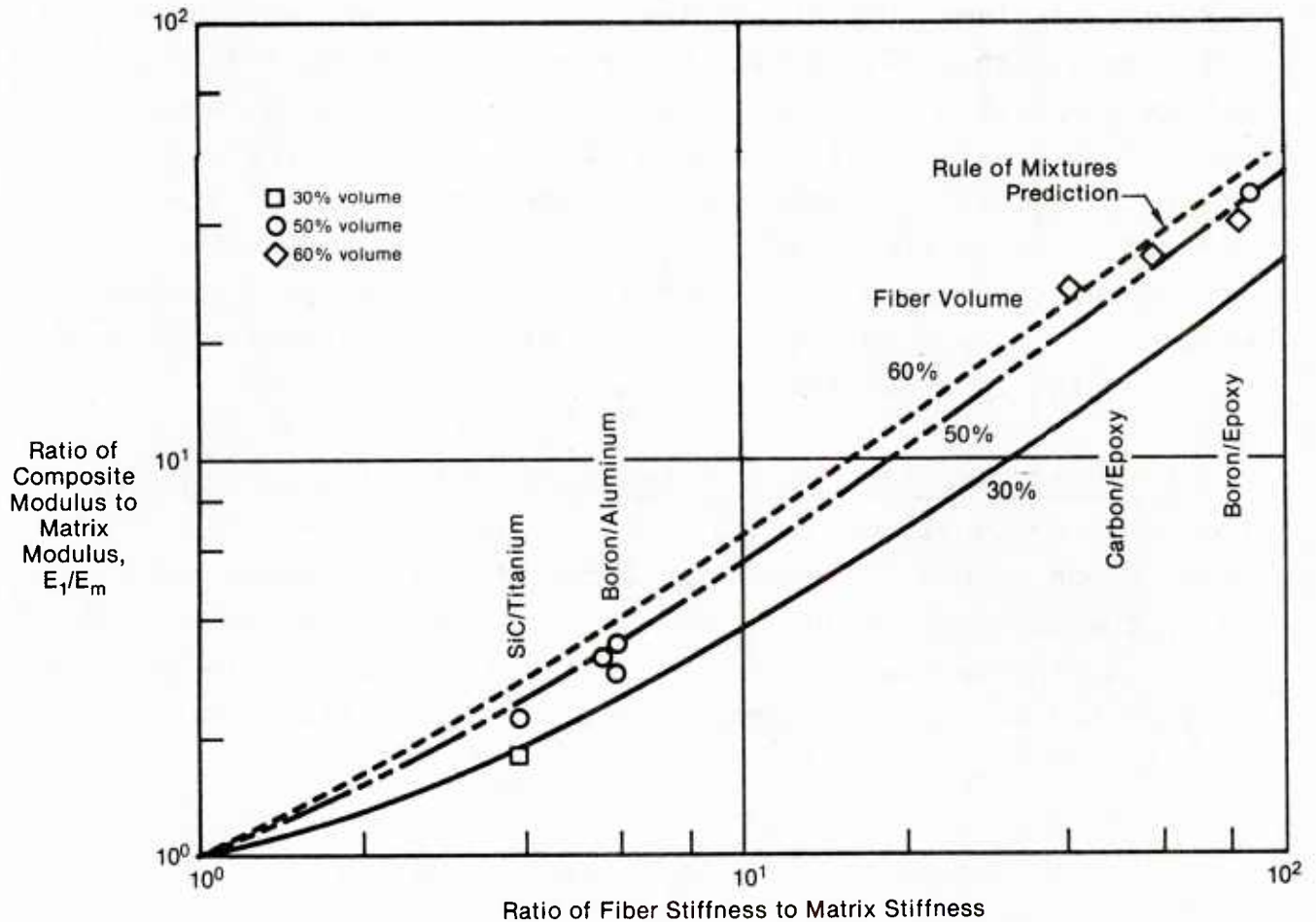
Figure 54. Prediction of the Effect of Fiber Volume by Rule of Mixtures
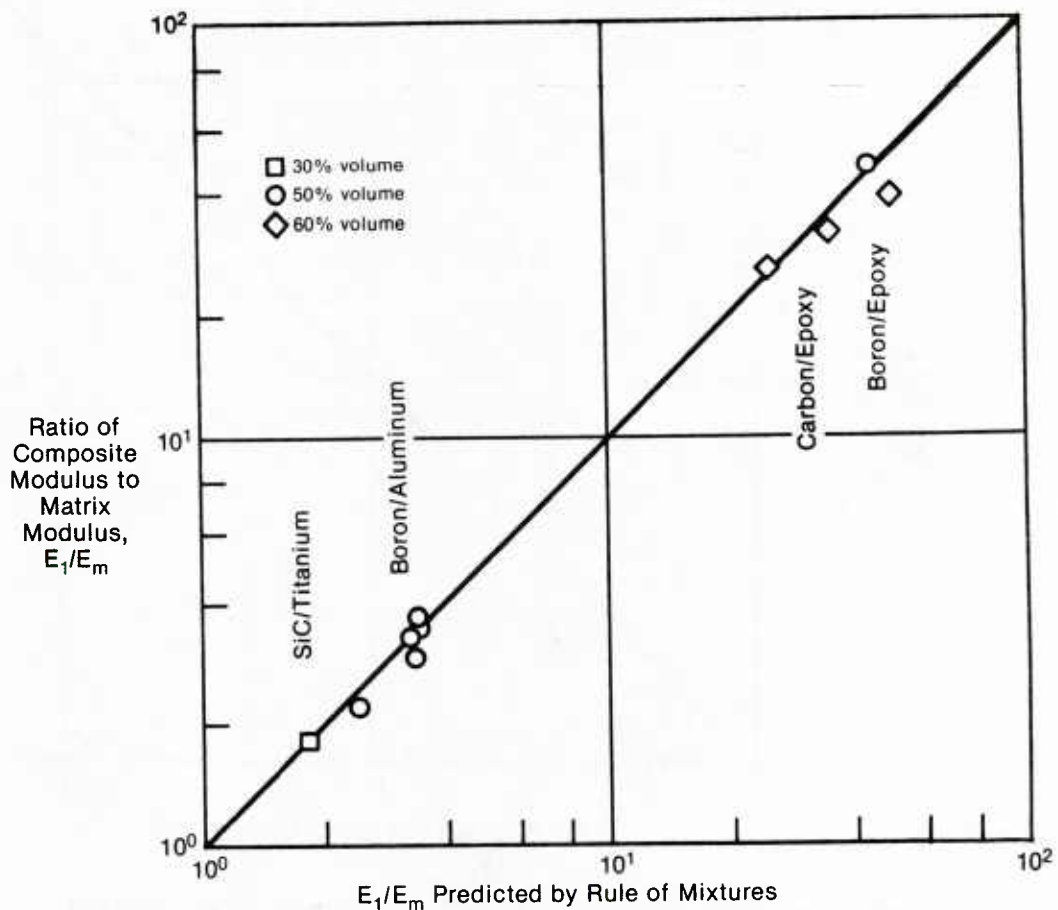
Figure 55. Correlation of Unidirectionally Reinforced Composite Stiffness by Rule of Mixtures

Rule of Mixtures analyses generally overestimate the strength of composite materials, Figure 56. Probably this is due to fiber strength degradation which may occur during composite fabrication. Sometimes this overall strength degradation is correlated using bundle theory to fit the overall fiber strength distribution in fibers leached from the matrix. Depending upon the severity of the temperatures and pressures required to fabricate the composite laminate, this fiber strength reduction can sometimes be substantial. This is particularly true of titanium matrix composites, where temperatures for material consolidation are as high as 1600° to 1700°F.

65
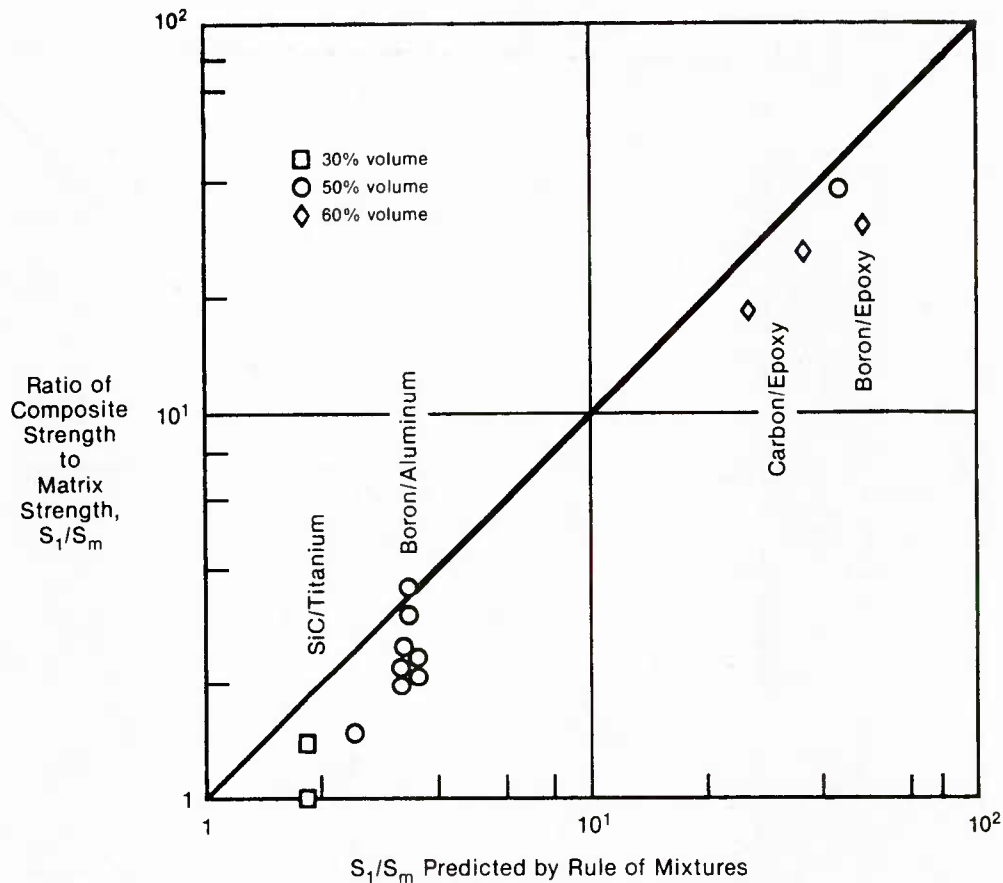
Figure 56. Correlation of Composite Strength by Rule of Mixtures

At these temperatures, there can be considerable fiber/matrix chemical interaction which can degrade the fiber strength. Often fibers developed for use in metal matrix composites are coated with chemically resistant coatings to reduce the possibility of chemical interaction between fiber and matrix. For analysis of metal matrix composites, we recommend that tests of unnotched unidirectionally reinforced material be used to estimate ply or lamina properties, rather than relying on a Rule of Mixtures approach.

This fiber/matrix interaction also affects the fiber-to-matrix adhesion strength and consequently the off-axis ply properties are reduced. Because of the fiber-to-matrix interaction zone degradation, we also recommend that the analyst

66

rely on off-axis tests of unidirectionally reinforced material to determine transverse and shear strengths of MMC plies. Predictions can be made using a Tsai-Hill type analysis, but its real value comes in correlating axial and off-axis strength data of unnotched MMC and providing estimates of the reduced lamina shear and transverse tension strengths (Figure 57). We recommend using
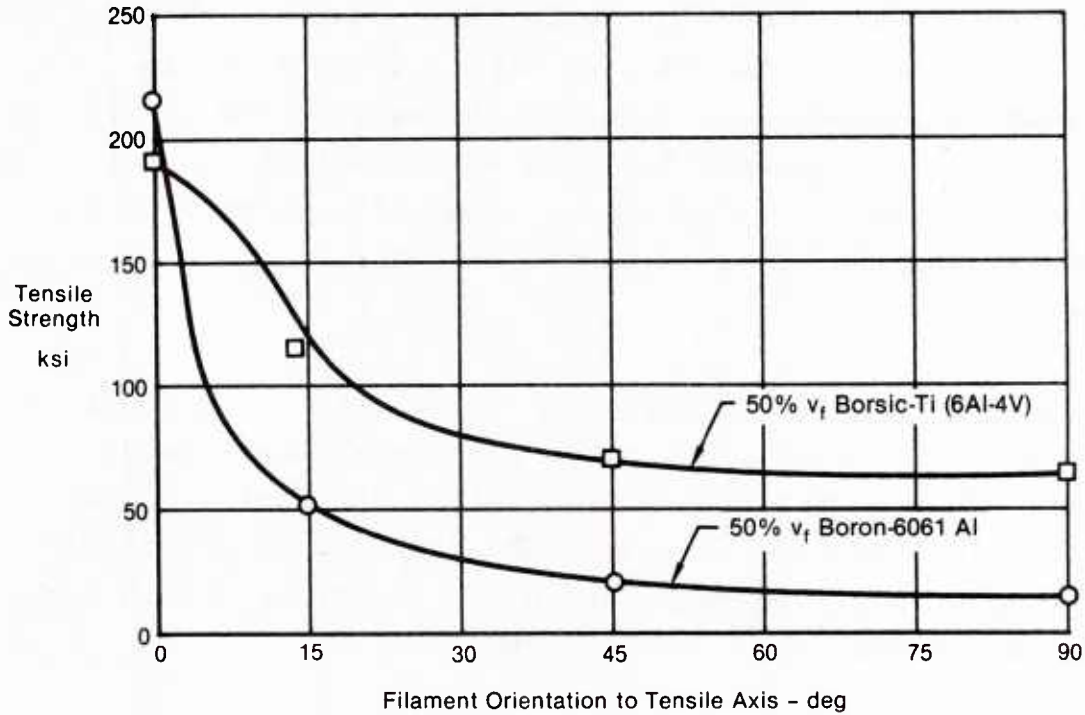
Figure 57. Correlation of Off-Axis Strength by Tsai-Hill Criterion

10° or 15° off-axis specimens and 90° specimens to determine shear and transverse strength properties, and testing a 45° specimen to confirm the analysis accuracy, as shown in Figure 57.

The Tsai-Hill failure criterion can be expressed, for any off-axis angle, θ, as

$$\cos^4\theta/F_x^2 + (1/F_{xy}^2 - 1/F_x^2)\cos^2\theta \sin^2\theta + \sin^4\theta/F_y^2 = 1/F_x^2$$

and can be used to derive F_x through an axial test, F_y through a 90° off-axis test, and F_{xy} through a 10°-15° off-axis test. Once the strength parameters, F_x, F_y, F_{xy} are known, the strength of any off-axis ply can be estimated.

67

It is important to note that the off-axis behavior of unidirectionally reinforced MMC is often quite plastic, due to the high strain tolerance of the matrix (Figure 51, Section III). In the analyses performed herein, we treated the matrix as an elastic-perfectly plastic material. Thus at strain levels below failure of the 0° plies, off-axis plies could and would show significant plastic strain. When this occurred, those plies would not pick up any additional load with increased strain. The ply stiffness was likewise reduced for transverse and shear loadings. When fatigue or strength failures were predicted to occur, the ply was assumed not to carry any transverse tension or shear loadings, and the ply's transverse and shear moduli were reduced to zero.

Laminate Stiffness/Strength - Given the ply properties at various strain levels, laminated plate analyses were used to predict the stresses and strains within the laminate. This analysis is iterative to insure that the stress and strain state within each ply is in agreement with the stress/strain behavior found in the unnotched lamina test.

Given the E_1, E_2, G_{12}, and v_{12} for each ply, the laminate stiffness is derived from laminated plate theory as follows:

$$Q_{11} = E_1 / (1-v_{12} v_{21})$$
$$Q_{12} = v_{21} Q_{11}$$
$$Q_{22} = E_2 / (1 - v_{12} v_{21})$$
$$Q_{66} = G_{12}$$

$$\bar{Q}_{11} = Q_{11}\cos^4\theta + 2(Q_{12} + 2Q_{66})\sin^2\theta\cos^2\theta + Q_{22}\sin^4\theta$$

$$\bar{Q}_{12} = (Q_{11} + Q_{22} - 4Q_{66})\sin^2\theta\cos^2\theta + Q_{12}(\sin^4\theta\cos^4\theta)$$

$$\bar{Q}_{22} = Q_{11}\sin^4\theta + 2(Q_{12} + 2Q_{66})\sin^2\theta\cos^2\theta + Q_{22}\cos^4\theta$$

$$\bar{Q}_{16} = (Q_{11} - Q_{12} - 2Q_{66})\sin\theta\cos^3\theta + (Q_{12} - Q_{22} + 2Q_{66})\sin^3\theta\cos\theta$$

$$Q_{26} = (Q_{11} - Q_{12} - 2Q_{66})\sin^3\theta\cos\theta + (Q_{12} - Q_{22} + 2Q_{66})\sin\theta\cos^3\theta$$

$$Q_{66} = (Q_{11} + Q_{22} - 2Q_{12} - 2Q_{66})\sin^2\theta\cos^2\theta + Q_{66}(\sin^4\theta + \cos^4\theta)$$

$$[A] = [Q]_i(h_i - h_{i-1})$$

$$[A] = \{[A]/t\}^{-1}$$

$$E_x = 1/A_{11} \qquad v_{xy} = -E_x\,A_{12}$$
$$E_y = 1/A_{22} \qquad G_{xy} = 1/A_{33}$$

These orthotropic plate properties are then used to determine stresses and strains in both notched and unnotched laminates.

Strength analysis of crossplied laminates is based upon determining individual ply stresses and strains. When yielding occurs the stress in the ply is limited to yield strength and the ply stiffness is reduced to the secant modulus, estimated for the final load condition. When ply failure occurs (that is, the ply strain allowable is exceeded), the modulus in tension and shear are reduced by three orders of magnitude, but the ply compression modulus is left unchanged, assuming that compression can be carried without buckling the laminate with these reduced properties.

The reductions in modulus that account for nonlinear ply behaviors require a reanalysis of laminate stiffness using laminated plate theory. The ply-by-ply failure condition (yielding or failure) is assumed to occur throughout the ply, whether the geometry is notched or unnotched. In unnotched geometries this assumption is easily accepted, but for notched geometries the assumption that cracking reduces the stiffness throughout the ply is less obvious. However, in notched plate analyses, the plate stiffnesses near the hole have the greatest effect on the local stress distributions. Therefore, as long as the ply stiffnesses throughout the notched laminate match the stiffnesses near the hole, the stresses near the hole are reasonably approximated by the notched laminate stress analysis.

2. <u>ELASTIC-PLASTIC MICROMECHANICS ANALYSIS</u> - Metal matrix composites differ from conventional resin matrix composites in that the matrix material can undergo plastic deformation without cracking. To investigate the effects of elastic-plastic behavior of the matrix material near cracks and notches, Dr. C. T. Sun, of Purdue University, performed a number of finite element analyses. Three specific cases of cracked, unidirectionally reinforced MMC materials were modeled. Each model consisted of six fibers and five matrix strips, as shown in Figure 58. In case 1, the crack cuts through two fibers and is perpendicular to the fibers. The crack tip resides at the fiber-matrix interface. In case 2 only the matrix strips are broken, while the fibers remain intact. In case 3 the crack cuts through the composite at a 45° angle.
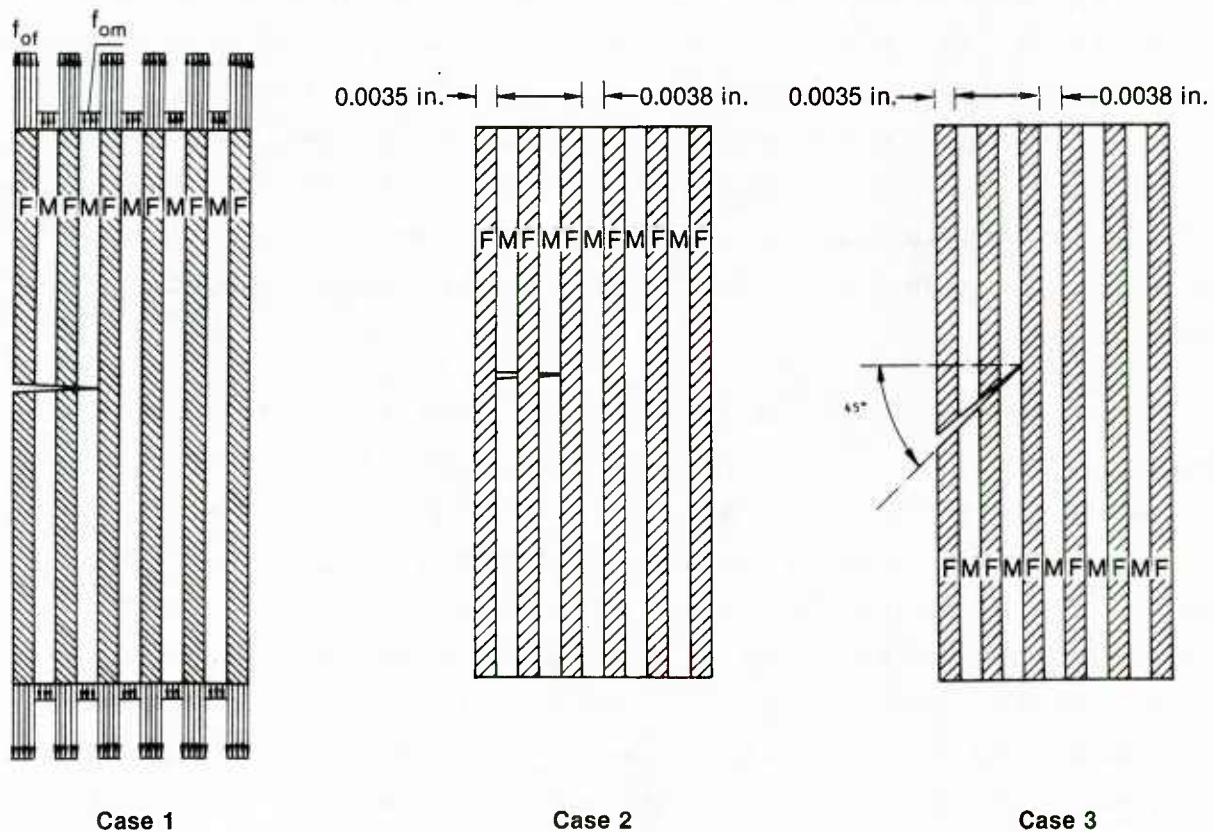
Figure 58. Geometry of Three Cases of a Cracked Panel

a. Constitutive Relations - In this study, the fiber was assumed to be elastic, while the elastic-plastic behavior of the matrix material was assumed to be bi-linear with a constant hardening slope E_T, a Young's modulus E, a Poisson's ratio ν, and an initial yield strength F_y.

Using the conventional plasticity theory approach, three properties, i.e., a yield criterion, a flow rule, and a hardening rule, in addition to the elastic stress-strain relations, are necessary to describe the elasto-plastic material behavior. In this study, a material model that follows the von Mises yield condition was employed along with the associated flow rule and isotropic hardening. From the isothermal condition and isotropic hardening, the von Mises yield function can be written as

$$J'_2 - k = 0$$

where J'_2 is the second deviatoric stress invariant and k is a variable which depends on the total plastic strain. Under the associated flow rule, the elastic-plastic moduli D^{ep}_{ij} are given by Reference 21 as

$$D^{ep}_{ij} = D^e_{ij} - \frac{D^e_{ik} |dJ'_2/df_k| |dJ'_2/df_l| D^e_{lj}}{H + |dJ'_2/df_m| D^e_{mn} |dJ'_2/df_n|}$$

in which D^e_{ij} are the elastic moduli, f is the stress vector, H is a scalar which can be determined using the work hardening hypothesis, normality condition, and the definitions of effective stress and effective plastic strain as

$$H = \frac{E_T}{1-E_T/E}$$

71

The relation of the elasto-plastic stress increment d_{fi} and the total strain increment de_i is then expressed as

$$df_i = D^{ep}_{ij} de_j$$

b. <u>Finite Element Solution</u> - In linear elastic analysis, singular finite elements have proven efficient for solving for the stress intensity factor for cracks at a bi-material interface. Since the nature of the singularity is not yet known in elasto-plastic analysis, the conventional 8-node isoparametric element was used in the current study. The incremental finite element equations for the small strain elasto-plastic problem can written in the matrix form as

$$\{\psi\} = {}_A [B]^T [D^{ep}][B]\{\Delta u\} - \{\Delta R\}$$

where $\{\psi\}$ is the unbalanced force vector, $[B]$ is the strain transformation matrix, $\{\Delta u\}$ and $\{\Delta R\}$ are the incremental nodal displacement vector and incremental nodal force vector, respectively.

At each load increment, the system of nonlinear equations was solved using the Newton-Raphson approach. The iteration procedure was performed until a convergence tolerance was reached. Strains and stresses were calculated at the 3x3 Gauss integration points. The state of stress at each Gaussian point was checked if it was on the yield surface during loading. Partial yield of an element was permitted. The elasto-plastic matrix D^{ep}_{ij} was updated within each iteration and was replaced by the elastic matrix D^e_{ij} for those Gaussian points if they were in the elastic region.

c. <u>Results for Cases 1 and 2</u> - The analysis of a crack normal to the fibers was carried out. Due to the symmetry only the upper domain was required to model the problem. Two hundred and fifty plane stress elements wre used; see Figure 59. The finite element mesh was refined near the crack tip. This

procedure was followed for both Case 1 and Case 2. However, for the latter case fixed boundary conditions (v=0) applied for the first two fibers along the crack line.
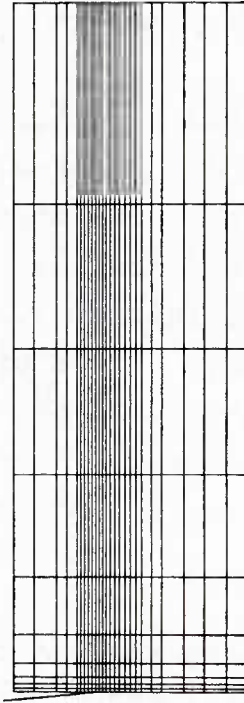
Figure 59. Finite Element Mesh for the Problem of a Crack Normal to an Interface

The properties of the constituent materials are given as:

Boron	$E = 5.8 \times 10^7$ psi	$\nu = 0.25$
Al	$E = 1.0 \times 10^7$ psi	$\nu = 0.25$
	$E_T = 1.0 \times 10^5$ psi	$F_y = 1.8 \times 10^4$ psi
Ti	$E = 1.53 \times 10^7$ psi	$\nu = 0.25$
	$E_T = 1.0 \times 10^5$ psi	$F_y = 1.6 \times 10^5$ psi

Note that the elastic constant hardening slope for the matrix, E_T, which is two orders of magnitude less than the corresponding Young's modulus, is assumed to represent the elastic-perfectly plastic behavior of the matrix material.

73

In order to keep the loaded boundary straight, piecewise uniform tensile stresses with different magnitudes were applied along the cross-sections of the fibers and the matrix, respectively. The ratio of the applied stresses f_{of}/f_{om} is equal to E_f/E_m, where f denotes the fiber and m the matrix.

Case studies are presented to illustrate the development of plastic zone in the matrix and the normal stress (f_y) in the fiber immediately ahead of the crack. The dimensionless stresses s_o and s_y shown in the figures are defined as: $s_o = f_{om}/F_{ym}$ and $s_y = f_y/F_{uf}$, where F_{ym} is the initial yield strength of the matrix, and F_{uf} is the ultimate stress of the fiber and its value is 4.5×10^5 psi. For convenience, Al-j and Ti-j are used as the case designations for the B/Al and B/Ti composites, respectively. For the full crack j=1 and for the partial crack (where matrix only is flawed) j=2.

Figures 60 and 61 indicate the deformed configurations with the loads for the cases of Al-1 and Ti-1, respectively. The dashed line shows the undeformed shape while the solid line represents the deformed body. Since the yield strength of aluminum is less than half that of the titanium matrix material, the elongation is small even though the applied stress on the aluminum matrix reaches the yield strength. However, the rotation is significant. Elongation and rotations are more pronounced in the case of B/Ti (Figure 61) because a much higher applied load is required to produce a stress on the matrix is half of the yield strength in titanium.

The deformed configurations of Al-2 and Ti-2 are plotted in Figures 62 and 63, respectively. Because only two strips of matrix were initially cracked and all the fibers still carried the load, the bending effect was small. Consequently, elongation is predominant. This can be seen from the figures.

$f_o/F_y = 0.10$ $f_o/F_y = 0.50$ $f_o/F_y = 1.00$
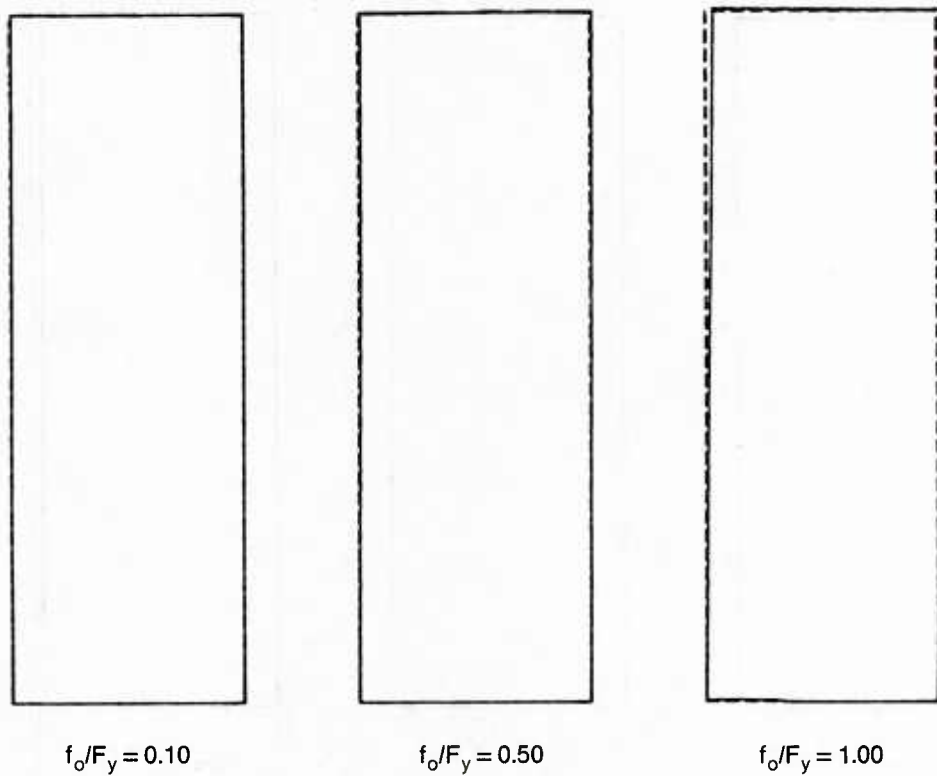
**Figure 60. The Deformed Configurations With Crack Through
Fibers and Matrix – Aluminum Matrix**

$f_o/F_y = 0.10$ $f_o/F_y = 0.30$ $f_o/F_y = 0.50$
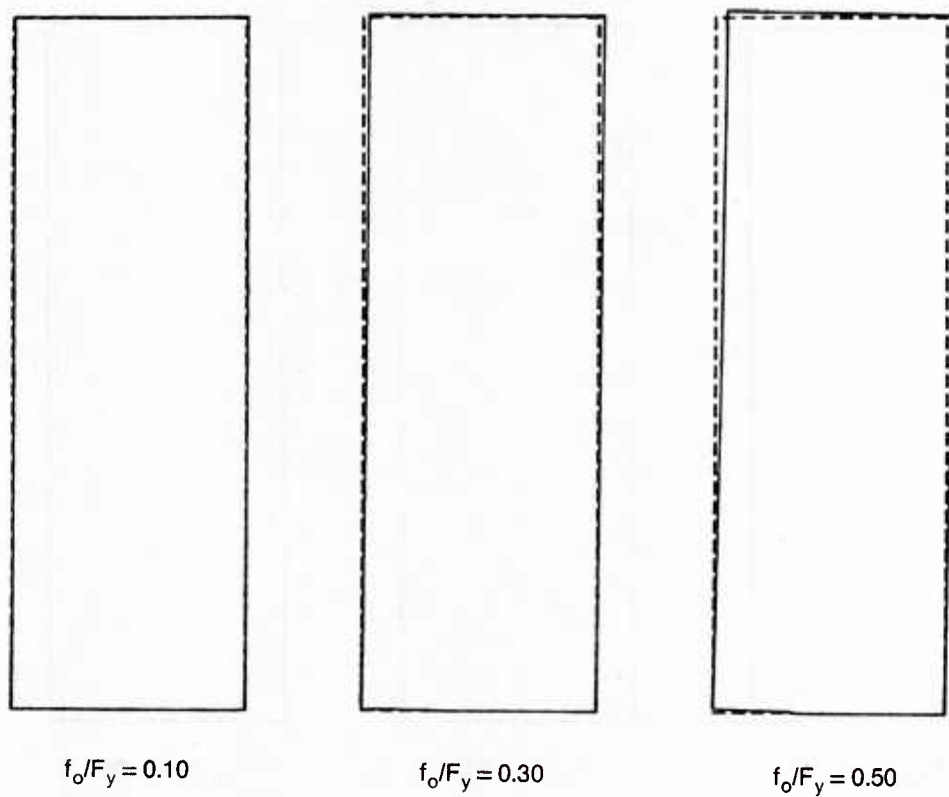
**Figure 61. The Deformed Configurations With Crack Through
Fibers and Matrix – Titanium Matrix**

75

$f_{om}/F_y = 0.40$ $f_{om}/F_y = 1.10$ $f_{om}/F_y = 1.60$
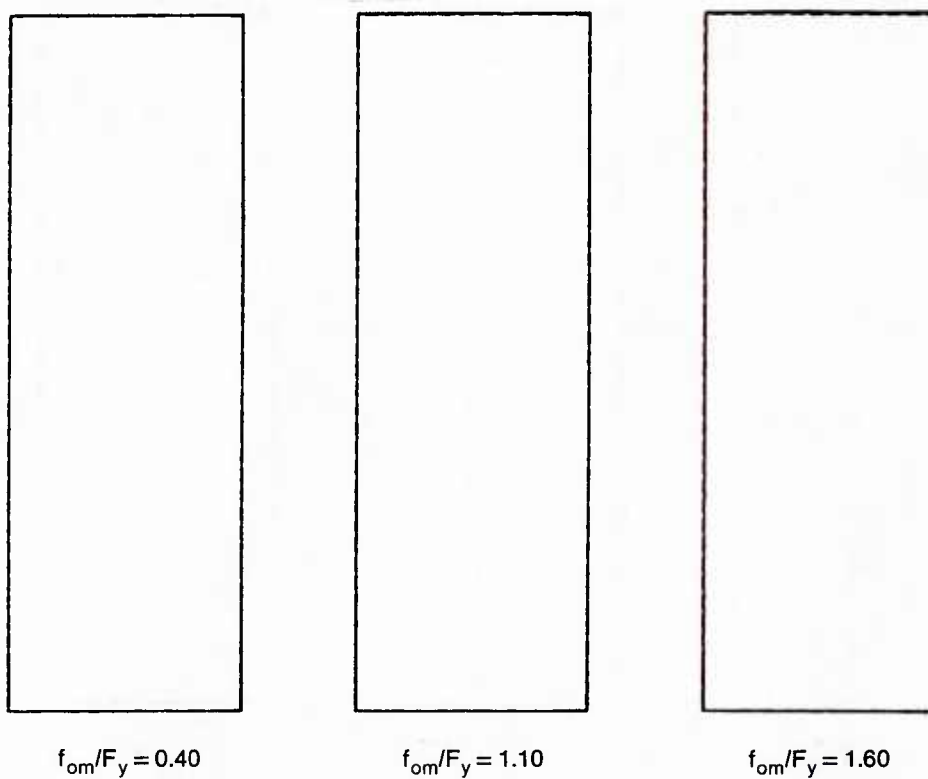
**Figure 62. The Deformed Configurations With Cracked Matrix/
Unflawed Fibers – Aluminum Matrix**

$f_{om}/F_y = 0.10$ $f_{om}/F_y = 0.50$ $f_{om}/F_y = 1.00$
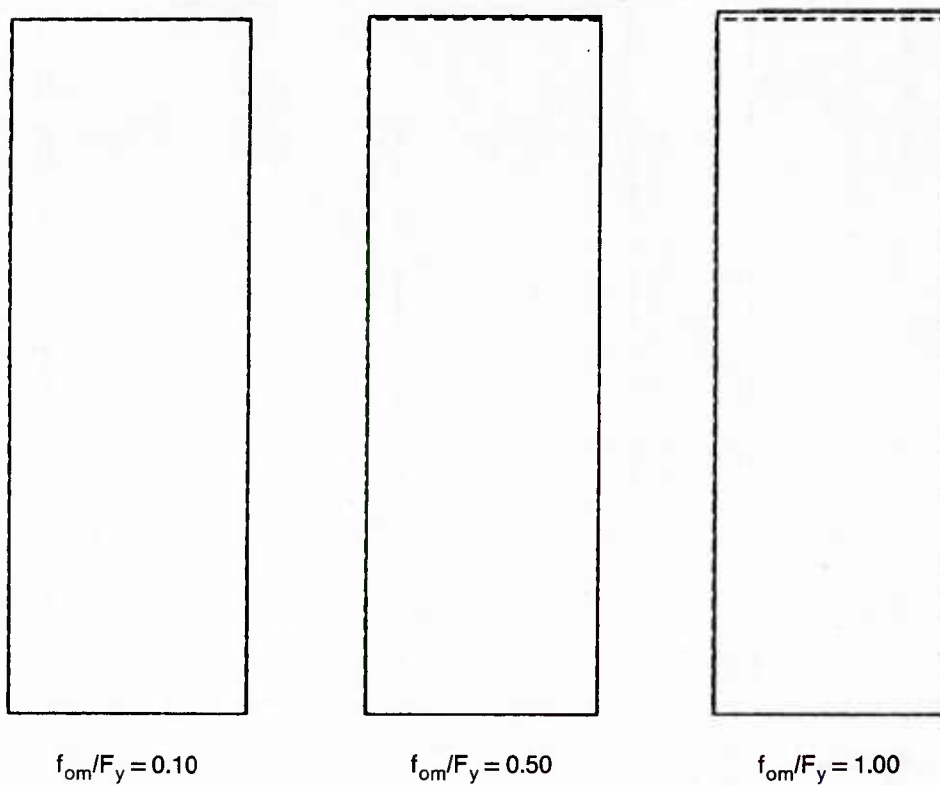
**Figure 63. The Deformed Configurations With Cracked Matrix/
Unflawed Fibers – Titanium Matrix**

76

In the numerical computation, the state of stress was checked at each Gaussian point. Figure 64 presents the yielded Gaussian points for Case Al-1 at different load levels. A dot shown in the figures denotes a yielded Gaussian point. It is found that plastic yielding starts at the Gaussian point in the aluminum strip nearest the crack tip. The plastic zone then extends from the region close to the crack tip near the loaded edge. A second plastic zone initiates at the point in the next matrix strip straight ahead of the crack as load increases. From Figure 64 we see that the plastic zone spreads further into the other matrix strips except for the region where compression due to bending reduces the level of tensile stresses.

Similar results of the growth of plastic yielding for Case Ti-1 are presented in Figure 65.

In Case 2 the initial cracks are assumed to exist in the left two matrix strips with a total of four crack tips. The finite element results showing plastic zones at different load levels are presented in Figures 66-67. As can be seen from these figures, both cases Al-2 and Ti-2 exhibit similar behavior.

Yielding in the matrix first appears in the areas near the tips of the inner crack and then in the region close to the tips of the outer crack. It should be noted that the growth of plastic zones is very slow. This means that the intensified stresses are produced only in the small regions near the crack tips. An overwhelming plastic yielding occurs when the applied stress s_o is nearly equal to one. As s_o becomes greater than one, the whole matrix yields except for the regions close to the cracks because of the stress free boundary condition.

A matrix crack near the fiber causes the fiber stress to rise. This increase in stress may induce fiber fracture. The dimensionless normal stress s_y distributions in the (third) fiber immediately ahead of the crack for the four cases studied are shown in Figures 68-71.

$f_{om}/F_y = 0.2$ $f_{om}/F_y = 0.3$ $f_{om}/F_y = 0.4$

$f_{om}/F_y = 0.5$ $f_{om}/F_y = 0.6$ $f_{om}/F_y = 0.7$
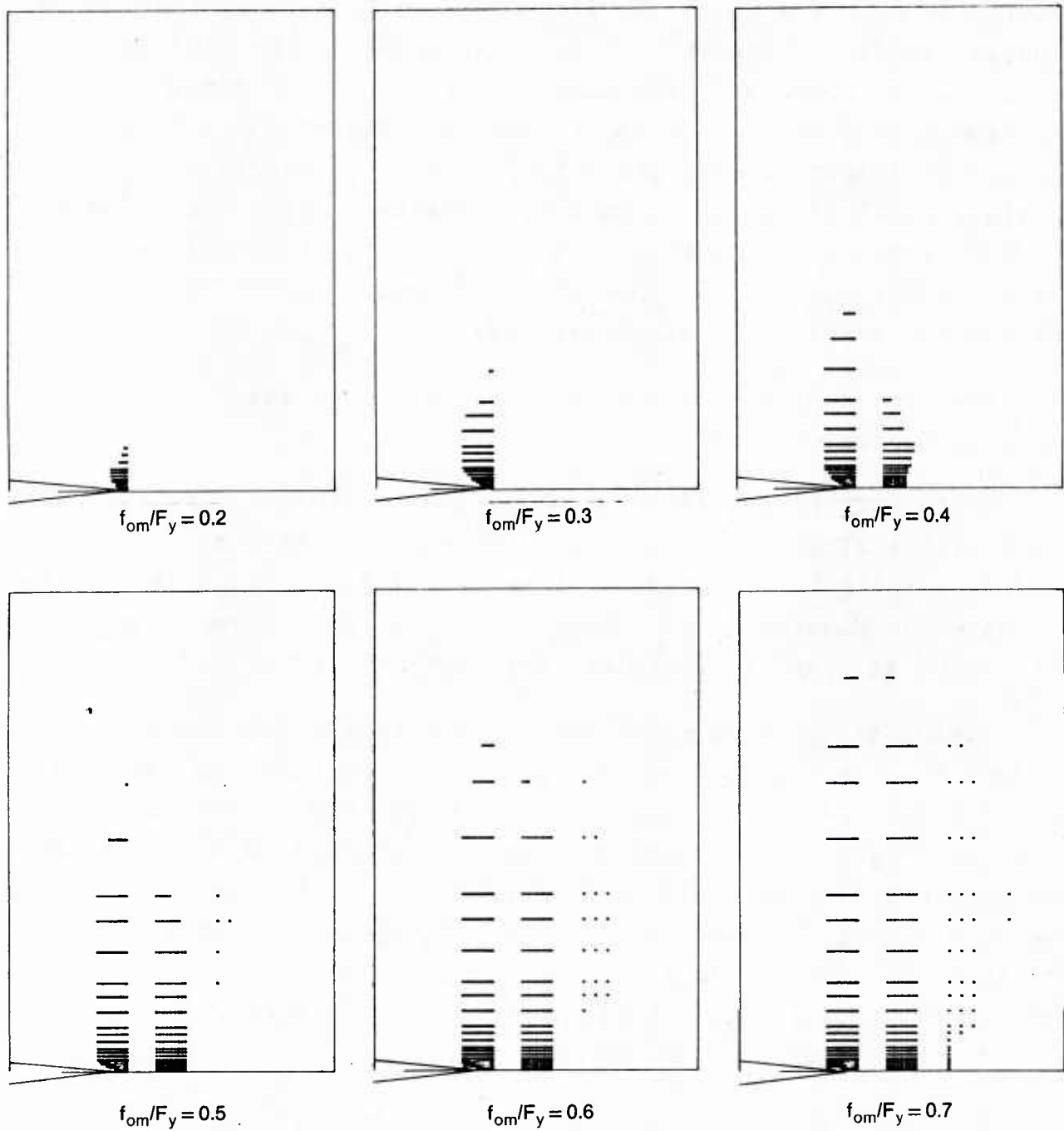
Figure 64. Matrix Yielding in Through Cracked Boron/Aluminum

$f_{om}/F_y = 0.2$ $f_{om}/F_y = 0.3$ $f_{om}/F_y = 0.4$

$f_{om}/F_y = 0.5$ $f_{om}/F_y = 0.6$
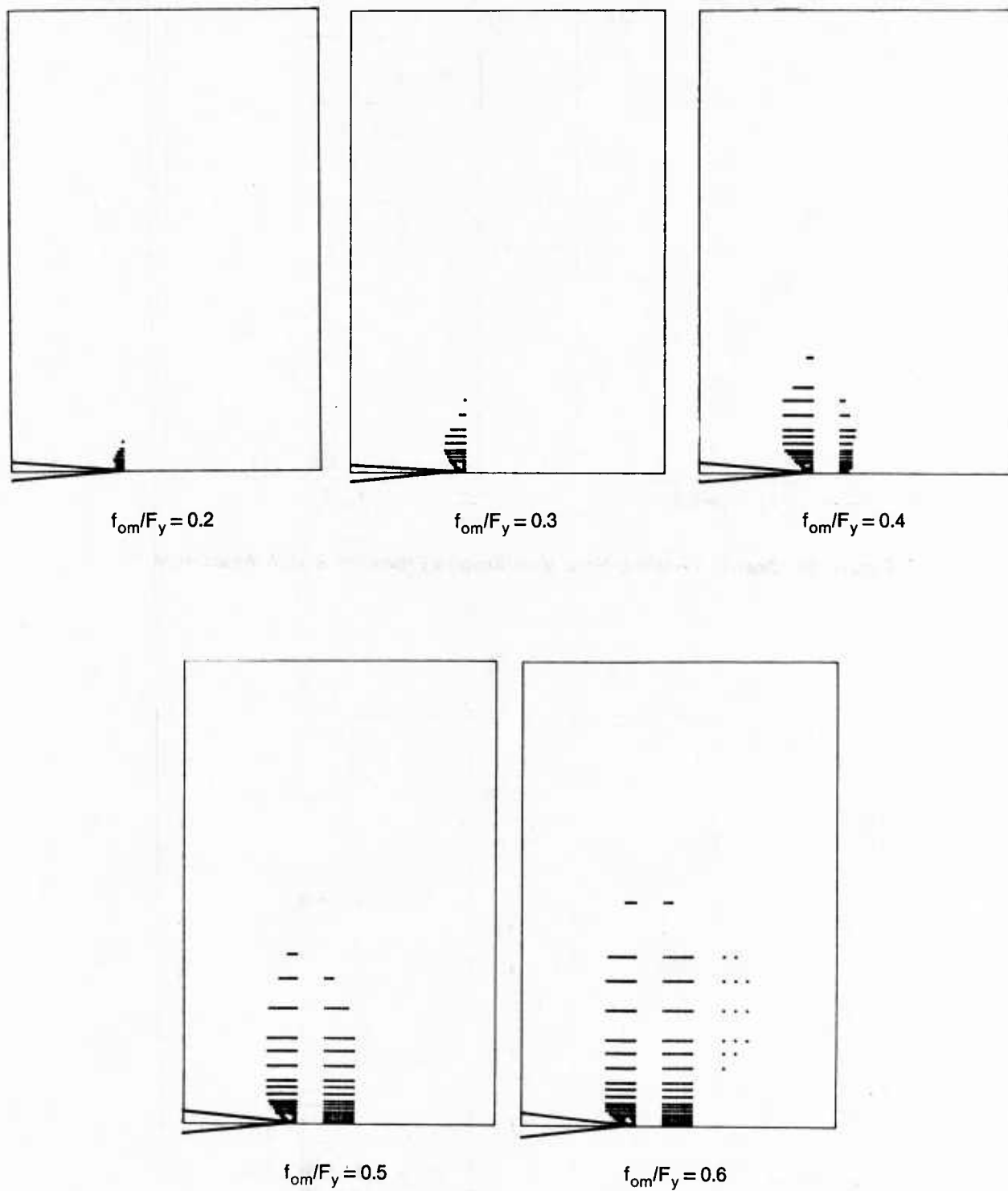
Figure 65. Matrix Yielding in Through Cracked Boron/Titanium

79
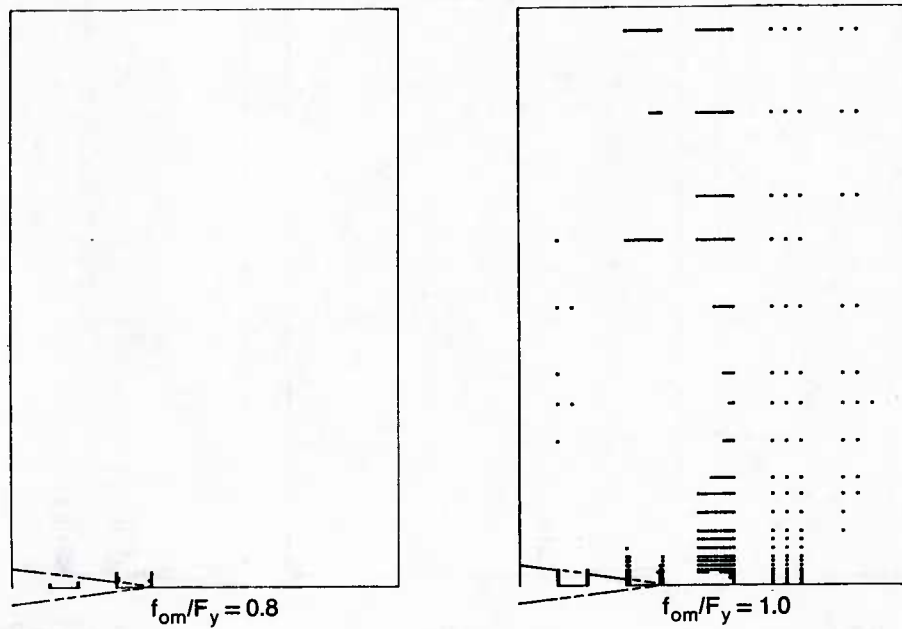
Figure 66. Matrix Yielding Near Continuous Fibers in Boron/Aluminum

$f_{om}/F_y = 0.8$ $f_{om}/F_y = 1.0$

$\sigma = 0.8\ \sigma_y$ $\sigma = 1.0\ \sigma_y$
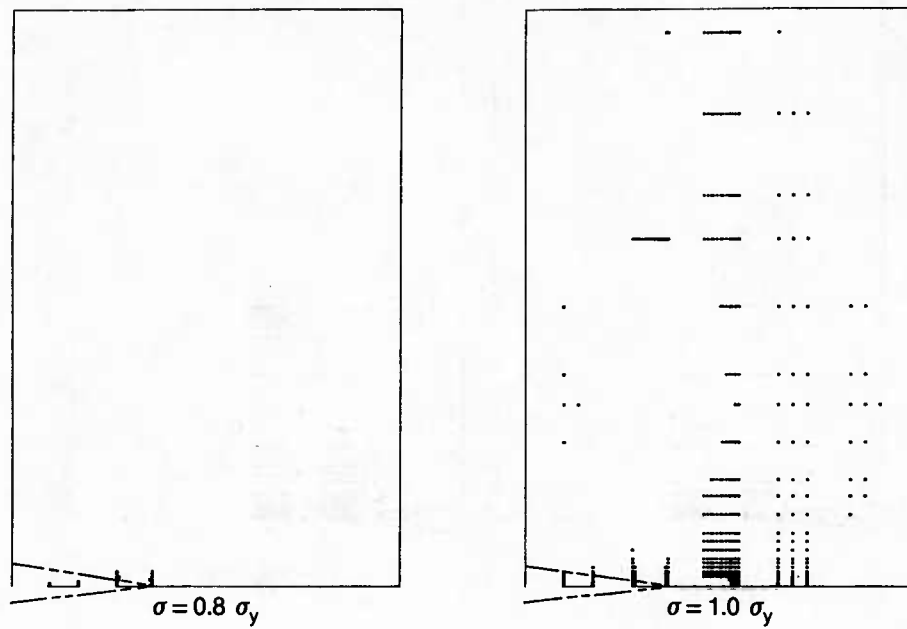
Figure 67. Matrix Yielding Near Continuous Fibers in Boron/Titanium
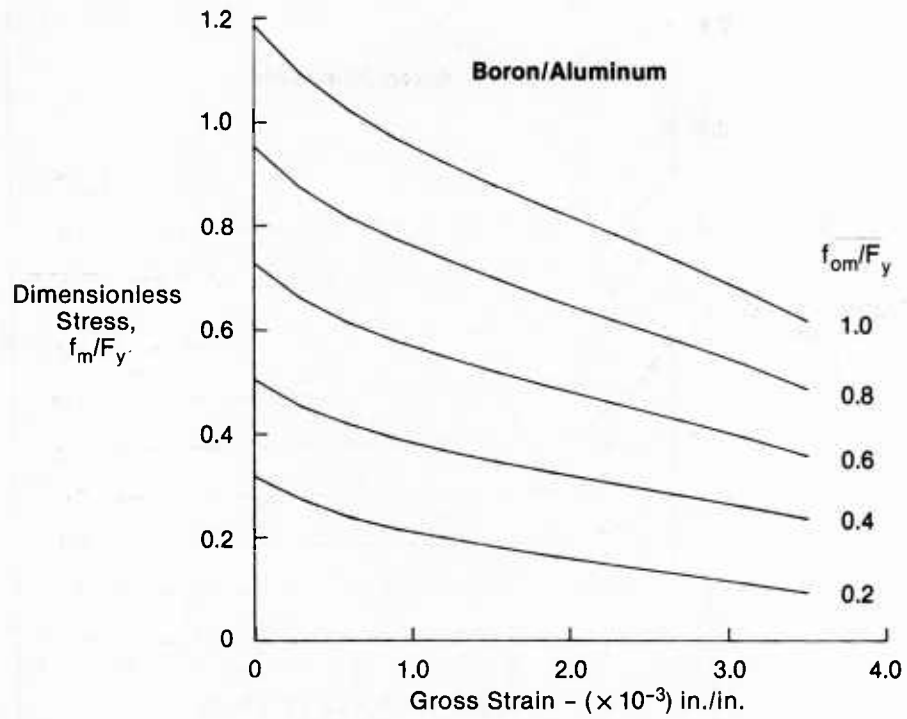
Figure 68. The Dimensionless Normal Stress Distributions in the Fiber Immediately Ahead of a Through Crack in Aluminum
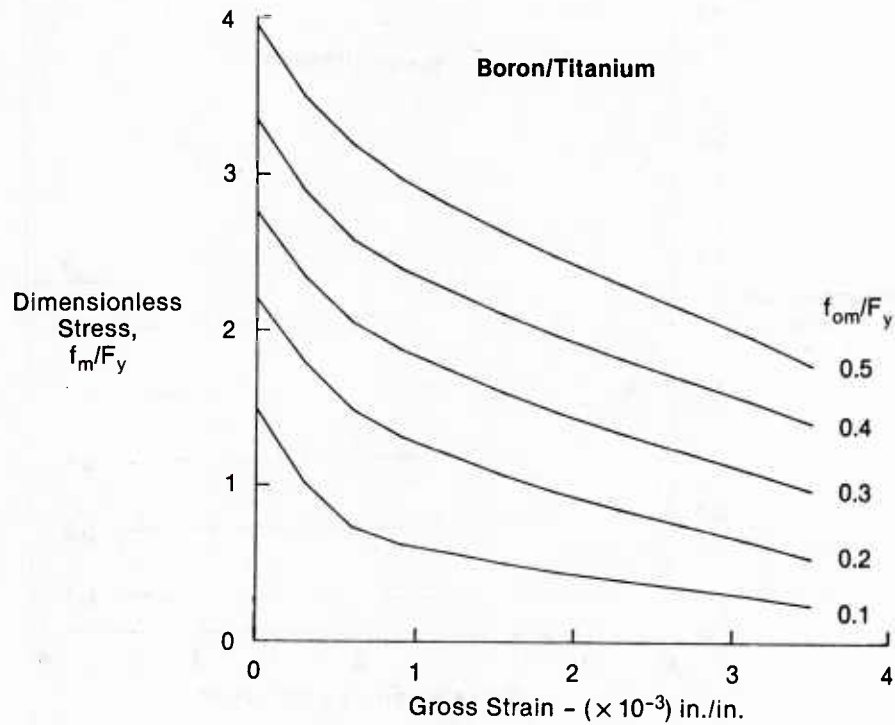
Figure 69. The Dimensionless Normal Stress Distributions in the Fiber Immediately Ahead of a Through Crack in Titanium

81
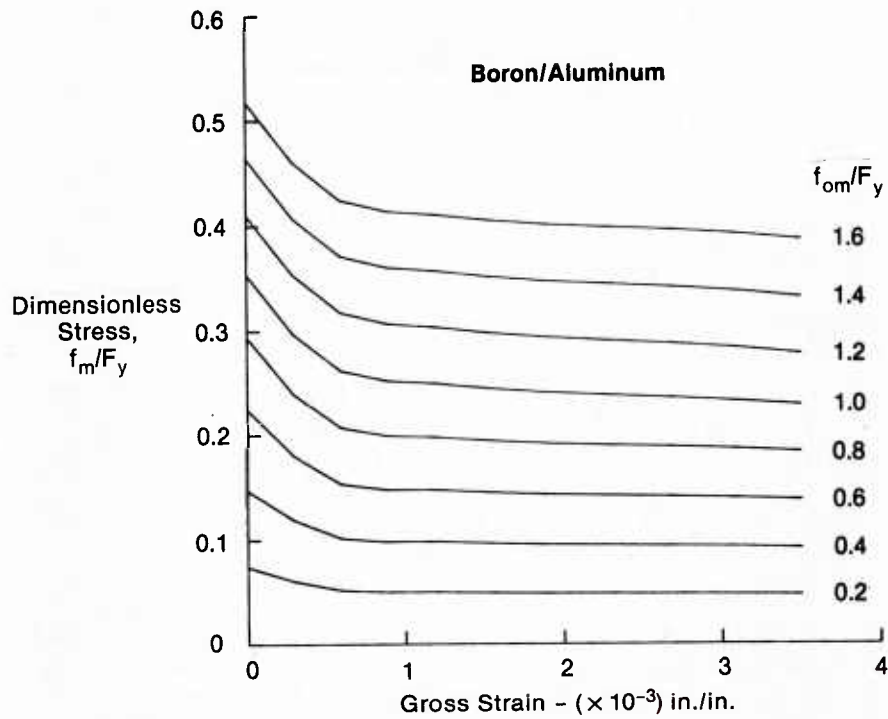
Figure 70. The Dimensionless Stress Distributions in the Third Fiber for Cracked Aluminum Matrix
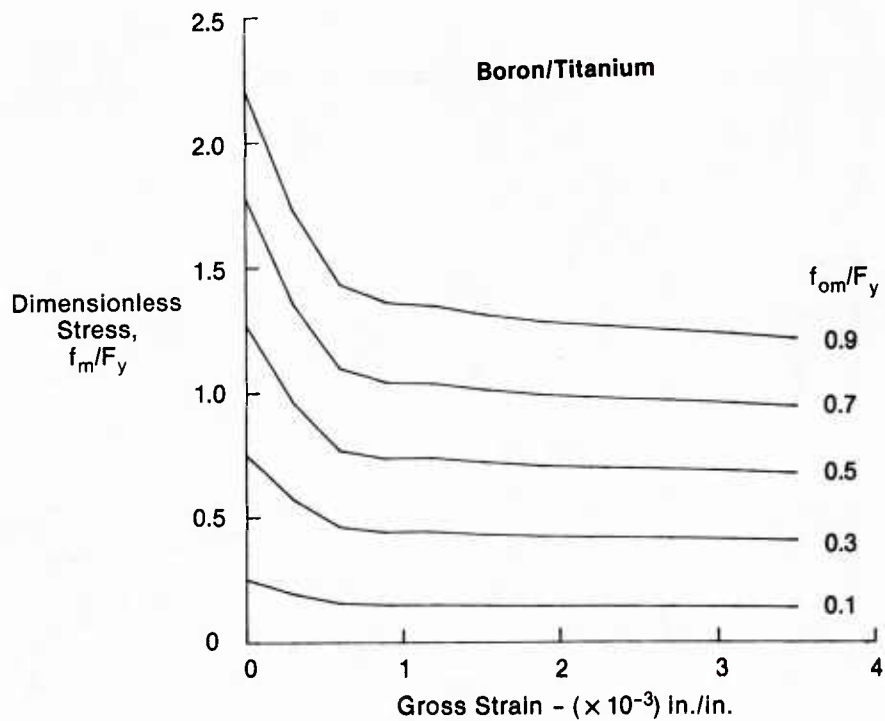
Figure 71. The Dimensionless Stress Distributions in the Third Fiber for Cracked Titanium Matrix

Note that in Figure 68 the dimensionless applied stress in the matrix strips $s_o = f_{om}/F_{ym}$ is nondimensionalized by the aluminum yield strength; while in Figure 69 for B/Ti s_o is nondimensionalized by the titanium yield strength. Thus, for the same numerical value of s_o, there is a much higher applied stress in the B/Ti composite.

From Figures 68 and 69 one can conclude that for B/Al it would be difficult to exceed the ultimate strength of the boron fiber even at the crack tip unless the applied stress is high enough to yield the aluminum matrix in the whole panel. On the other hand, in the B/Ti material the near tip stress in the fiber can easily surpass its ultimate strength at a relative low load, $s_o = 0.1$. This explains why it is so much more difficult to drive a crack perpendicular to the fibers through a B/Al composite panel than through a B/Ti panel.

The results presented in Figure 71 indicate that a matrix crack between unfailed fibers in the B/Ti composite can cause fiber stresses high enough to propagate the crack through boron fibers. Of course high loads (above half of matrix yield strength) are required to initiate this failure.

d. <u>Results for Case 3</u> - The case of a crack situated at an angle 45° to the fiber was considered. The crack was assumed to start from the left boundary and end at the interface of the second matrix strip and the third fiber, see Figure 58. A total of 37 x 37 elements was used to model the whole domain. The physical dimensions of the model were 0.04 inch thick x 0.24 inch wide. For convenience, both 8-node quadrilateral and 6-node triangular elements were employed in the region near the crack.

Figure 72 shows a part of the finite element mesh in this region. The vertical displacement v was fixed along the bottom boundary. In order to avoid rigid body motion, the longitudinal displacement u at the lower left corner was suppressed. Uniform

83

tensile stress but with different magnitude was applied on the cross-sections of the fiber and the matrix along the top boundary. The ratio, f_{of}/f_{om} of the applied stresses on the cross-sections was set equal to E_f/E_m, where $_f$ denotes the fiber and $_m$ the matrix.
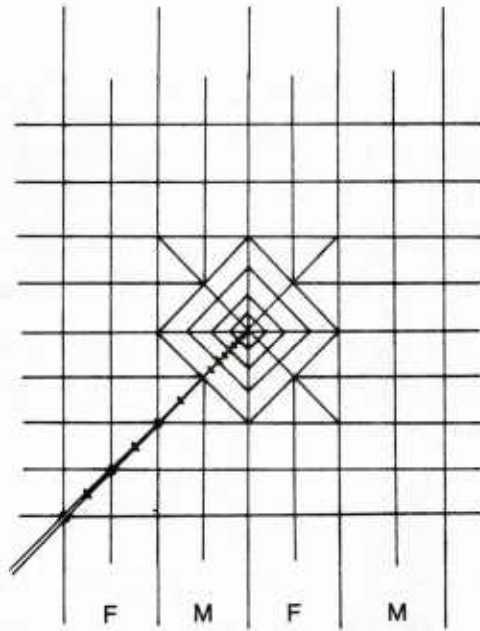
Figure 72. Finite Element Mesh in the Region Near the Crack Tip

Figure 73 presents the development of the plastic zone in the matrix strips. As shown in Figures 73 and 74, for both composites the first plastic zone appears in the upper region at the crack tip; then the second emerges in the lower part. However, when the load increases, the second plastic zone extends faster. Subsequent loading makes the plastic zone symmetric with respect to the horizontal line passing through the crack tip.

The dimensionless normal stress distribution of s_y in the fiber immediately ahead of the crack for the two composites is plotted in Figures 75 and 76. The stress was calculated along the line at y = constant through the crack tip. Comparing the stress distributions in these figures and those for the transversely cracked panel (Figures 68-69), we note a similar trend.

84

$f_{om}/F_y = 0.1$　　　　$f_{om}/F_y = 0.2$　　　　$f_{om}/F_y = 0.3$　　　　$f_{om}/F_y = 0.4$

$f_{om}/F_y = 0.5$　　　　$f_{om}/F_y = 0.6$　　　　$f_{om}/F_y = 0.8$　　　　$f_{om}/F_y = 1.0$
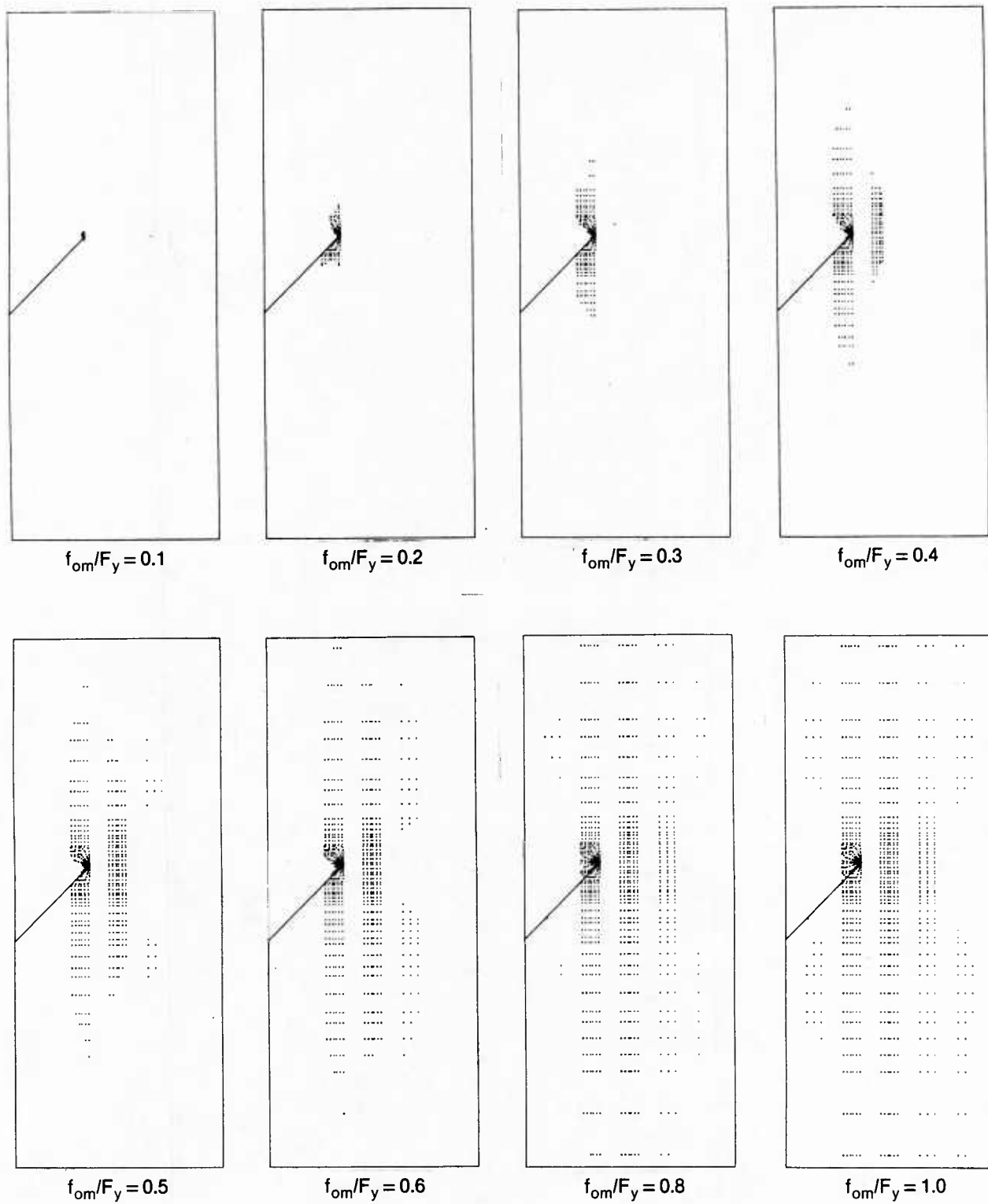
Figure 73. Matrix Yielding Near an Off-Axis Crack in Boron/Aluminum

85

$f_{om}/F_y = 0.1$ $f_{om}/F_y = 0.2$ $f_{om}/F_y = 0.3$ $f_{om}/F_y = 0.4$

$f_{om}/F_y = 0.5$ $f_{om}/F_y = 0.6$ $f_{om}/F_y = 0.8$ $f_{om}/F_y = 1.0$
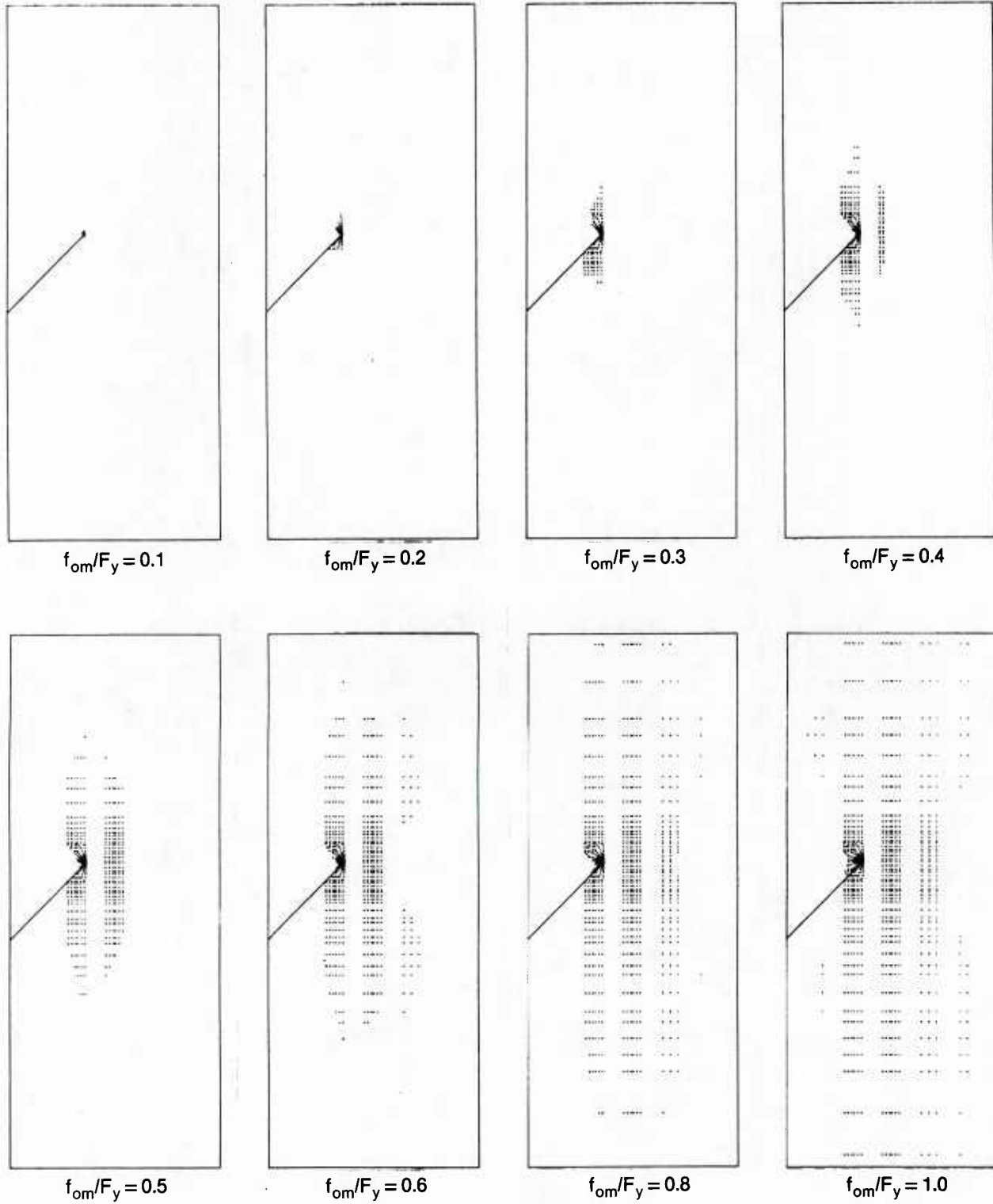
Figure 74. Matrix Yielding Near an Off-Axis Crack in Boron/Titanium

86
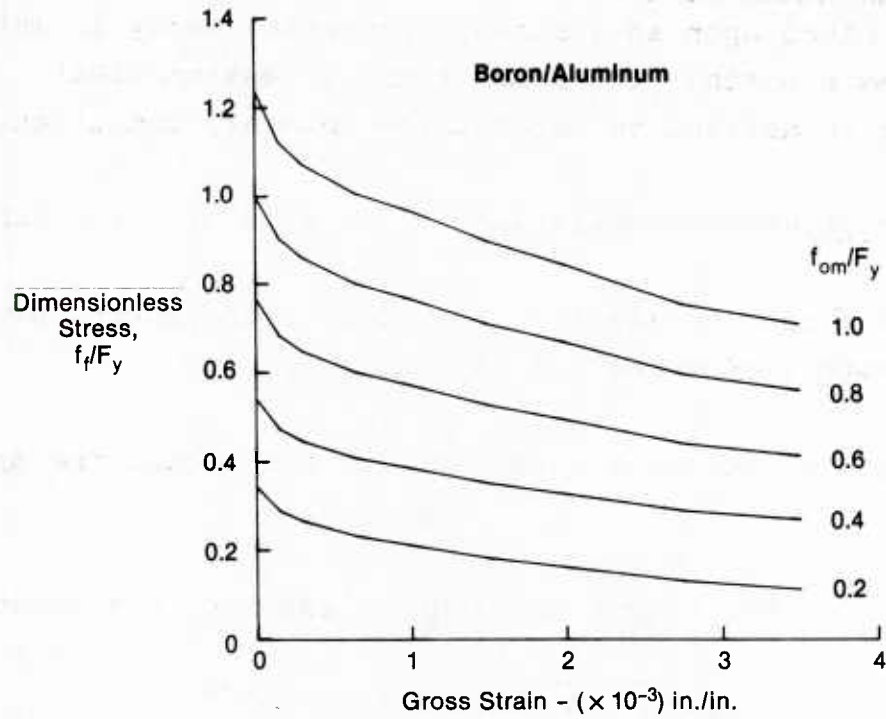
Figure 75. Normal Stress Distributions in the Fiber Immediately Before the Crack Tip in Boron/Aluminum Composite With Off-Axis Crack
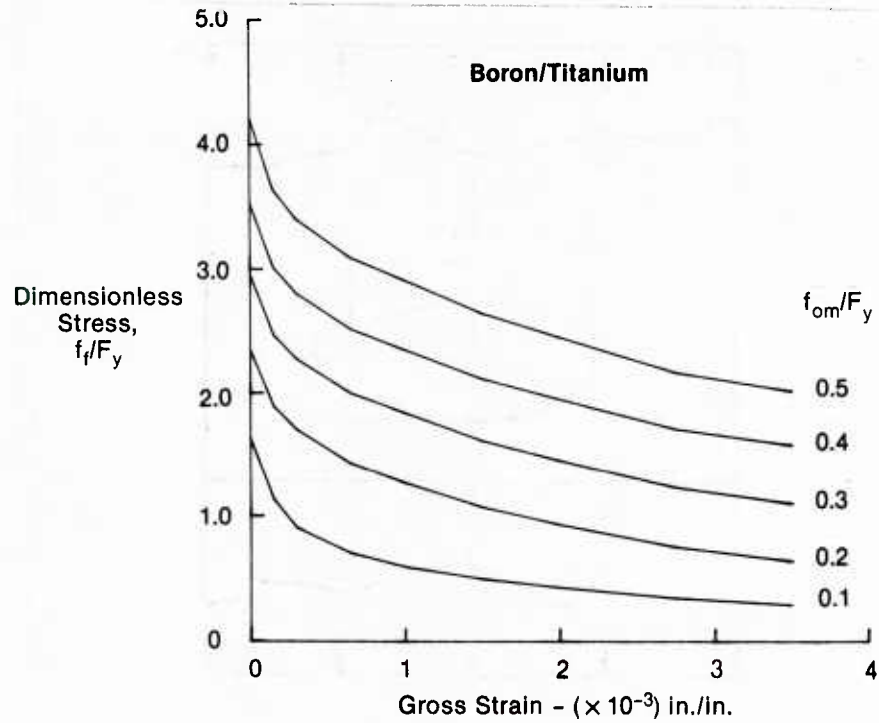
Figure 76. Normal Stress Distributions in the Fiber Immediately Before the Crack Tip in Boron/Titanium Composite With Off-Axis Crack

87

3. NOTCHED LAMINATE STRESS ANALYSIS - WIDTH EFFECTS - The stress analysis is based upon an assumed exponential decay in any stress gradient from a notch. The form of the stress gradient relationship is derived to match three boundary conditions:

1) the stress concentration at the edge of the notch, K_t

2) the stress gradient at the edge of the notch, given by Seely and Smith (Reference 22) as $C_1 K_t / \rho$

3) the load across the net section must equal the applied load.

The form of the stress gradient is assumed to represented by

$$f/f_g = A + B[1 + (x-a)/\rho]^{-C}$$

where $\rho = b^2/a$ and the notch parameters are shown in Figure 77.
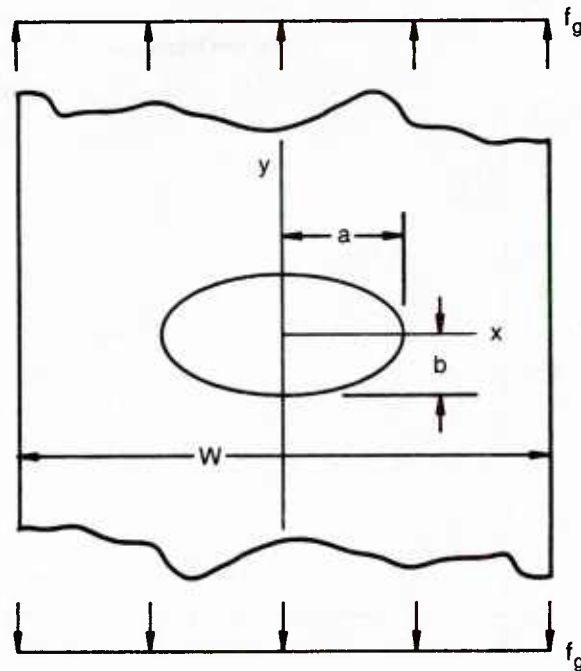
Figure 77. Elliptic Notch in a Finite Width Plate

88

From Condition (1),

$$f/f_g(x=a) = K_t = A + B$$

From Condition (2),

$$df/dx(x=a) = -C_1 K_t/\rho \text{ or}$$

$$C = C_1 K_t/B$$

Condition (3) is used to determine B. The basic expression of Condition (3) is

$$P = Wtf_g = 2t \int_a^{W/2} f dx$$

This can be rewritten as

$$1 = 2a/W \int_1^{W/2a} (f/f_g)\, d(x/a)$$

With proper substitutions it can be shown that

$$B = \frac{1-K_t(1-2a/W)}{(2a/W-1)+2b^2/(Wa(1-C))\{[1-(a/b)^2+(a/b)2W/2a]^{1-C}-1\}}.$$

Because B and C are bound up in the second condition, the solution is iterative in the strictest sense. However, for infinite plates, A = 1 and B = K_t-1. We used this expression and some known conditions to solve for C_1. Assuming an infinite width plate, the second condition becomes

$$C = C_1 K_t/(K_t-1)$$

For an elliptical notch, K_t approaches infinity as the ellipse collapses to a crack. Therefore, for a crack C must equal C_1 and C_1 must approach 0.5 so that the solution will approach the

theoretical stress gradient ahead of a crack in an infinite plate. For the circular hole in an infinite plate, $C_1 = 3.25$, was found to give good correlation with the classical stress gradient solution, Figure 78. For an elliptical hole having a 1 to 3 aspect ratio, $C_1 = 1.71$, was found to give good correlation with Inglis' results (Reference 23). Therefore, C_1 was selected to be

$$C_1 = 0.5 + 1.6667\sqrt{b/a}$$

To account for the reduction in gradient which occurs as $2a/W$ approaches 1, we used the finite width correction of Koiter (Reference 24). The final expression becomes

$$C_1 = (0.5 + 1.6667\sqrt{b/a})\sqrt{1-2a/W}$$

Having C_1, the remaining terms can be determined directly.
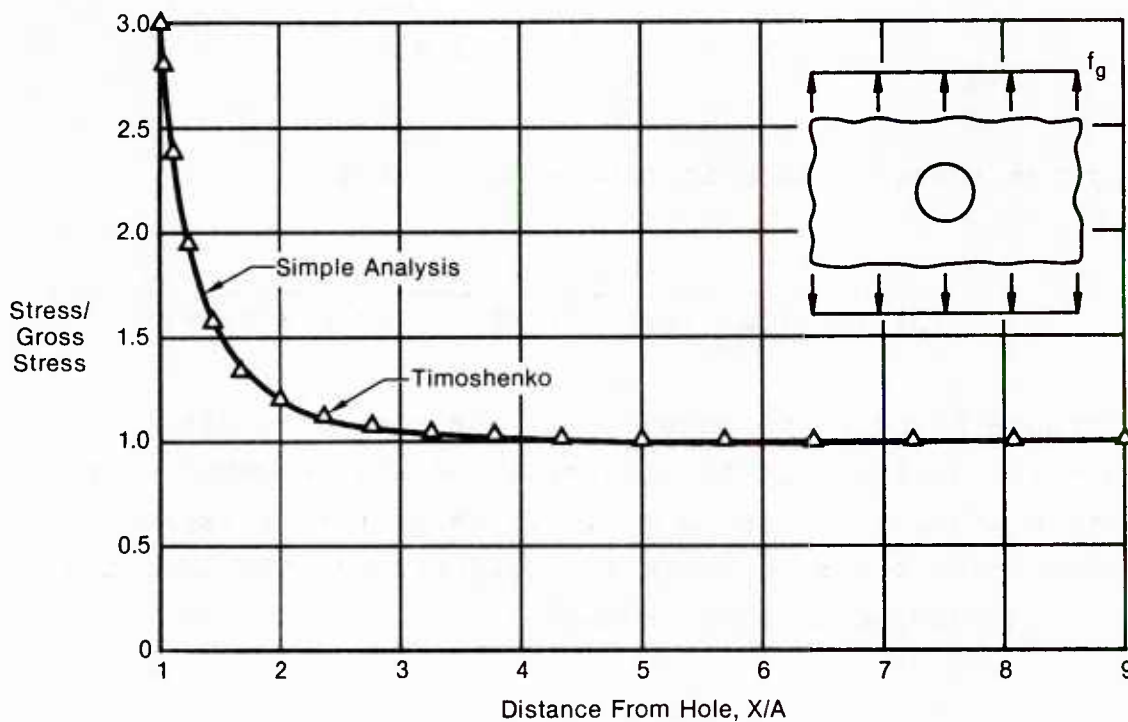
Figure 78. Stresses Near Holes in Infinite Isotropic Plates

90

To account for geometry and material orthotropy, we need only know the effect of these parameters on K_t. K_t is the gross stress concentration determined as

$$K_t = K_{t\ net}/(1-2a/W)$$

We currently express K_t net as a fit to the elliptical notch results in Peterson's handbook (Reference 25), as shown in Figure 79. The fit is expressed as

$$K_{t\ net} = 2+f_1f_2{}^2+f_1f_2{}^4+0.643f_3(1-f_4{}^2)+0.167f_3(1-f_4{}^4)+0.109f_3f_5(2a/W)$$

where

$$f_1 = K_{tg}/2-1$$

$$f_2 = 1-2a/W$$

$$f_3 = a/b-1$$

$$f_4 = 4a/W-1$$

$$f_5 = 1-(2a/W)^{100}$$

and

$$K_{tg} = 1 + a/b[E_1/G_{12}-2v_{12}+2\sqrt{E_1/E_2}]^{1/2}$$

which is the exact solution derived by Lehknitskii (Reference 26) for orthotropic plates of infinite width and degenerates to the well known K_t of 3 for infinite, isotropic plates.

This stress analysis was verified by comparison with many known limiting cases for plates of finite and infinite width in both isotropic and orthotropic materials. The comparison with infinite, isotropic plate results was shown in Figure 78.
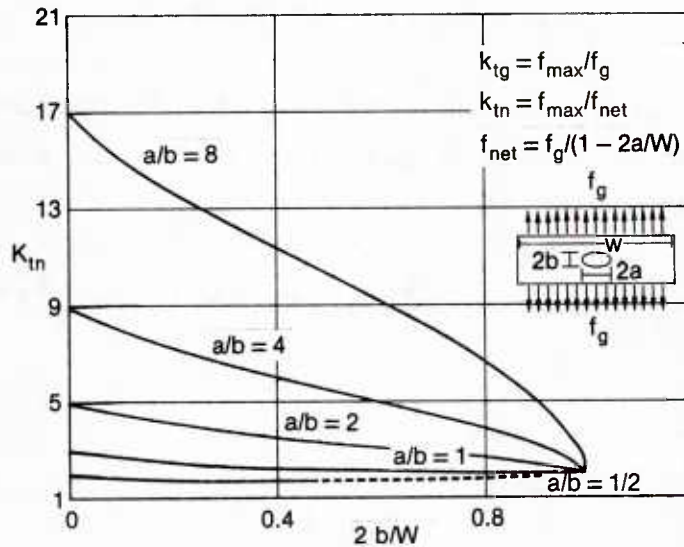
Figure 79. Stress Concentration Factors for an Elliptical Hole in a Finite Width Plate in Tension

For isotropic materials, comparisons were made to solutions from Inglis (Reference 23), Figure 80, for elliptical slots in infinite width plates, Howland (Reference 27), Figure 81, for circular holes in finite width plates, and with finite element analyses, for circular holes in very narrow plates, Figure 82. In addition, when the hole diameter is very nearly as wide as the plate, the K_t approaches $2/(1-D/W)$ as shown by Peterson (Reference 25) and the stress is almost linear across the net section, as shown in Figure 82.

For orthotropic plates with central notches, the analysis is derived to be exact for infinite plates and was verified by comparisons with Lekhnitskii's solutions for highly orthotropic plates, as shown in Figure 83. For finite width plates, the analysis was compared with both finite element and boundary collocation analyses (Figure 84).
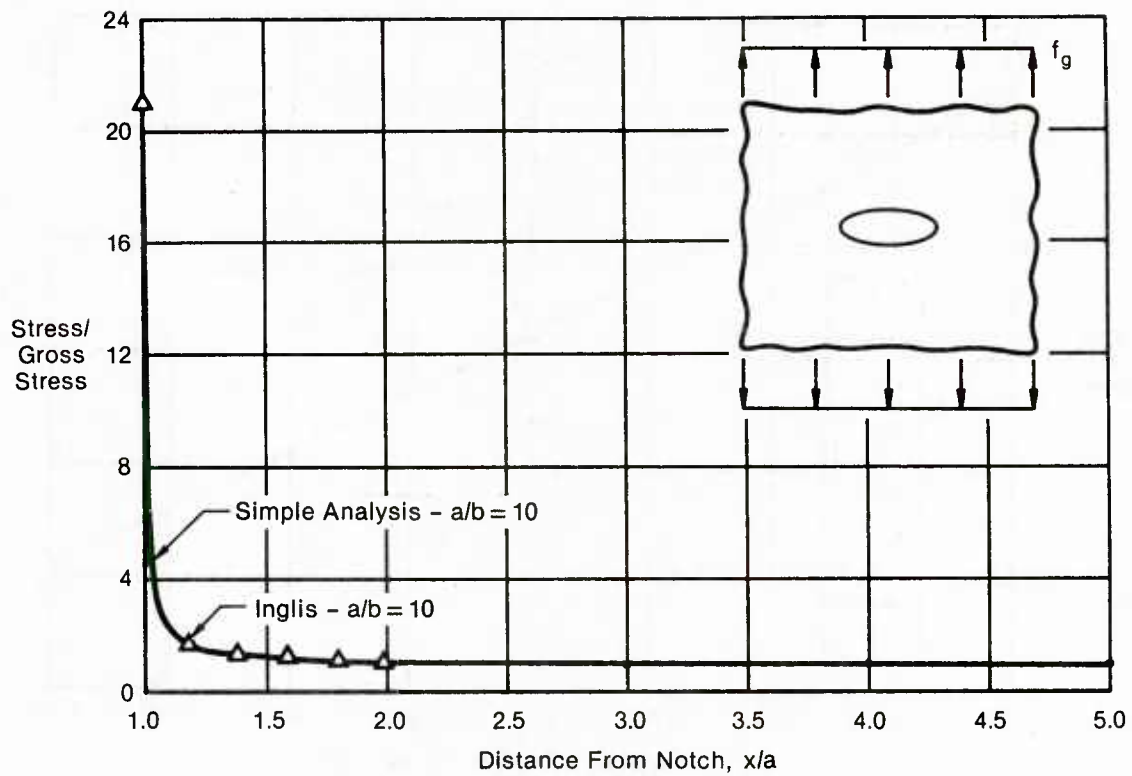
Figure 80. Stresses Near an Ellipse in an Isotropic Plate
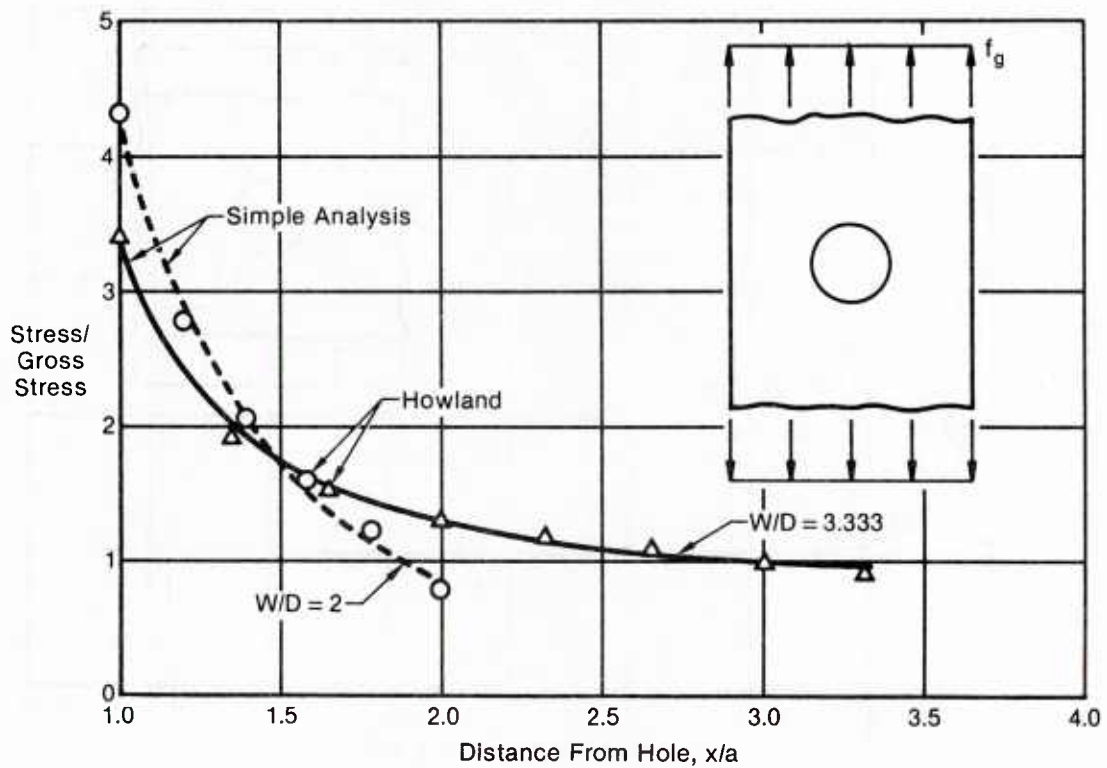
Figure 81. Stresses Near Holes in Finite Isotropic Plates

93
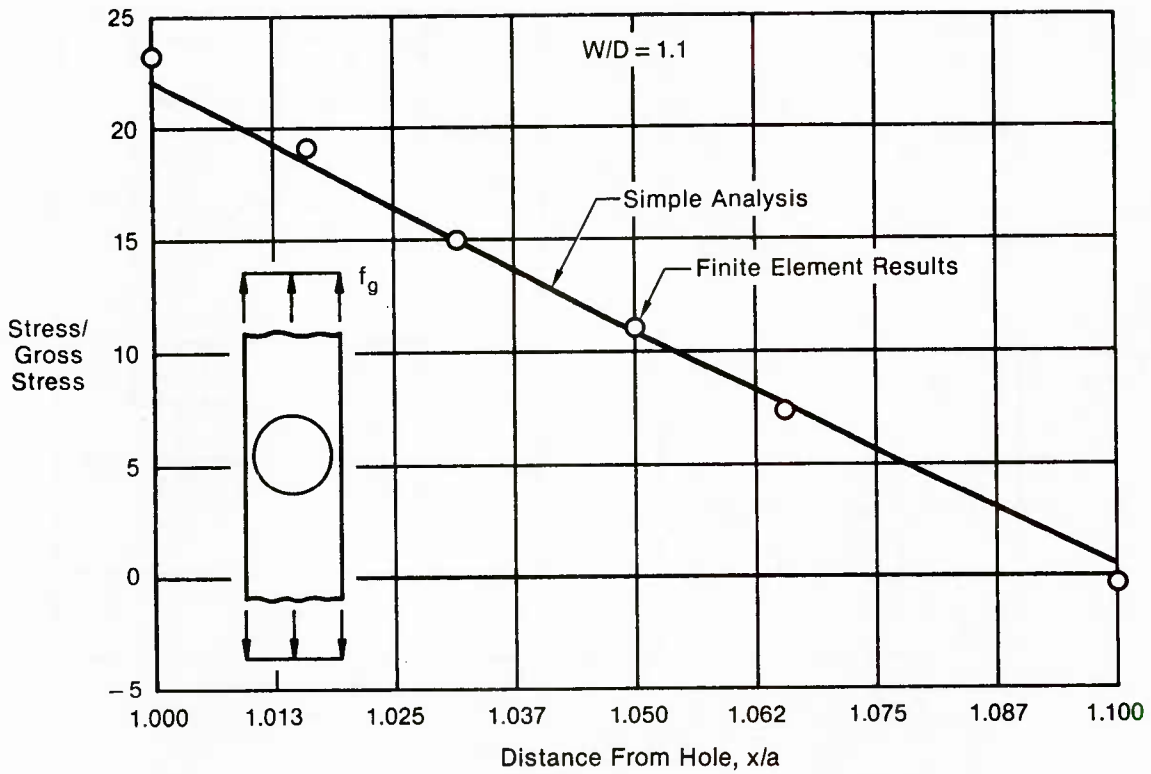
Figure 82. Stresses Near Holes in Very Narrow Plates
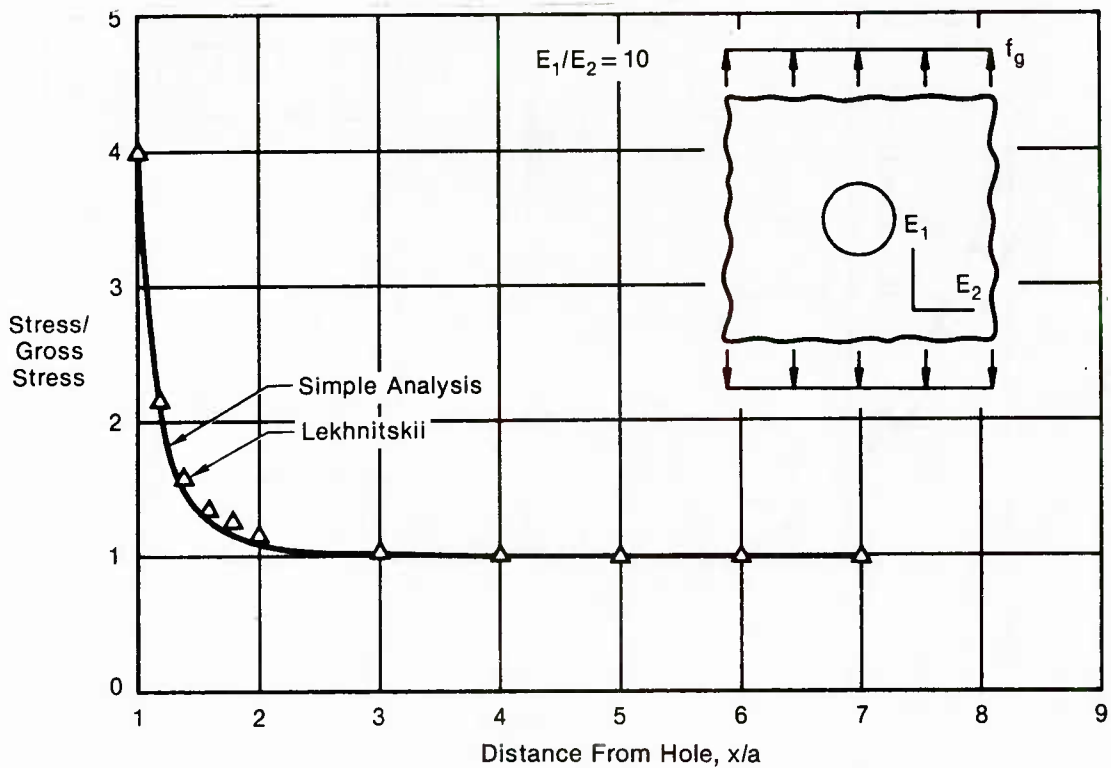
Figure 83. Stresses Near Holes in Infinite Orthotropic Plates

94
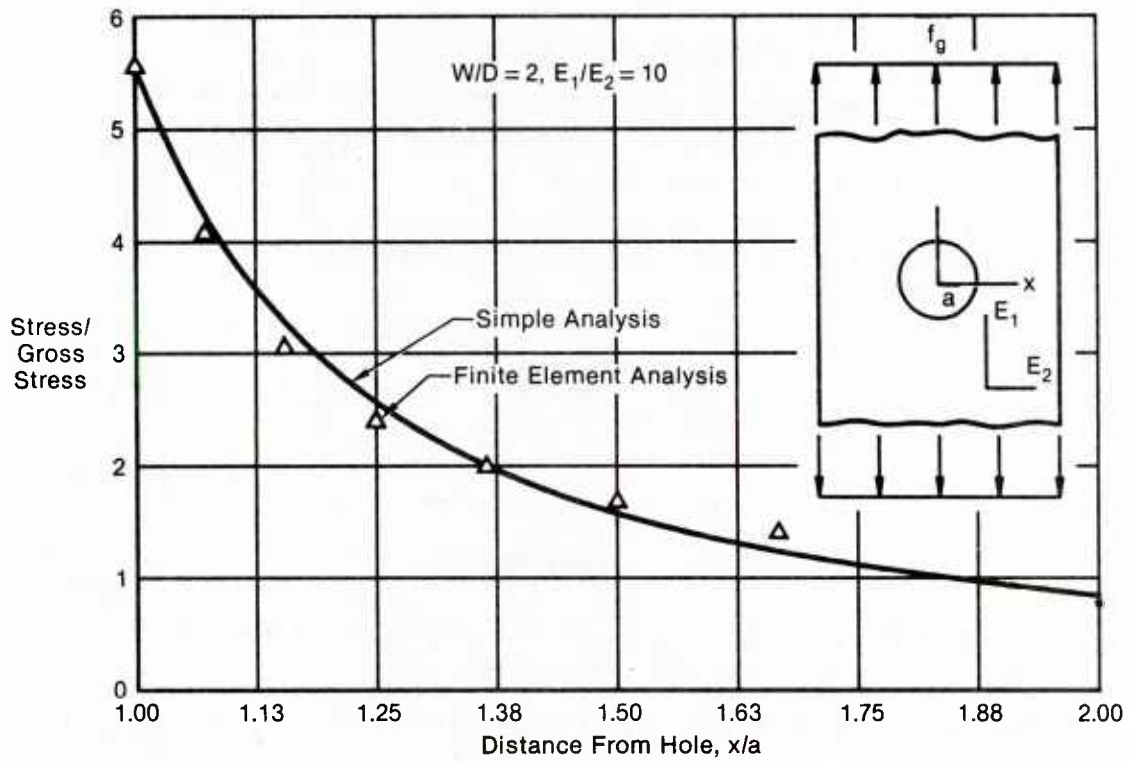
Figure 84. Stresses Near Holes in Finite Orthotropic Plates

An even more extensive check of the analysis was performed, using boundary collocation analyses, to check the specific geometries tested in this program (Figure 85). The comparison shown encompasses a wide range of orthotropic materials. With the net section K_t we can compute the net section stress distribution very accurately using the methods described herein, however, to determine how MMC materials fail in fatigue, we need to be able to compute the stresses around the hole boundary as well.

In order to compute the stresses at any location around the hole boundary, we first examined the elasticity solutions for stresses about holes in isotropic and orthotropic plates having infinite width. Lekhnitskii's (Reference 26) results show that the stress tangent to a hole in an orthotropic plate can be expressed as

$$f_t/f_g = E_y/E_x[1/2(1+n-\sqrt{E_y/E_x}) - 1/2(1+n+\sqrt{E_y/E_x})\cos 2\theta]$$

where $n = [E_y/G_{yx} - 2v_{yx} + 2\sqrt{E_y/E_x}]^{1/2}$.

95
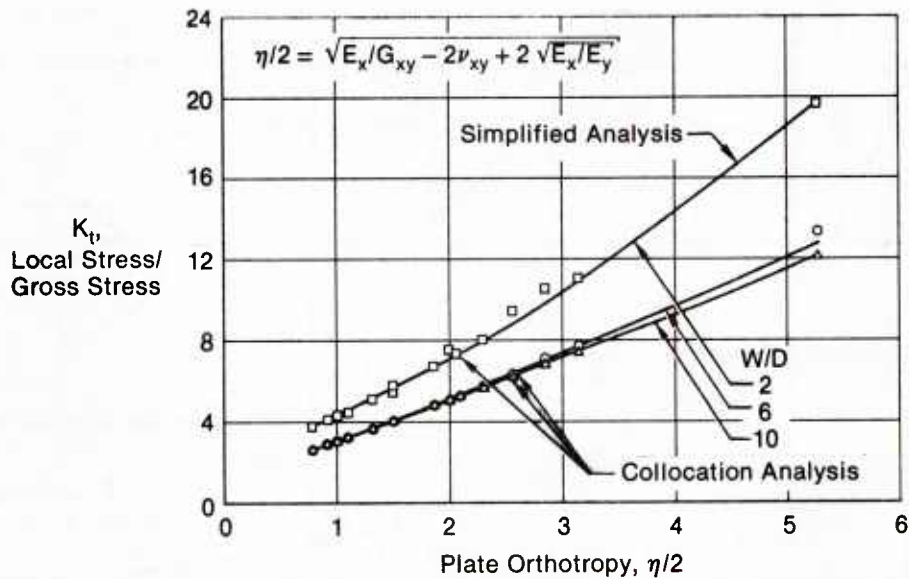
Figure 85. Stress Concentrations Predicted by Simple Analysis Agree With Collocation Results

Recognizing the $n + 1 = K_t$ at $\theta = 90°$ and $-E_y/E_x = K_{t0}$, the K_t at $0°$, it appeared that the stress distribution about a hole in any infinite plate (isotropic or orthotropic) can be expressed as a combination of the K_t at the $0°$ and $90°$ points:

$$f_t/f_g = E_t/E_y[1/2(K_t A + K_{t0}B) - 1/2(K_t A - K_{t0}B)]\cos 2\theta$$

By choosing $\theta = 0°$ and $90°$ and solving for A and B an expression for the tangential stress at any point on the hole periphery can be found from:

$$f_t/f_g = 1/2[E_t/E_y K_t + E_t/E_x K_{t0}] - 1/2[E_t/E_y K_t - E_t/E_x K_{t0}]\cos 2\theta$$

Moreover, as long as K_t and K_{t0} are computed for the finite width of the structure being analyzed, this expression can be used to accurately and rapidly compute the tangential stress about an open hole in any plate. The effect of finite width on K_t is determined as discussed previously. The expression for stress concentration at the top of the hole was derived as

$$K_{t0} = -\frac{\sqrt{Ey/Ex} + 2.8/(W/D)^2}{1 + 0.00865/(W/D)^{2.76}}$$

96

Results from this analysis are compared with NASTRAN finite element results in Figure 86.

Given K_t and K_{t0} and the expression for tangential stresses around a central hole in a plate, we can easily compute the shear stress in the loading direction at any location around the hole periphery through the use of Mohr's circle

$$f_{12} = 1/2(f_1 - f_2) \sin 2\theta$$

where $f_2 = 0$. Substitution yields

$$f_{12}/f_g = 1/4[K_t E_t/E_y + K_{t0} E_t/E_x] \sin 2\theta$$
$$- 1/4[K_t E_t/E_y - K_{t0} E_t/E_x]\sin 2\theta \cos 2\theta$$

A comparison of this analysis with the results of an exact boundary collocation analysis is shown in Figure 87.
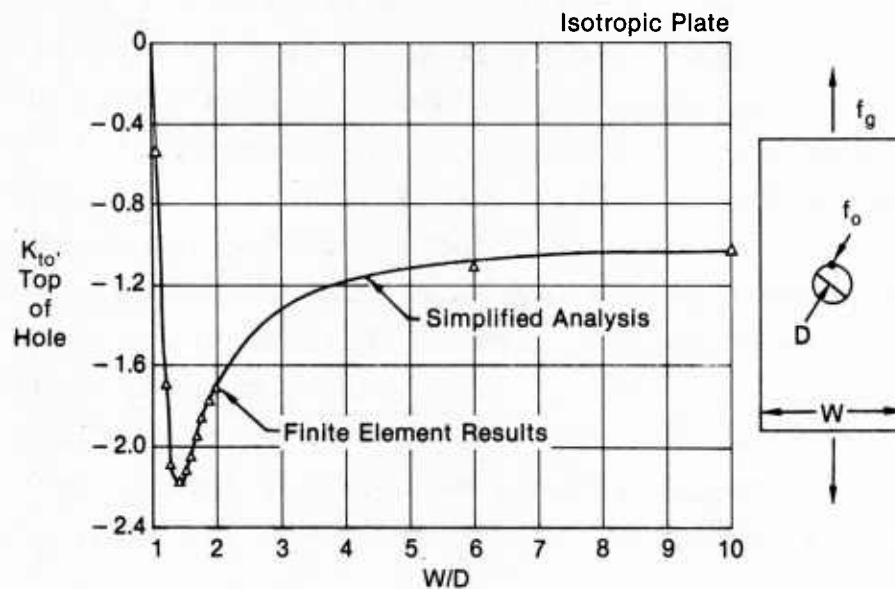
Figure 86. Analysis Results for Stress Concentration at the Top of Hole
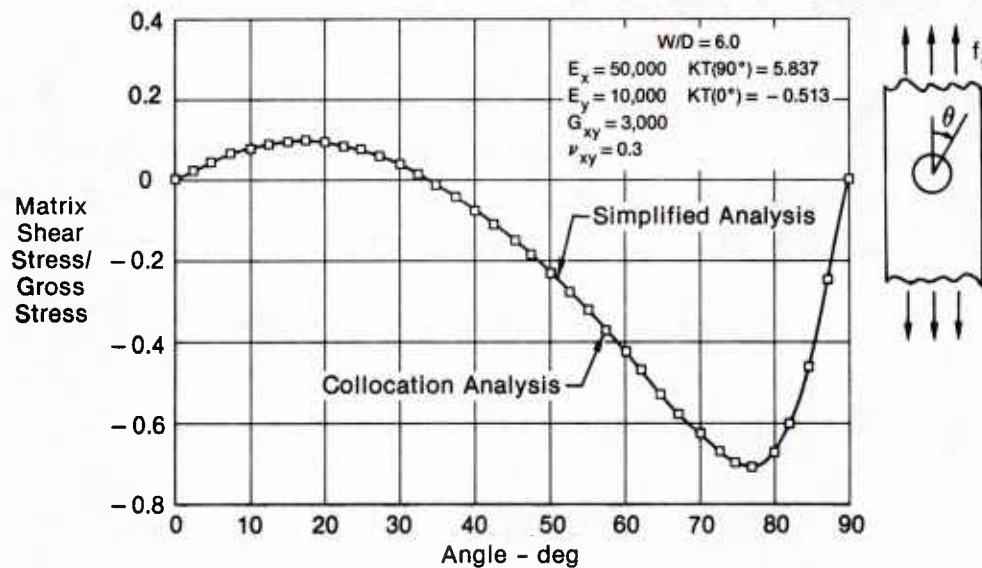
Figure 87. Matrix Shear Stress Concentrations Are Accurately Predicted by Simple Analysis

4. STRENGTH ANALYSIS OF NOTCHED METAL MATRIX COMPOSITES - Our initial approach toward formulating an analysis method for predicting strength of metal matrix composites was based on application of the Bolted Joint Stress Field Model (BJSFM), a model developed at MCAIR and verified by tests performed under Air Force contract (Reference 28), as shown in Figure 88. This model uses lamina property input and laminate plate theory to describe the stresses and strain states near a hole in a laminated composite plate. This model was found to predict the location of maximum matrix shear stress (where matrix cracking was found to initiate), as was shown in Figure 1. With adjustments to the ply properties to allow for the yielding that occurs in metal matrix composites, the model was shown to be capable of predicting the strength of metal matrix composites having loaded holes very well, as shown by F. M. Grimsley in AFWAL-TR-84-3063, (Reference 29).

There were two limitations of this model, however, that needed to be removed so that the model could be applied to analysis of metal matrix composite specimens such those tested in this program. The first limitation was that BJSFM does not

98

predict the stresses near open holes in finite width plates. It does not account for the finite width effects on the stress distribution. This limitation was removed through the analysis methods described in the previous discussion.
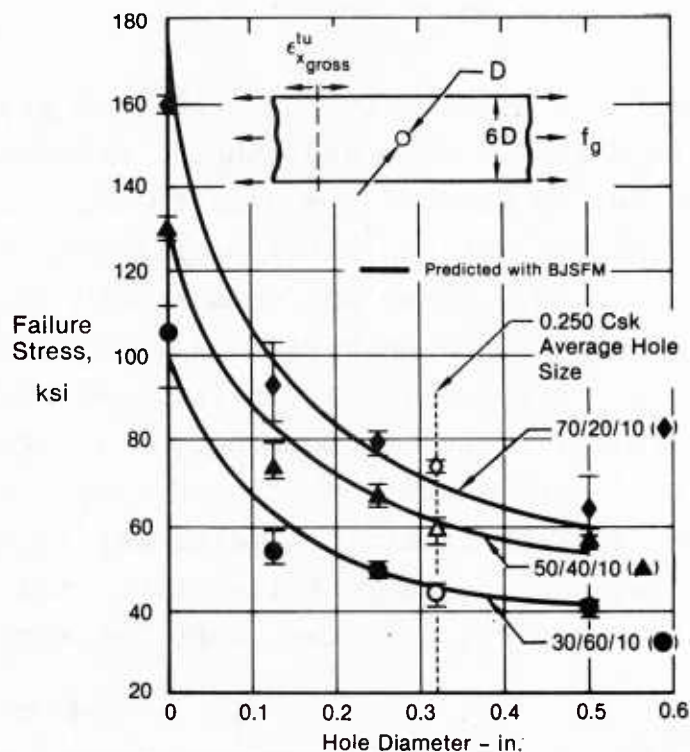
Figure 88. Effect of Hole Size on Unloaded Hole Tensile Strength

The second limitation was that the model did not handle material nonlinearity effects. Plasticity plays an important role in the failure processes of metal matrix composites, and a purely elastic stress analysis like that of BJSFM was not considered sufficient to describe the failures that occurred in our tests without considerable modification of the lamina properties to account for plasticity effects. For example, to account for the effects of matrix yielding to lower the transverse and shear moduli, one ran the analysis twice. Once to determine the location and ply in which yielding first occurred, and, provided no fiber failure had occurred, then the appropriate moduli were reduced and the analysis was performed again. If several plies could yield at different loads, then the analysis had to be run

several times, with failure checks each time. Otherwise one had to guess the failure load and yield state within the laminate and check to see that the analysis was consistent at the failure load. This process was considered too cumbersome to be used in a design mode for material and geometry selection.

During the literature survey phase of this program we became aware of the work done by Goree and others (References 9-11) and Reedy (Reference 30) on shear lag models to describe the matrix yielding that occurs in notched metal matrix composite monolayers, loaded along the fibers. These analyses showed that a shear lag model could predict well the post yield and static crack growth behavior of notched unidirectionally reinforced metal matrix composites (Figure 89). The micromechanics analyses of Dr. Sun (presented earlier in this section) showed that yielding in notched, unidirectionally reinforced metal matrix composites would occur largely between the first unfailed fiber and the first notched fiber, in agreement with the shear lag analyses.
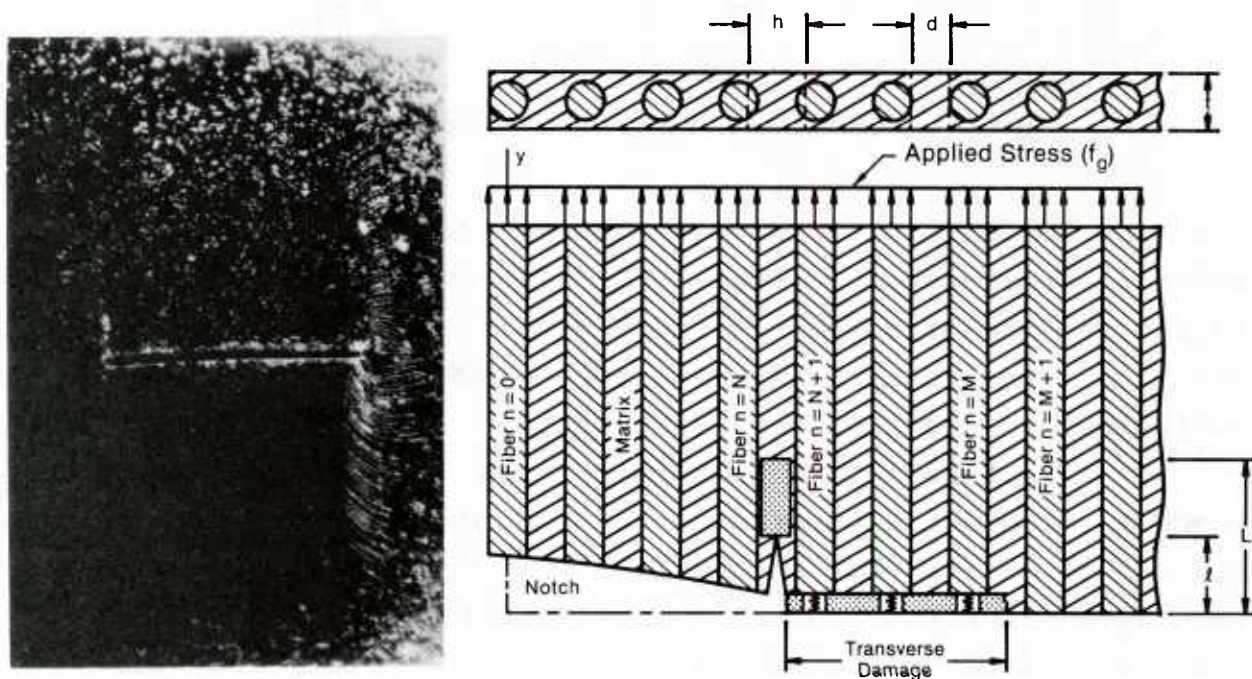
Figure 89. Yield Pattern (Brittle Coating) an Modeling of Unidirectional Boron/Aluminum
Goree and Jones

100

Based on the agreement of the analyses and their correlation with the behavior of MMC materials, we decided to incorporate a very simple shear lag model in our strength analysis. The engineering approach we took is described, schematically in Figure 90. The location of first yielding around the hole periphery was assumed to be the site from which yielding would subsequently progress along unfailed fibers.

$$L = \frac{D(P - P_o)}{2AF_{SU}}$$
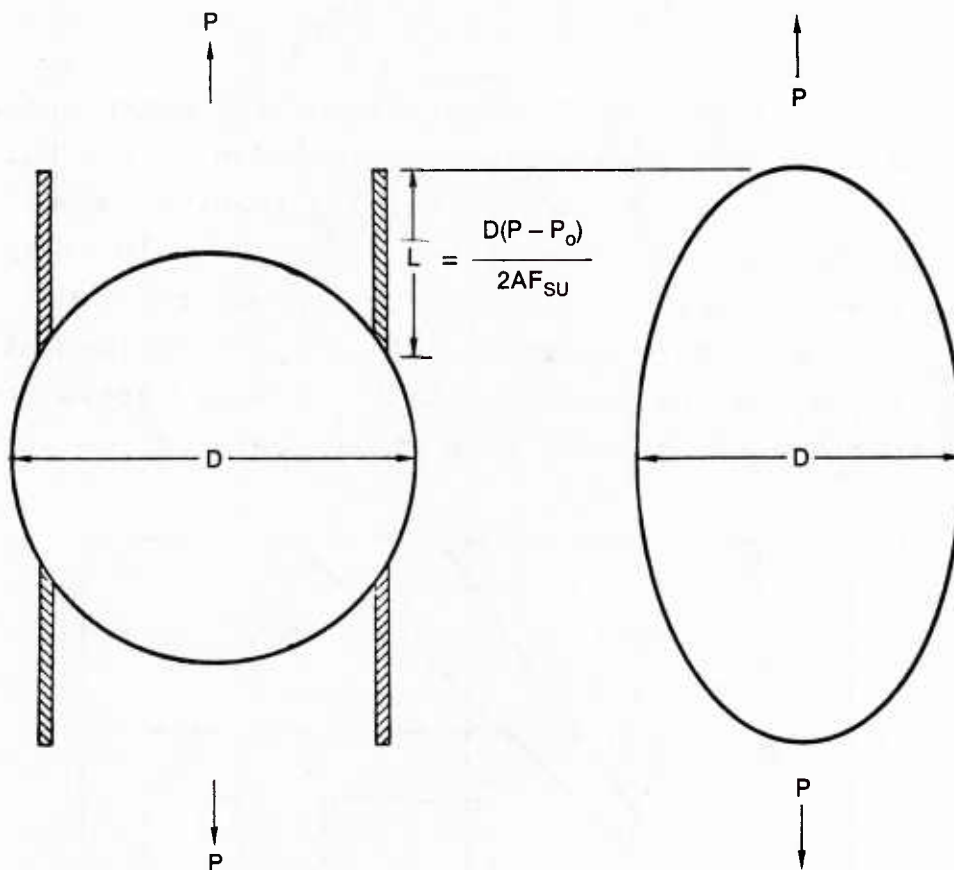
Figure 90. Yielding and Cracking Along Fibers Lowers Stress Concentrations in Boron/Aluminum

The length of the yield zone was determined by the amount of load that this area would have to carry around the hole in shear. The amount of load to be carried by the matrix at shear yield is the amount of load through the hole that cannot be carried

101

elastically, $(P - P_0)Dt/2A$, where P is the applied load, P_0 is the load at which yielding first occurs in the matrix, t is the ply thickness, and A is the gross area of the ply (Wt). This load had to be carried by the matrix at shear yield over the length, L, so

$$s_y L = (P - P_0)D/2A$$

or, as shown in Figure 90,

$$L = (P - P_0)Dt/2AF_Y$$

This yielding along the fiber significantly reduces the stress in the first continuous fiber at the edge of the hole. This effect was shown in Dr. Sun's analysis results as well. We accounted for this K_t reduction by analyzing the hole as an ellipse whose axis along the fiber direction was related to the length of yielding along the fibers. This K_t reduction was verified by comparing the predicted displacements across the hole and in the specimen net section with those measured, as shown in Figure 91.
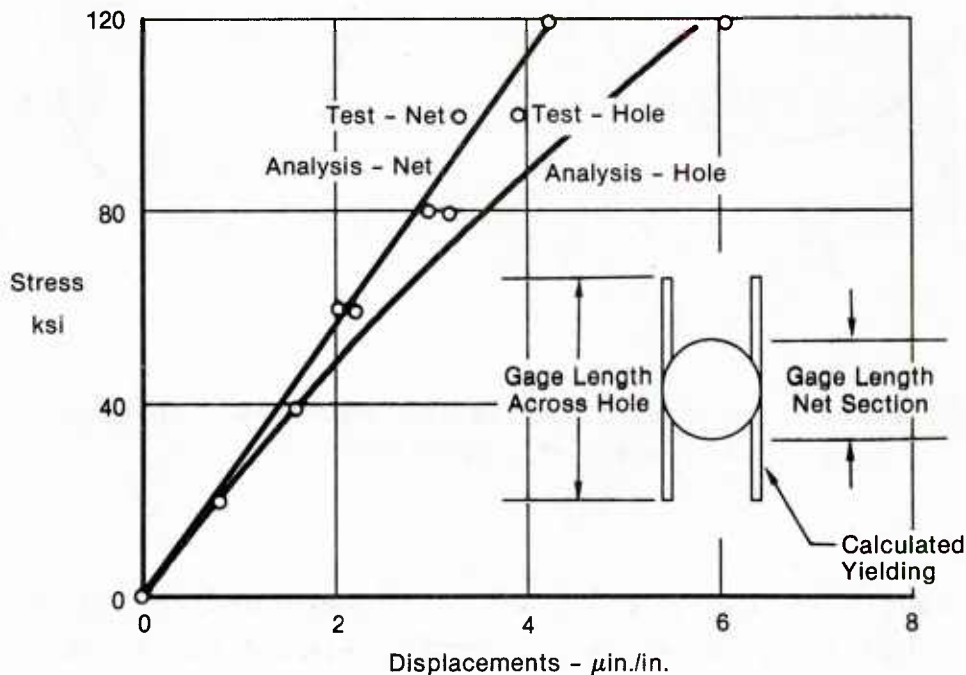
Figure 91. Correlation of Predicted and Measured Displacements

102

The final proof though was in application to the static strength results. The correlation for strength analysis with the test data for all static strength tests (unnotched as well as notched) is shown in Figure 92. These predictions were made by incorporating the stress analysis of the previous section into laminated plate theory and incorporating the shear lag analysis described in this section to reduce the hole Kt when necessary. A failure load is assumed and the ply properties and yield zone length are computed, based on an assumed elastic-perfectly plastic properties, and the fiber stresses at the edge of the hole are computed. If the fiber stresses are too low to cause fiber failure, then a higher load is selected and the analysis is performed iteratively until the load at which fiber failure occurs is determined, within some tolerance.
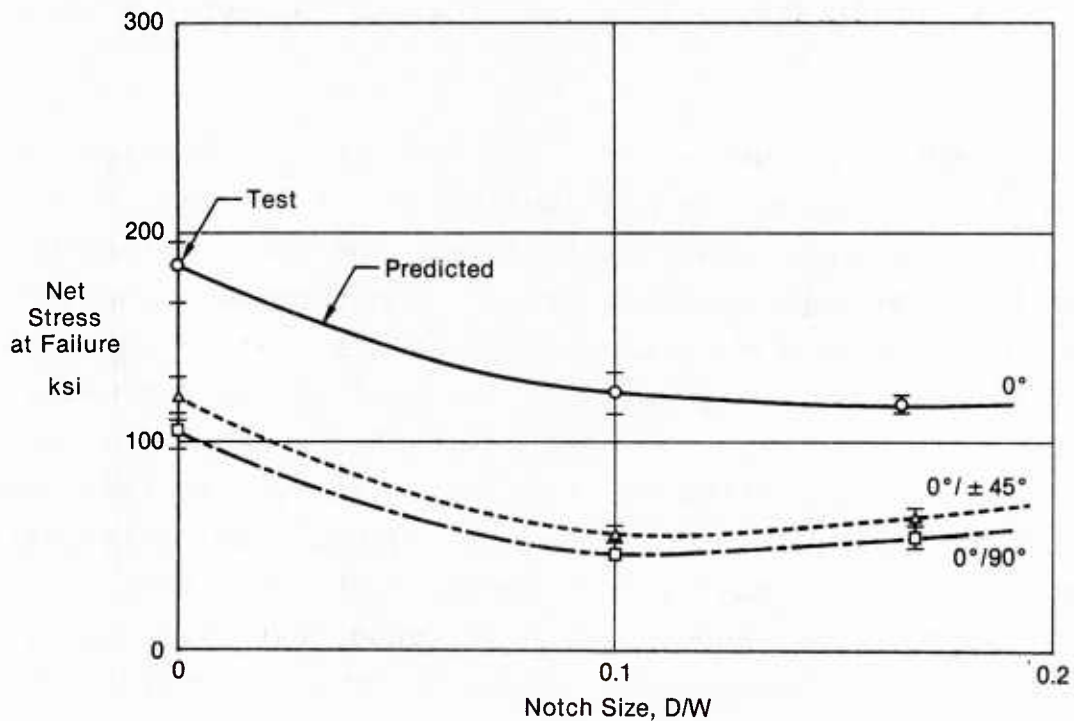
Figure 92. Correlation of Finite Width Effects on Strength of Notched Boron/Aluminum

The computer routine, MMCAN, described in Appendix A, is used to perform this analysis. The routine can be used to predict the unnotched strengths as well as notched strengths simply by assuming the hole geometry to be infinitely long in the loading direction. This is done for the analyst when he selects an unnotched configuration. This procedure allows the same analysis to be used to predict unnotched as well as notched strengths.

Crossplied MMC materials can also be analyzed with this routine. Currently, an elastic-plastic analysis of the off-axis plies is used to predict their properties. This analysis limits the ply shear and transverse tension stresses to their maximum values until fiber failure is predicted to occur. This requires a multistep analysis be done to determine when each ply yields until failure occurs. The computer routine is programmed to do this progressive failure search automatically until last ply failure is predicted to occur and to print the results as each ply yields or fails.

At present the concept of a characteristic dimension is not used in this analysis. We are looking at the material most adjacent to the hole to define failure. The fiber strength then becomes the most important parameter for determining the strength of the unidirectionally reinforced materials. While this procedure has worked very well for analysis of the MMC materials examined in this program, we have reservations about the general application of this method to other material systems that might have significantly different fiber strengths. The characteristic dimension concept is easily incorporated into this analysis and will be incorporated whenever data is found that irrefutably requires it. We do not intend to use it if not required, however.

5. <u>FATIGUE LIFE ANALYSIS</u> - Fatigue life analysis development efforts were concentrated on prediction of whether cracks would initiate at the hole edge and progress across the section as in conventional metallic materials or would initiate in the matrix

and propagate along unfailed fibers. The second failure mode, characteristic of weak matrix composites such as aluminum or epoxy, results in very short crack initiation lives but long crack growth lives. The primary physical properties that seem to determine the type of failure mode are the matrix shear strength and the fiber/matrix interface strength. As shown in Figure 1, the first failure mode is characteristic of titanium matrix materials and the second is characteristic of aluminum matrix materials.

a. Failure Modes - The stress analysis described in the previous section helps to understand why fatigue failure modes differ between aluminum and titanium matrix composites. If the stresses in the first unnotched fiber and the maximum matrix shear stresses are plotted as a function of the applied load for boron/aluminum, as in Figure 93, the effect of matrix yielding on the stress concentration in the fiber adjacent notch is evident. Aluminum matrix yielding, occurring at such a low load level, will result in early fatigue failure at that location if those loads are repeated often, as in fatigue. The fiber strengths are more than sufficient to carry the load without failure, and, since the matrix shear cracking that occurs is not near the maximum stress point in the fiber, the fiber is not expected to fail.

It should be noted that a net section failure can be induced if the load is high enough to fail unnotched fibers at the hole boundary. Since fiber strengths usually have large scatter, these fibers can often be failed by loads greater than 75 percent of the static strength of the coupon. At these loads the fiber stresses are above 80 percent of their average failure strength, and weak fibers will fail.

Below the load at which matrix yielding takes place, the matrix fatigue lives are very long. While the existence of a fatigue limit stress level is difficult to prove, the lives at these stress levels are certainly beyond those of interest for airframe load spectra.
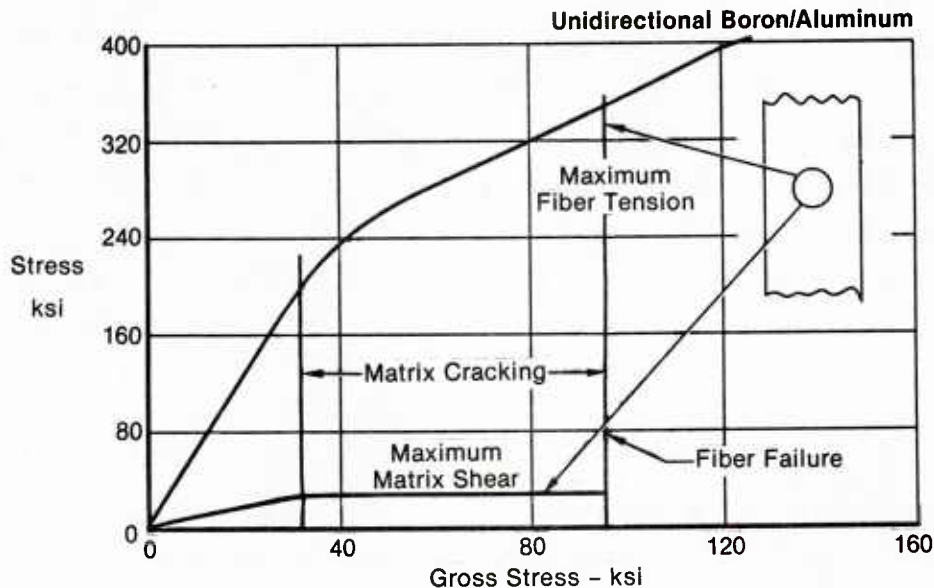
**Figure 93. Maximum Fiber and Matrix Stresses Determine
Failure Modes in Boron/Aluminum**

By comparison the stress analysis of the boron/titanium
material is much different (Figure 94). First, the matrix shear
strength is high enough to preclude yielding at the maximum matrix
shear location until fibers fail at the net section. Therefore,
the failure mode in this material system will be a net section
failure, similar to that in its parent metal. Recall that the
matrix strength of this system is so high that even in the net
section the fractographic evidence showed that fiber failed even
before the crack propagated to that location (Figure 43, Section
III).

These analysis results were compiled into a chart shown in
Figure 95 for loads of about 50 percent of ultimate strength. The
lamina longitudinal and shear strengths were selected as
parameters to define the fiber and matrix or fiber/matrix
strengths. The plate orthotropy parameter was selected to
describe how much of the load in the MMC coupon was being carried
around the hole in shear. In addition to the boron/aluminum and
boron/titanium materials, we have shown the comparable values for
isotropic metals and for unidirectionally reinforced carbon/epoxy

106

with a hole for comparison. The metal matrix materials tested in this program have very similar orthotropic stiffnesses (E_1 and E_2 are very close). Thus all of these results fall at nearly the same value of plate orthotropy.
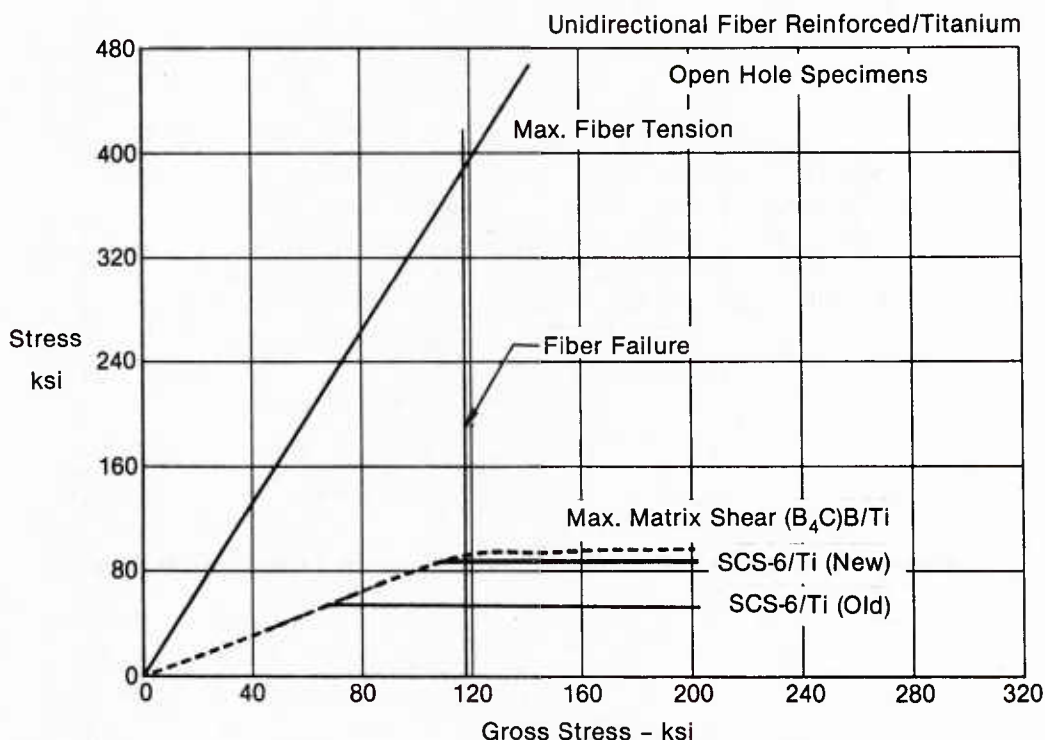
Figure 94. Maximum Fiber and Matrix Stresses Determine Failure Modes in (B₄C)B/Ti

The ratio of longitudinal to shear strengths of boron/ aluminum is shown in Figure 95 to be well above the threshold for cracking along the fiber. Boron/titanium is nearly sufficiently below the threshold to show a net section failure. The SCS-6/ titanium materials shown are from two different panels. The first panel was one of the very first SCS-6 reinforced panels produced and showed matrix cracking similar to that in boron/aluminum. The second panel results are for a later panel in which the processing had been improved. The second panel showed a net section failure in fatigue (Figure 96). The difference in these behaviors is predicted well by comparing the longitudinal and shear strengths

107

of the lamina. The shear strength of the first panel was almost half of that in the second panel. This difference may have been due to poor fiber spacing in the first panel (Figure 97) or due to poor fiber/matrix interface strength. In either case the fatigue failure mode is predictable.
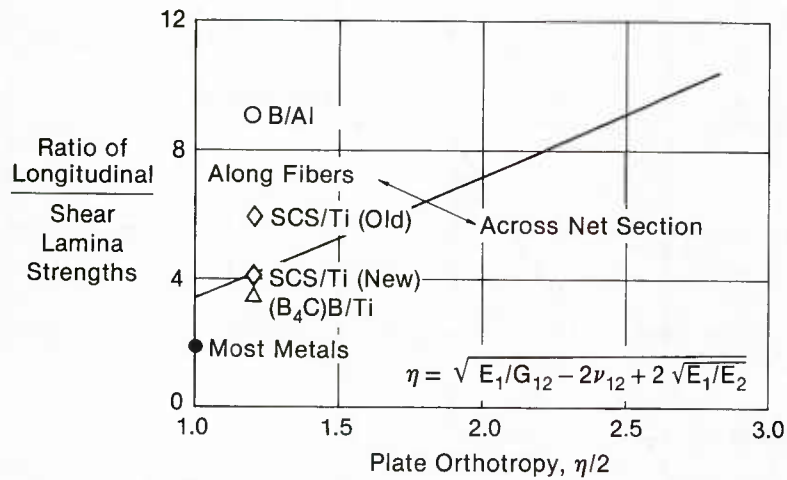
Figure 95. Fatigue Failure Mode Predictions for FRMMC Materials

With Poor Shear Properties   **With Better Shear Properties**
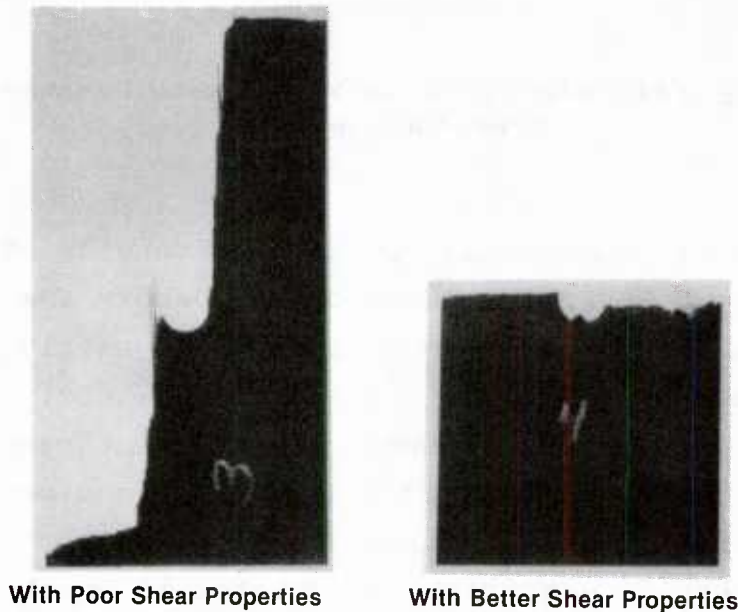
Figure 96. Effects of Improved Matrix Properties on Fatigue Failure
Mode in SCS-6/15-3 Titanium
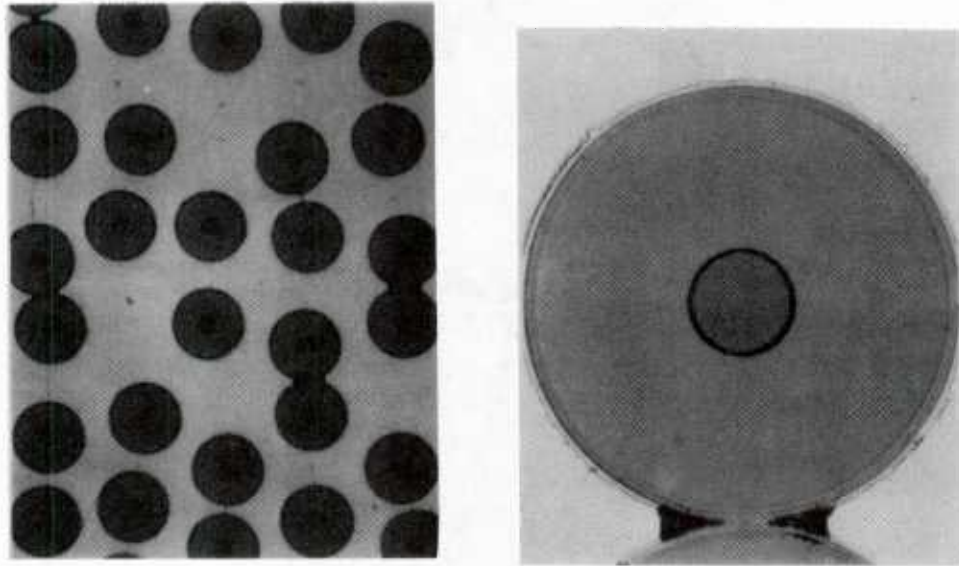
**Figure 97. Irregular Fiber Spacing in SCS-6/15-3Ti
Can Contribute to Poor Shear Properties**

When the material properties are such that analysis shows the material to straddle the threshold between the cracking modes, this behavior is also reflected in the crack growth behavior. At loads about fifty percent of ultimate, in the second panel of SCS-6/titanium, the analysis cannot discriminate the failure mode. At this load level the fatigue failures show evidence of both modes, as shown in Figure 98. At this load level, the fibers do not fail, but they allow so much matrix deformation that cracks initiate and grow, both along the fibers and across the net section.

It is important to note that the failure mode analysis presented in Figure 95 is load level dependent. At high load levels net section failures can be induced, even in boron/aluminum. The data shown in the Figure, and the analytical prediction is based on a maximum stress level about fifty percent of ultimate strength.
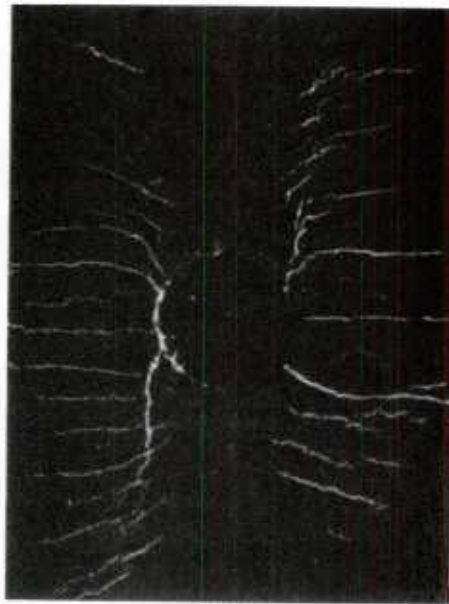
**Figure 98. Fatigue Failure Mode in SCS-6/15-3 Titanium
at Low Stress Levels**

Thus, the fatigue crack initiation life of MMC composites depends on the fiber and matrix properties. To accurately describe the initiation lives of these materials one needs to determine both the life to fiber failure and the life to matrix crack initiation.

b. Crack Initiation Analysis for Unidirectional Composites - To predict the lives of unidirectionally reinforced MMC materials, we used our baseline notched fatigue test data to develop two stress/life curves, one representing the life to matrix crack initiation, the other representing the life to fiber failure. Figure 99 shows an example of such data for boron/aluminum under constant amplitude fatigue at R=0.02. The fiber life curve is obtained from net section failures (at high stress levels). The matrix crack initiation curve is obtained from crack growth data taken during duplicate tests at lower stress levels.

110
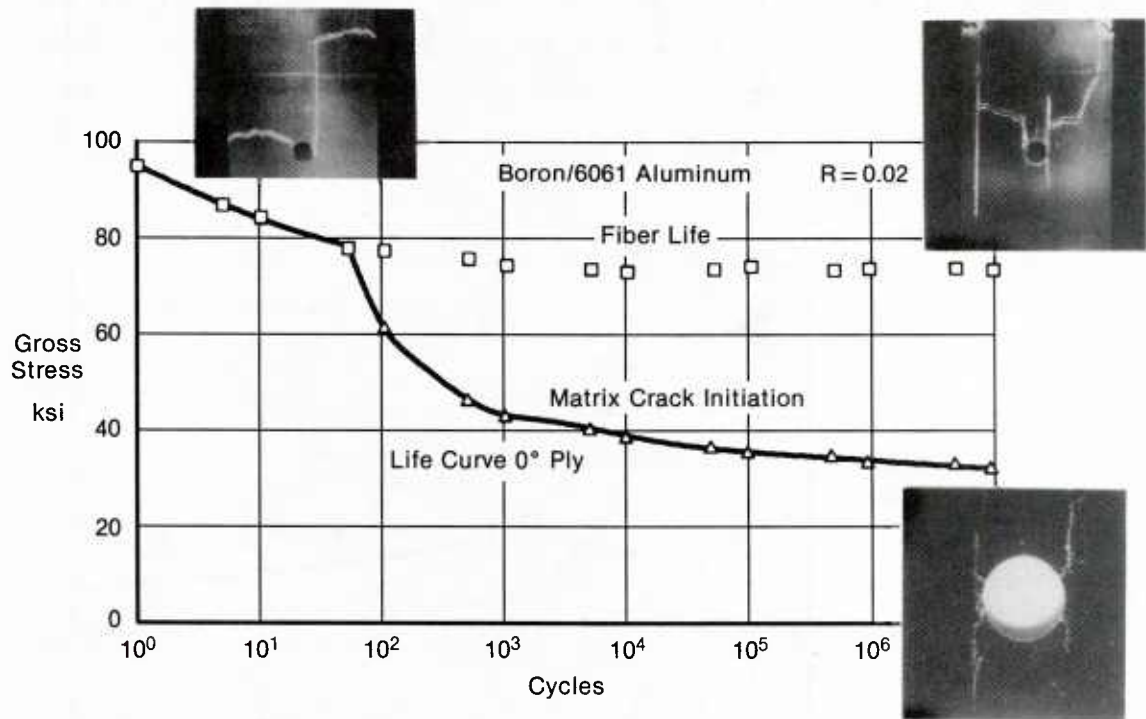
Figure 99. Crack Initiation Lives and Failure Modes in Unidirectional Boron/Aluminum

Data like that shown in Figure 99 was used along with the stress analysis module of the MMCAN routine to predict the crack initiation life for boron/aluminum at various stress ratios. In these analyses, we assumed that maximum stress level alone was the primary driver for fiber failures, so that the fiber failure curves are identical for both R=0.02 and R=-1. We used a standard stress ratio correction for metals to predict the effect of stress ratio on fatigue crack initiation in the matrix. The parameter we used is an effective strain version of a stress parameter developed by Smith, Watson, and Topper (Reference 31)

$$e_{eff} = \sqrt{f_{max} \, \Delta e / 2E}$$

This parameter has been shown to correlate stress ratio effects on crack initiation in a wide variety of metallic materials.

111

The correlation of the crack initiation analysis and test lives to initiation of an 0.05 inch long initial flaw is shown in Figure 100. The correlation shown is good and the fatigue life to specimen rupture at the higher stress levels was unaffected by the stress ratio, as anticipated.
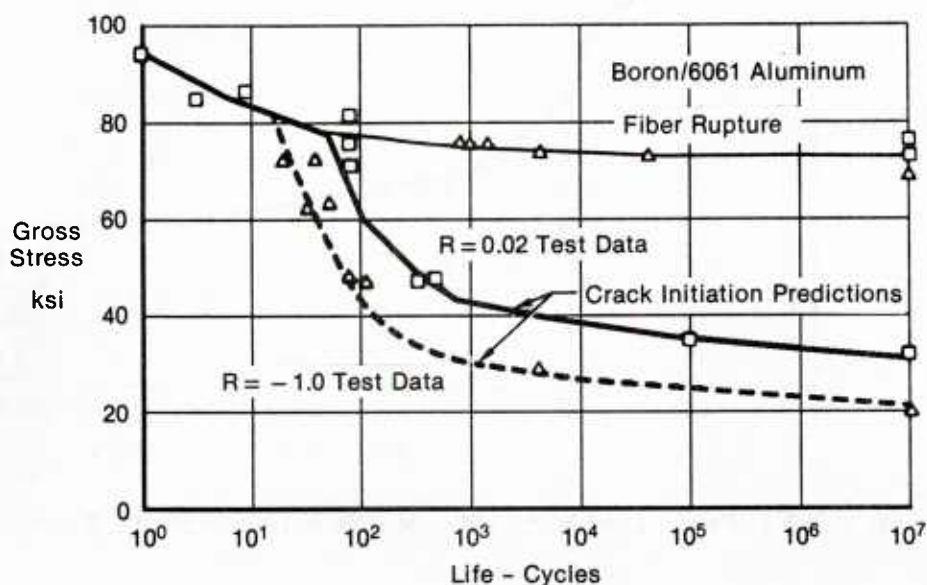
Figure 100. Comparison of Predicted and Test Lives – Unidirectional Boron/Aluminum

One reason that the net section failures of the unidirectionally reinforced boron/aluminum material were unaffected by stress ratio is that the net section stress concentration in compression is significantly less than that in tension, as shown in Figure 101. While the effect of the pin in the hole can reduce the magnitude of the stress concentration slightly if the pin is a neat fit, in compression, even a rather sloppy fit will provide a significant reduction in K_t. Figure 102 presents the results of NASTRAN finite element analyses using gap elements between the pin and the hole wall in a boron/aluminum component. These results show that the pin in the hole affects the compression K_t much more that the tension K_t, all the more so when the gap is large. In addition, the effect of pin/hole gap is affected by the load

112

applied. At low load levels the pin may not be effective in propping the hole. That is why the effect of pin propping was ignored in the crack initiation analysis.

    c. <u>Crossplied Laminate Life Analysis</u> - Fatigue life analysis is handled in essentially the same manner as that for the unidirectionally reinforced materials and is computed from the unidirectionally reinforced material data. Matrix crack initiation in each ply is predicted based on the shear and tension stresses around the notch boundary. As each ply is predicted to crack, the plate properties are modified to reflect that cracking. In the heavily 0° dominated laminates tested in this program, failure of the 0° plies determined failure, but the effective stiffness of the crossplies played a key role in the load level at which this failure occurred.
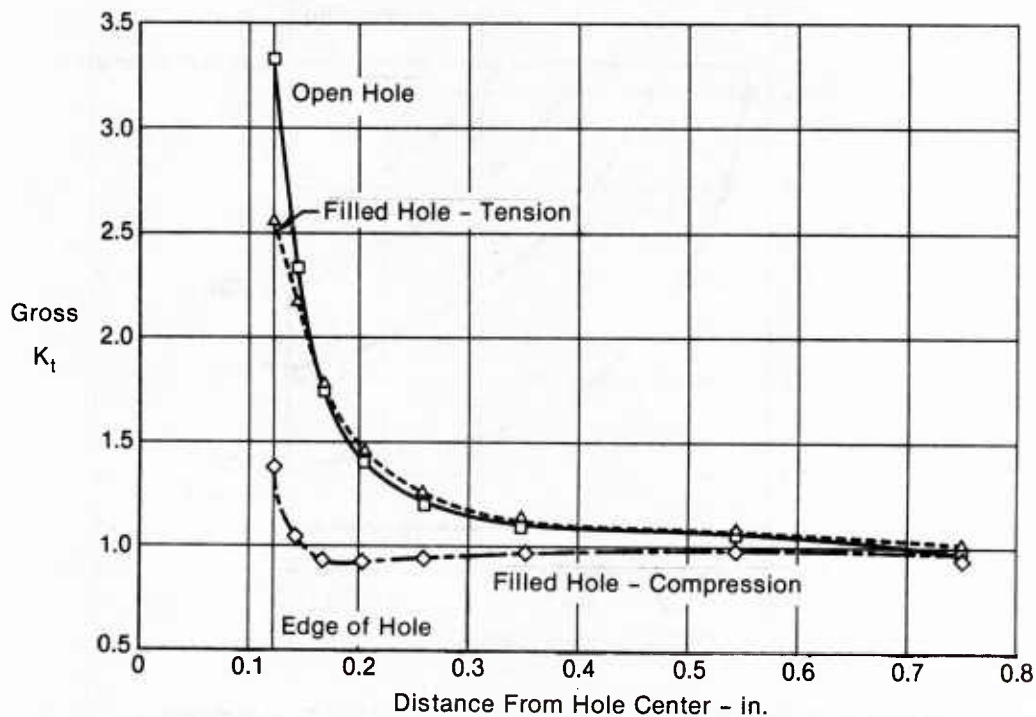
Figure 101. Tension and Compression Stress Gradients Near Filled Holes in Boron/Aluminum
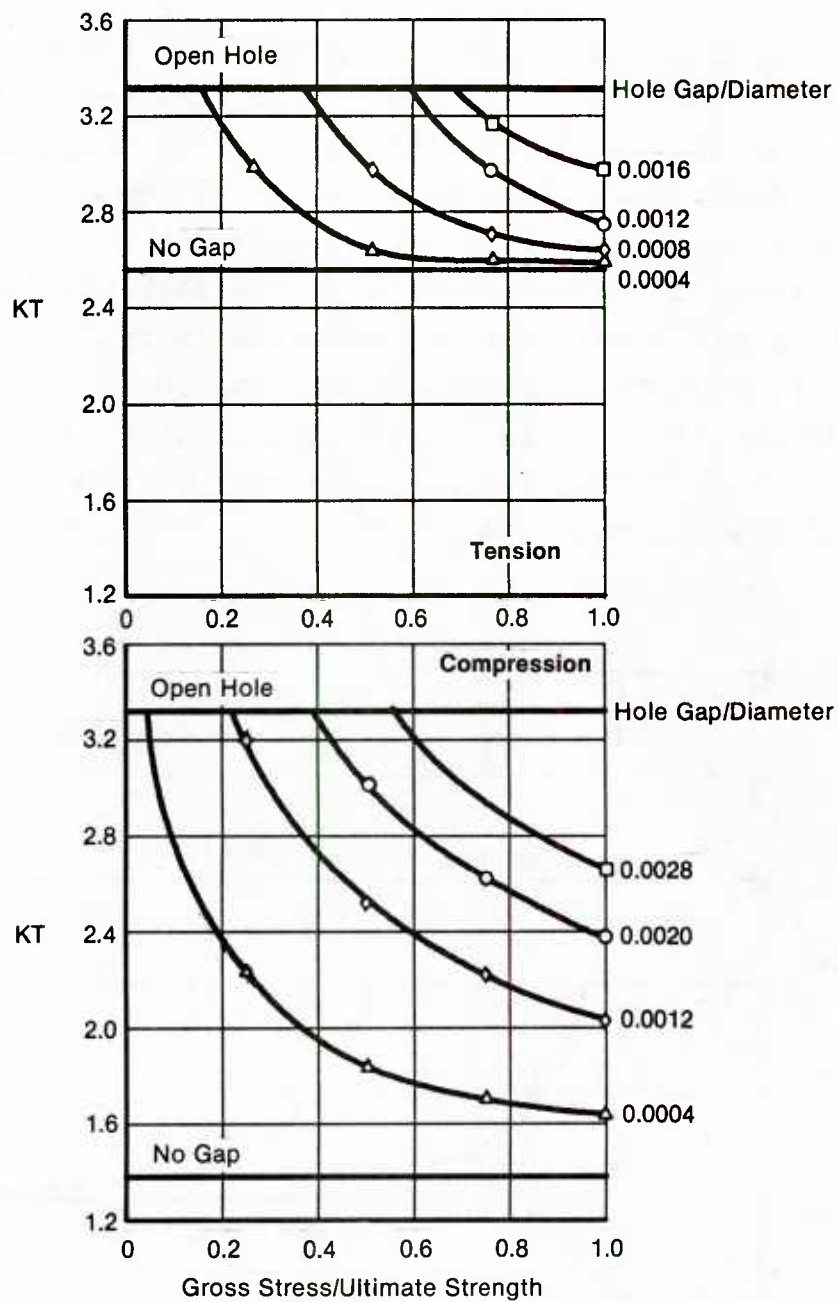
Figure 102. Effect of Pin-to-Hole Gap on Stress Concentration

114

The analysis results shown in Figure 103 present matrix crack initiation curves for the +45° plies, crack initiation in the 0° plies, and rupture life for the 0° plies. The life to specimen rupture data shown in the figure are from Dr. Sun's tests and show good agreement with the rupture life predictions from the model. Unfortunately, no data was taken in this test program to verify the accuracy of the crack initiation life predictions in the crossplies.
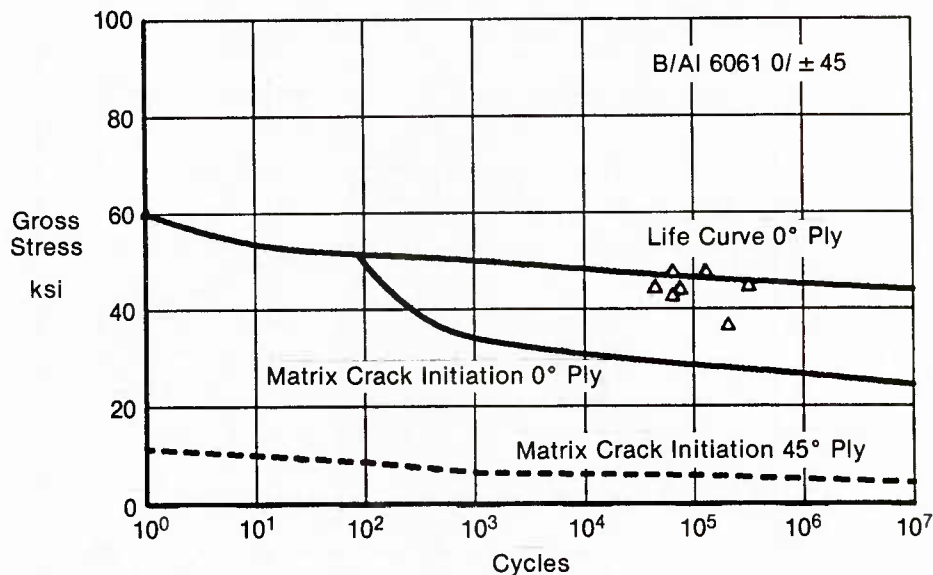
Figure 103. Comparison of Crossplied Laminate Lives With Analysis for 0/ ± 45

6. <u>CRACK GROWTH ANALYSIS</u> - The selection of crack growth analysis used to predict fatigue lives in this program was dependent on the failure mode as described in the previous section. When the flaws grow in shear along the first unfailed fiber, then the analysis was configured to predict flaw growth in the matrix constrained by the orthotropic material on either side. When the flaw growth was predicted to occur across the net section, then more conventional fracture mechanics analysis was used. In crossplied laminates, flaw growth within individual plies was predicted based on the unidirectionally reinforced material results, but verification was based solely on the flaw growth in the outermost 0° plies.

115

a. Cracking Along Fibers - In unidirectionally reinforced boron/aluminum, cracking along the fibers is the primary failure mode. When such cracking occurred in test, measurements showed that the crack growth rates were relatively constant, as shown in Figure 104. Note that while two of the flaws grew at faster rates than the other two, the cracking was consistently uniform in rate until the cracks approached the grips, about 0.9 inches away from the hole. The crack growth rates fall when the cracks approach the grips because the shear deformation at that location becomes constrained by the grips.
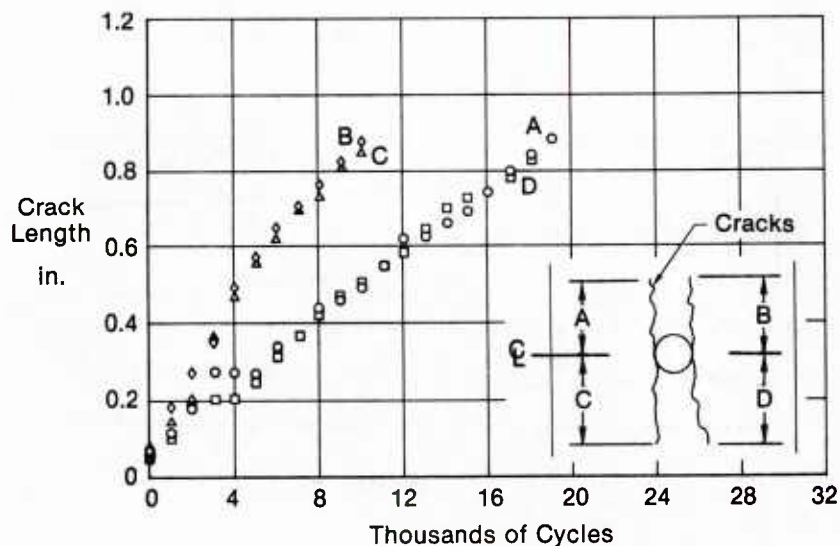
Figure 104. Crack Growth in Notched, Unindirectional Boron/Aluminum

Note that the two flaws which grew faster occurred at opposite sides of the notch. This is likely due to uneven load introduction in the specimen, with the majority of load going from the upper right hand side to lower left hand side of this specimen as viewed in Figure 104. This was a relatively common occurrence and made recovery of crack growth rate data difficult from these tests, although the factor of two difference in crack growth rate shown was not significant in comparing the fatigue lives in this test program. Generally, stress ratio and stress level had much greater impact on crack growth rates than a factor of two, as shown in Figure 105.

116
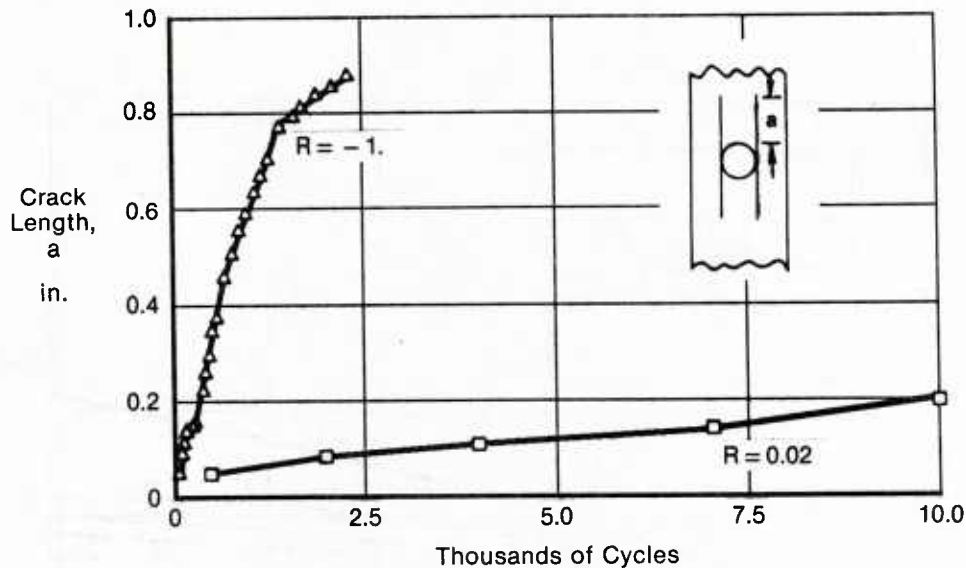
**Figure 105. Effect of Stress Ratio on Crack Growth
From a Notch in 0° Boron/Aluminum**

Analysis of this crack growth behavior was performed by considering the stress intensity factors for cracks being grown in shear in an isotropic medium sandwiched between two orthotropic media. The solution for these stress intensity factors is given by Sih in his Handbook of Stress Intensity Factors (Reference 32). The solution, in terms of matrix modulus, E_m, orthotropic modulus, E_1, crack length, a, and fiber spacing, 2h, is shown in Figure 106. The stress intensity factors are normalized by stress level in this figure to demonstrate that, as the matrix crack lengths exceed the fiber spacing by any appreciable amount, the stress intensity factors become very nearly constant. Thus, we see the crack growth likewise becomes a constant for a given load level.

That these solutions can be used with conventional fracture mechanics approaches to predict growth rates in MMC materials has been demonstrated by several authors (References 33-35). However, to apply these solutions to crack growth in metal matrix composites, we must also have some way to predict the effects of transverse and shear stresses on crack growth in the matrix.

117
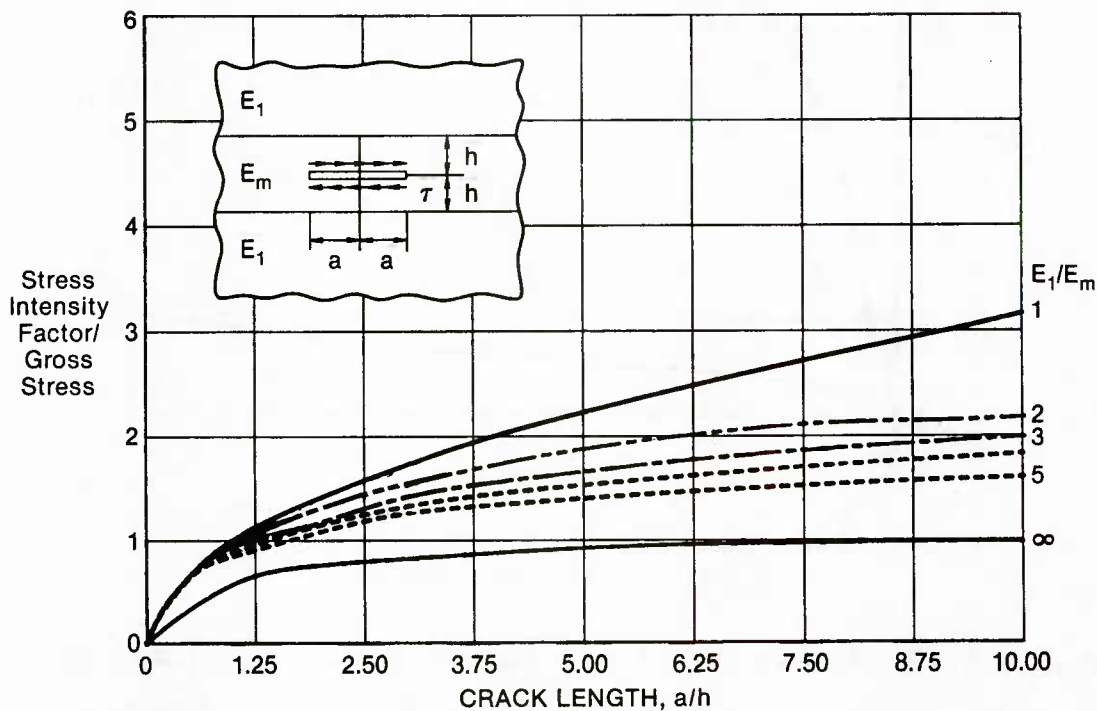
**Figure 106. Stress Intensity Factors for Matrix Cracks in Shear
Are Almost Constant When Cracks Are Visible**

Two of the most frequently used parameters for analysis of coupled shear and tension on crack growth in composite materials are strain energy release rate and strain energy density factors. These parameters couple the shear and normal stress intensity factors to assess damage severity and flaw growth rates. Strain energy density has the advantage that it can be applied to either cracked or uncracked structures since the strain energy (W) per unit volume (V) can be expressed as a product of local stress (f_{ij}) and strain (e_{ij}),

$$dW/dV = 1/2 \ f_{ij} \ e_{ij}$$

For cracked structures the strain energy density can be expressed in terms of strain energy density factor (S) or stress

118

intensity factors, accounting for material anisotropy, stress state and flaw size, where

$$dW/dV = S/r$$

r is the radial distance from a crack tip and

$$S = a_{11} K_{12} + a_{12} K_1 K_2 + a_{22} K_{22}$$

where K1 and K2 are the opening and shearing mode stress intensity factors, r is the distance from the crack tip (Reference 36), and

$$a_{11} = 1/16G_{12}[(3 - 4v - \cos\theta)(1 + \cos\theta)]$$

$$a_{12} = 2/16G_{12} \sin\theta [\cos\theta - 1 + 2v]$$

$$a_{22} = 1/16G_{12} [4(1 - v)(1 - \cos\theta) + (1 + \cos\theta)(3 \cos\theta - 1)]$$

When the crack grows continuously along the fibers, as in boron/aluminum, this formulation can be considerably simplified. Noting that the trajectory does not deviate from that along the fibers, then θ will be 0 and the expressions for a_{ij} simplify to

$$a_{11} = 4/16G_{12} (1 - 2v)$$

$$a_{12} = 0$$

$$a_{22} = 4/16G_{12}$$

So that the strain energy density factor S has the same form as the strain energy release rate

$$S = a_{11} K_1^2 + a_{22} K_2^2$$

This is the same form of parameter as that used by Mahulikar, et. al (Reference 35), to correlate crack growth rates in titanium

119

matrix materials, when cracks grow across the fibers (Figure 107). It was found to work equally well in correlating crack growth rates in unidirectionally reinforced boron/aluminum tested in this program (Figure 108).

A weight function approach was used to compute stress intensity factors for the data in Figure 108. The weight function approach uses the unnotched stress distribution along the crack path and a point load solution to determine the stress intensity factors according to the following equation

$$K = \int_a f(x)\ g(x,a)\ dx$$
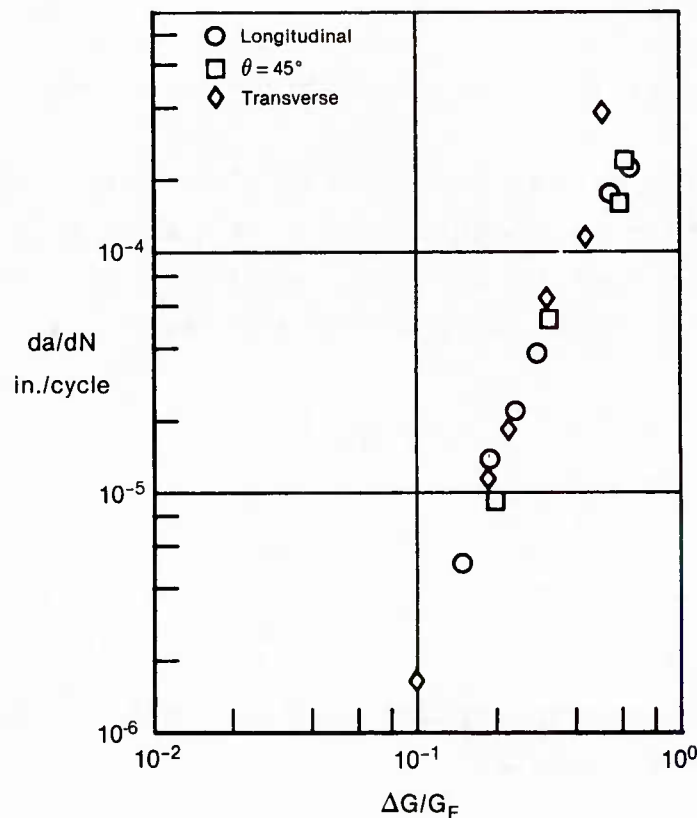
Figure 107. Mahulikar's Use of Strain Energy Release Rate to Correlate Crack Growth Rate Data in $(B_4C)B/6\text{-}4$ Titanium

120
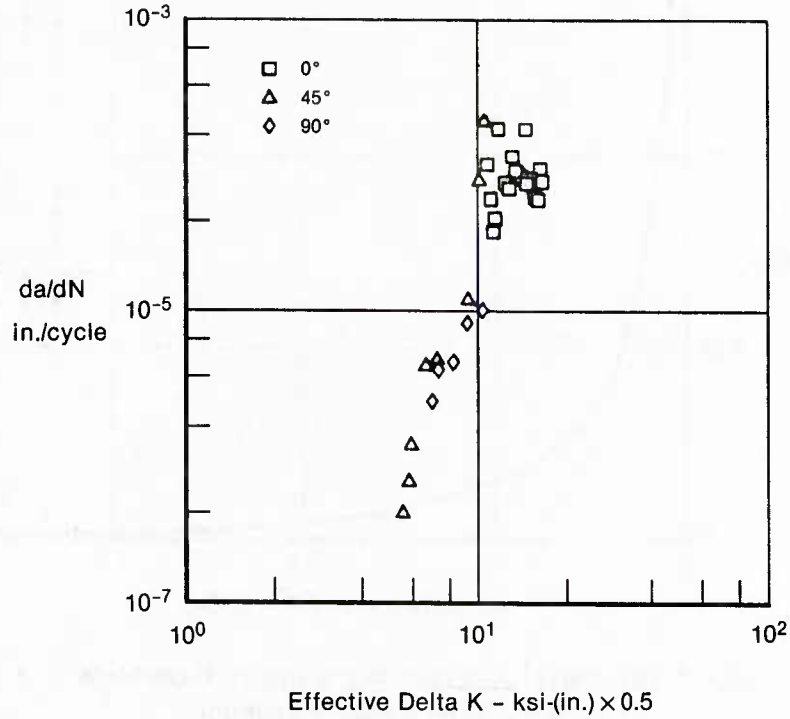
Figure 108. Unidirectional Flaw Growth Test Results

The stress distribution along the unnotched fibers adjacent to the hole in the fiber reinforced MMC was determined from boundary collocation analyses. The shear stress distribution along the fibers is shown in Figure 109. The weight function was taken from the point load solutions of Reference 32. For both tension and shear loads the weight function is given for an isotropic medium as

$$K = 2P/\sqrt{\pi a(1-(x/a)^2)}$$

$$g(x,a) = dK/dx = 2f(x)/\sqrt{\pi a(1-(x/a)^2)}$$

The stress intensity factor developed by these methods and used in analyzing the growth of flaws in shear in boron/aluminum are shown in Figure 110.

121
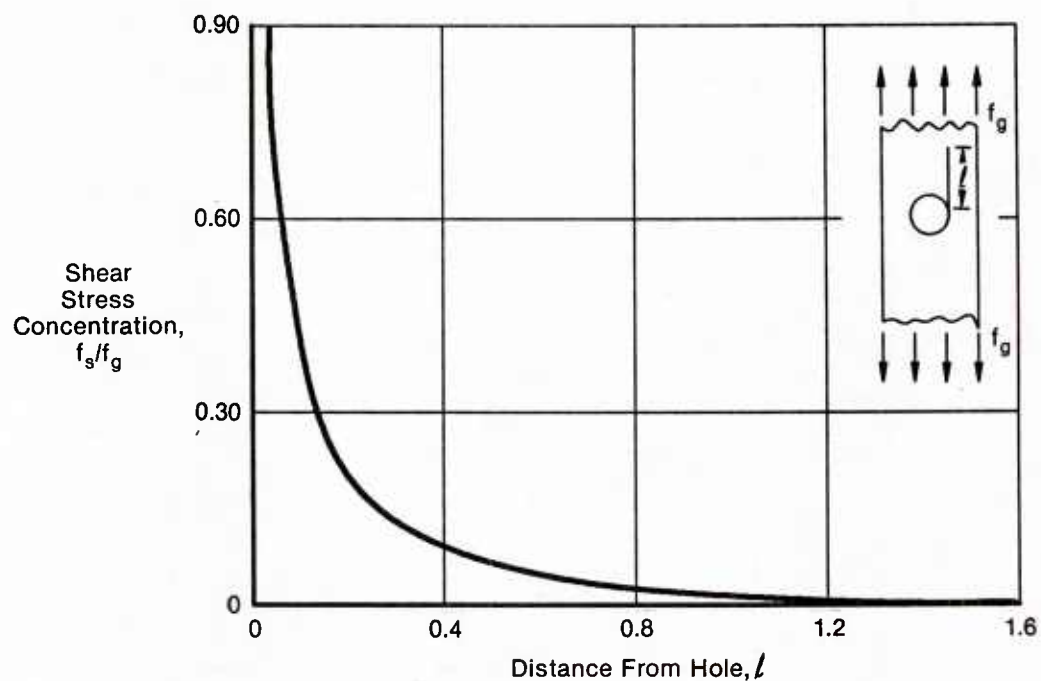
Figure 109. Shear Stresses Along Fibers From Hole in Unidirectional Boron/Aluminum
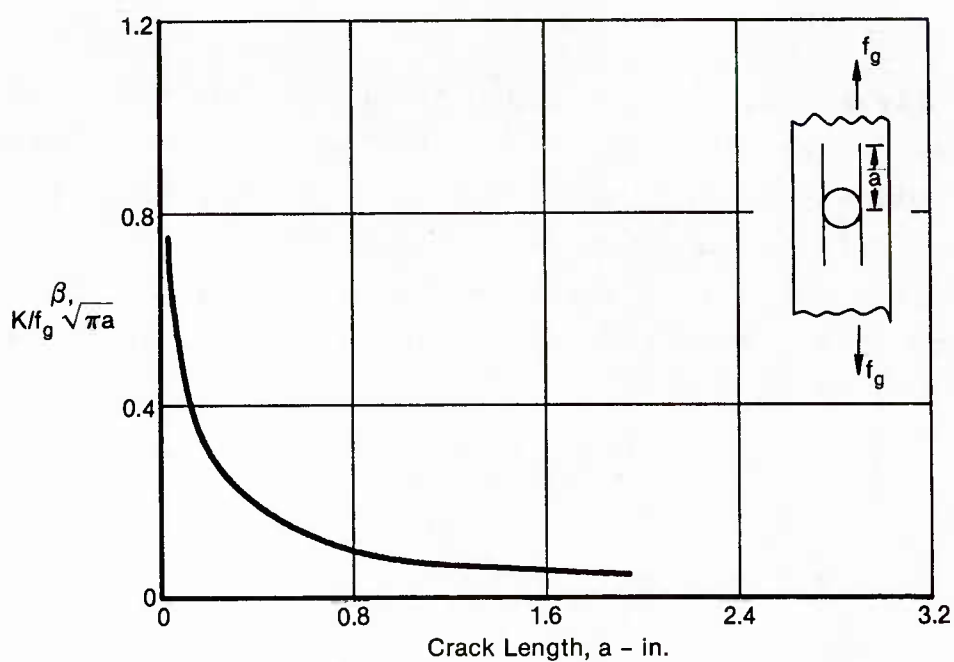
Figure 110. Stress Intensity Factors for Flaw Growth Along Fibers From a Hole in Boron/Aluminum

These stress intensity factors, in conjunction with the crack growth data of Figure 108 were used to predict flaw growth along fibers in unidirectional boron/aluminum. The results of one analysis is compared with test results in Figure 111. The analysis generally tends to underestimate crack growth rates as the cracks approach the grip because it was assumed that the displacement at the end of the load tab was uniform deformation of the adhesive bond between the specimen and load tab probably allows more than zero in-plane shear at the tab and consequently allows greater crack growth.
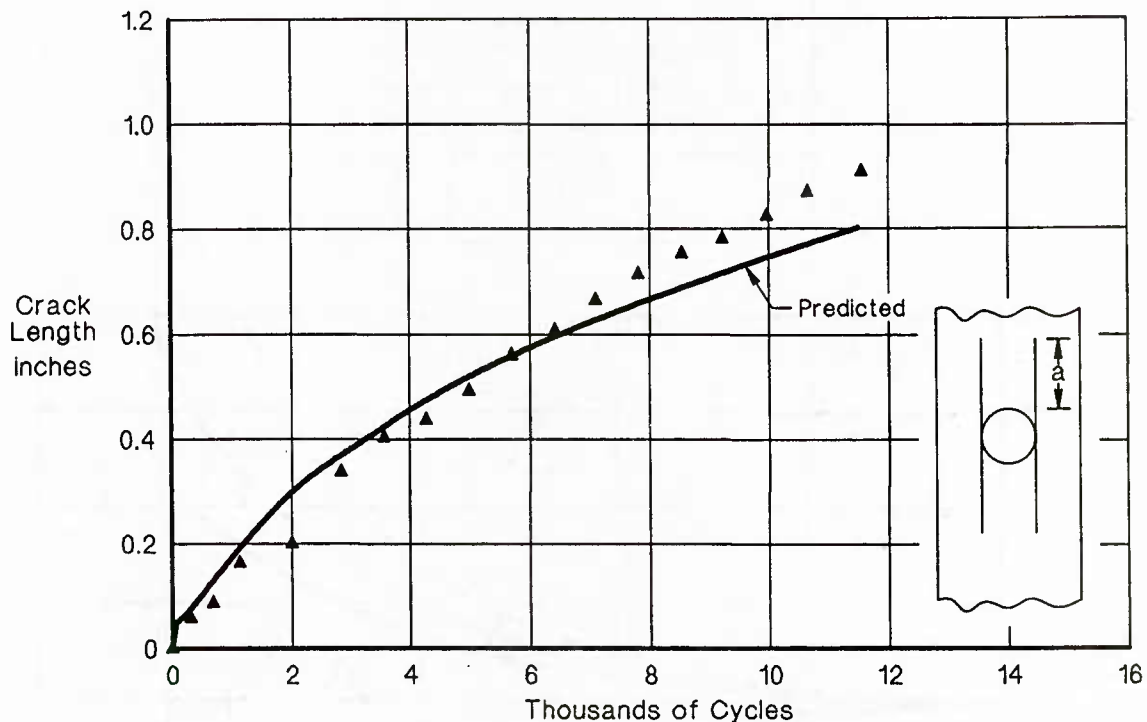
**Figure 111. Prediction of Flaw Growth Along
Fibers in Boron/Aluminum**

b. <u>Cracking Across Net Section</u> - When cracks propagate across the net section, as in boron/titanium in this program, isotropic stress intensity factors can be used with some confidence to correlate and predict flaw growth. As shown by a plot of Sih's handbook solutions (Reference 32) for cracks growing in the matrix perpendicular to the fibers and load (Figure 112),

the stress intensity factor for cracks in the matrix alone falls off as the flaw approaches the first fiber. However, since the ratio of matrix modulus to composite modulus is about 0.5 for boron/titanium, this decrease is not as large as the solutions shown in Figure 112. Furthermore, as the cracks grow through the fibers, the ratio of the modulus of the material severed by the crack gets closer to overall composite modulus, and the stress intensity factor solution approaches the isotropic solution.
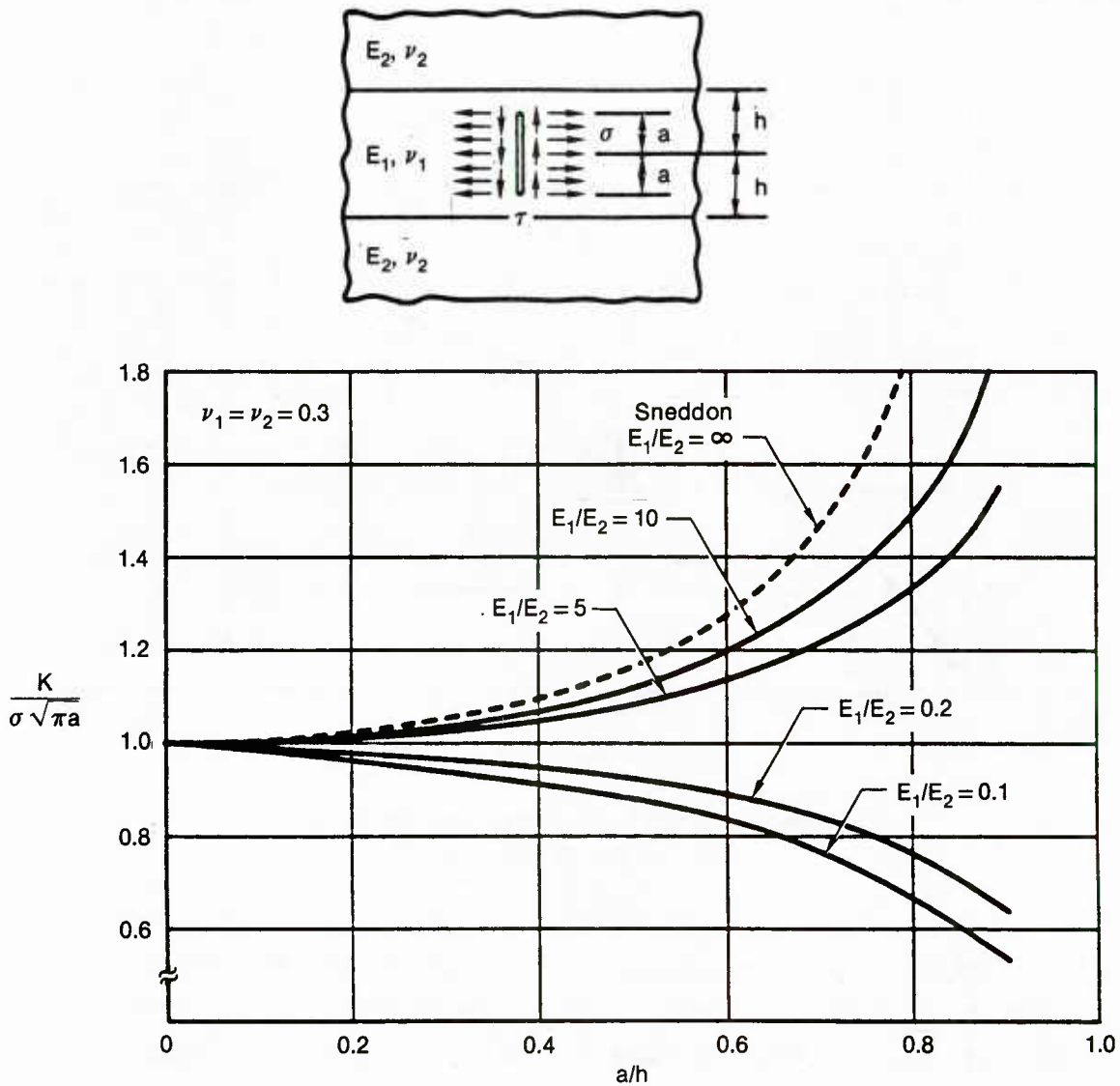
Figure 112. Stress Intensity Factors for Crack Perpendicular to Interface

Since crack growth rates for flaws growing across 0° fibers can be related to isotropic stress intensity factors, these crack growth rates can be directly compared with those from the parent matrix material for materials characterization, as shown in Figure 113. Not only can these results be used to compare materials, but they can also be used to predict spectrum crack growth, using conventional fracture mechanics based analysis methods. The results of one such prediction is shown in Figure 114 in comparison to some early MCAIR test data.
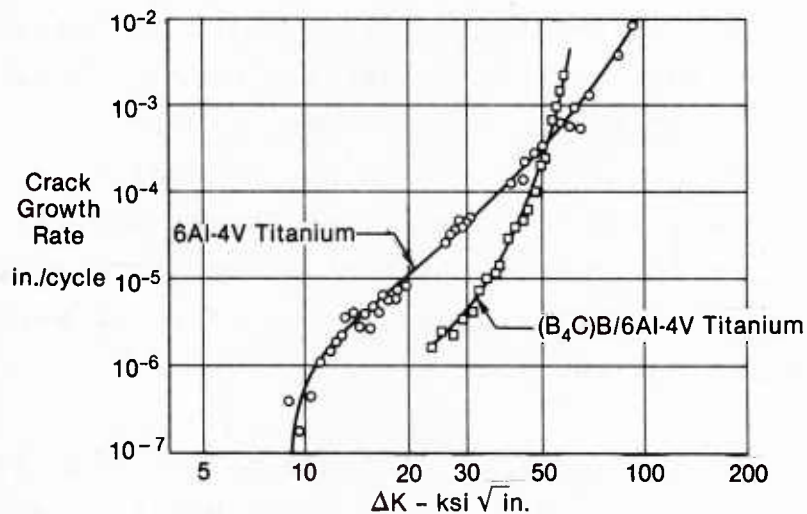
Figure 113. Crack Growth in (B₄C)B/Ti Is Similar to That of the Titanium Matrix
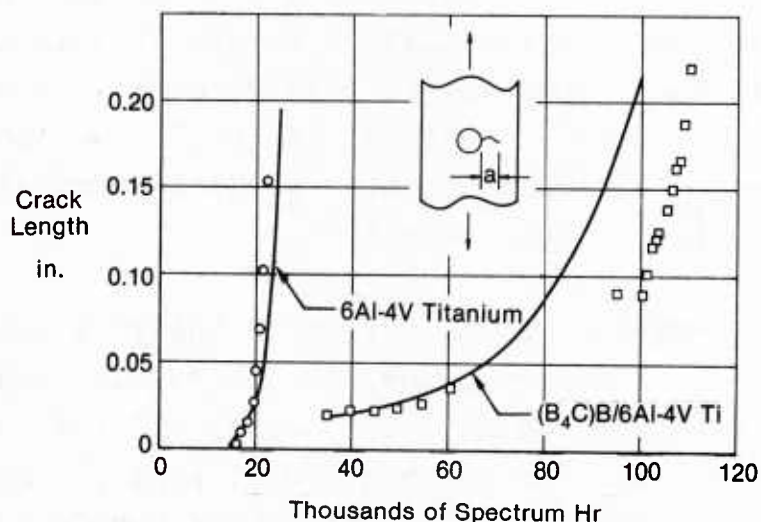
Figure 114. Conventional Fracture Mechanics Analysis Can Be Used to Predict Flaw Growth in (B₄C)B/Ti

125

c. <u>Analysis of Crossplied Laminates</u> - Analysis of the crack propagation in crossplied MMC materials is complicated. Recall that our prediction of crack initiation in these materials indicated that crossplies cracked very early in life. The crack growth in these plies can be predicted using (1) the stress intensity factors and strain energy parameters developed in the previous sections, (2) a formulation for ply stiffness that accounts for cracking within the ply, and (3) laminated plate theory to describe the strains and stresses within each ply.

No testing was performed in this program to determine the crack propagation rates in the crossplies of laminated boron/ aluminum material. This cracking occurs at very low stress levels - far below those that limit life in the 0° dominated laminates tested. Rather, what we found was that the crossplies could be cracked throughout their width without affecting the life of a component, as long as the stresses in the 0° plies were below that found to cause net section failure.

The stress levels required to cause net section failure of the 0° plies are so high that once a flaw initiates across fibers the critical stress intensity factor is exceeded after very little growth. For example, the stress level in a 0° ply must be at least 75 percent of the ultimate strength to cause fibers to break in fatigue. If a net section failure occurs at this stress level, the apparent fracture toughness of this material (15 ksi/in) will limit the maximum flaw size to 0.001 inches. Thus, once a fiber breaks, fracture mechanics principles predict immediate failure, and essentially that is what happens.

7. <u>RESIDUAL STRENGTH</u> - Residual strength analyses depend, as do the life and crack growth analyses, on the failure mode predicted to occur under fatigue loading. In general, if the failure mode is one of cracking along the fibers, in 0° plies, a simple strength analysis, accounting for the stress concentration reduction due to yielding and cracking, can be used to accurately

126

predict residual strength. If the failure mode is that of cracking across the net section, then fracture mechanics methods can be used to accurately predict the residual strength.

Simonds showed that in unidirectionally reinforced boron/ aluminum the residual strength of center cracked panels after fatigue cycling was sometimes higher than that found in static strength tests alone (Figure 115). This strength increase appears to be caused by the effect of the cracking parallel to the fibers to segregate the notch and reduce the stress concentration.
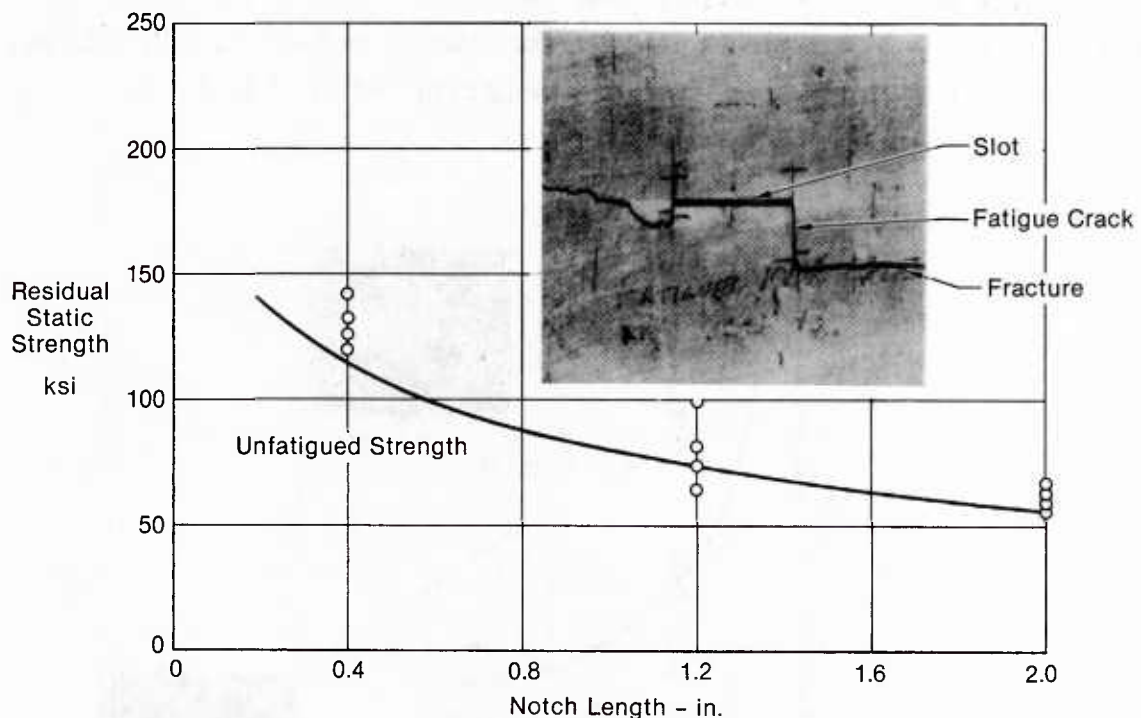
Figure 115. Fatigue Cracking Along 0° Fibers Does Not
Affect Longitudinal Strength

The analysis incorporated in MMCAN (Appendix A) performs strength analyses based on both static strength and fracture mechanics criteria. The least strength found from these two criteria is considered the most accurate prediction. The strength

based prediction is conservative because, while it contains the effects of matrix yielding to reduce the notch stress concentration, it does not account for the effect of cracking along the fibers to further reduce the notch stress concentration. However, the conservatism is not great (as was shown in Figure 115).

The fracture mechanics criterion is generally unconservative when applied to those cases in which the flaw grows across the net section. This lack of conservatism may be due to the selection of fracture toughness used in these analyses. For the results shown in Figure 116, the fracture toughness was chosen to be the value of stress intensity factor that resulted in unstable crack growth in fatigue test. Certainly the value derived from a static test of a precracked specimen (as is done with metallic materials) would have provided a better correlation with the data.
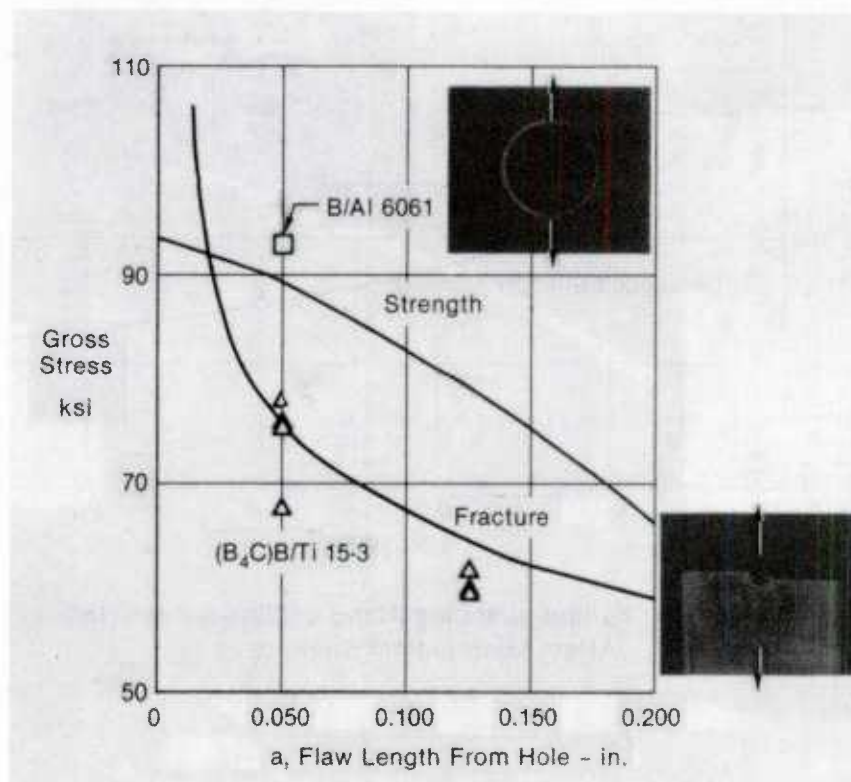
Figure 116. Residual Strength Depends on Failure Mode

128

8.   <u>PREDICTION OF VERIFICATION TEST RESULTS</u> - The methods of
analysis described in the preceding sections were used, along with
the analysis development data, to predict the results of the model
verification tests.   These tests involved different geometries,
stress levels, and stress ratios than those used in the model
development test program.   In addition, the boron/titanium
material was also tested to verify the failure mode change shown
in previous MCAIR testing.   These predictions were made before the
start of the verification tests described in the next section.
Correlation of the test results with the strength, life, and
residual strength predictions are summarized in Section VI.

MODEL VERIFICATION TESTING

In this test phase 150 tests of FRMMC specimens were used to verify the strength, life, residual strength, and failure mode prediction models. One hundred of these specimens were fabricated from the boron/6061 aluminum composites used in Task II testing, and 50 from the (B_4C)boron/15-3-3-3 titanium composite chosen in Task II. The model verification test plan is outlined in Figures 117 and 118.

Test Objective	Laminate/No. of Tests			Total Tests
	0°	0°/90°	0°/±45°	
Static Properties				
Baseline (Panel-to-Panel Bias)	2	2	2	6
Thin (Panel-to-Panel Bias)	2	2	2	6
Large Hole	2	2	2	6
Small W/D	2	2	2	6
Fatigue Life Tests				
Stress Life				
R=0	2	2	2	6
R=−1	4	2	2	8
Stress Ratio				
R=0.5	2	2	2	6
R=−2.0	2	2	2	6
Geometry				
Thin	4	2	2	8
Large Hole	4	2	2	8
Small W/D	4	2	2	8
Countersink	4	2	2	8
Residual Strength Tests				
Thin	2	2	2	6
Large Hole	2	2	2	6
Small W/D	2	2	2	6
Total Tests	40	30	30	100

Figure 117. Verification Testing in Boron/Aluminum

Test Objective	Test Description	Specimen Type	Number of Replications	Total Tests
Static Properties				
Unnotched Strength	Tension	Unnotched	2	2
	Compression	Unnotched	2	2
	Transverse Tension	Unnotched	2	2
Baseline (Panel-to-Panel Bias)	Tension (3 Panels)	Baseline	2	2
		Thin	2	4
Fatigue Life Tests				
Stress Ratio				
R = 0	R = 0, 2 Stress Levels	Baseline	2	4
R = −1	R = −1, 2 Stress Levels	Baseline	2	4
R = −∞	R = −∞, 2 Stress Levels		2	4
Baseline (Panel-to-Panel Bias)	R = 0, 2 Panels	Thin	2	4
Unnotched Specimen	R = 0	Unnotched	2	2
	R = −1	Unnotched	2	2
Center Cracked Panel	R = 0	Thin Center Cracked	2	2
	R = −1	Center Cracked	2	2
Residual Strength Tests				
Baseline				
Tension Residual	R = 0, 2 Stress Levels	Thin	2	4
	R = −1, 2 Stress Levels	Baseline	2	4
Compression Residual	R = −1, 2 Stress Levels	Baseline	2	4
Center Cracked Panel				
Tension Residual	R = 0	Thin Center Cracked	2	2
Total Tests				**50**

Figure 118. Verification Testing in Boron/Titanium

1. <u>MATERIALS AND LAYUPS</u> - The same layups were used for verification testing in the boron/aluminum materials as were used in the development testing. All boron/titanium FRMMC was fabricated with unidirectional layups. The high transverse strength of titanium metal matrix composites eliminates the need to cross-ply.

2. <u>SPECIMEN GEOMETRIES</u> - The baseline specimen (Figure 11) was used in most of the tests. It was selected because it represents the most common type of fatigue damage initiation site in any structural material: bolt holes and cut-outs. Specimens having only eight plies of FRMMC (Figure 119) were used to investigate thickness effects in both unidirectional and crossplied boron/ aluminum and also to reduce specimen costs for tension-only tests in the boron/titanium material. Thickness was expected to have

131

greatest effect on crossplied FRMMC material in which interlaminar stresses work to degrade fiber-to-matrix bonds. The influence of thickness on life in unidirectional FRMMC was evaluated in the boron/aluminum tests prior to committing to this specimen in boron/titanium.
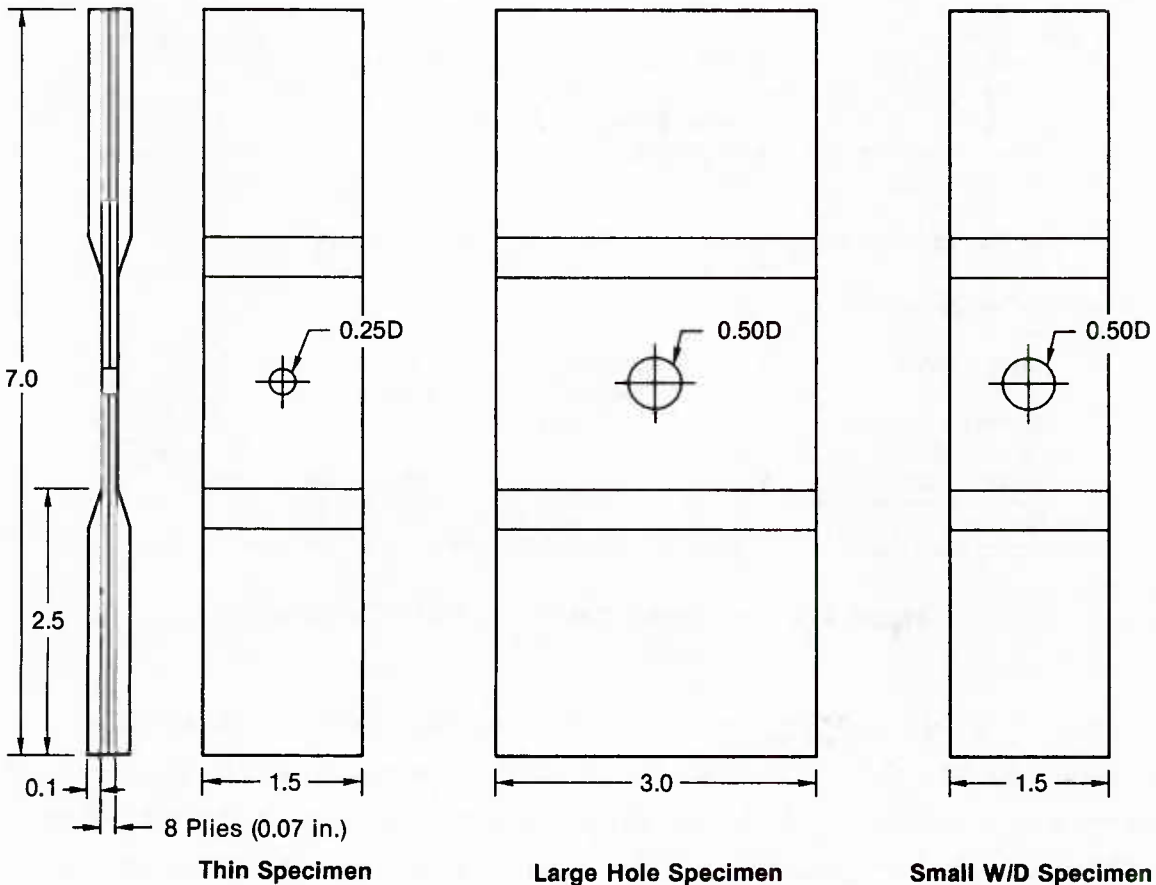
Figure 119. Specimen Geometries for Verification Testing

To verify the ability of the analysis methodology to predict the effects of stress concentrations on fatigue life in FRMMC structures, static and fatigue tests were conducted on specimens having large holes, small W/D, and countersink fastener holes.

The large fastener hole specimen is shown in Figure 119.
Hole size is known to significantly affect fatigue life in metals.
In tests performed at MCAIR, we have found large differences in
life between metal specimens having different hole sizes, even
when stress levels are selected to give the same predicted stress
at the hole boundary for each hole size. Carbon/epoxy materials,
particularly those having highly fiber dominated layups, show
little sensitivity in fatigue to hole size for unloaded holes,
although hole size is known to affect the strength of notched
carbon/epoxy laminates.

Metal and carbon/epoxy material systems differ in the way
damage progresses under fatigue loadings. In both materials, the
initial stress distribution is significantly affected by hole
size. Although the stress distribution affects crack growth in
metals, in fiber dominated composites, cracking extends from the
hole along the fibers and reduces stress concentrations. Thus,
life in the composite material depends primarily on net section
stress rather than on the unflawed local stress. Tests of
specimens with larger holes were used to determine the effect of
stress gradient on damage progression in FRMMC.

The final specimen shown in Figure 119 was used to investi-
gate small W/D. Using the larger hole size for these tests
allowed greater specimen size and more room to track flaw growth.

Countersink fastener holes and flush head fasteners are
commonly used to attach skins to airframes. These holes produce
higher stress concentrations than do cylindrical holes. In
carbon/epoxy laminates, an average hole size was found to produce
good correlation between strength predictions using BJSFM and test
data. In metals, strength is accurately predicted using net
stress. Tests of the specimens of Figure 120 were used to
determine which analysis best predicts strength in FRMMC and
verify that life analyses developed in this program are applicable
to these common hole types.

Dimensions are in inches
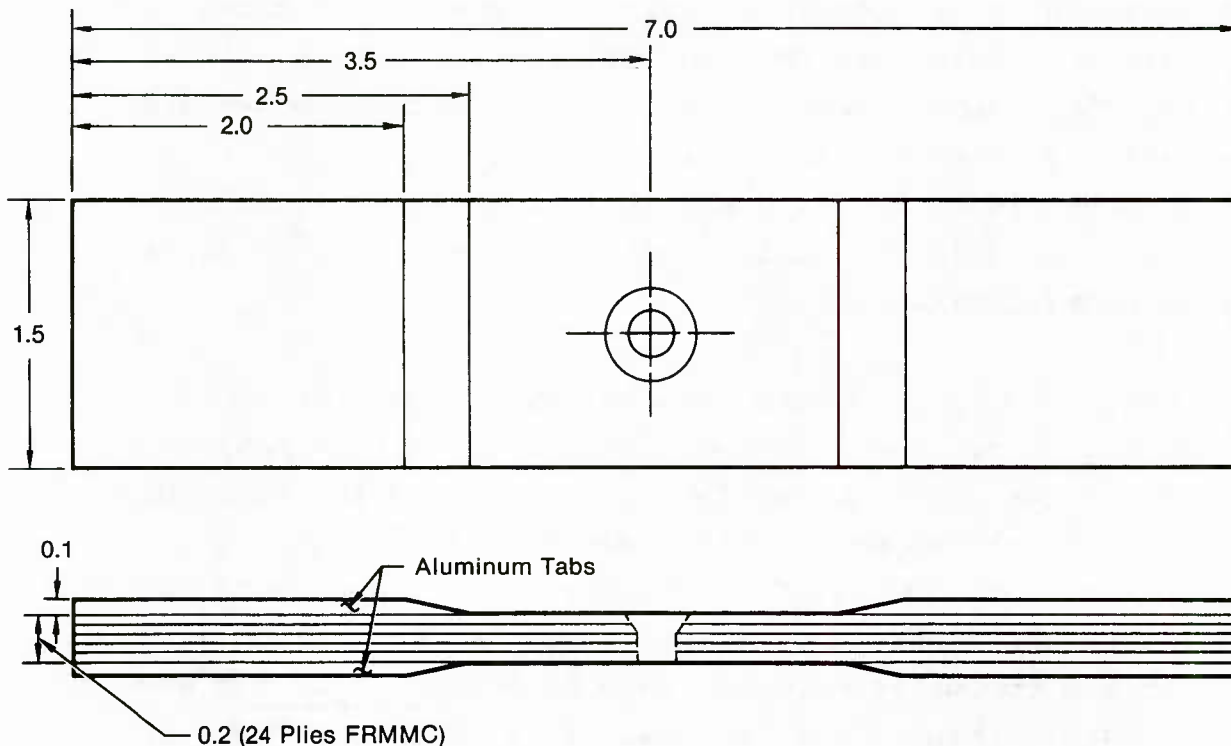
Figure 120. Countersink Hole Specimen

Center cracked panels (Figure 11) were tested only in the boron/titanium material. Based on our previous testing and analysis, we expected to find that cracks grow across the net section in the unidirectional boron/titanium. These tests were used to verify that standard fracture mechanics methodology can be accurately applied to this material system.

3. <u>STATIC PROPERTIES</u> - The tests outlined in Figure 121 were performed to determine the static ultimate tension strengths of the boron/aluminum specimens used during verification testing. The notched specimens, the baseline specimen (Figure 11) and the thin specimen (Figure 119), were used to measure tensile strength variations between panels.

134

Specimen Type	Laminate	Specimen No.	Specimen Type			Predicted Strength (kip)	Predicted Strength (ksi)	Measured Strength (kip)	Measured Strength (ksi)
			Width (in.)	Thick (in.)	Diameter (in.)				
Baseline	0	1-4-61	1.50	0.172	0.25	25.40	118.14	26.50	123.26
	0	1-4-71	1.50	0.172	0.25	25.40	118.14	28.35	131.86
	0/90	2-2-93	1.50	0.172	0.25	12.50	58.14	11.24	52.28
	0/90	2-2-92	1.50	0.172	0.25	12.50	58.14	11.69	54.37
	0/45	3-2-62	1.50	0.172	0.25	14.05	65.35	14.61	67.95
	0/45	3-2-52	1.50	0.172	0.25	14.05	65.35	12.77	59.40
Thin Baseline	0	1-6-11	1.50	0.060	0.25	8.50	113.33	8.68	115.73
	0	1-6-12	1.50	0.060	0.25	8.50	113.33	8.67	115.60
	0/90	2-3-23	1.50	0.060	0.25	4.30	57.33	4.05	54.00
	0/90	2-3-15	1.50	0.060	0.25	4.30	57.33	4.59	61.20
	0/45	3-3-15	1.50	0.060	0.25	5.20	64.33	4.35	58.00
	0/45	3-3-23	1.50	0.060	0.25	5.20	64.33	4.15	55.33
	0/45	3-3-25	1.50	0.060	0.25	5.20	64.33	4.30	57.33
Large Hole W/D = 6	0	1-5-25	3.00	0.060	0.50	14.30	95.33	8.68	57.87
	0	1-5-26	3.00	0.060	0.50	14.30	95.33	8.67	57.80
	0/90	2-3-26	3.00	0.060	0.50	7.20	48.00	7.59	50.00
	0/90	2-3-34	3.00	0.060	0.50	7.20	48.00	8.75	58.33
	0/45	3-3-26	3.00	0.060	0.50	8.80	58.67	8.29	55.27
	0/45	3-3-31	3.00	0.060	0.50	8.80	58.67	8.90	59.33
Small W/D W/D = 3	0	1-5-21	1.50	0.060	0.50	6.30	105.00	6.29	104.83
	0	1-5-22	1.50	0.060	0.50	6.30	105.00	6.00	100.00
	0/90	2-3-16	1.50	0.060	0.50	3.20	53.33	3.05	50.83
	0/90	2-3-17	1.50	0.060	0.50	3.20	53.33	3.81	63.50
	0/90	2-3-11	1.50	0.060	0.50	3.20	53.33	3.23	53.83
	0/45	3-3-11	1.50	0.060	0.50	3.90	65.00	3.44	57.33
	0/45	3-3-17	1.50	0.060	0.50	3.90	65.00	3.93	65.00
Countersink	0		1.50	0.172	0.25	21.60	100.47	22.88	106.42

Figure 121. Static Strength Results for Boron/Aluminum Laminates

The large hole and small W/D (Figure 119) specimens were tested as outlined in Figure 120 to provide a comparison base for subsequent residual strength tests of these specimen types. Static test predictions and results are presented in Figure 122 for $(B_4C)B/15$-3 titanium.

4. FATIGUE LIFE TESTS - The results from the 58 fatigue tests outlined in Figure 123 were used to determine methodology accuracy in the areas of stress level, stress ratio, and geometry for boron/aluminum. The stress level tests outlined in Figure 115 differ from those performed in the model development testing (Figure 52, Section III).

Specimen Type	Test Type	Specimen No.	Specimen Geometry			Predicted Strength (kip)	Predicted Strength (ksi)	Measured Strength (kip)	Measured Strength (ksi)
			W (in.)	T (in.)	D (in.)				
Unnotched	Tension	4-1-13	1.25	0.172	—	29.1	135.3	26.55	123.5
		4-1-14	1.25	0.172	—	29.1	135.3	26.30	122.3
	Compression	4-1-15	1.25	0.172	—	45.4	211.2	34.10	158.6
		4-1-16	1.25	0.172	—	45.4	211.2	31.85	148.1
	Trans. Tension	4-1-19	1.25	0.172	—	10.8	50.2	11.73	54.6
		4-2-17	1.25	0.172	—	10.8	50.2	9.15	42.6
Notched Baseline		4-2-11	1.5	0.172	0.25	18.9	87.9	24.90	115.8
		4-2-12	1.5	0.172	0.25	18.9	87.9	25.30	117.7
Thin (Panel 1)	Tension	4-6-11	1.5	0.06	0.25	6.3	84.0	6.99	93.2
		4-6-12	1.5	0.06	0.25	6.3	84.0	6.91	92.1
Thin (Panel 2)		4-7-11	1.5	0.06	0.25	6.3	84.0	6.94	92.5
		4-7-12	1.5	0.06	0.25	6.3	84.0	7.33	97.7

Figure 122. Static Strength Results for Unidirectional Boron/Titanium

Specimen Type	Specimen Number	Specimen Type			Loading			Predicted Life Cycles	Measured Life Cycles
		W (in.)	T (in.)	D (in.)	R	P_{max} (kip)	Stress (ksi)		
Baseline	1-4-81	1.5	0.172	0.25	0.02	18	83.7	10,000	9,200
	1-4-91	1.5	0.172	0.25	0.02	18	83.7	10,000	12,400
	1-4-13	1.5	0.172	0.25	−1	15.5	72.1	300	880
	1-4-33	1.5	0.172	0.25	−1	15.5	72.1	300	810
	1-4-43	1.5	0.172	0.25	−1	12.7	59.1	1,000	2,000
	1-4-53	1.5	0.172	0.25	−1	12.7	59.1	1,000	2,220
	1-4-63	1.5	0.172	0.25	0.5	20	93.0	400,000	600,000 NF
	1-4-73	1.5	0.172	0.25	0.5	20	93.0	400,000	809,000 NF
	1-4-83	1.5	0.172	0.25	−2	12.7	59.1	1,000	1,075
	1-4-93	1.5	0.172	0.25	−2	12.7	59.1	1,000	600
Thin Baseline	1-6-13	1.5	0.06	0.25	0.02	9	120.0	1	12
	1-6-16	1.5	0.06	0.25	0.02	7.5	100.0	10,000	41
	1-6-14	1.5	0.06	0.25	0.02	6	80.0	100,000	118,453
	1-6-17	1.5	0.06	0.25	0.02	6	80.0	100,000	60,000
Large Hole W/D=6	1-5-13	3	0.06	0.5	0.02	13.3	88.7	100	100
	1-5-14	3	0.06	0.5	0.02	11.9	79.3	10,000	6,300
	1-5-15	3	0.06	0.5	0.02	10.3	68.7	50,000	31,000
	1-5-16	3	0.06	0.5	0.02	10.3	68.7	50,000	17,000
Small W/D W/D=3	1-6-26	1.5	0.06	0.5	0.02	5.2	69.3	1,000	750
	1-6-27	1.5	0.06	0.5	0.02	4.2	56.0	10,000	21,700
	1-6-28	1.5	0.06	0.5	0.02	3.5	46.7	100,000	260,000
	1-6-29	1.5	0.06	0.5	0.02	3.5	46.7	100,000	200,000
Countersink	1-3-92	1.5	0.172	0.25	0.02	13.3	61.9	10,000	133
	1-4-62	1.5	0.172	0.25	0.02	10.3	47.9	100,000	623,000
	1-4-72	1.5	0.172	0.25	0.02	12	55.8	100,000	625,000

Figure 123. Fatigue Life Results for Unidirectional Boron/Aluminum

136

Tests were performed using R = 0.5 and R = -2.0, to determine
model accuracy in predicting the effects of stress ratio. Results
of these tests (Figure 123) can be compared to those performed in
model development (Figure 52).

The final, and perhaps most significant, tests performed in
fatigue life verification for boron/aluminum were those evaluating
the effects of geometry. Specimens having only eight plies of
FRMMC (Figure 119) were used to investigate thickness effects.
Verification tests were performed using the large hole specimen to
evaluate the effects of hole size in comparison to the model
development tests which used the smaller hole baseline specimen
(Figure 11). To complete the investigation of effects of
cylindrical hole geometry on life behavior, tests were performed
with W/D = 3 specimens (Figure 119) to contrast with the result of
the baseline W/D = 6 specimen (Figure 11) behavior. At small
W/D, specimen width significantly increases the stress concentra-
tion and can affect the fatigue life behavior.

Countersinks increase stress concentrations. Results of
tests to evaluate the ability of the models to predict this effect
are outlined in Figure 123.

A similar series of tests was performed on the 0/90 and 0/±45
crossplied boron/aluminum laminates. The test results are
compared with analytical predictions in Figure 124. Crossplied
laminates showed much more scatter than the unidirectional
material because the crossplies fail early and can initiate
failures in the 0° plies earlier than predicted assuming no such
interaction.

To test our prediction capability in boron/titanium, the test
program outlined in Figure 125 was performed. This testing
parallels the model development testing for boron/aluminum to
determine if analysis results can be accurately extrapolated to

other material systems. Stress ratio tests (R = 0, -1, -∞) were performed at multiple stress levels, to evaluate the effect of stress ratio on life and model accuracy.

Specimen Type	Laminate	Specimen No.	Specimen Type			Loading			Predicted Life Cycles	Measured Life Cycles
			W (in.)	T (in.)	D (in.)	R	P_{max} (kip)	Stress (ksi)		
Baseline	0/90	2-2-72	1.50	0.172	0.25	−99	11.00	51.16	NF	270,000 NF
	0/90	2-2-82	1.50	0.172	0.25	−99	11.00	51.16	NF	270,000 NF
	0/45	3-2-72	1.50	0.172	0.25	0	11.50	53.49	30,000	60,213
	0/45	3-2-82	1.50	0.172	0.25	0	12.00	55.81	20,000	22,000
	0/90	2-2-12	1.50	0.172	0.25	−1	9.00	41.86	2,000	18,785
	0/90	2-2-33	1.50	0.172	0.25	−1	9.00	41.86	2,000	5,247
	0/45	3-2-92	1.50	0.172	0.25	−1	9.00	41.86	50,000	200,000 NF
	0/45	3-2-32	1.50	0.172	0.25	−1	11.00	51.16	100	8,880
	0/90	2-2-73	1.50	0.172	0.25	−0.5	10.00	46.51	1,000	6,760
	0/90	2-2-83	1.50	0.172	0.25	−0.5	10.00	46.51	1,000	5,466
	0/45	3-2-43	1.50	0.172	0.25	0.5	12.00	55.81	200,000	100,000 NF
	0/45	3-2-53	1.50	0.172	0.25	0.5	14.00	65.12	40,000	72,154
	0/90	2-2-53	1.50	0.172	0.25	2	7.50	34.88	NF	270,000NF
	0/90	2-2-43	1.50	0.172	0.25	2	8.50	39.53	NF	200,000 NF
	0/45	3-2-73	1.50	0.172	0.25	−2	6.00	27.91	250,000	100,000 NF
	0/45	3-2-83	1.50	0.172	0.25	−2	7.00	32.56	70,000	22,840
Thin Baseline	0/90	2-3-21	1.50	0.060	0.25	−1	3.10	41.33	2,000	103
	0/90	2-3-22	1.50	0.060	0.25	−1	3.10	41.33	2,000	6,400
	0/45	3-2-73	1.50	0.172	0.25	−1	3.20	42.67	20,000	27,500
	0/45	3-2-83	1.50	0.172	0.25	−1	3.10	41.33	30,000	72,300
Large Hole W/D = 6	0/90	2-3-12	3.00	0.060	0.50	−1	5.51	36.73	8,000	7,320
	0/90	2-3-13	3.00	0.060	0.50	−1	5.51	36.73	8,000	7,320
	0/45	3-3-12	3.00	0.060	0.50	−1	5.51	36.73	70,000	139,774
	0/45	3-3-13	3.00	0.060	0.50	−1	5.51	36.73	70,000	131,684
Small W/D W/D = 3	0/90	2-3-31	1.50	0.060	0.50	−1	2.34	39.00	8,000	5,790
	0/90	2-3-32	1.50	0.060	0.50	−1	2.34	39.00	8,000	6,970
	0/45	3-3-34	1.50	0.060	0.50	−1	2.50	41.67	50,000	30,300
	0/45	3-3-32	1.50	0.060	0.50	−1	2.34	39.00	90,000	74,766
Countersink	0/90	2-2-42	1.50	0.172	0.50	−99	9.00	52.33	NF	200,000 NF
	0/45	3-2-12	1.50	0.172	0.50	−99	9.50	55.23	NF	200,000 NF

Figure 124. Fatigue Life Results for Crossplied Boron/Aluminum

138

Specimen Type	Specimen No.	Specimen Geometry			Loading			Predicted Life Cycles	Measured Life Cycles
		W (in.)	T (in.)	D (in.)	Stress Ratio	P_{max} (kip)	Stress (ksi)		
Baseline	4-2-13	1.5	0.172	0.25	0.02	7.3	34.0	100,000	138,900
	4-2-14	1.5	0.172	0.25	0.02	9.7	45.1	50,000	29,121
	4-2-15	1.5	0.172	0.25	0.02	13.1	60.9	5,000	4,770
	4-2-16	1.5	0.172	0.25	0.02	13.1	60.9	5,000	5,032
	4-3-11	1.5	0.172	0.25	−1	6.6	30.7	100,000	154,778
	4-3-12	1.5	0.172	0.25	−1	6.6	30.7	100,000	128,160
	4-3-13	1.5	0.172	0.25	−1	11.8	54.9	5,000	6,845
	4-3-14	1.5	0.172	0.25	−1	11.8	54.9	5,000	7,620
	4-3-15	1.5	0.172	0.25	−50	22.5	104.7	100,000	438,000+
	4-3-16	1.5	0.172	0.25	−50	22.5	104.7	100,000	300,000+
Thin (Panel 2)	4-6-15	1.5	0.06	0.25	0.02	2.4	32.0	100,000	134,810
	4-6-16	1.5	0.06	0.25	0.02	2.4	32.0	100,000	177,640
Thin (Panel 3)	4-6-17	1.5	0.06	0.25	0.02	2.4	32.0	100,000	227,430
	4-6-18	1.5	0.06	0.25	0.02	2.4	32.0	100,000	149,982
Unnotched	4-1-11	1.25	0.172	—	0.02	15	69.8	50,000	50,732
	4-1-12	1.25	0.172	—	0.02	15	69.8	50,000	60,402
	4-4-11	1.25	0.172	—	0.02	15	69.8	50,000	114,825
	4-5-11	1.25	0.172	—	0.02	15	69.8	50,000	185,582
Center Crack	4-6-19	1.5	0.06	0.25	0.02	2.5	33.3	50,000	47,900
	4-7-15	1.5	0.06	0.25	0.02	2.4	33.3	50,000	83,800
	4-5-16	1.5	0.172	0.25	−1	6.6	30.7	50,000	80,840
	4-5-17	1.5	0.172	0.25	−1	6.6	30.7	50,000	95,980

Figure 125. Fatigue Life Results for Unidirectional Boron/Titanium

Three panels were required to fabricate the specimens for fatigue testing in the boron/titanium verification testing. Two specimens (Figure 11) from each of two panels were tested at R = 0, and results compared to the tests of the third panel (included in the R=0, stress ratio test series) to permit evaluation of panel-to-panel bias on life behavior.

Tests of center cracked panels (Figure 11) were performed to determine if flaw growth rates obtained from this specimen can be related to rates observed in fastener hole tests. The results shown in Figure 114 show the accuracy of the predictions versus the test results.

139

5. RESIDUAL STRENGTH TESTS - In the verification test program 16 residual strength tests were performed in the boron/aluminum system (Figure 126). These tests were designed to evaluate prediction accuracy in the area of specimen geometry. Thin, large hole, and small W/D specimens had the largest geometry variations from the baseline specimen, and were used in this investigation. The specimens were subjected to R = 0.02 constant amplitude fatigue cycling until a particular crack length was obtained. Then the specimen was statically failed to determine residual tension strength.

| Specimen Type | Laminate | Specimen No. | Specimen Type | | | Loading | | | Crack Length (in.) | Predicted Strength (kip) | Predicted Strength (ksi) | Measured Strength (kip) | Measured Strength (ksi) |
			Width (in.)	Thick (in.)	Hole Dia (in.)	R	P_{max} (kip)	Stress (ksi)					
Thin Baseline	0	1-6-18	1.50	0.060	0.25	0.02	5.67	75.6	0.05	8.50	113.3	8.28	110.4
	0	1-6-19	1.50	0.060	0.25	0.02	5.67	75.6	0.05	8.50	113.3	8.34	111.2
	0/90	2-3-25	1.50	0.060	0.25	−99	3.00	40.0	NA	3.40	45.3	4.02	53.6
	0/45	3-3-23	1.50	0.060	0.25	−99	3.00	40.0	NA	4.20	56.0	4.18	55.7
	0/45	3-3-24	1.50	0.060	0.25	0.02	3.00	40.0	NA	4.20	56.0	3.96	52.8
Large Hole W/D=6	0	1-5-23	3.00	0.060	0.50	0.02	9.50	63.3	0.05	14.30	95.3	13.42	89.5
	0	1-5-24	3.00	0.060	0.50	0.02	9.50	63.3	0.05	14.30	95.3	13.44	89.6
	0/90	2-3-34	3.00	0.060	0.50	−99	3.00	20.0	NA	5.80	38.7	6.96	46.4
	0/45	3-3-31	3.00	0.060	0.50	0.02	2.50	16.7	NA	7.00	46.7	8.83	58.9
	0/45	3-3-33	3.00	0.060	0.50	0.02	2.50	16.7	NA	7.00	46.7	8.21	54.7
Small W/D W/D=3	0	1-5-11	1.50	0.060	0.50	0.02	4.20	70.0	0.05	6.30	105.0	6.16	102.7
	0	1-5-12	1.50	0.060	0.50	0.02	4.20	70.0	0.05	6.30	105.0	*	*
	0/90	2-3-14	1.50	0.060	0.50	−99	3.00	50.0	NA	2.60	43.3	2.99	49.8
	0/90	2-3-16	1.50	0.060	0.50	−99	3.00	50.0	NA	2.60	43.3	3.04	50.7
	0/45	3-3-14	1.50	0.060	0.50	0.02	2.50	41.7	NA	3.10	51.7	3.24	54.0
	0/45	3-3-16	1.50	0.060	0.50	0.02	2.50	41.7	NA	3.10	51.7	3.70	61.7

*Machine malfunction

Figure 126. Residual Strength Results for Boron/Aluminum Laminates

In the boron/titanium system 18 residual strength tests were performed. The majority of these tests were performed using the baseline specimen (Figure 11), to determine if the predictive methodology could account for the differences in failure modes between the aluminum and titanium matrix materials. These tests were performed in the same manner as in the aluminum matrix

140

system, with the addition of compression residual strength tests
for a few specimens. In addition, for the titanium matrix system,
two residual tension tests were performed following R = 0 fatigue
cycling, using center cracked panels. These tests were used to
verify correlation of fracture mechanics based residual strength
predictions with the results from fastener hole and center cracked
specimens. The results are shown in Figure 127.

Specimen Type	Specimen No.	Specimen			Loading			Crack Length (in.)	Predicted Strength (kip)	Predicted Strength (ksi)	Measured Strength (kip)	Measured Strength (ksi)
		W (in.)	T (in.)	D (in.)	Stress Ratio	P_{max} (ksi)	Stress (kip)					
Thin Baseline	4-6-13	1.5	0.06	0.25	0.02	2.4	32.0	0.05	6.6	88.0	5.92	78.9
	4-7-13	1.5	0.06	0.25	0.02	2.4	32.0	0.05	6.6	88.0	6.77	90.3
	4-6-14	1.5	0.06	0.25	0.02	2.0	26.7	0.125	5.65	76.3	*	*
	4-7-14	1.5	0.06	0.125	0.02	2.0	26.7	0.125	5.65	75.3	5.22	69.6
Baseline Tension	4-4-14	1.5	0.172	0.25	0.02	7.3	34.0	0.05	18.9	87.9	18.9	87.9
	4-4-15	1.5	0.172	0.25	0.02	7.3	34.0	0.05	18.9	87.9	19.0	88.4
	4-4-16	1.5	0.172	0.25	0.02	7.0	32.6	0.125	16.2	75.3	15.4	71.6
	4-4-17	1.5	0.172	0.25	0.02	7.0	32.6	0.125	16.2	75.3	14.95	69.5
Baseline Compression	4-5-13	1.5	0.172	0.25	0.02	7.3	34.0	0.05	−40.9	−190.2	−48.8	227.0
	4-5-13	1.5	0.172	0.25	0.02	7.3	34.0	0.05	−40.9	−190.2	−47.2	219.5
	4-5-14	1.5	0.172	0.25	0.02	7.0	32.6	0.125	−38.8	−180.5	−45.0	209.3
	4-5-15	1.5	0.172	0.25	0.02	7.0	32.6	0.125	−38.8	−180.5	−45.5	211.6
Thin Center Crack	4-7-16	1.5	0.06	0.25	0.02	2.0	26.7	0.25	5.4	72.0	5.3	70.7
	4-7-17	1.5	0.06	0.25	0.02	2.0	36.7	0.25	5.4	72.0	5.44	72.5

*Machine malfunction during gripping

Figure 127. Residual Strength Results for Unidirectional Boron/Titanium

6. <u>FAILURE MODE IDENTIFICATION</u> - Failure modes in the analysis
verification testing were determined using the best NDE techniques
from those evaluated during model development testing. These were
found to be visual examinations and displacement monitoring during
test.

After failure, the failure mechanisms were identified using
the scanning electron microscope. With this instrument we can
identify areas of fatigue fracture, static fracture, fiber
pullout, and the character of suspected local initiation sites and
inclusions.

141

COMPARISON OF ANALYSIS AND TEST RESULTS

As shown in the tabulated data of the previous section, the correlation of test results and predicted behavior of both titanium and aluminum MMC materials was good. However, it is difficult to assess the accuracy of a technique from data tabulations alone. In this section the predictions and test results for all of the analyses and test results used to evaluate the analysis methods are compared, graphically wherever possible.

1. STRENGTH ANALYSIS VERIFICATION - The results of the strength analysis verification tests in unidirectional boron/aluminum are shown in Figure 128. There was very good correlation between the predicted and measured strengths for all of the specimens tested.
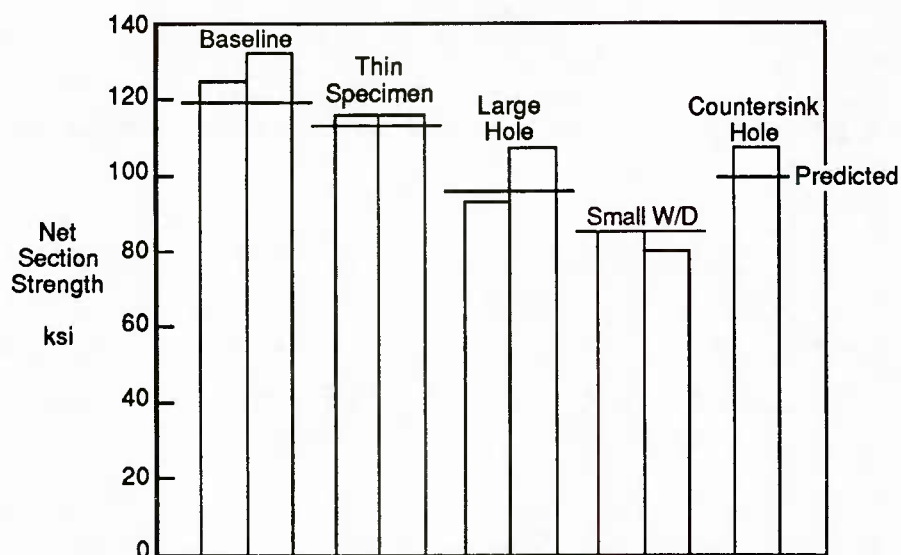
Figure 128. Notched Strength Analysis Verification in Boron/Aluminum

The thin specimens, as predicted, showed strengths one third those of the thicker specimens. The large hole specimens, twice as large as the thin baseline specimen, were predicted to have strengths slightly less than twice those of the thin baseline specimens. The reduction is due to the fact that, even though the extent of yielding is about the same as that for the smaller specimen, the stress concentration at the larger hole is not reduced quite as much. Thus, the load at failure is not quite twice as high as that for the thin baseline specimen.

For the W/D=3 specimen the strengths were predicted to be about 80 percent of those in the baseline specimen due primarily to the slightly higher net section stress level. This specimen has a slightly higher K_t than the baseline specimen but, in this specimen, the higher K_t primarily results in earlier yielding in the matrix, it does not directly affect the strength.

For the crossplied boron/aluminum specimens the same type of correlation was found with the predicted strengths (Figure 129). Since the strengths of these layups were dominated by the 0° plies, the behavior is easily predicted from the 0° unidirectional results, modified by the stiffness reduction in the crossplies that accounts for the yielding and cracking that occurs in those plies.
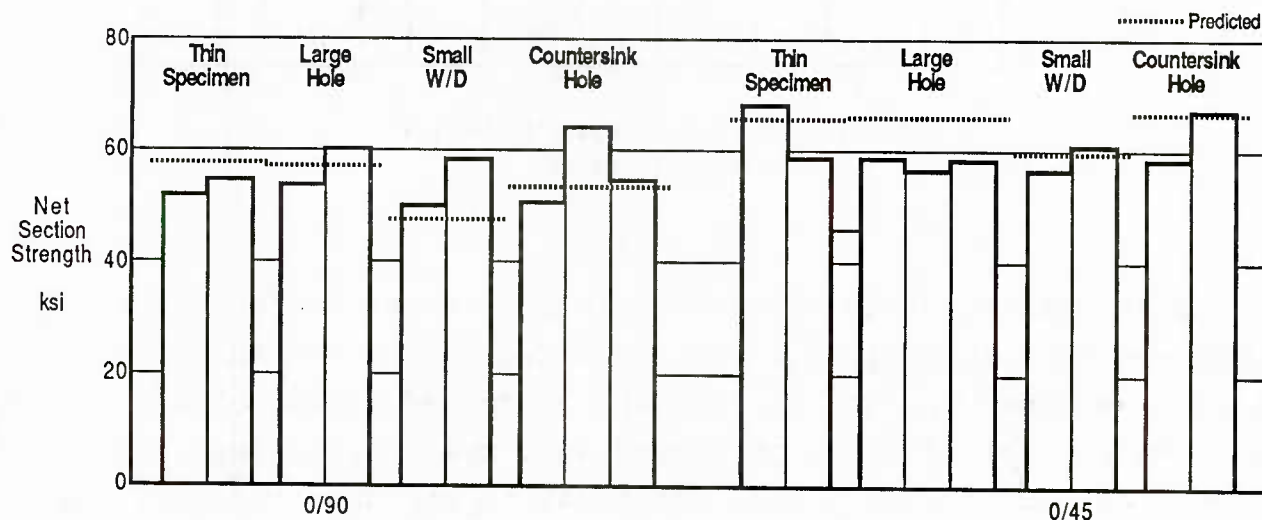
Figure 129. Notched Strength Analysis Verification Results in Crossplied Boron/Aluminum

143

One of the biggest surprises in all of the verification test results was that of the boron/titanium tests of unnotched and open hole tests, as shown in Figure 130. We had originally assumed that the fiber strengths in the boron/titanium material would be above 300 ksi. While this strength would still make the material vulnerable to net section cracking in fatigue, it would still make the strength, in either notched or unnotched conditions, fiber strength controlled as in the boron/aluminum. Thus the predictions showed a significant reduction in notched versus unnotched strengths.
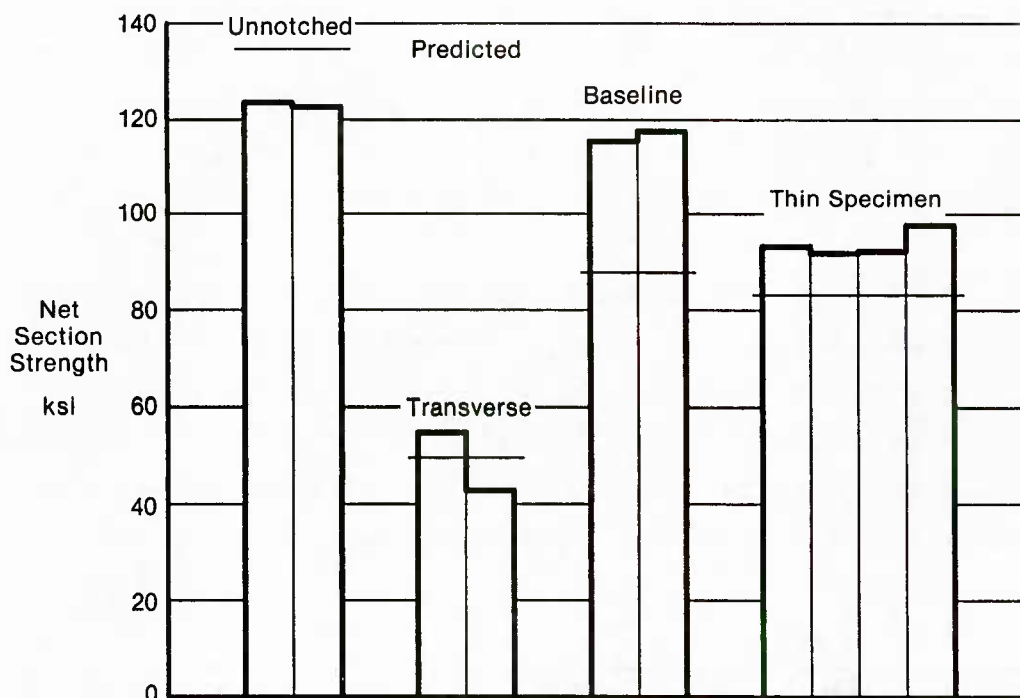
Figure 130. Strength Analysis Verification
in Boron/Titanium

This difference in strength between notched and unnotched specimens in boron/titanium was not borne out by the test results at all, as shown in Figure 130. The unnotched strengths were about 90 percent of those predicted and, most surprising, the notched strengths were almost identical to the unnotched values. This behavior was almost like that of unreinforced metals.

144

Examination of the unnotched static test results shows why this occurred. The load displacement plot, shown in Figure 131 for an unnotched boron/titanium specimen, shows that there is significant nonlinearity in response to load. To correlate this nonlinearity with the analysis technique requires that the fiber strengths be less than 200 ksi. Once that fiber strength is used in the analysis, the correlation between the analysis results and the unnotched and notched test data is significantly improved (Figure 132).
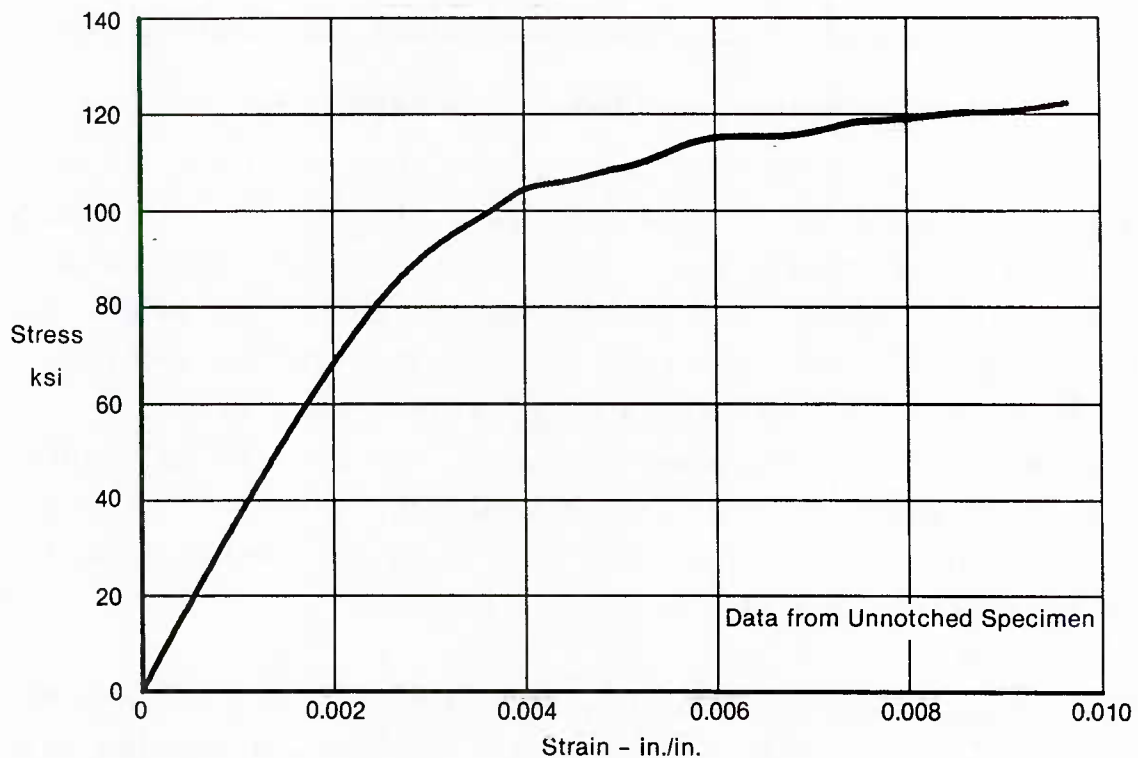
Figure 131. Stress-Strain Behavior of $(B_4C)B/Ti$ After SPF/DB Cycle Is Highly Nonlinear

145
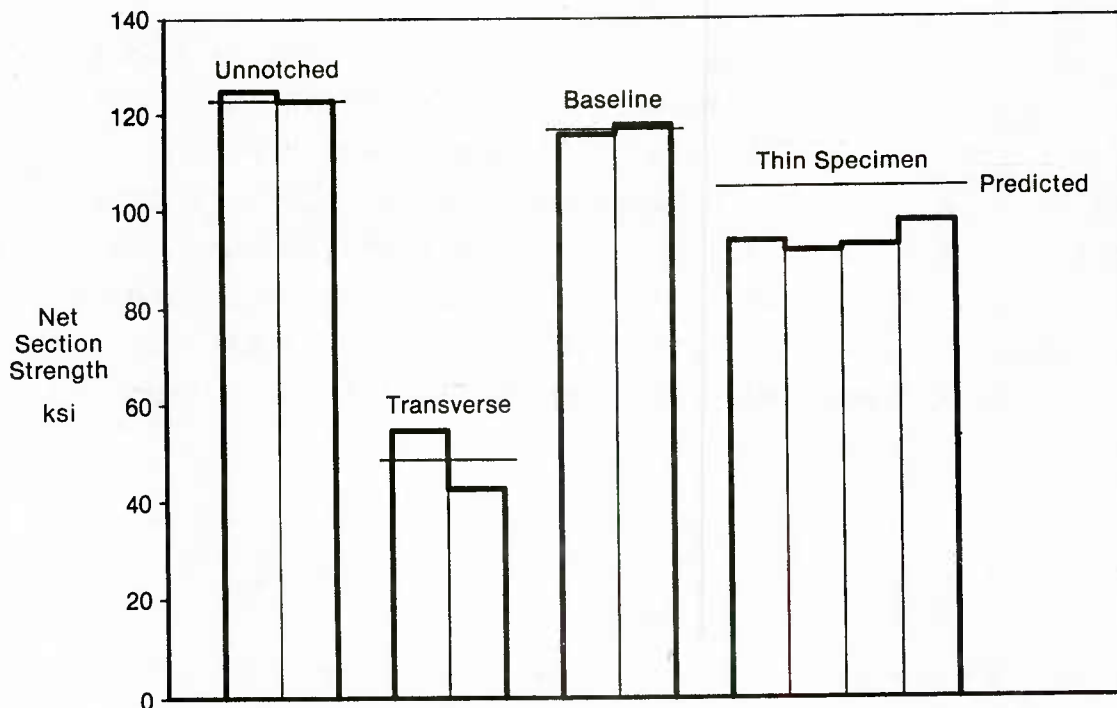
Figure 132. Revised Boron/Titanium Strength Analysis Results

There is a good reason for this low fiber strength in the boron/titanium material. This material, after consolidation, was put through an extensive superplastic forming/diffusion bonding (SPF/DB) thermal cycle to simulate its projected use in aircraft structure (specifically the F-15 horizontal stabilator torque box). This SPF/DB cycle was known to cause fiber strength degradations. This was shown by Niemann and Dorr in Reference 37, as shown in Figure 133. There are ramifications of this loss in fiber strength that are addressed in subsequent sections as they affect the correlation of analysis and test.

2. <u>FATIGUE FAILURE MODE ANALYSIS</u> - Figures 134 and 135 summarize the correlation of fatigue failure lives and failure modes between the predictions and verification test results. In general the fatigue failure modes in the verification tests were predicted to be always along the fibers in the unidirectionally reinforced boron/aluminum and always across the net section in the boron/titanium material. To a certain extent these results were dictated by the stress levels used to obtain reasonable lives in
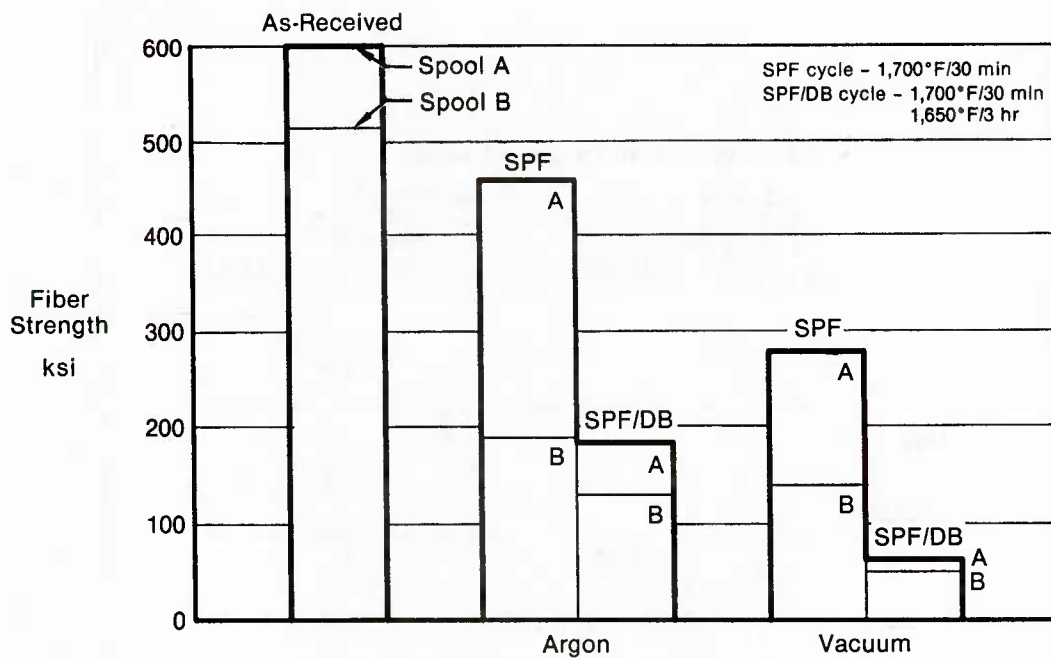
Figure 133. The Effect of SPF/DB Cycle in (B₄C)B Fiber Strength
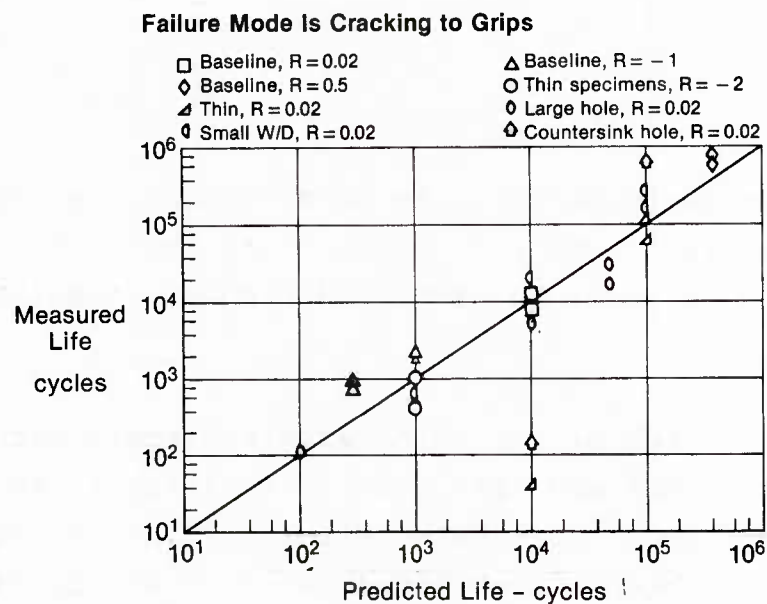
Figure 134. Boron/Aluminum Model Verification Test Results
Undirectional Reinforced

147

Failure Mode Is Net Section Fracture

□ Baseline, R = 0.02   △ Baseline, R = −1
◇ Baseline, R = −∞   ○ Thin specimens, R = 0.02
▲ Unnotched, R = 0.02   ◐ Unnotched, R = −1
◖ Center cracked panel, R = 0.02   ◇ Center cracked panel, R = −1
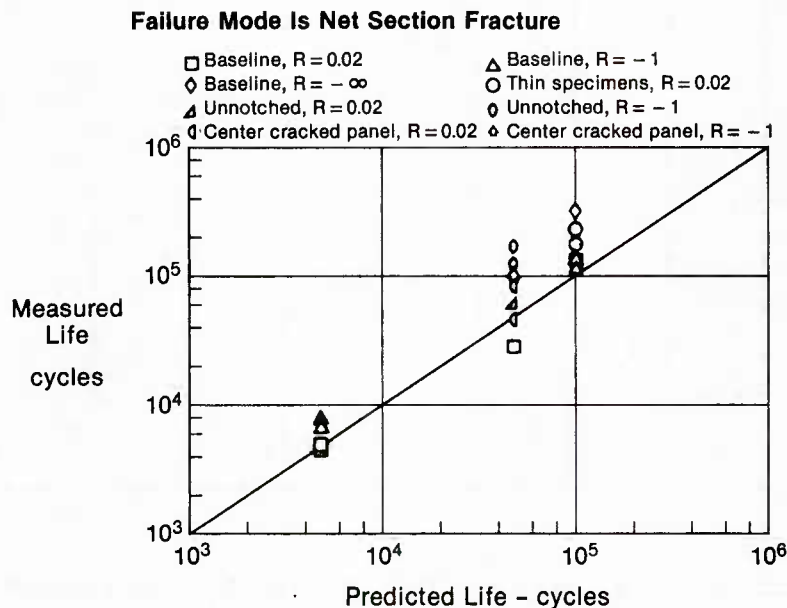
Figure 135. (B₄C)B/15-3 Titanium Model Verification Test Data
Undirectionally Reinforced

the boron/aluminum material. As shown before, the stress level in boron/aluminum can be raised to the point that a net section failure can occur, but the lives under those conditions are very short.

In fact, in two of the boron/aluminum tests (shown in Figure 134) net section failures did occur, resulting in very short fatigue lives. In one of these tests, a thin specimen tested at R = 0.02, a very high stress level was applied initially, then reduced to the desired level. Evidently the high load was applied long enough to initiate a net section failure that continued to propagate very rapidly, even under the lower load level. Failure occurred in less than 100 cycles.

148

The second test in which an early failure occurred was that of one of the countersink fastener hole specimens. In the first test of such a specimen, a net section failure occurred in about 200 cycles. No explanation was ever found for this failure throughout the course of this program. It was felt that an extensive modeling of this specimen would be required to determine if the K_t at the short edge of this specimen at the base of the countersink might be sufficient to produce the net section failure obtained. More analytical effort in this area needs to be done.

The net section failure modes predicted for the boron/titanium material were all substantiated by test.

3.   <u>FATIGUE LIFE TEST RESULTS</u> - When the failure mode was predicted correctly, the life to failure was almost always predicted accurately by the analysis techniques. The correlation of analysis and test results shown in Figures 134 and 135, show that the analysis is generally more accurate for the boron/aluminum material than for the boron/titanium material. It tends to be a little more conservative for the boron/titanium than for the boron/aluminum. However, it is important to note that the boron/titanium results were based on only 5-10 test results from previous material lots, while the boron/aluminum predictions were based on the results of 150 tests of specimens from the same material lot.

In the unidirectionally reinforced materials there was remarkably little scatter within a test condition. With as few replications as were performed in this test program, this was fortunate. In the crossplied boron/aluminum materials this was not the case.

In the crossplied materials the scatter in lives within a particular condition was much higher, much more like that found in crossplied carbon/epoxy materials. In the aluminum matrix materials the fatigue failure mode was always one of cracking in the off-axis plies acting to initiate cracks in the matrix of the 0° plies and eventually producing fiber failures leading to rapid net section fracture. The life of the crossplied materials therefore depends almost entirely on how long it takes to develop cracking in the 0° plies once the off-axis plies are cracked. We know from our earlier analyses, that the off-axis plies crack very early in fatigue, often within ten cycles at reasonable stress levels (50 percent of ultimate). In this program we did not attempt to model the initiation of cracking in the 0° plies caused by off-axis ply cracking or the failure of fibers caused by matrix cracking. These are areas which still require analytical development.

One other interesting note on the crossplied boron/aluminum data is its agreement with graphite/epoxy data for life as a function of percent of ultimate tensile strength (Figure 136). The implication of this agreement is that when a good model is developed for one of these systems, it should do a good job of predicting the results of the other system.

Our predictions of crossplied boron/aluminum fatigue lives were based on the rupture lives of unidirectional boron/aluminum and stress analysis of the laminate, assuming all cross-plies are cracked and carry load only in the fiber direction. This analysis method was shown to predict fatigue failure lives of crossplied graphite/epoxy specimens having unloaded holes as well (Figure 137). Not only does the method predict the gross strain to failure well but it can also predict the effect of stress ratio on life, as shown in Figure 138.

150
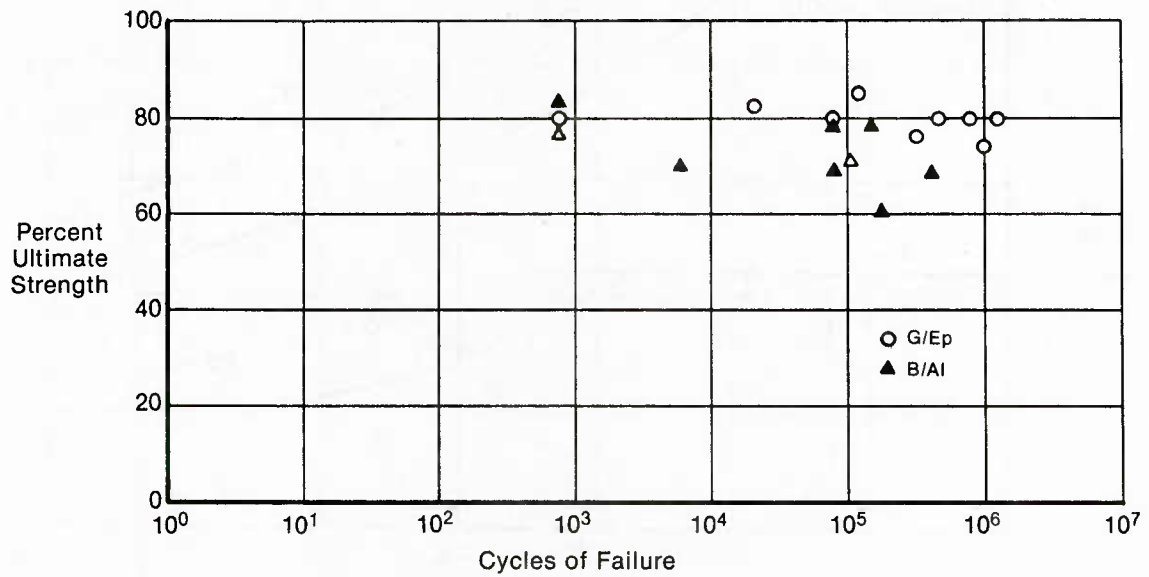
Figure 136. Comparison of 0/±45 B/Al and G/Ep Fatique Lives
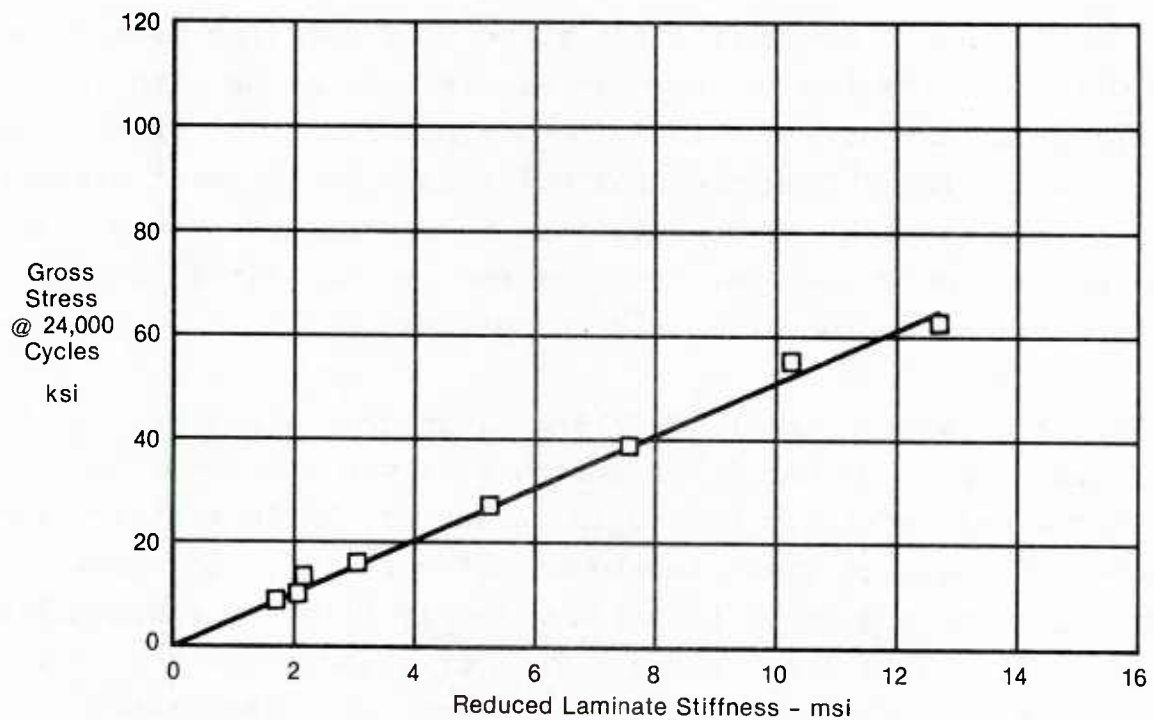
Figure 137. Carbon/Epoxy Laminate Fatigue Life Analysis
R = –1

151
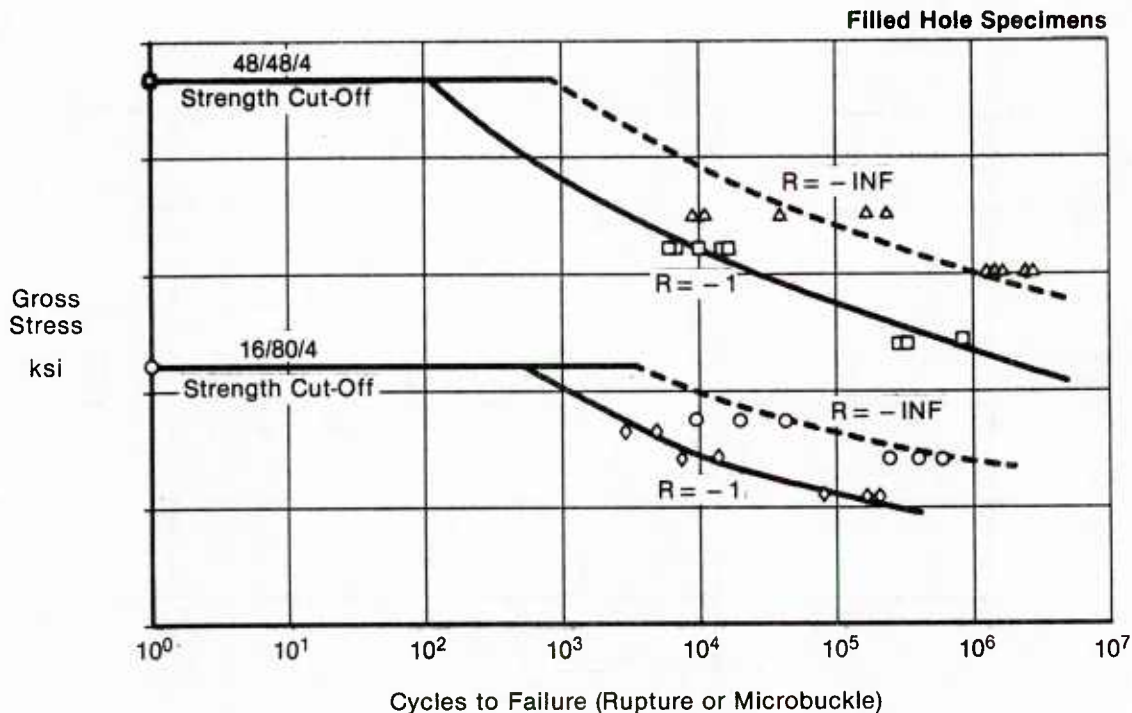
Figure 138. Effects of Stress Ratio on Fatigue Life of Graphite/Epoxy

The fatigue crack initiation curve used for life prediction of B_4C)B/15-3 titanium is shown in Figure 139, along with the verification test data obtained in this program. The crack growth curve was developed from previous MCAIR data in the same system. The correlation with the results from this program is good. As shown by the few R = -∞ results, compression has little effect on the life of notched metal matrix composites.

Crack growth in the (B_4C)B/15-3 titanium was not as significantly influenced by the fiber strength as was the boron reinforced 6-4 materials tested in an earlier MCAIR test program (Figure 112, Section IV). As shown in Figure 140, the crack growth rate in boron/15-3 titanium was only slightly reduced from that in the 15-3 material alone. The curve shown for the 15-3 material is from tests of matrix foil material consolidated under the same conditions as the boron/titanium material tested herein and subjected to the same SPF/DB cycle. Thus, the data plotted in Figure 140 represents the results of fiber reinforcement alone.

152
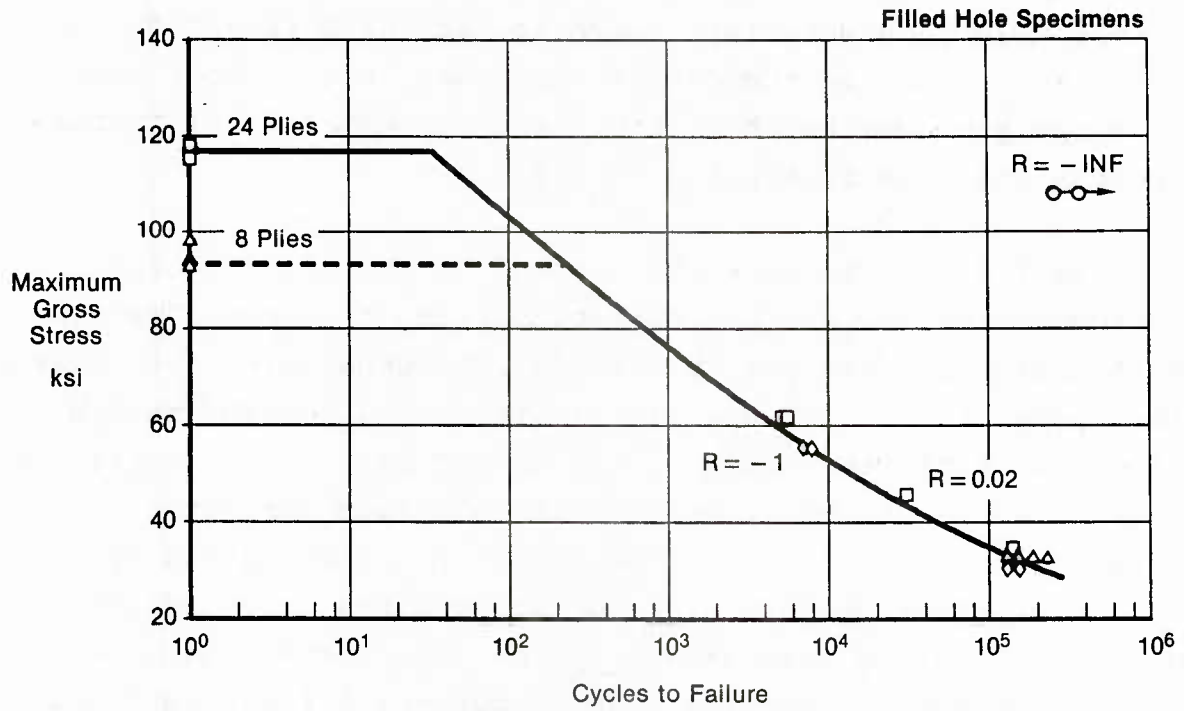
Figure 139. Fatigue Life Data for Boron/15-3 Titanium
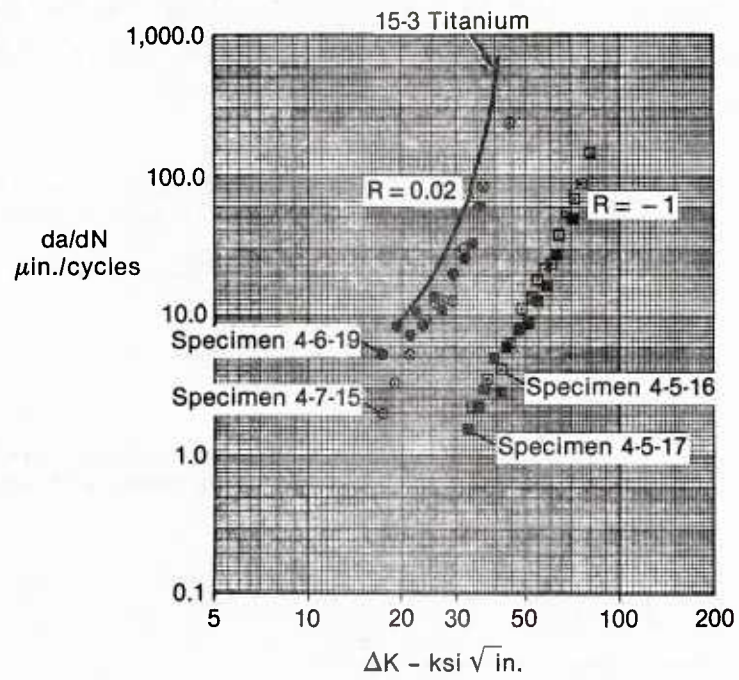
Figure 140. Crack Growth Rates in (B₄C)B/15-3 Titanium

153

As shown this effect is very small because the fiber strengths were so low in this material. Such low strength fibers do not restrict the strain in the matrix very much, rather they perform in much the same way as short fiber reinforcement does; increasing the stress for a given applied strain.

We feel it may be possible to predict the effects of fiber reinforcement on the crack growth properties of a metal matrix material, provided the matrix crack growth behavior can be characterized accurately. As shown in Figure 141, given the matrix crack growth rate, the threshold in an MMC material is controlled to a large extent by the fiber/matrix interface strength. A low interface strength will not allow the matrix deformation to be picked up by the fiber and will not produce the fiber failure required to continue flaw growth in the same plane. As shown earlier, in the case when the flaw encounters a fiber bundle in titanium, the flaw must then find a weak fiber at which to initiate a new crack plane. This is the most obvious mechanism found in these tests for the reduction in flaw growth in fiber reinforced titanium. When the crack is initiating in the matrix of reinforced titanium, a weak fiber/matrix interface can prevent the flaw from ever developing.
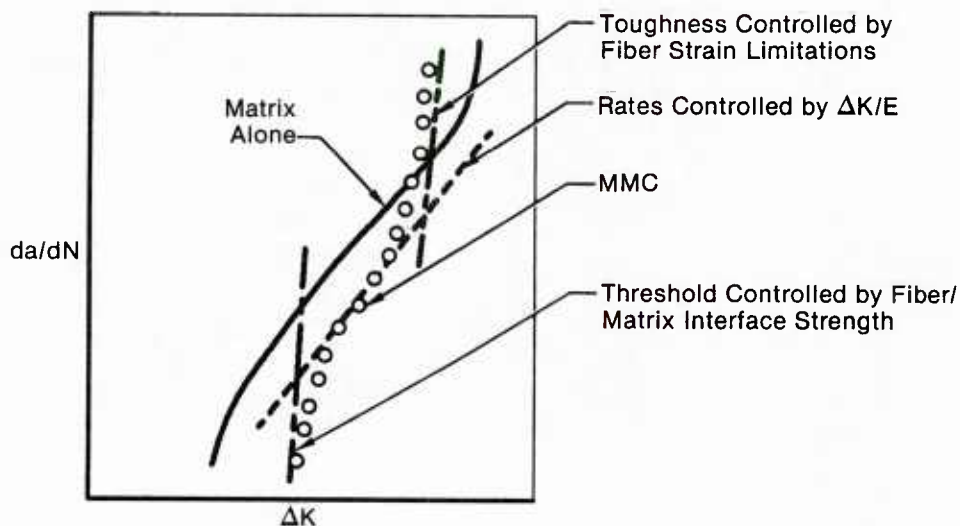
Figure 141. Effects of Fiber Reinforcement on Crack Growth Rates
in Metal Matrix Composite

154

The fracture toughness of fiber reinforced metals is controlled by fiber strain limits. In the same way that fracture toughness in metals is controlled by the ductility of the metal, the effect of the fiber to limit that ductility will reduce the toughness of the material system. In just the opposite manner very elastic aramid fibers are used to reinforce ALCOA's ARALL material to improve its toughness. Obviously the best fiber for a metal matrix material is the highest strain fiber available that still produces the desired increases in stiffness and strength.

4. RESIDUAL STRENGTH VERIFICATION RESULTS - With the agreement of the failure mode, crack growth, and fatigue life analysis, it is not surprising to find that the analysis accurately predicts residual strength as well. The comparison of analysis and test results is shown in Figure 142 for both boron/titanium and boron/aluminum. As was found in the model development testing the residual strength of boron/aluminum is strength controlled, depending only on the amount of remaining net section. In the titanium matrix material, the residual strength is accurately predicted by a fracture mechanics approach.
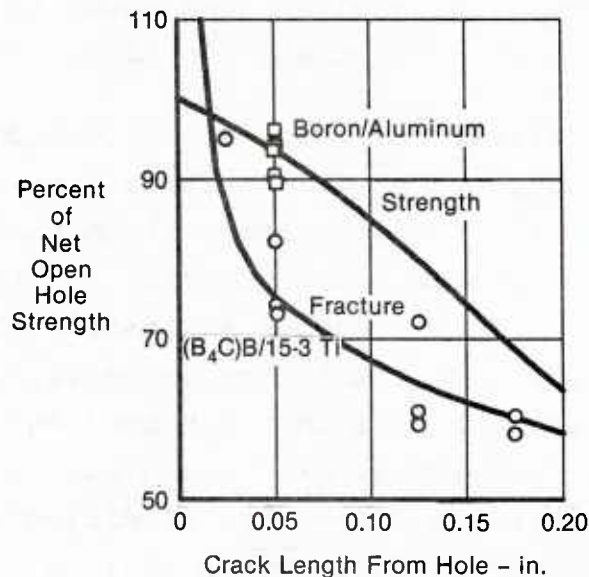
Figure 142. Residual Strength Verification

SECTION VII

CONCLUSIONS

The objective of this program was to develop and verify methods for predicting the durability of metal matrix composite structures. In the course of performing this program methods were derived for predicting stiffness and stress in notched metal matrix lamina, stiffness loss in fatigue of crossplied laminates, strength, crack initiation life, fatigue failure mode, crack growth, and residual strength of continuous fiber reinforced metal matrix composites. All of the analysis methods have been verified by predicting the results of 150 strength, fatigue, and residual strength tests.

1. <u>ANALYSIS METHODS</u> - A very simple stress analysis method for predicting the stresses near notches in finite width plates in isotropic or orthotropic materials was developed. The analysis accounts for yielding in both the 0° and off-axis plies and performs a non-linear laminate analysis to determine laminate stiffness as plies yield and crack. For the 0° dominated layups tested in this program, the analysis was shown to accurately predict the strengths of notched and unnotched coupons.

Fatigue crack initiation lives were predicted using the results of notched coupon test data. The stress analysis was used to examine the hole wall to determine maximum fiber tensile stresses and maximum matrix shear stresses. These stress values were compared with the fiber tension and matrix shear strengths to determine if the cracks would initiate as matrix cracks or as fiber breaks. The fatigue life to fiber breakage was controlled by the maximum fiber tension stress regardless of stress ratio. The matrix crack initiation lives were predicted using standard crack initiation schemes based on metal fatigue, i.e., Miner's rule applied to the local stress condition. Stress ratio effects can be predicted using any standard metals analysis; a variation of the Smith, Watson, Topper method was used herein.

156

The fatigue crack initiation locations and subsequent failure modes were found to depend on the ratio of the maximum stresses in the fiber and the matrix to the respective strengths of the fiber and matrix. Thus, the failure modes were found to depend on laminate orthotropy (which determines how much load is taken by the matrix in shear) and the relative strengths of the matrix and fiber. In cases in which the two failure modes are close to occurring simultaneously, the fiber/matrix interface plays a role in the fatigue failure mode. These observations were used to develop a simple approach for determining the fatigue failure mode in MMC materials.

Crack growth analyses were based on a strain energy density approach so that changes in failure mode could be predicted. However, for the materials examined in this program, failure modes did not change during the course of any test. For cases in which flaws propagated along the fibers in the loading direction (as in boron/aluminum) the strain energy density factor was based solely on the shear stress intensity factor. For the boron/titanium material which failed across the net section (because of its poor fiber strength) the strain energy density function became controlled solely by the opening mode stress intensity factor. Thus, for the most part, standard fracture mechanics approaches were found to accurately predict flaw growth in these two materials, once their failure modes were determined by matrix and fiber strengths and stiffnesses.

The only time the strain energy density factor was exercised was in the crack growth tests of off-axis laminates. In those cases it has the same form as the strain energy function proposed by Mahulikar and Marcus (Reference 35) to estimate the effect of fiber angle on SCS/titanium crack growth. This parameter was shown to collapse the boron/aluminum data obtained herein equally well.

In the same way, the residual strength behavior of MMC materials was completely dependent on the failure mode. When flaws grow along the fibers in the loading direction, the simple strength analysis can be used to predict residual strength conservatively. When flaws grow across the net section, either along fibers or across fibers, standard fracture mechanics methodology will accurately predict the strength of the part.

2. <u>TEST METHODOLOGY</u> - At the beginning of this program a notched, central hole specimen was recommended for the majority of the tests because it does not presuppose a particular failure mode, such as matrix cracking or fiber failure. As a result of the tests performed herein, the central hole specimen was found to provide valuable information about the mechanisms that drive failure modes as well, since crack initiation location changed with fiber/matrix strength ratios. This discrimination in mechanisms was a valuable asset for model development. This specimen is recommended for further studies of this type, in which new material systems are evaluated and failure modes cannot readily be forecast.

Once failure modes are determined and the parameters which define them have been determined, then center cracked panels or unnotched specimens can be used to develop basic mechanical properties data of value for analysis.

Visual observation of the failure progression in these materials was found to be the best method for defining failure modes in this program. It was the only way to obtain accurate crack length measurements during the fatigue tests. Simple automated monitoring of specimen displacement behavior during test was another valuable way to discern failure mode changes during testing, in crossplied composites particularly. Acoustic emission (AE) monitoring has a place in describing failures in MMC materials because of the energy involved in failures of the large fibers used. It is the author's opinion, however, that AE is a more valuable tool in full scale component tests, where failure

158

location and magnitude are difficult to assess in real time without such a system. Sectioning and scanning electron microscopy (SEM) techniques were also valuable tools for post-test analysis and understanding the progression of flaws in metal matrix materials.

Ultrasonic inspections and static tests of unidirectionally reinforced materials, both on axis and off-axis, are still the best means for determining initial quality of MMC materials. Ultrasonic inspection will detect delaminations and poor bonds in a panel, but nothing short of a strength test was found to reliably detect low strength fibers, poor fiber/matrix interface strength, or degraded matrix material properties. X-radiography needs development before it can be reliably used to detect fiber breaks or matrix cracking in multiply titanium matrix materials. The resolution of fiber and matrix is not yet great enough using our current procedures. Eddy current methods, although not used in this program, have promise for detection of crack initiation in notched MMC components, as well as assessment of initial notch quality in terms of fiber damage during notch fabrication.

3.   ASSESSMENT OF DURABILITY OF METAL MATRIX COMPOSITES - Fiber reinforcement of metals offers many enhancements to their properties: better strength, stiffness, and in increased useful temperature ranges. For durability, fiber reinforcement offers a mixed blessing. The number of cycles to crack initiation is often reduced by the fiber reinforcement because a cut fiber, either at the side of an unnotched specimen or at the hole wall of a notched specimen, is a natural crack initiation site for matrix or fiber/matrix interface cracking. In the boron/aluminum tests performed herein, some flaws formed in the matrix as soon as multiple loads were applied. Likewise in boron/titanium fiber breaks occurred very early in test (However this assessment is not fair, perhaps, because of the very low strengths of the fibers after the extended SPF/DB cycle applied.). The stress levels at

159

which no cracking occurred were about 30 percent of ultimate in both notched materials (36 ksi in boron/aluminum and 40 ksi gross in boron/titanium).

The positive aspect of durability of MMC materials is that flaws grow very slowly due to the fiber reinforcement. If flaws grow in the loading direction along the fibers, the fibers carry the load and the component will not fail catastophically unless the net section is reduced to the point that fiber ultimate strengths are exceeded. This crack growth is slow and constant since it is driven by shear. The flaw growth rate does not increase with length as in conventional failure modes. If the MMC is being used for unidirectional reinforcement, then cracking such as that described may be permissible since it does not degrade the longitudinal strength of the part.

There are two cautions to note with regard to permissible cracking like that described above. First, these cracks are generally through-the-thickness flaws. Fluids cannot be contained by skins in which such cracking is allowed. Second, transverse loads cannot be carried by cracked unidirectional MMC materials like that described above. Care will have to be taken in such applications to ascertain that transverse load capability is not required of the MMC.

When flaws grow perpendicular to the load and across fibers, as in the titanium materials, all of the durability concerns associated with conventional metals apply. And, in general, the methods developed for metallic materials can be safely applied, as long as the material has been adequately characterized by tests for initiation and crack growth data. Fibers in these materials provide two methods for slowing the rate of crack propagation. First, the fibers control the strains in the matrix. Even when the fiber/matrix interface is not strong, the overall strain in the matrix is reduced by the load carrying capability of the fiber. When the fiber/matrix interface is very weak, local matrix

160

strains can cause cracking, but the matrix cracks may not cause fiber failures. This occurred in earlier tests of SCS-6/15-3 titanium.

The fiber/matrix interface provides the second method for slowing net section flaw growth. When the interface is weak, it fractures easily. When flaws are small and strains are only locally high, a weak interface will relieve the strains in the fiber at the crack tip and prevent crack propagation through the fibers. In order for the flaw to propagate through the fiber in a weak interface material, the flaw must find a weak area in the fiber, and the flaw must reinitiate in a new fracture plane. This process causes FRMMC materials to require a much higher stress intensity factor to cause continuous crack growth through the fibers and is demonstrated by a higher threshold stress intensity factor and slower crack growth rates at low stress intensity factors in the FRMMC material than in its matrix metal.

Damage tolerance of MMC materials then is good for slow crack growth structure, however, the overall toughness of these materials is reduced by the strain limitation of the fibers. Thus these materials cannot withstand as large a flaw as can the matrix material alone. Their damage tolerance is also directionally dependent. Damage in a direction along the primary fiber reinforcement direction is common under impact loads, and these materials are vulnerable to transverse loads in these cases, even though they show excellent tolerance under longitudinal loads.

REFERENCES

1. Dorr, D. J., "Two-Sheet Available Fiber/Matrix Composite Design Development for Airframes," AFWAL-TR-86-3065, March 1986.

2. Johnson, S. R. and Ravenhall, R. "Metal Matrix Composite Shaft Research Program," AFWAL-TR-87-2007, May 1987.

3. Bates, W. F., Cornell, B. L., and Sensenbrenner, J. E., "Preliminary Design Concepts for Metal Matrix Composite Aircraft Structures," AFWAL-TR-85-3123, April 1986.

4. Hayes, S. V., Knight, R. C., "Metal Matrix Composite Structural Demonstration for Missiles," AFWAL-TR-86-3097, January 1987.

5. Steelman, T. E., Bakalyar, A. D., and Konopka, L., "Aluminum Matrix Composite Structural Design Development," AFWAL-TR-86-3087.

6. Lockheed-Georgia, "MMC Structural Data Development," Air Force Contract F33615-81-C-3264.

7. United Technologies Research Center, "MMC Structural Data Development for Spacecraft," Air Force Contract F33615-81-C-5128.

8. Saff, C. R., "Durability of Continuous Fiber Reinforced Metal Matrix Composites," AFWAL-TR-85-3107, February 1986.

9. Goree, J. G. and Jones, W. F., "Fracture Behavior of Unidirectional Boron/Aluminum Composite Laminates," NASA-CR-3753, December 1983.

REFERENCES (Continued)

10. Goree, J. G., Lokeswarappa, R. D., and Jones, W. F., "Mathematical Modeling of Damage in Unidirectional Composites,"NASA-CR-3453, August 1981.

11. Goree, J. G. and Gross, R. S., "Analysis of a Unidirectional Composite Containing Broken Fibers and Matrix Damage," Engineering Fracture Mechanics, Vol. 13, 1980, pp. 395-405.

12. Dill, H. D. and Saff, C. R., "Effects of Fighter Attack Spectrum on Crack Growth," AFFDL-TR-76-112, March 1977.

13. Badaliance, R. and Dill, H. D., "Effects of Fighter Attack Spectrum on Composite Fatigue Life," AFWAL-TR-81-3001, March 1981.

14. Badaliance, R. and Dill, H. D., "Compression Fatigue Life Prediction Methodology for Composite Structures," NADC-83060-60, September 1982.

15. Saff, C. R., "Effects of Layup and Loading Frequency on Fatigue Life of Graphite/Epoxy," NADC-81017-60, October 1982.

16. Cooke, C. M., Cammett, E. D., and Smith, P. R., "Edge Preparation of Titanium Matrix Composite Specimens for Mechanical Testing," Microstructural Science, Vol. 10, Elsevier Science PublishingCo., Inc., pp. 221-228.

17. Johnson, W. S., "Modeling Stiffness Loss in Boron/Aluminum Below the Fatigue Limit," NASA-TM-83294, March 1972.

18. Johnson, W. S., "Mechanisms of Fatigue Damage in Boron/ Aluminum Composites," Damage in Composite Materials, ASTM STP 775, 1981, pp. 83-102, (Also NASA-TM-81926, December 1980).

REFERENCES (Continued)

19. Johnson, W. S., Bigelow, C. A., and Bahei-El-Din, Y. A., "Experimental and Analytical Investigation of the Fracture Processes of Boron/Aluminum Laminates Containing Notches, "NASA-TP-2187, September 1983.

20. Awerbuch, J., "Fracture Behavior of Boron/Aluminum Composites at Room and Elevated Temperatures," AFOSR-TR-82-0038, September 1980.

21. Klaus-Jurgen Bathe, <u>Finite Element Procedures in Engineering Analysis</u>, Prentice-Hall, 1982, p. 388.

22. Seely, F. B. and Smith, J. O., <u>Advanced Mechanics of Materials</u>, Wiley & Sons, 1952.

23. Inglis, C. E., "Stresses in a Plate Due to the Presence of Cracks and Sharp Corners," <u>Transactions of the Institute of Naval Architechs</u>, Vol. 55, Part 1, 1913.

24. Koiter, W. T., <u>Quarterly Journal of Applied Mathematics</u>, Vol. 15, p. 303.

25. Peterson, R. E., <u>Stress Concentration Design Factors</u>, Wiley & Sons, 1953.

26. Lekhnitskii, S. G., <u>Anisotropic Plates</u>, Gordan and Breach Science Publishers, 1968.

27. Howland, R. C. J., On the Stresses in the Neighborhood of a Circular Hole in a Strip Under Tension," <u>Philosophical Transactions of the Royal Society</u> (London), Vol. 229A, p. 49, 1930.

REFERENCES (Continued)

28. Garbo, S. P. and Ogonowski, J. M., "Effect of Variances and Manufacturing Tolerances on the Design Strength and Life of Mechanically Fastened Composite Joints," AFWAL-TR-81-3041, Vol.1, April 1981.

29. Grimsley, F. M., "Static and Fatigue Behavior of Pin-Loaded Metal Matrix Joints," AFWAL-TR-84-3063, June 1984.

30. Reedy, E. D., Jr., "On the Specimen Dependence of Unidirectional Boron/Aluminum Fracture Toughness," Journal of Composite Materials Supplement, Vol. 14, 1980, pp. 119-131.

31. Smith, K. N., Watson, P. and Topper, T. H., "A Stress-Strain Function for the Fatigue of Metals," Journal of Materials, ASTM, Vol. 5, No. 4, December 1970, pp. 767-778.

32. Sih, G. C., Handbook of Stress Intensity Factors, Lehigh University, Bethlehem, Pa., 1973.

33. Hancock, J. R., "The Initiation and Growth of Fatigue Cracks in Filament Reinforced Aluminum Alloys," AFML-TR-71-82, March 1971.

34. Waszczak, J. P., "Applicability of Linear Elastic Fracture Mechanics to 5.6 Mil. Boron/6061 Aluminum," Journal of Aircraft, Vol. 13, No. 10, 1976, pp. 770-777.

35. Mahulikar, D. S., Park, Y. H., and Marcus, H. L., "Environmental Influences on the Fracture and Fatigue Properties of Titanium Metal Matrix Continuous Fiber Composites," Fracture Mechanics:Fourteenth Symposium - Volume II: Testing and Applications, ASTM STP 791, 1983, pp. 579-597.

REFERENCES (Concluded)

36. Badaliance, R., "Mixed Mode Fatigue Crack Propagation'"
    <u>Proceedings of First USA-Greece Symposium on Mixed Mode Crack
    Propagation</u>, edited by G. C. Sih and P. S. Theocaris,
    Sijthoff and Noordhoff, 1981, pp. 77-98.

37. Dorr, D. J., "Two-Sheet Available Fiber/Matrix Composite
    Design Development for Airframes," AFWAL-TR-84-3041, August
    1984.

APPENDIX A

USER'S GUIDE FOR MMC ANALYSIS PROGRAM

1. <u>OVERALL SUMMARY</u>

a. <u>Purpose and General Arrangement</u> - A multi-stage program for MMC analysis is being developed. This program is capable of analyzing lamina and laminate stiffnesses, stresses about a notch and through the net section, the laminate strength (notched or unnotched), laminate crack initiation lives, laminate crack growth, and laminate residual strength. This user-friendly program emphasizes simple analysis techniques which allow the program to be run interactively. Each section is programmed as a separate module and can be used individually.

The program is designed to be as user-friendly as possible. Input data can be entered either interactively or through an input file. Once entered, the data can be modified through the use of a data echo/edit routine. This routine is menu driven and can be used to display the data for each analysis routine and to change some or all of it. This echo/edit routine also allows one to use additional analysis options and input the corresponding data. Similarly, the routine allows one to delete analysis options. After the input data has been finalized, the program will write the data to a file, if so desired.

The output data from the program execution can be written to a file and saved or displayed interactively. All file names are specified by the user and may contain up to 20 characters.

b. <u>Discussion of Methods</u> - Each module in the analysis program employs simple and rapid analysis techniques.

Stiffness - The stiffness module is a two-part routine. It allows the evaluation of lamina or laminate stiffnesses. Currently, the program is limited to a total of three different fiber/ matrix material systems. It is also limited to eight different combinations of ply materials and fiber orientations. These numbers were arbitrarily selected and can be changed.

Given separate fiber and matrix properties (moduli and Poisson's ratios), the program uses a Rule of Mixtures formulation to develop the lamina or ply properties. If the lamina properties are known, they may be input directly.

Laminate properties are determined from the lamina properties, the number of plies, the ply orientations, and the thickness of each ply. Laminated plate theory is used to determine these properties (Reference A.1). The routine is not sensitive to stacking sequence, therefore, two identical plies that are not located next to each other in the laminate may be input as one ply with twice the thickness.

Stress - The stress routine evaluates stress concentrations around a circular or elliptical notch and predicts the stress distribution through the net section of a notched laminate.

Given a uniaxially loaded laminate with a center notch, the general expression for the tangential stress concentration at any point along the periphery is:

$$\frac{s_t}{s_0} = \frac{1}{2} \left[\frac{E_t}{E_x} K_t + \frac{E_t}{E_y} K_{t0} \right] - \frac{1}{2} \left[\frac{E_t}{E_x} K_t - \frac{E_t}{E_y} K_{t0} \right] \cos 2\Theta$$

where K_t is the stress concentration at the edge of the hole ($\Theta = 90°$) and K_{t0} is the stress concentration at the top of the hole ($\Theta = 0°$). Substituting into this equation the expressions for K_t and K_{t0} for an infinite plate, this equation is identical to the equation developed by Lekhitskii (Reference A.2). Based upon

results from finite element and boundary collocation analyses for notched laminates with varying stiffness properties and width to diameter ratios, we have generated expressions for K_t and K_{t0}. Using these expressions in the above equation provides a completely general expression for the tangential stress concentrations which accounts for finite width plates and plate orthotropy. The accuracy of this simplified approach is demonstrated in Figure 87 where the matrix shear stress at angles between 0° and 90° from the loading axis is calculated and compared to boundary collocation analysis.

The stress routine also allows one to determine the stress distribution through the net section of a notched laminate. The expression for the stress distribution is assumed to be an exponential decay of the stress gradient from the notch. The exact form of this equation is determined through the application of three boundary conditions. These conditions state the following:

1) the stress concentration at the edge of the hole must equal K_t,

2) the stress gradient at the edge of the hole must equal CK_t/p (Reference A.3), and

3) the load across the net section must equal the applied load.

In these equations, C is a constant based upon the geometry of the notch and panel and p is the notch radius. Figure 84 compares this simplified analysis to a finite element analysis for a finite width orthotropic plate.

Strength - The strength module consists of a lamina or ply strength analysis and a laminate strength analysis. The module is capable of predicting strengths of notched or unnotched specimens.

The lamina analysis is based on a Rule of Mixtures formulation. Given the fiber and matrix strengths and the fiber volume percentage, an unnotched lamina strength will be made. Although Rule of Mixtures predicts lamina stiffnesses very well, it is not as accurate in predicting strengths. Strength predictions made by Rule of Mixtures are unconservative. It is recommended that the user input lamina strengths directly, if known. Three lamina strengths are required: 1) the strength parallel to the fibers, 2) the strength perpendicular to the fibers, and 3) the shear strength. If the shear strength is unknown, the user may input any off-axis strength. The program will then use the Tsai-Hill failure criteria to predict the shear strength.

The laminate notched strength analysis module is based upon a linear elastic theory with allowance for matrix yielding in the zero degree plies of the laminate and an elastic-perfectly plastic theory for off-axis plies. Allowable strains are calculated for each ply in the laminate and as the laminate strain at the notch exceeds an allowable strain, the corresponding ply either fails, for a zero degree ply, or loses its stiffness contribution to the laminate, for any off-axis ply. The off-axis plies are treated as elastic-perfectly plastic in that they still carry load after their allowable strain has been exceeded.

If the shear strength of the matrix material is low, then a notched zero degree ply will initiate a crack from the notch and it will grow along the fibers. Matrix yielding is modeled through the use of a very simple shear lag model (Reference A.4). The length of the yield zone from the notch is determined by the amount of load sheared around the hole. This load divided by the yield zone length and the specimen thickness is equated to the ultimate matrix shear stress. The net effect of the matrix yielding is a reduction of the stress concentration at the edge of the notch. The reduction in K_t is modeled by analyzing the hole as an ellipse whose axis along the fiber direction is related to the length of the yield zone.

170

Fatigue Crack Initiation Life - The crack initiation portion
of the MMC analysis program will predict the life to a .05 in.
flaw and the associated failure mode for a laminate when subjected
to constant amplitude loading. In zero degree plies, cracks will
initiate either across the net section or along the fibers away
from the notch. The failure mode is dependent upon the magnitude
of the stress level and the ratio of the ply longitudinal strength
to the matrix shear strength (Figure 95).

For each fiber/matrix system in the laminate, two types of
data are required: 1) gross stress vs. cycles to fiber breakage
and 2) gross stress vs. cycles to matrix crack initiation. The
fiber breakage data must be obtained from either a notched or an
unnotched zero degree laminate. The matrix crack initiation data
must be obtained from one of four specimens:

    1) an unnotched off-axis laminate,
    2) an unnotched matrix material specimen,
    3) a notched zero degree laminate which cracks along the
fibers, or
    4) a notched ninety degree laminate.

The routine permits the use of life data from either notched
or unnotched specimens for prediction of life in either notched or
unnotched components. It is recommended, however, that unnotched
input data be used to predict initiation lives for unnotched
laminates and that the notched input data be used to predict
initiation lives for notched specimens.

The gross stresses in the input curves are converted to
represent the local stress at the point of the initiation. For
example, the gross stress from a notched zero degree laminate is
multiplied by the stress concentration at the edge of the notch,
K_t, to determine the local stress at the point of crack initiation
for a laminate which initiates a crack across the net section. In
addition, the matrix crack initiation input data files are scaled

171

with respect to the matrix strength such that at the point of crack initiation the local stress in the ply equals the matrix strength. This allows the user to input only one matrix crack initiation data file for plies of the same fiber/matrix system, but of different orientations.

The initiation life predictions are made on a ply-by-ply basis. Given a gross stress level, the first step in the analysis procedure is to determine which plies in the laminate have failed. The overall properties of the laminate are recalculated accounting for the failed plies. Next, the stress concentrations around the notch are determined. The gross stress is then converted to local stress by multiplying by the stress concentration factors. Each ply is then examined to determine its life to initiation by looking up the local stress in the converted input data files for the appropriate material system. There are two data files for each material system, one that predicts lives to initiation across the fibers and one that predicts lives to initiation up along the fibers. The lowest of the two lives for the two failure modes is the crack initiation life for that ply at the associated gross stress level.

A standard stress ratio correction for metals is used to predict the effect of stress ratio on fatigue crack initiation in the matrix. The parameter used is an effective strain version of a stress parameter developed by Smith, Watson, and Topper and has been shown to correlate stress ratio effects on crack initiation in a wide variety of metallic materials (Reference A.5).

The output from this routine consists of a stress vs. life data for each ply in the laminate. This data is stored in a file in a form which allows for easy plotting. The crack initiation life for the entire laminate is represented by the lowest curve on the plot.

Fatigue Crack Growth Analysis - The crack growth analysis module is capable of predicting flaw growth rates in a laminate whether the flaws grow in the matrix along the fibers or across

172

fibers. The type of crack growth is determined in the crack initiation section of the program. This routine is restricted to constant amplitude loading only.

Test data from MMC materials or matrix materials is used to evaluate matrix controlled crack growth (via off-axis crack growth tests) and fiber controlled crack growth (via longitudinal tests). Each fiber/matrix system requires the following input files: one that describes crack growth in the matrix along the fibers and one that describes crack growth across the fibers. This test data can be in the form of crack length, a, vs. cycles, N, or crack growth rate, da/dN, vs. delta K. If the data is entered as crack length vs. cycles, the program will convert the data to crack growth rate vs. delta K. In this case, it is also necessary to provide a description of the laminate tested, including specimen width, notch radius, applied stress level, and associated stress ratio.

If one or both of the input data files are unavailable for a particular fiber/matrix system, then the user must provide a file with crack growth data for the matrix material. This data will be used to represent the matrix crack growth along the fibers. Crack growth across the fibers will be estimated by scaling the stress intensity by the ratio of the laminate modulus to the matrix modulus.

Some material systems will crack along the fibers even in a zero degree orientation. This type of crack growth has a constant crack growth rate and stress intensity. If the user provides matrix crack growth data from this type of specimen, only one da/dN vs. delta K point will be generated. Therefore, it is required that the user supply a matrix material crack growth curve. The single da/dN vs. delta K point generated from the zero degree lamina data will be used to shift the da/dN vs. delta K curve of the matrix material. This will provide the user with an estimated matrix crack growth curve.

173

As in the crack initiation life analysis module, the crack growth analysis is performed on a ply-by-ply basis. Given an applied stress level and stress ratio, the gross strain for the laminate is calculated. Then the stress and delta K for each ply is determined. Next, the crack initiation life and failure mode are determined for the ply. The crack growth rate is read from the input curve for the material system and failure mode. The crack length is then incremented in each ply. The final output from the crack growth module is a data file of crack length vs. number of cycles for each ply in the laminate. This file is formatted in such a way as to allow for easy plotting.

Residual Strength - The final section of the MMC analysis program is the residual strength module. In this section, the strength of a flawed laminate is predicted. This routine is based on the assumption that the flaw initiates from a circular notch and grows symmetrically through the net section of the specimen. Also, it is assumed that the flaw described is all that is known about the damage in the laminate and that this flaw is through the thickness.

Two types of failure criteria are evaluated in this routine. A simple strength analysis, which accounts for stress concentration reduction due to yielding and cracking, is used to predict the residual strength for laminates with low shear strength and that crack up along the fibers in zero degree plies. A fracture mechanics approach is used to predict residual strength for laminates which fail through the net section. The residual strength of a laminate is calculated using the strength based analysis and the fracture mechanics based analysis. The lowest of the two calculated residual strengths for the different failure modes will drive the laminate.

The user is asked to supply a value for the critical stress intensity factor, K_c for the laminate. This is used in the fracture mechanics analysis. If K_c is not known, the routine will

make an estimate. The estimate is made by performing the strength analysis for the specified laminate with a narrow ellipse in the center of the panel. The ellipse is used to approximate a center crack. The failing stress and the major radius of the ellipse which represents the critical crack size is used to calculate an estimate for the critical stress intensity.

The type of output from this routine is specified by the user. Given a specified flaw length the program will calculate a single residual strength. If a flaw length is not specified, the program will start with a 0.01 inch flaw and calculate a residual strength at every 0.01 inch increment up to 0.20 inch. This data is stored in a file for easy plotting.

2. HOW TO USE MMC ANALYSIS PROGRAM - I/O - This program is designed to be a quick running, easy to use routine that runs interactively. The program runs from a set of input data that can either be input interactively or can be read from a specified file. Once the data has been input to the program, the user may review the data and edit it as necessary. After successful execution the program will write the input data in a file, if desired.

To assist the user when answering questions interactively, the routine has error traps programmed into it. These error traps are designed to catch simple typographical errors, such as typing an alphabetic character when a number is required. Without these error traps the program execution would stop and the program would have to be run from the start. Another type of error trap included in the routine checks a numeric response when responding to a choice of numbered options. If your entry does not appear in the given list, then the program will ask you to re-input your answer.

The echo/edit routine is used to modify an existing set of data. Once the data has been read into the program or entered interactively, the user is asked if editing of the data is necessary. If this option is selected, the user is then presented a

menu which consists of a list of the analysis modules for which
data may be edited. The editing process starts with an echoing of
the input data for that section of analysis. The user is asked if
this data is correct. If it is correct, the routine exits to the
first menu. If the data is incorrect, the user may modify all or
some of the data listed. The editing routine also allows one to
add data sets for analysis modules not originally selected.
Similarly, one may eliminate an analysis option. One can also add
or delete material systems.

   a. <u>Description of Input Data</u> - In this section, a list of
the input data and a description of each input variable is provi-
ded. An input file may be created from the following list of
data, however it is easier to enter the data interactively and
then store that data in a file after a successful program
execution.

   Analysis Selection
   IRES3(I) - A combination of numbers between 1 and 6.
            Maximum of 6 entries.
            Options include:
                 1 - Stiffness Analysis
                 2 - Stress Analysis
                 3 - Strength Analysis
                 4 - Crack Initiation Life Analysis
                 5 - Crack Growth Analysis
                 6 - Residual Strength Analysis
            Each input module has different input data. The
            input for each module is listed below. Execution
            of some modules requires that the user supply
            input data for other modules. For example, if the
            user selects option 4, then input for options 1,
            2, and 3 are also required. The input require-
            ments for each module are specified in Table A-1.
            Output will be displayed for only the modules
            specified by the user.
   /   - Ends IRES3 input.

NUMMAT - Number of fiber/matrix material systems.
        Maximum of 3 materials.
        For I=1, NUMMAT:
           NF(I) - Name of fiber
                   Maximum of 20 characters.
           NM(I) - Name of matrix
                   Maximum of 20 characters.
           FVOL(I) - Fiber volume percentage (%)
           IRES4(I) - Lamina stiffness calculation flag.
                   Options include:
                       1 - Calculate lamina stiffness (ROM).
                       2 - Enter lamina stiffness directly.
           If IRES4(I)=1
                EF(I),VF(I) - Fiber modulus (ksi) and
                              Poisson's ratio
                EM(I),VM(I) - Matrix modulus (ksi) and
                              Poisson's ratio
           IF IRES4(I)=2
                E1(I),E2(I),G12(I),V12(I)
                     - Lamina properties:
                         longitudinal stiffness (ksi)
                         transverse stiffness (ksi)
                         shear stiffness (ksi)
                         Poisson's ratio
                EM(I) - Matrix modulus (ksi)
           IRES5 - Laminate stiffness calculation flag
                   Options include:
                       Y or y - Calculate laminate stiffnesses.
                       N or n - Don't calculate laminate
                                stiffnesses.
           NUMPLY - Number of plies in laminate
                    (Maximum of 8)

177

```
                    For I=1, NUMPLY
                        MATO(I) - Material identification number
                        ANG(I) - Fiber orientation (degrees)
                        PLYTHK(I) - Ply thickness (in)
                    ALPHA - Angle of laminate to loading axis (degrees)


Stress Module Input
        Input for Stiffness Module with following exceptions:
            IRES5 - No input required by user (Flag set to 'Y')


        RX,RY - Radius of notch in x and y direction (in)
                (X direction is parallel to loading)
        W - Width of laminate (in)
        NOUT - Number of locations where stress is calculated
                through the net section

Strength Module Input
        Input for Stiffness Module with following exceptions:
                IRES5 - No input required by user (Flag set to 'Y')
        Input for Stress Module

        For I=1, NUMMAT
            If IRES4(I)=1
                    XF(I) - Fiber strength (ksi)
                    XM(I),SM(I) - Matrix longitudinal strength (ksi)
                                    and matrix shear strength (ksi)
            If IRES4(I)=2
                    X(I),Y(I),
                    Z(I),ZA(I) - Lamina strengths:
                                    longitudinal strength (ksi)
                                    transverse strength (ksi)
                                    shear strength or any off-axis
                                        strength (ksi)
                                    off-axis angle (0 if shear
                                        strength is entered)
                    XM(I),SM(I) - Matrix longitudinal strength (ksi)
                                    and matrix shear strength (ksi)
```

178

Crack Initiation Life Module Input

Input for Stiffness Module with following exceptions:
IRES5 - No input required by user (Flag set to 'Y')

Input for Stress Module

Input for Strength Module

For I=1, NUMMAT
IRES7A(I) - Flag which specifies type of laminate
from which fiber rupture data was
obtained.
Options include:
1 - Notched 0 degree laminate
2 - Unnotched 0 degree laminate
FFILE1(I) - Name of file containing fiber rupture
data (Stress vs. Life). Format of this
file is shown in Table A-2.
Maximum of 20 characters.
RF(I) - Stress ratio for fiber rupture data.
If IRES7A(I)=1
FRX(I),FRY(I) - Radius of notch in x and y
direction (in) for fiber rupture
data.
FW(I) - Width of laminate (in) for fiber rupture
data.
IRES7B(I) - Flag which specifies type of laminate
from which matrix crack initiation data
was obtained.
Options include:
1 - Notched 0 degree laminate
2 - Notched 90 degree laminate
3 - Unnotched off-axis unidirectional
laminate
4 - Unnotched matrix material

179

FFILE2(I) - Name of file containing matrix crack
initiation data (Stress vs. Life).
Format of this file is shown in Table
A-2.
Maximum of 20 characters.

RM(I) - Stress ratio for matrix crack initiation
data.

If IRES7B(I)<3

TRX(I),TRY(I) - Radius of notch in x and y
direction (in) for matrix crack
initiation data.

TW(I) - Width of laminate (in) for matrix crack
initiation data.

If IRES7B(I)=3

TANG(I) - Off-axis angle (degrees)

SRM,SRF - Stress ratio for the matrix and the fibers for
the laminate analysis. Typically SRM=SRF. One
example in which SRM doesn't equal SRF is when
your laminate has a filled notch and is
subjected to R=-1 loading. In this case, SRM=-1
and SRF=0 (.02) because the fibers are not
affected by the compression loads.

Crack Growth Module Input

Input for Stiffness Module with following exceptions:
IRES5 - No input required by user (Flag set to 'Y')

Input for Stress Module

Input for Strength Module

Input for Crack Initiation Life Module

For I=1, NUMMAT

180

IRES8A(I) - Flag specifying if you will provide fiber
crack growth data.
Options include:
Y or y - Data will be provided.
N or n - data will not be provided.
If IRES8A(I)=Y
IRES8B(I) - Curve type flag
Options include:
1 - Crack length (in) vs. cycles
(a vs. N)
2 - Crack growth rate (in/cycle)
vs. stress intensity (ksi/in)
(da/dN vs. del K)
FFILE3(I) - Name of file containing fiber crack
growth data. Format of this file is
shown in Table A-2.
Maximum of 20 characters.
If IRES8B(I)=1
RF2(I),GSLF(I) - Stress ratio and gross
stress level (ksi) for
fiber crack growth data.
FRX2(I),FRY2(I) - Radius of notch in x and
y direction (in) for
fiber crack growth data.
FW2(I) - Width of laminate (in) for fiber
crack growth data.
IRES8C(I) - Flag specifying if you will provide
matrix crack growth data.
Options include:
Y or y - Data will be provided.
N or n - data will not be provided.
If IRES8C(I)=Y
IRES8D(I) - Curve type flag
Options include:
1 - Crack length (in.) vs. cycles
(a vs. N)

181

```
                    2 - Crack growth rate (in/cycle)
                        vs. stress intensity (ksi√in)
                        (da/dN vs. del K)
        FFILE4(I) - Name of file containing matrix crack
                    growth data.  Format of this file is
                    shown in Table A-2.
                    Maximum of 20 characters.
If IRES8D(I)=1
        RM2(I),GSLM(I) - Stress ratio and gross
                            stress level (ksi) for
                            matrix crack growth data.
        TRX2(I),TRY2(I) - Radius of notch in x and
                            y direction (in) for
                            fiber crack growth data.
        TW2(I) - Width of laminate (in) for fiber
                    crack growth data.
If IRES8A(I)=Y and IRES8C(I)=Y and TANG2(I)=0. or
    IRES8A(I)=Y and IRES8C(I)=N or
    IRES8A(I)=N and IRES8C(I)=Y or
    IRES8A(I)=N and IRES8C(I)=N
        IRES8E(I) - Flag specifying if the matrix
                    material crack growth curve is
                    the same as a curve already
                    input.  Options include:
                        Y or y - File has already been
                                    input.
                        N or n - File has not been
                                    input yet.
                No input necessary if I=1.
If IRES8E(I)=Y
        MATM(I) - Material number for matrix
                    material with same crack growth
                    curve.
                    No input necessary if I=1.
```

182

```
If IRES8E(I)=N
    IRES8F(I) - Curve type flag
            Options include:
                1 - Crack length (in) vs.
                    cycles (a vs. N)
                2 - Crack growth rate
                    (in/cycle) vs. stress
                    intensity (ksi/in)
                    (da/dN vs. del K)
    FFILE5(I) - Name of file containing matrix
            material crack growth curve.
            Format of this file is shown in
            Table A-2.
            Maximum of 20 characters.
    If IRES8F(I)=1
        RMM(I),GSLMM(I) - Stress ratio and
                    gross stress level
                    (ksi) for matrix
                    material crack
                    growth curve.
        TRXM(I),TRYM(I) - Radius of notch in x
                    and y direction (in)
                    for matrix material
                    crack growth curve.
        TWM(I) - Width of laminate (in) for
                    matrix material crack growth
                    curve.
STRCG - Stress level (ksi) for crack growth laminate
        analysis.
SRM2,SRF2 - Stress ratio for the matrix and the fibers for
        the laminate analysis.  Typically SRM2=SRF2.
        One example in which SRM doesn't equal SRF is
        when your laminate has a filled notch and is
        subjected to R=-1 loading.  In this case,
        SRM=-1 and SRF=0 (.02) because the fibers are
        not affected by the compression loads.
```

183

Residual Strength Module Input

> Input for Stiffness Module with following exceptions:
>> IRES5 - No input required by user (Flag set to 'Y')

> Input for Stress Module

> Input for Strength Module

> IRES9 - Residual strength output flag
>> Options include:
>>> 1 - Single residual strength calculation
>>> 2 - Residual strength vs. flaw length data
>> If IRES9=1
>>> FLN - Length of flaw from hole (in)
>> EKC - Fracture toughness (ksi/in)
>>> Enter '0' if unknown - an estimate will be made.

End of Input

b. <u>Description of Output</u> - The user has the option of displaying the output on the screen or having it written to a file for later printing. The output displayed from each analysis module is controlled by the user when selecting the analysis modules. Some data generated by the analysis modules are written to files in a format which allows for plotting. These files are written to the user's directory during execution. The output displayed and files created by each module are described in this section.

Stiffness Module
> Lamina or Ply Stiffness
>> E1 - Stiffness parallel to fibers (ksi)
>> E2 - Stiffness perpendicular to fibers (ksi)
>> G12 - Shear stiffness (ksi)
>> V12 - Poisson's ratio

Lamina or Ply Unnotched Strengths

    X - Strength parallel to fibers (ksi)

    Y - Strength perpendicular to fibers (ksi)

    S - Shear strength

Laminate Stiffness

    EX - Stiffness parallel to loading axis (ksi)

    EY - Stiffness perpendicular to loading axis (ksi)

    GXY - Shear stiffness

    VXY - Poisson's ratio

Stress Module

    Stress Concentrations About Notch

        KTNET - Net stress concentration at edge of notch, 90° from loading axis.

        KTGROSS - Gross stress concentration at edge of notch, 90° from loading axis.

        KTTOP - Stress concentration at top of notch, 0° from loading axis.

        KS - Maximum shear stress/gross stress, shear stress concentration at angle, THETA, from loading axis.

        THETA - Angle from loading axis where maximum KS occurs.

    Stress Distribution Through Net Section

        ALPHA, BETA, GAMMA - Constants in stress gradient equation determined through application of boundary conditions.

        X - Distance from center of laminate (in) through net section.

        A - Distance from edge of notch (in) through net section.

        X/R - Distance from center of laminate/radius in y direction.

        KT - Local stress parallel to fibers X/ gross stress.

Strength Module

    Lamina or Ply Yielding or Failing Data

        Ply material number and orientation

        Gross stress at which ply yields or fails (ksi)

        Net stress at which ply yields or fails (ksi)

        Load at which ply yields or fails (ksi)

    Laminate Notched or Unnotched Strength

        Gross strength of laminate (ksi)

        Net strength of laminate (ksi)

        Failing load of laminate (ksi)

    Note: 1) The term 'fail' for an off-axis ply refers to
              the point at which the ply goes from elastic to
              perfectly-plastic. The ply loses all stiffness
              contribution but still carries load.

           2) If the stiffness data printout is requested, the
              new laminate stiffnesses will be displayed each
              time a ply fails or yields.

Crack Initiation Life Module

    Output Displayed

        STRESS - Gross stress level of laminate (ksi)

        LOG10(LIFE) - The $\log_{10}$ of the life to a .05 in.
                      crack in each ply at the specified
                      STRESS.

        M - Flag which indicates that a .05 in. crack has
            initiated in the matrix along the fibers.

        T - Flag which indicates that a .05 in. crack has
            initiated along the fibers 90° from the loading
            axis.

        F - Flag which indicates that the ply has failed
            through the net section.

Output Written to Files

File Name	Output Description
MMUNCIFi.DAT	Unnotched fiber life data - This file is created from the user supplied fiber rupture curves. It contains the local stresses (ksi) and lives to fiber breakage. i = 1, 2, and 3 for the three material systems.
MMUNCIMi.DAT	Unnotched matrix crack initiation data - This file is created from the user supplied matrix initiation curves. It contains local stresses (ksi) and lives to 0.05 in. cracks. i = 1, 2, and 3 for the three material systems.
MMCIPi.DAT	Crack initiation data for ply # i in laminate. This file contains gross laminate stresses (ksi) and lives for 0.05 in. crack to initiate in the ply.
MMCISM.DAT	Crack initiation life summary of each ply in the laminate

Crack Growth Module

Displayed Output

For user specified stress level, STRCG, the following information is displayed:

1) material number and orientation of plies that have failed; and

2) material number, orientation, initiation life, and failure mode for plies that have initiated a 0.05 in. crack.

DELTA K - Stress intensity (ksi/in) for ply

DA/DN - Crack growth rate (in/cycle) at DELTA K for ply

Output Written to Files

File Name	Output Description
MMCGM.DAT	Matrix crack growth data for all material systems.
MMCGF.DAT	Fiber crack growth data for all material systems.
Note:	These files contain da/dN (in/cycle) vs. delta K (ksi/in) data created from the user supplied data files. If the user supplies da/dN vs. delta K data, then this file is identical to the users input data. The data for each material system is stacked on top of each other.
MMCGPi.DAT	Crack growth data for ply # i in the laminate. This file contains crack length (in) vs. cycle data.

Residual Strength Module

Displayed Output

KC - Critical stress intensity factor (ksi/in) - only displayed if an estimate was requested by user.

FLN - Length of flaw from hole (in) as specified by user

RST - Residual strength (ksi) for FLN

MODE - Flag that indicates if failure was driven by strength or fracture mechanics criteria.

Output Written to Files - Multiple Point Calculation Only

File Name	Output Description
MMRS.DAT	1) Residual strength (ksi) vs. flaw length (in) data based on fracture mechanics criteria.
	2) Residual strength (ksi) vs. flaw length (in) data based on strength criteria.

188

TABLE A-1

Program Execution Control

When user specifies:	Program requires input for:
1 - Stiffness Analysis	1 - Stiffness Module
2 - Stress Analysis	1 - Stiffness Module 2 - Stress Module
3 - Strength Analysis	1 - Stiffness Module 2 - Stress Module 3 - Strength Module

4 - Crack Initiation
    Life Analysis
	1 - Stiffness Module
	2 - Stress Module
	3 - Strength Module
	4 - Crack Initiation
	    Life Module

5 - Crack Growth Analysis	1 - Stiffness Module 2 - Stress Module 3 - Strength Module 4 - Crack Initiation Life Module 5 - Crack Growth Module
6 - Residual Strength Analysis	1 - Stiffness Module 2 - Stress Module 3 - Strength Module 6 - Residual Strength Module

TABLE A-2

Format for Input Data Files

Crack Initiation Files - Fiber rupture and matrix crack
initiation data

```
        Line 1      - Title for data (80 character max)
        Line 2      - Number of points in data file, NPT
        Line 3      - Shortest life , Highest Stress Level (ksi)
           .             .        ,        .
           .             .        ,        .
           .             .        ,        .
        Line NPT+2 - Longest Life, Lowest Stress Level (ksi)
```

Crack Growth Files - Crack growth data for growth across
                     fibers, along fibers, or in matrix
                     alone.

1) Crack length vs. cycle format

```
        Line 1      - Title for data (80 character max)
        Line 2      - Number of points in data file, NPT
        Line 3      - 0      , 0
        Line 4      - Lowest Cycle # , Smallest crack length
                                                         (in)
           .             .        ,        .
           .             .        ,        .
           .             .        ,        .
        Line NPT+2 - Highest Cycle #, Largest crack length (in)
```

2) Crack growth rate vs. delta stress intensity format
      (in/cycle)   (ksi√in)

    Line 1   - Title for data (80 character max)
    Line 2   - Number of points in data file, NPT
    Line 3   - Lowest delta K , Smallest da/dN
        .   .   ,   .
        .   .   ,   .
        .   .   ,   .
    Line NPT+2 - Highest delta K, Largest da/dN

3. EXAMPLE PROBLEMS

Data may be input into the program interactively or through the use of input files. If the data is input interactively, the program will store the data in an input file, if the user desires.

Five different example problems are listed in this section to demonstrate the input file format and to display some sample output. The data in the input files must appear on the appropriate lines as shown, but the column spacing in each row is arbitrary. If there is an error in the input file the program will terminate execution. Therefore, the simplest way to create an input file is to enter the data interactively and let the program create and save the file.

a. Example 1 - Stiffness

Input File

```
          1
 /
          2
 (B4C)B
 Ti-15-3
   40.00000
          1
   56000.00      0.3000000
   15600.00      0.3000000
 Boron
 AL6061
   48.00000
          1
   56000.00      0.3000000
```

```
        10000.00        0.3000000
    Y
              4
              1   0.0000000E+00   0.01
              1    45.00000       0.01
              1   -45.00000       0.01
              1    90.00000E+00   0.01
        0.0000000E+00
```

Output File

```
        ****************************************

                  COMPOSITE STIFFNESSES

        ****************************************

          *** LAMINA PROPERTIES ***

              MATERIAL NO. 1

        (B4C)B/Ti-15-3    40.00000        % FIBER VOLUME
        E1 = 31760.00    E2 = 21927.71    G12 = 8433.733    V12 = 0.300

              MATERIAL NO. 2

        Boron/AL6061     48.00000         % FIBER VOLUME
        E1 = 32080.00    E2 = 16509.43    G12 = 6349.782    V12 = 0.300

          *** LAMINATE PROPERTIES ***

        EX = 24986.90    EY = 24986.90    GXY = 9618.924    VXY = 0.298
```

b. <u>Example 2 - Stress</u>

<u>Input File</u>

```
          2
 /
          1
 Boron
 Al6061
   48.00000
          2
   30250.00          20630.00          9780.000          0.2500000
   10000.00
          1
          1   0.0000000E+00   0.01
 0.0000000E+00
 0.1250000        0.1250000
    1.500000
         10
```

<u>Output File</u>

```
 ****************************************

      LAMINATE STRESS DISTRIBUTION

 ****************************************


   *** FIBER STRESSES ***

 KTNET =   2.794711     KTGROSS =   3.353653
 ALPHA = 0.9861588     BETA =   2.367494     GAMMA =   2.696295
```

194

X	A	X/R	KT
0.1250	0.0000	1.0000	3.3537
0.1327	0.0077	1.0617	2.9205
0.1559	0.0309	1.2469	2.1263
0.1944	0.0694	1.5556	1.5520
0.2485	0.1235	1.9877	1.2536
0.3179	0.1929	2.5432	1.1148
0.4028	0.2778	3.2222	1.0508
0.5031	0.3781	4.0247	1.0204
0.6188	0.4938	4.9506	1.0052
0.7500	0.6250	6.0000	0.9973

*** MAXIMUM MATRIX SHEAR STRESS ***

KT (TOP OF HOLE) = -0.904

MAXIMIUM MATRIX SHEAR STRESS/GROSS STRESS = -0.876

  LOCATION --- THETA = 66.000

c. <u>Example 3 - Strength</u>

<u>Input File</u>

```
         3
 /
         1
Boron
Al6061
  48.00000
         2
 30250.00       20630.00        9780.000       0.2500000
 10000.00
         3
         1  0.0000000E+00  0.02
         1   45.00000      0.01
         1  -45.00000      0.01
```

```
0.0000000E+00
0.1250000        0.1250000
 1.500000
          2
 181.3000        25.80000        62.50000        15.00000
 80.00000        27.00000
```

Output File

    *** LAMINA PROPERTIES ***

       MATERIAL NO. 1

X =   181.3000   Y =   25.80000   S =   16.67867

   ****

       LAMINATE STRENGTHS

   ****

   ***   45.0 DEGREE PLIES OF MATERIAL # 1 HAVE REACHED
          THEIR STRENGTH LIMIT

THE PLY GROSS STRENGTH IS   9.901 KSI.
THE PLY NET STRENGTH IS   11.881 KSI.
THE LOAD IN THE PLY IS   0.594 KIPS

    *** -45.0 DEGREE PLIES OF MATERIAL # 1 HAVE REACHED
          THEIR STRENGTH LIMIT

THE PLY GROSS STRENGTH IS   9.901 KSI.
THE PLY NET STRENGTH IS   11.881 KSI.
THE LOAD IN THE PLY IS   0.594 KIPS

```
***    0.0 DEGREE PLIES OF MATERIAL # 1 HAVE YIELDED AT AN
     ANGLE OF  62.00 DEGREES FROM THE TOP OF THE HOLE


THE LENGTH OF THE YIELD ZONE IS   0.334 IN. FOR MATERIAL # 1


***    0.0 DEGREE PLIES OF MATERIAL # 1 HAVE REACHED
              THEIR STRENGTH LIMIT


THE LAMINATE GROSS STRENGTH IS   53.653 KSI.
THE LAMINATE NET STRENGTH IS   64.384 KSI.
THE LOAD IN THE LAMINATE IS    3.219 KIPS
```

d. <u>Example 4 - Crack Initiation and Crack Growth</u>

<u>Input File</u>

```
1 2 3 4 5
 /
          1.
Boron
AL6061
  48.00000
          2
  30250.00        20630.00        9780.000        0.2500000
  10000.00
          1
          1  0.0000000E+00  0.1000000
0
  0.1250000        0.1250000
  1.500000
          2
  181.3000        25.80000        62.51000        15.00000
  80.00000        27.00000
          1
```

```
LIFF
 2.0000000E-02
 0.1250000       0.1250000
  1.500000
          1
LIFM
 2.0000000E-02
 0.1250000       0.1250000
  1.500000
 2.0000000E-02   2.0000000E-02
N
Y
          1
BALMCG
 2.0000000E-02    70.00000
 0.1250000       0.1250000
   1.500000
 0.0000000E+00
          2
AL6061CG
  70.00000
 2.0000000E-02   2.0000000E-02
```

Output File

```
    ****************************************


          COMPOSITE STIFFNESSES


    ****************************************


    *** LAMINA PROPERTIES ***

        MATERIAL NO. 1

 Boron/AL6061      48.00000        % FIBER VOLUME
 E1 = 30250.00    E2 = 20630.00    G12 = 9780.000    V12 = 0.250
```

X =   181.3000   Y =   25.80000   S =   16.68171

   *** LAMINATE. PROPERTIES ***

EX = 30250.00   EY = 20630.00   GXY = 9780.000   VXY = 0.250

   ****

      LAMINATE STRESS DISTRIBUTION

   ****

   *** FIBER STRESSES ***

KTNET =   2.794711   KTGROSS =   3.353653
ALPHA = 0.9861588   BETA =   2.367494   GAMMA =   2.696295

       X   A   X/R   KT
    0.1250   0.0000   1.0000   3.3537
    0.7500   0.6250   6.0000   0.9973
   *** MAXIMUM MATRIX SHEAR STRESS ***

 KT (TOP OF HOLE) = -0.904
MAXIMUM MATRIX SHEAR STRESS/GROSS STRESS = -0.876
 LOCATION --- THETA = 66.000

   ****

         LAMINATE STRENGTHS

   ****

   ***   0.0 DEGREE PLIES OF MATERIAL # 1 HAVE YIELDED AT AN
      ANGLE OF 66.00 DEGREES FROM THE TOP OF THE HOLE

THE LENGTH OF THE YIELD ZONE IS   0.301 IN. FOR MATERIAL # 1

199

```
***   0.0 DEGREE PLIES OF MATERIAL # 1 HAVE REACHED
              THEIR STRENGTH LIMIT

THE LAMINATE GROSS STRENGTH IS   95.821 KSI.
THE LAMINATE NET STRENGTH IS  114.985 KSI.
THE LOAD IN THE LAMINATE IS    14.373 KIPS

   ****************************************

            CRACK INITIATION LIFE

   ****************************************


STRESS    LOG10(LIFE)
 (KSI)    0 (1)
-------   -------
   95.82  0.00 F
   91.54  0.29 F
   87.27  0.65 F
   82.99  1.13 F
   78.71  1.65 F
   74.43  1.76 M
   70.16  1.83 M
   65.88  1.90 M
   61.60  1.99 M
   57.33  2.15 M
   53.05  2.33 M
   48.77  2.54 M
   44.50  2.82 M
   40.22  3.63 M
   35.94  4.79 M
   31.66  6.96 M
   27.39  8.30 M
   23.11  9.85 M
   18.83 10.00 M
   14.56 10.00 M
   10.28 10.00 M
```

```
*****************************************

          CRACK GROWTH LIFE

*****************************************

THE    0.0 DEGREE PLY OF MATERIAL # 1 HAS  INITIATED
A CRACK GROWING  ALONG THE FIBERS AFTER  0.676913E+02 CYCLES

DELTA K    DA/DN
 15.46    0.10E-03
 15.60    0.11E-03
 15.72    0.11E-03
 15.83    0.11E-03
 15.92    0.11E-03
 16.01    0.12E-03
 16.09    0.12E-03
 16.15    0.12E-03
 16.21    0.12E-03
 16.26    0.12E-03
 16.31    0.12E-03
 16.35    0.13E-03
 16.38    0.13E-03
 16.41    0.13E-03
 16.43    0.13E-03
 16.45    0.13E-03
 16.47    0.13E-03
 16.48    0.13E-03
 16.49    0.13E-03
 16.49    0.13E-03
```

e. Example 5 - Residual Strength

Input File

```
        6
 /
        1
(B4C)B
Ti-15-3
   40.00000
         2
  32000.00         23000.00         9000.000         0.2500000
  16000.0
         1
         1  0.0000000E+00   0.1000000
 0
 0.1250000        0.1250000
  1.500000
 2
  129.0000         48.00000         97.00000         0.0000000E+00
  180.0000         105.0000
         2
  57.50000
```

Output File

```
*****************************************

            RESIDUAL STRENGTH

*****************************************
```

FLAW LENGTH	RESIDUAL STRENGTH	MODE
0.000	107.50	STRENGTH DRIVEN
0.010	105.78	STRENGTH DRIVEN
0.020	89.24	FRACTURE DRIVEN
0.030	80.80	FRACTURE DRIVEN
0.040	76.37	FRACTURE DRIVEN
0.050	73.57	FRACTURE DRIVEN
0.060	71.56	FRACTURE DRIVEN
0.070	69.95	FRACTURE DRIVEN
0.080	68.57	FRACTURE DRIVEN
0.090	67.33	FRACTURE DRIVEN
0.100	66.18	FRACTURE DRIVEN
0.110	65.09	FRACTURE DRIVEN
0.120	64.04	FRACTURE DRIVEN
0.130	63.03	FRACTURE DRIVEN
0.140	62.06	FRACTURE DRIVEN
0.150	61.12	FRACTURE DRIVEN
0.160	60.20	FRACTURE DRIVEN
0.170	59.32	FRACTURE DRIVEN
0.180	58.46	FRACTURE DRIVEN
0.190	57.63	FRACTURE DRIVEN
0.200	56.82	FRACTURE DRIVEN

REFERENCES

A.1 Jones, Robert M., Mechanics of Composite Materials,
      McGraw-Hill Book Company, New York, 1975, pp. 147-236.

A.2 Lekhnitskii, S.G., Anisotropic Plates, Gordon and Breach
      Science Publishers, 1968.

A.3 Seely, F.B. and Smith, J.O., Advanced Mechanics of Materials,
      Wiley & Sons, 1952.

A.4 Goree, J.G., Lokeswarappa, R.D., and Jones, W.F.,
      "Matematical Modeling of Damage in Unidirectional
      Composites," NASA-CR-3453, August 1981.

A.5 Smith, K.N., Watson, P. and Topper, T.H., "A Stress-Strain
      Function for the Fatigue of Metals," Journal of Materials,
      ASTM, Vol. 5, No. 4, December 1970, pp. 767-778.

U235039